

Renewable Fuels and Chemicals from the Organic Fraction of Municipal Solid Waste

Aritha Dornau

PhD

University of York
Biology
September 2019

Abstract

Municipal solid waste (MSW) is any non-industrial waste produced in households and public or commercial institutions. 3.4 billion tonnes of MSW will be produced annually by 2050, but unsustainable practices like landfilling and incineration currently dominate MSW management. The organic fraction of MSW (OMSW) typically comprises ~50% lignocellulose-rich material but is underexplored as a biomanufacturing feedstock.

This thesis investigated OMSW as a feedstock for producing renewable biofuels and chemicals. Uniquely, the OMSW-derived fibre used in this project was produced via a commercial autoclave pre-treatment from a realistic and reproducible MSW mixture. The OMSW fibre was subjected to comprehensive compositional analysis and hydrolysis, and OMSW hydrolysate was analysed for sugars, metals and marker inhibitors to evaluate fermentability. Waste residues were investigated as a feedstock for biogas production. Next, the growth and productivity of eight diverse and biotechnologically useful microbial species was characterised on OMSW fibre hydrolysate supplemented with 1% yeast extract and the best candidate was further characterised and improved for industrial applications.

The OMSW fibre contained a large polysaccharide fraction, comprising 38% cellulose and 4% hemicellulose. Hydrolysate of OMSW fibre was high in D-glucose and D-xylose, low in inhibitors, deficient in nitrogen and phosphate and abundant in potentially toxic metals. Hydrolysis residues contained a six-fold greater metal concentration but generated 33.4% more biomethane in anaerobic digestion compared to unhydrolysed fibre. Microbial screening identified three species that robustly and efficiently fermented OMSW fibre hydrolysate: *Saccharomyces cerevisiae*, *Zymomonas mobilis* and *Rhodococcus opacus*. These species could theoretically produce 139 Kg and 136 Kg of ethanol and 91 Kg of triacylglycerol (TAG) per tonne of OMSW, respectively. *R. opacus* had the highest fermentation productivity, concurrently using D-glucose and D-xylose and producing TAG to 72% of maximum theoretical yield. Expression of a heterologous thioesterase in *R. opacus* to augment lauric acid production proved unsuccessful and requires further work.

Overall, this study showed that OMSW is a promising renewable feedstock for biomanufacturing. The microorganisms identified through this work grew robustly and efficiently on OMSW fibre hydrolysate and are promising candidates for developing an OMSW biorefining platform.

Table of Contents

| | |
|--|----|
| <u>List of Tables</u> | 7 |
| <u>List of Figures</u> | 9 |
| <u>Acknowledgements</u> | 13 |
| <u>Authors Declaration</u> | 16 |
| Chapter 1: General Introduction | 17 |
| 1.1 Anthropogenic Climate Change: A Brief History | 17 |
| 1.2 Biorefining | 20 |
| 1.2.1 Renewable Feedstocks | 22 |
| 1.2.2 Pre-treatment | 25 |
| 1.2.3 Enzymatic Hydrolysis | 27 |
| 1.2.4 Fermentation | 29 |
| 1.2.5 Other Outputs | 39 |
| 1.3 Municipal Solid Waste | 42 |
| 1.3.1 Global Impact | 42 |
| 1.3.2 MSW Management in the United Kingdom | 45 |
| 1.3.3 Municipal Solid Waste as a Feedstock | 47 |
| 1.3.4 Wilson Bio-Chemical and the Wilson System® | 49 |
| 1.4 Aims and Objectives | 52 |
| Chapter 2: Compositional Analysis of Organic Municipal Solid Waste Fibre | 54 |
| 2.1 Introduction | 54 |
| 2.1.1 Aims of this Chapter | 56 |
| 2.2 Materials & Methods | 57 |
| 2.2.1 Production of the OMSW Fibre | 57 |
| 2.2.2 Compositional Analysis | 60 |
| 2.2.3 Total Solids, Moisture & Ash content | 60 |
| 2.2.4 Lignin | 60 |
| 2.2.5 Hemicellulose & Cellulose | 61 |
| 2.2.6 Oil | 63 |
| 2.2.7 Protein | 63 |
| 2.2.8 Metals | 63 |
| 2.2.9 OMSW Washing | 64 |
| 2.2.10 Soxhlet Extraction & Extractives | 64 |
| 2.3 Results | 66 |
| 2.3.1 Composition of the Constructed OMSW Fibre | 66 |

| | | |
|--|---|-----|
| 2.3.2 | Appearance and Moisture content | 66 |
| 2.3.3 | Structural Components: Lignocellulose and Ash..... | 67 |
| 2.3.4 | Non-Structural Components: Metals..... | 70 |
| 2.3.5 | Non-Structural Components: Extractives | 72 |
| 2.3.6 | Summative Composition | 75 |
| 2.4 | Discussion..... | 76 |
| Chapter 3: Evaluating Hydrolysis, Fermentability and Biogas Production from OMSW Fibre | | 82 |
| 3.1 | Introduction..... | 82 |
| 3.1.1 | Aims of this Chapter | 85 |
| 3.2 | Materials and Methods..... | 87 |
| 3.2.1 | Determining Cellulase Activity as Filter Paper Units | 87 |
| 3.2.2 | Small-scale hydrolysis | 87 |
| 3.2.3 | Large-scale hydrolysis | 87 |
| 3.2.4 | Hydrolysate sterilisation | 88 |
| 3.2.5 | Calculating hydrolysis efficiency..... | 89 |
| 3.2.6 | Determining Specific Gravity..... | 89 |
| 3.2.7 | Hydrolysate analysis | 91 |
| 3.2.7.1 | Reducing sugars..... | 91 |
| 3.2.7.2 | Monosaccharides and oligosaccharides | 92 |
| 3.2.7.3 | Metals | 92 |
| 3.2.7.4 | Marker inhibitors..... | 92 |
| 3.2.7.5 | Nutrients | 93 |
| 3.2.8 | Anaerobic Digestion Assays | 94 |
| 3.2.8.1 | Small-scale Anaerobic Digestion Assay..... | 94 |
| 3.2.9 | Automated Biomethane Potential Assay..... | 96 |
| 3.2.9.1 | Set-up, Sampling and Feeding | 97 |
| 3.2.9.2 | Chemical Oxygen Demand | 98 |
| 3.2.9.3 | Microbial Community Characterisation | 98 |
| 3.3 | Results..... | 100 |
| 3.3.1 | Hydrolysis of OMSW fibre | 100 |
| 3.3.1.1 | Inhibitor and metal content | 104 |
| 3.3.1.2 | Nutrient analysis..... | 108 |
| 3.3.2 | Methane production from residual solids of OMSW fibre hydrolysis..... | 109 |
| 3.3.2.1 | Small-scale anaerobic digestion assay | 109 |
| 3.3.2.2 | Automated lab-scale anaerobic digestion assay | 111 |

| | | |
|--|--|-----|
| 3.4 | Discussion..... | 116 |
| Chapter 4: Identifying Microorganisms for Optimal OMSW Fibre Hydrolysate | | |
| | Fermentation..... | 120 |
| 4.1 | Introduction..... | 120 |
| 4.1.1 | Aims of the Chapter..... | 123 |
| 4.2 | Materials and Methods..... | 124 |
| 4.2.1 | Microorganisms, Chemicals and Media..... | 124 |
| 4.2.2 | Seed Cultures..... | 125 |
| 4.2.3 | Nutrient Growth Assays with <i>E. coli</i> | 126 |
| 4.2.3.1 | Assays with Chemical Nutrients..... | 126 |
| 4.2.3.2 | Assays with Nutritional Adjuncts..... | 126 |
| 4.2.4 | Fermentations..... | 127 |
| 4.2.4.1 | Fermentation Medium..... | 127 |
| 4.2.4.2 | Fermentation Assays..... | 127 |
| 4.2.4.3 | TAG Production Time Courses..... | 129 |
| 4.2.5 | Light Microscopy..... | 129 |
| 4.2.6 | Biochemical Analytical Methods and Calculations..... | 130 |
| 4.2.6.1 | Glucose and Xylose..... | 130 |
| 4.2.6.2 | Ethanol, Butanol and Acetone..... | 130 |
| 4.2.6.3 | Final Cell Dry Weight..... | 131 |
| 4.2.6.4 | Calculating Fermentation Yield Parameters..... | 131 |
| 4.2.6.5 | Calculating the Carbon to Nitrogen Ratio..... | 133 |
| 4.2.6.6 | Fatty Acid Profiling and Triacylglycerol Quantification..... | 134 |
| 4.2.6.7 | Calculating the Cetane Number..... | 135 |
| 4.2.7 | Molecular Biology..... | 136 |
| 4.2.7.1 | Plasmids..... | 136 |
| 4.2.7.2 | Primers, PCR and Sequencing..... | 138 |
| 4.2.7.3 | Agarose Gel Electrophoresis..... | 139 |
| 4.2.7.4 | Synthetic DNA Design and Synthesis..... | 140 |
| 4.2.7.5 | In-Fusion Cloning..... | 141 |
| 4.2.7.6 | Transformation by Heat Shock..... | 143 |
| 4.2.7.7 | Purifying Plasmids from <i>E. coli</i> | 143 |
| 4.2.7.8 | <i>Rhodococcus opacus</i> Competent Cell Production..... | 144 |
| 4.2.7.9 | Transformation by Electroporation..... | 144 |
| 4.2.7.10 | Purifying Plasmids from <i>R. opacus</i> | 145 |
| 4.2.8 | Recombinant Gene Expression..... | 145 |

| | | |
|--|--|-----|
| 4.2.8.1 | SDS-PAGE | 145 |
| 4.2.8.2 | Expression Time-Course..... | 146 |
| 4.3 | Result | 147 |
| 4.3.1 | Evaluation of OMSW Fibre Hydrolysate Fermentability | 147 |
| 4.3.2 | Time-Course Kinetics of Eight Species Grown on OMSW Fibre Hydrolysate .. | 151 |
| 4.3.2.1 | <i>Clostridium saccharoperbutylaceticum</i> | 151 |
| 4.3.2.1 | <i>Escherichia coli</i> | 152 |
| 4.3.2.2 | <i>Geobacillus thermoglucosidasius</i> | 154 |
| 4.3.2.3 | <i>Pseudomonas putida</i> | 155 |
| 4.3.2.4 | <i>Rhodococcus opacus</i> | 156 |
| 4.3.2.5 | <i>Saccharomyces cerevisiae</i> | 158 |
| 4.3.2.6 | <i>Schizosaccharomyces pombe</i> | 159 |
| 4.3.2.7 | <i>Zymomonas mobilis</i> | 160 |
| 4.3.3 | Evaluating Relative Fermentation Efficiency between Species..... | 162 |
| 4.3.4 | Characterising OMSW Fibre Hydrolysate Fermentation by <i>R. opacus</i> | 166 |
| 4.3.5 | Engineering Lauric Acid Production in <i>Rhodococcus opacus</i> | 171 |
| 4.4 | Discussion | 176 |
| Chapter 5: General Discussion | | 183 |
| Appendices | | 191 |
| Appendix I: Percentage composition of constructed OMSW fibre | | 191 |
| Appendix II: Concentration of metals measured in constructed OMSW fibre | | 192 |
| Appendix III: Shannon Index..... | | 193 |
| Appendix IV: Taxonomic Tables of AD Community Analysis..... | | 194 |
| Appendix V: Screening of <i>Schizosaccharomyces pombe</i> strains | | 198 |
| Appendix VI: Sugar fermentation data for each species | | 199 |
| Appendix VII: Fatty acid profile of <i>Rhodococcus opacus</i> MITXM-61 grown in 40 ml OMSW fibre hydrolysate supplemented with 1% vitamin-enriched yeast extract..... | | 200 |
| Appendix VIII: Cloning of ACP-BTE into pTip-QC1 | | 202 |
| Appendix IX: Biochemical steps in the TAG biosynthesis pathway of oleaginous <i>Rhodococcus</i> species..... | | 207 |
| <u>Index of Abbreviations</u> | | 208 |
| References | | 211 |

List of Tables

| | |
|---|-----|
| Table 2.1: Composition of waste materials used for production of OMSW fibre on the Wilson Bio-Chemical Pilot Rig..... | 57 |
| Table 2.2: Composition of lignocellulose (cellulose, hemicellulose and lignin) in OMSW fibre..... | 68 |
| Table 2.3: Monosaccharide composition of the hemicellulose fraction of OMSW fibre | 68 |
| Table 2.4: Metal levels in washed and unwashed OMSW fibre..... | 71 |
| Table 2.5: Composition of OMSW fibre and Soxhlet extracted OMSW fibre..... | 74 |
| Table 2.6: Theoretical concentration of metals in hydrolysate of OMSW fibre after 20% solids loading hydrolysis..... | 79 |
| Table 2.7: Metal levels measured in industrial OMSW compared to metal levels in OMSW used in this project..... | 81 |
| Table 3.1: Organic acids, aldehydes and metals measured in OMSW fibre hydrolysate and the minimum inhibitory concentration (M.I.C) of each analyte for the model fermentative microorganism <i>Escherichia coli</i> | 106 |
| Table 3.2: Levels of phosphorus, orthophosphate, sulphate, nitrogenous compounds and calculated yeast available nitrogen (YAN) in OMSW fibre hydrolysate..... | 108 |
| Table 4.1: Microorganisms, media and culture conditions used in this study..... | 124 |
| Table 4.2: Composition of MOPS minimal medium..... | 125 |
| Table 4.3: PCR primers used throughout this project and their respective applications..... | 138 |
| Table 4.4: PCR reaction components..... | 138 |
| Table 4.5: PCR protocol..... | 139 |

| | |
|---|-----|
| Table 4.6: 10x Tris-Borate-EDTA Buffer Recipe..... | 139 |
| Table 4.7: Recipe for MB + 1.5% glycine..... | 144 |
| Table 4.8: Recipe for preparation of SDS-PAGE resolving and stacking gel..... | 146 |
| Table 4.9: Level of phosphorus, orthophosphate, sulphate, nitrogenous compounds and calculated yeast available nitrogen (YAN) in OMSW fibre hydrolysate and OMSW fibre hydrolysate supplemented with 1% vitamin-enriched yeast extract (VYE)..... | 150 |
| Table 4.10: Key fermentation yield parameters for eight species grown on OMSW fibre hydrolysate..... | 164 |
| Table 4.11: Fatty acids composition profile of <i>Rhodococcus opacus</i> MITXM-61 growth on OMSW fibre hydrolysate for 72 hours and the calculated cetane index of each fatty acid..... | 167 |

List of Figures

| | |
|--|----|
| Figure 1.1: Overview of the carbon cycle, including natural and anthropogenic carbon sources and sinks..... | 18 |
| Figure 1.2: Overview of the greenhouse effect..... | 19 |
| Figure 1.3: General overview of an integrated biorefining process chain..... | 22 |
| Figure 1.4: Structural configuration of lignocellulose within the plant cell wall | 23 |
| Figure 1.5: Common byproducts derived from lignocellulosic biomass during physicochemical pre-treatment..... | 26 |
| Figure 1.6: The enzymatic degradation of cellulose by endoglucanases, exoglucanases, β -glucosidases and LPMOs | 28 |
| Figure 1.7: A model fermentation pathway..... | 30 |
| Figure 1.7: The Embden-Meyerhof Pathway..... | 33 |
| Figure 1.8: The Entner-Doudoroff Pathway | 34 |
| Figure 1.9: Triacylglycerol structure and mechanism of transesterification to Biodiesel.... | 35 |
| Figure 1.10: Triacylglycerol Metabolism..... | 36 |
| Figure 1.11: Value-added products synthesised from lactic acid..... | 38 |
| Figure 1.12: Value-added products synthesised from lignin..... | 39 |
| Figure 1.13: Overview of Anaerobic Digestion..... | 41 |
| Figure 1.14: Contribution of different greenhouse gas emissions sectors to the net mean global temperature changes projected for the next 20 years | 43 |
| Figure 1.15: Prevalence of landfilling (left) and incineration (right) across European Union member states in 2015. | 44 |
| Figure 1.16: Overview of mechanical and biological processing stages operating within an integrated materials recovery facility (MRF) | 46 |
| Figure 1.17: Major constituents of British MSW by percentage. | 47 |
| Figure 1.18: Overview of the Wilson System [®] | 50 |
| Figure 1.19: The Wilson System Autoclave..... | 51 |
| Figure 2.1: The Wilson Bio-Chemical Pilot Rig..... | 58 |

| | |
|--|-----|
| Figure 2.2: Schematic of Wilson Bio-Chemical Ltd. Pilot Rig | 59 |
| Figure 2.3: Anatomy of a Soxhlet extractor (image by author) | 65 |
| Figure 2.4: Appearance of the OMSW fibre..... | 66 |
| Figure 2.5: Composition of lignocellulose (cellulose, hemicellulose and lignin) in three batches of OMSW fibre..... | 69 |
| Figure 2.6: Concentration of hemicellulose-derived monosaccharides in OMSW fibre and Soxhlet extracted OMSW fibre..... | 74 |
| Figure 2.7: Percentage composition of OMSW fibre..... | 75 |
| Figure 2.8: Percentage composition of OMSW reported for a range of cities and in this study..... | 77 |
| Figure 2.9: Abundance of metals in Wilson Fibre® produced on an industrial Wilson System® over 32 months..... | 80 |
| Figure 3.1: Methodological overview of experimental aims and approaches investigated in Chapter 3..... | 86 |
| Figure 3.2: Measuring Specific Gravity..... | 90 |
| Figure 3.3: Schematic of the small-scale anaerobic digestion apparatus..... | 95 |
| Figure 3.4: Anaerobic Digestion Mini-bioreactor Assembly..... | 96 |
| Figure 3.5: Automated Lab-Scale Anaerobic Digestion System..... | 97 |
| Figure 3.6: Preliminary trial of OMSW fibre hydrolysis using a range of enzyme loadings.. | 100 |
| Figure 3.7: Images of the key stages in the large-scale hydrolysis of OMSW fibre..... | 102 |
| Figure 3.8: Concentration and abundance of monosaccharides measured in hydrolysate of OMSW fibre..... | 103 |
| Figure 3.9: Fractionation of metals in the liquid and solid fractions produced after OMSW fibre hydrolysis..... | 107 |

| | |
|--|-----|
| Figure 3.10: Cumulative biomethane yield from anaerobic digestion of OMSW fibre hydrolysis residual material over 46 days..... | 110 |
| Figure 3.11: total solids content of digestate from anaerobic digestion of OMSW fibre and residuals..... | 111 |
| Figure 3.12: Chemical oxygen demand of digestate from anaerobic digestion of OMSW fibre and residuals..... | 112 |
| Figure 3.13: Cumulative biogas and methane production from anaerobic digestion of OMSW fibre and residuals | 113 |
| Figure 3.14: Taxonomic abundance of microbial communities after 43 days of anaerobic digestion with OMSW fibre or residuals, based on groupings of 16s rRNA sequences..... | 115 |
| Figure 4.1: Microaerobic fermentation set-up; (Image by Author)..... | 128 |
| Figure 4.2: Map of plasmid pTip-QC1 with close-up of MCS..... | 137 |
| Figure 4.3: Published protein sequence of Acyl-acyl Carrier Protein Thioesterase BTE from <i>Umbellularia californica</i> | 140 |
| Figure 4.4: DNA sequence synthesised using GeneArt Synthesis Service..... | 141 |
| Figure 4.5: Overview of Quick-Fusion Protocol..... | 142 |
| Figure 4.6: Growth of <i>Escherichia coli</i> LW06 on OMSW fibre hydrolysate supplemented with nutrients | 149 |
| Figure 4.7: Fermentation kinetics of <i>Clostridium saccharoperbutylacetonicum</i> growth on OMSW fibre hydrolysate..... | 152 |
| Figure 4.8: Fermentation kinetics of <i>Escherichia coli</i> grown on OMSW fibre hydrolysate.. | 153 |
| Figure 4.9: Fermentation kinetics of <i>Geobacillus thermoglucosidasius</i> grown on OMSW fibre hydrolysate..... | 154 |
| Figure 4.10: Fermentation kinetics of <i>Pseudomonas putida</i> growth on OMSW fibre hydrolysate..... | 156 |

| | |
|--|-----|
| Figure 4.11: Fermentation kinetics of <i>Rhodococcus opacus</i> grown on OMSW fibre hydrolysate..... | 157 |
| Figure 4.12: Fermentation kinetics of <i>Saccharomyces cerevisiae</i> grown on OMSW fibre hydrolysate..... | 158 |
| Figure 4.13: Fermentation kinetics of <i>Schizosaccharomyces pombe</i> grown on OMSW fibre hydrolysate..... | 160 |
| Figure 4.14: Fermentation kinetics of <i>Zymomonas mobilis</i> grown on OMSW fibre hydrolysate..... | 161 |
| Figure 4.15: Fermentation kinetics of eight different microorganisms grown on OMSW fibre hydrolysate..... | 163 |
| Figure 4.16: Light microscopy images of <i>Rhodococcus opacus</i> cells after 24, 48 and 72 hours of growth on OMSW fibre hydrolysate..... | 169 |
| Figure 4.17: Comprehensive TAG production kinetics of <i>R. opacus</i> grown on OMSW fibre hydrolysate | 170 |
| Figure 4.18: SDS-PAGE of induced and non-induced <i>R. opacus</i> ^{pTip-QC1_ACP-BTE} | 173 |
| Figure 4.19: Cell dry weight and TAG production over 144 hours by thiostrepton induced <i>R. opacus</i> ^{pTip-QC1_ACP-BTE} and <i>R. opacus</i> ^{pTip-QC1} | 174 |
| Figure 4.20: Laurate (C12:0) production over time by thiostrepton induced <i>R. opacus</i> ^{pTip-QC1_ACP-BTE} and <i>R. opacus</i> ^{pTip-QC1} | 175 |
| Figure 4.21: Time-course profile of the major long-chain fatty acids produced by <i>R. opacus</i> ^{pTip-QC1_ACP-BTE} and <i>R. opacus</i> ^{pTip-QC1} | 175 |
| Figure 4.22: Percentage abundance of the major fatty acids produced by <i>R. opacus</i> MITXM-61 reported in the literature compared to this project..... | 179 |

Acknowledgements

A PhD is a personal journey. A substantial intellectual undertaking and a trial of perseverance. At times it has been emotionally challenging, and on occasion even physically demanding. I am fortunate to have had two excellent supervisors, Simon McQueen-Mason and Gavin Thomas, without whom my pursuit of this thesis would have been abandoned long ago. Simon's supervision was always supportive, understanding and delivered with a laid-back attitude and good humour. He taught me that science is the icing on the cake of life, and on occasions when I was frustrated or demotivated by my work, he always told me to go home, enjoy the hypothetical sunshine (this is Britain, after all) and not to return until I had resurrected a clear and motivated mind. Gavin taught me new ways to think about and approach science. He is a master of asking the right questions, and his love for microbiology inspired me to seek answers. I always left our meetings feeling more confident and re-energised about my research, even in the darkest of times. I sincerely thank them both for their mentorship and invaluable help over the last four years.

I was also lucky to have a supportive and engaged Thesis Advisory Panel. I thank Neil Bruce and Peter Young for their encouragement and insight, and for occasionally asking hard questions. I also extend my thanks to Peter Metcalf, my industrial supervisor and representative on behalf of Wilson Bio-Chemical, for providing insight into the industrial aspects of MSW management and of course for preparing the first batch of OMSW fibre for my project. Additionally, I thank the individuals who kindly donated strains to this project, including Professor Anthony J. Sinsky (Massachusetts Institute for Technology, USA) for *Rhodococcus opacus* MITXM-61, Professor Neil Bruce (University of York, UK) for *Pseudomonas putida* NCIMB8249, Professor Nigel Minton (University of Nottingham, UK) for *Geobacillus thermoglucosidasius* DSM2542, and Dr Daniel Jeffares (University of York, UK) for *Schizosaccharomyces pombe* JB953.

To all the kind, generous and helpful individuals in the McQueen-Mason and Thomas labs – thank you for sharing your wisdom and expertise, for chatting, supporting, consoling and frequently baking. For their advice and help with my experiments I particularly thank Leonardo Gomez, Alexandra Lanot, Rachael Hallam, Reyme Herman, Ivan Gyulev, Emmanuelle Severi, Giovanna Pesante and Federico Sabbadin. Michelle Rudden

and Sophie Rugg also deserve a big thank you for sparing an afternoon to help me dewater 6 Kg of OMSW fibre - I hope the beer was sufficient recompense.

It is also of utmost importance that I acknowledge James Robson, who helped me conduct my maverick anaerobic digestion experiments and laughed an appropriate amount when I stabbed myself with a sludge contaminated needle (twice). He started out as a strange smelly sludge lizard and turned into an irreplaceable friend. I thank him for being the only person interested in my rock collection, for joining me on mushroom hunts, having lunch with me almost every day and for always being up for Star Trek, Asian food and of course, beer.

The last four years would have been very difficult to survive without all my fellow PhD student friends – we did an excellent job distracting one another and commiserating over our plight, and we will do an even better job celebrating once this is all over. There are a few humans that I have grown particularly fond of who deserve acknowledgement: Caroline Pearson (for being my designated extrovert, and the first person on Earth to call me their coolest friend), John Armstrong (for always being available to chill out, and for trying ever so patiently to teach me to sing in harmony and play my banjo in time), David Kuntin (for turning me into a snobby coffee-obsessed hipster, and introducing me to much good music) and Jack Munns (for his unexpected humour, and for loving my snakes almost as much as I do).

There are also many to thank who have been with me long before I started this PhD, but without whom I would have never made it this far. First, to my father, who was a true naturalist in the traditional sense. He knew the names of all things and instilled in me a lifelong love for biology. To my mother, who gave everything so that I could fulfil my dream of going to university and fixing all the world's problems, and whose wisdom and guidance always help me stay grounded and true to myself. And of course, to Nick, who followed me around the world so that I could become a scientist. Ten years ago, when I was filled with uncertainty, he convinced me that I was clever enough to study biology - it took him another nine years to convince me to marry him. Without Nick I would be but a shadow of my true self, and for his existence I am forever indebted to the universe.

To my brother Gonzo, who looked at a shelf of LB medium and asked if biologists are too busy to use the toilet. Thank you for helping me be a little less serious about life. I must also thank my uncle Robert, who truly understood the challenges that faced me at university and who, together with my aunt Julia, have supported me over many long years. To my Oma Brigitte, who sent me my first microscope when I was 11 and carried on where my father left off by sending me many inspiring books. And with all my heart I thank my Oma Karin and Opa Charly, who love me no matter what happens, and whose home is always a comforting refuge.

A penultimate thanks goes out to the 40-odd jars of pickled gherkins that bravely met their end over the course of writing this thesis - I salute you and your delightful sour crunchiness. May you rest in peace.

Finally, I humbly thank my microorganisms for deigning to grow,
most of the time.

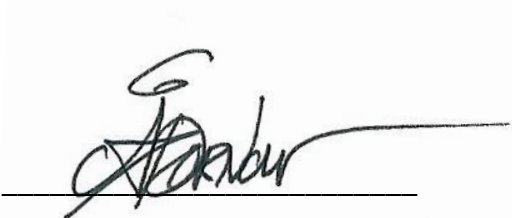
Authors Declaration

I declare that this thesis is a presentation of original work and I am the sole author. This work has not previously been presented for an award at this, or any other, University. All sources are acknowledged as references.

The data presented in Chapter 3, sections 3.3.2.1 and 3.3.2.2 was carried out in collaboration with James F. Robson of the Department of Biology at the University of York. James provided guidance on the experimental design of anaerobic digestion trials and subsequently carried out sequencing and bioinformatics analysis of microbial communities in sludge samples from these experiments. These data are presented in Chapter 3, Figure 3.13 and Figure 3.14, and in Appendix III & IV.

Material from this thesis is currently under review with the following citation:

Dornau A., Robson, J.F., Thomas G.H. and McQueen-Mason S.J. (2018). *Robust microorganisms for biofuel and chemical production from municipal solid waste*. Manuscript submitted for publication.



Aritha Dornau

Chapter 1: General Introduction

1.1 Anthropogenic Climate Change: A Brief History

Humans have been converting raw organic materials into useful and more valuable products for thousands of years – wine, beer, vegetable oil, textiles and paper are all traditionally made by refining biomass through stages of pre-treatment, processing, separation and/or conversion. Until approximately 200 years ago, renewable sources of energy were used to power these processes where necessary, including wood burning and wind or water-driven mills (Edinger & Kaul, 2000). Technological innovations during the industrial revolution enabled the manufacture of desirable products in a mechanised way on a larger scale than ever before. Consequently, craft and manual labour was rapidly replaced by automated, power driven machines fuelled with fossil fuels, including coal, petroleum and natural gas. As the human population grew and socioeconomic structures shifted, the demand for products escalated and these industries expanded and diversified (Pandey et al, 2015). Simultaneously, reliance upon fossil fuels became consolidated into the foundation of our industries, economies and societies (Mitchell, 2009).

Today fossil fuels supply 80% of the world's energy (IEA, 2016). Globally 84 million barrels of oil are used per day, with the majority supplying the transport sector. Byproducts of fossil fuel refining such as naphtha are also used to produce chemicals and plastics (Cherubini, 2010). Many projections suggest that fossil fuel reserves will be depleted by the end of the century (Abas et al, 2015; Aleklett & Campbell, 2003; Höök & Tang, 2013). This inevitability greatly threatens global socioeconomic and political stability as the world is now almost exclusively reliant upon energy and products derived from fossil fuels (Mitchell, 2009). A secondary but pivotal consequence of our fossil fuel dependence is the major effect it is having on global climate. Fossil fuels are formed over millions of years from degrading organic material and when they are excavated and combusted the carbon is released back into the atmosphere, primarily as CO₂ and CH₄. We have been liberating this carbon within a miniscule fraction of the time that was necessary to sequester it, thereby disrupting the global carbon cycle (**Figure 1.1**) and enhancing the greenhouse effect (**Figure 1.2**) (Cassia et al, 2018; Cavicchioli et al, 2019).

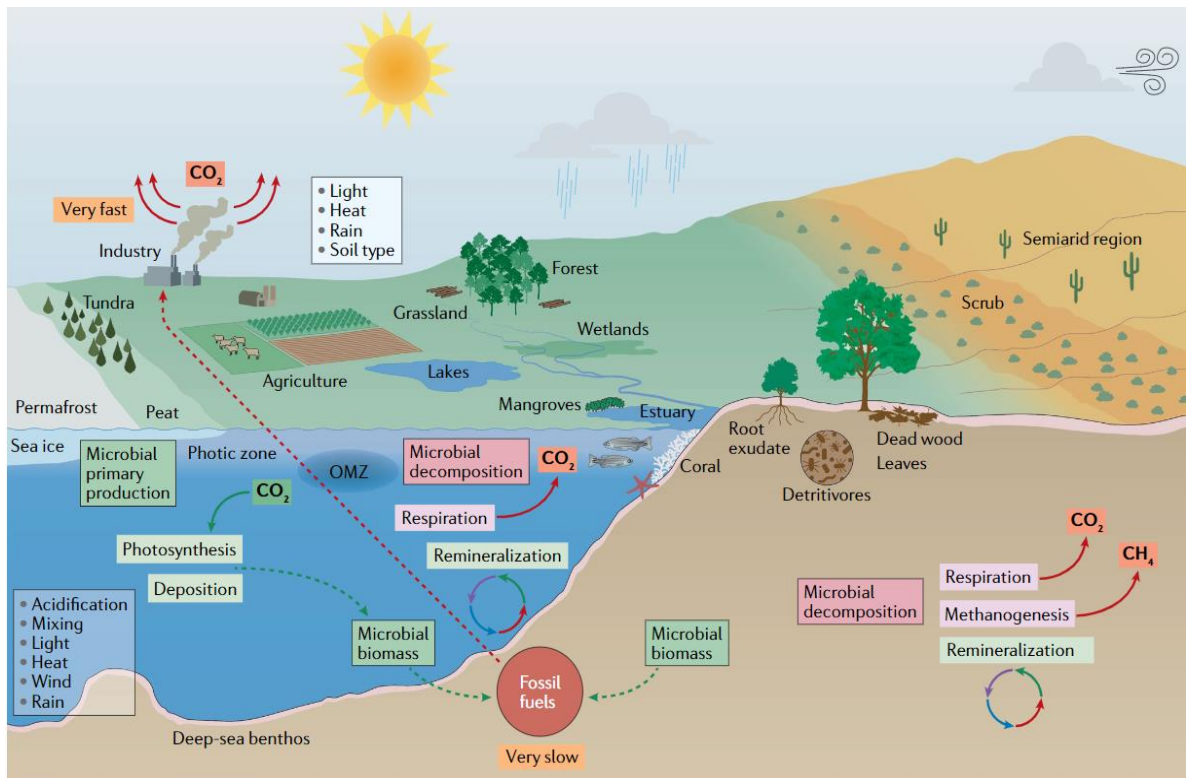


Figure 1.1: Overview of the carbon cycle, including natural and anthropogenic carbon sources and sinks (Figure taken from Cavicchioli et al, (2019))

Boxes shown in red, orange and pink are major sources of carbon emissions.

Boxes in green are major carbon sinks.

The **carbon cycle** involves the balanced interconversion of carbon compounds in the environment. Carbon is sequestered in carbon sinks such as forests, peatlands, wetlands, permafrost and oceans. Carbon is also incorporated into living things. To balance this cycle, carbon is naturally released, primarily through microbial decomposition of living things and respiration. When plants, animals and microorganisms die and become buried under anoxic conditions, their carbon-based organic matter is converted to **fossil fuels** over millions of years. Fossil fuels represent an important global carbon sink. Extracting and burning fossil fuels to power industry, agriculture and human activities rapidly releases fixed carbon sources into the atmosphere, thereby disrupting the balance of the carbon cycle. Other human activities also contribute to the disruption of natural carbon sinks, for example by deforestation and destruction of wetlands.

Since the industrial revolution began, emissions from burning fossil fuels in concomitance with intensified agriculture and deforestation have significantly increased the concentration of greenhouse gasses in the atmosphere - CO₂ levels have risen by 40%, CH₄ by ~150% and NO₂ by ~20%. All in all this has led to a global atmospheric temperature rise of 0.8°C above pre-industrial levels which has already triggered accelerated changes in global weather and climate. The most noticeable consequences thus far include a

significant reduction in arctic sea ice, a rise in sea levels and elevated ocean temperatures (Pethica & Ostriker, 2014) as well as wide-ranging negative impacts on biodiversity and ecosystem function (Abrahms et al, 2017). In fact, it is projected that over a third of species will be on an irreversible trajectory toward extinction by 2050, predominantly as a consequence of anthropogenic climate change (Thomas et al, 2004).

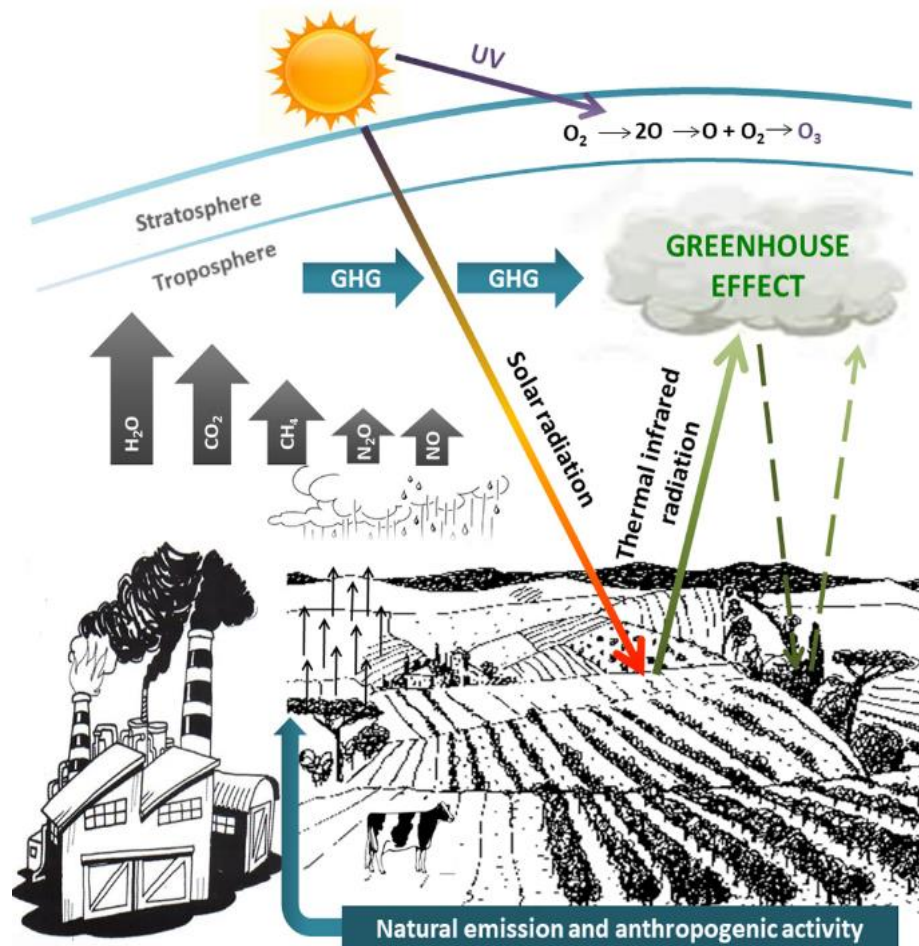


Figure 1.2: Overview of the greenhouse effect (Figure adapted from Cassia et al, (2018))

The **greenhouse effect** is a natural phenomenon by which solar radiation is trapped within the Earth's troposphere (lower atmosphere). When solar radiation hits the planet's surface it is reflected back into the atmosphere as thermal infrared radiation. This radiation is absorbed and subsequently emitted by **greenhouse gasses** (GHGs), including water vapour, ozone (O_3), CO_2 , CH_4 , N_2O and NO . The greenhouse effect is critical for keeping the Earth

It has been estimated that the Earth will continue to warm at a rate of 0.3 - 0.7°C every 30 years unless greenhouse gas emissions are curbed substantially (Folland et al, 2018). The consequences of a much warmer planet are unpredictable, but there is general consensus that a global temperature increase of >1.5°C above pre-industrial levels will pose a dangerous threat to humanity, while uncontrolled warming is likely to have far reaching, catastrophic effects for all life on Earth (Xu & Ramanathan, 2017). The Paris Agreement, put forward in 2015 by the United Nations Framework Convention on Climate Change, has been ratified by 183 nations and the EU. These nations have committed to reducing net GHG emissions to zero by the year 2300 and taking immediate actions to ensure greenhouse gas emissions do not exceed 2.7°C above the pre-industrial baseline by 2050 (UNFCCC, 2015). Although these commitments are encouraging, meeting these goals will require an unprecedented degree of societal, industrial and political transformation as well as technological innovation (de Coninck et al, 2018; Xu & Ramanathan, 2017).

1.2 Biorefining

Developing renewable alternatives to fossil fuels is crucial if we are to mitigate the impacts of anthropogenic climate change. While carbon-neutral, renewable energy sources such as wind, solar and hydroelectric power are increasingly being adopted to meet domestic energy needs (de Coninck et al, 2018), the demand for sustainable liquid transport fuels and renewable raw materials for industrial manufacturing remains largely unmet (Berntsson et al, 2014). Efforts in this area have led to the conception of biorefining, comprehensively defined as *“the sustainable processing of biomass into a spectrum of marketable biobased products (food, feed, chemicals and materials) and bioenergy (biofuels, power and/or heat)”* (IEA, 2008). Unlike fossil fuel refineries, biorefineries run on renewable sources of biomass (feedstocks) that are replenishable over the course of a human lifetime, thereby ensuring that any carbon released into the atmosphere can be sequestered back into raw materials at a comparable rate (Kircher, 2015). Biorefineries also aim to integrate the recovery, valorisation and recycling of waste streams into their process flow, thereby ensuring more sustainable, circular manufacturing processes in which materials and energy are not wasted (Cherubini, 2010).

A basic biorefining process (**Figure 1.3**) involves taking a renewable source of biomass and subjecting it to successive stages of physical and/or chemical processing, followed by conversion of these pre-processed components into products such as fuels, chemicals or materials by fermentation with specialised microorganisms (Yamakawa et al, 2018). Biotechnology, the technological application of biological systems, living things or their derivatives for industry, is central to achieving sustainable biorefining. Compared to traditional chemical manufacturing, bio-based processes can operate at lower temperatures, produce fewer byproducts and toxic wastes, are highly selective and can even be re-usable and self-replicating (Gavrilescu & Chisti, 2005). Furthermore, through modern genetic engineering techniques, bioprocesses can be designed that produce novel products or products that are challenging to synthesise by chemical processes (Lee & Kim, 2015). Biorefinery processes can potentially be made even more sustainable through heat integration and energy generation from waste streams. For example, waste residues from fermentation and product purification can be incinerated or, along with waste water, converted to biogas (Pandey et al, 2015). Heat recaptured from fermentation processes can also be harnessed. Furthermore, any excess heat and energy produced in this way can be sold back to the national grid (IEA, 2018).

The advent of biorefining has impelled initiatives to replace the linear economic model that has been central to industrialisation (in short, take-make-dispose) with a circular economic model. In a circular economy waste is a resource, to be recycled through closed materials loops or revalorised in further manufacturing processes and industrial symbioses (Venkata et al, 2016). Biorenergy Task 42, of which the United Kingdom is one of eleven members, was set up in 2007 by the International Energy Agency (IEA) to promote the global bioeconomy by developing and implementing highly efficient biorefineries with zero-waste value chains (IEA, 2016). However, in order to achieve fully sustainable, circular systems across all industries and to meet the energy demands of the future, we must not only improve the sustainability of well-established biorefinery value chains but also identify new feedstocks and develop methods for their valorisation.

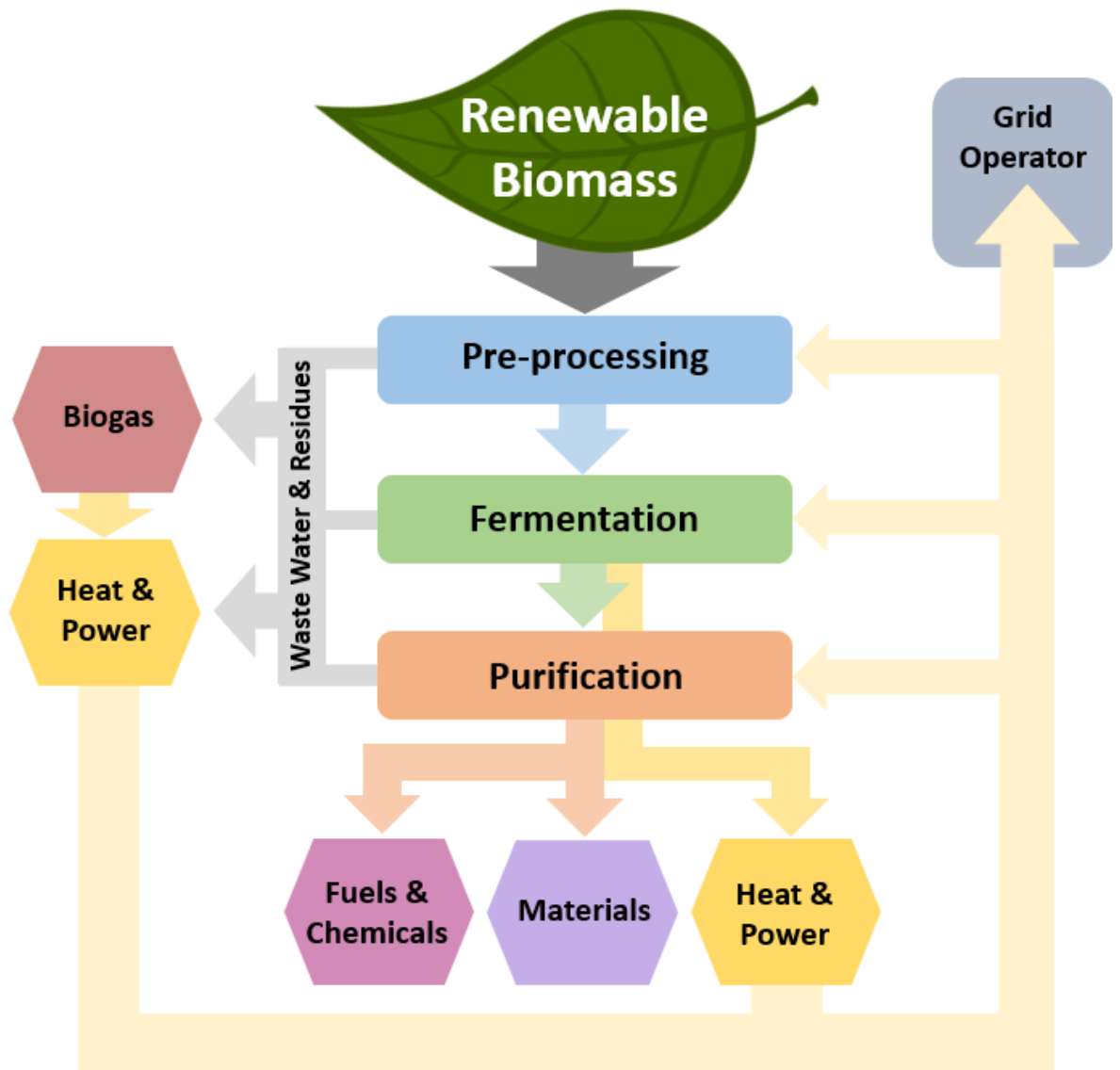


Figure 1.3: General overview of an integrated biorefining process chain
(Figure by author)

1.2.1 Renewable Feedstocks

Renewable sources of biomass are vital for sustainable bio-manufacturing. Lignocellulose, the major component of the inedible parts of plants, is the most abundant source of renewable carbon on the planet and is widely considered the best feedstock for sustainable biorefining (Ghatak, 2011). Lignocellulose contains up to 75% polysaccharides in the form of cellulose and hemicellulose (**Figure 1.4**) which can be broken down into their constituent sugars and used as a carbon source for fermentation. Cellulose and hemicellulose typically make up between 25-55% and 23-40% of lignocellulose composition in higher plants, with the remaining 7-35% comprising lignin, an amorphous aromatic heteropolymer (Marriott et al, 2016).

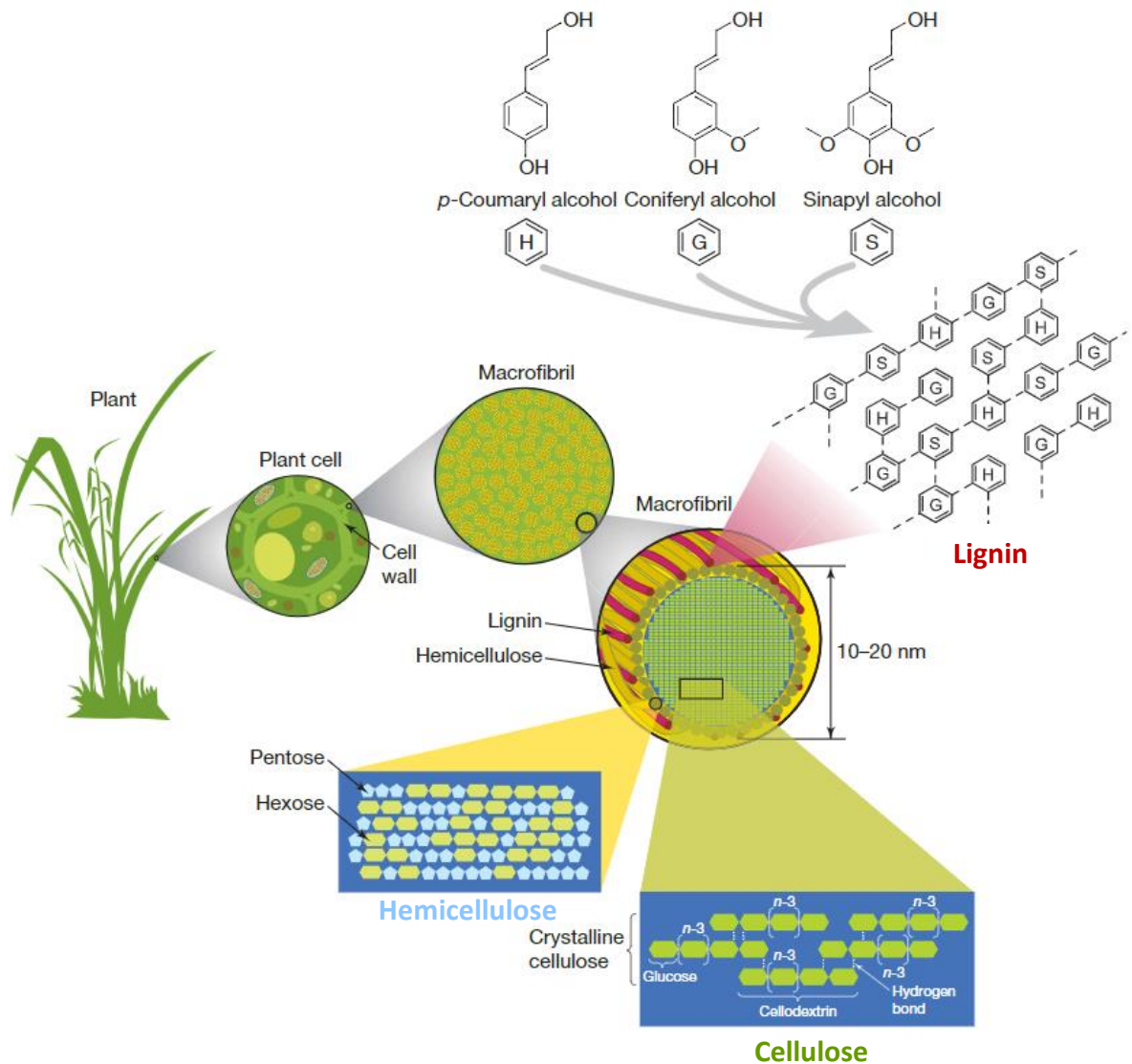


Figure 1.4: Structural configuration of lignocellulose within the plant cell wall
(Adapted from Rubin, 2008).

The non-edible, woody parts of plants and plant-derived materials such as paper are primarily composed of **lignocellulose**, the major structural component of plant secondary cell walls. Lignocellulose consists of up to 75% polysaccharides in the form of **cellulose** and **hemicellulose** (Marriot et al, 2006). **Cellulose** is composed of **D-glucose** molecules linked by β -1,4-glycosidic bonds and bundled into **crystalline microfibrils**. The microfibrils are linked together through hydrogen bonding with long-chain polysaccharides of **hemicellulose**, which contains backbones composed of a range of **hexose** sugars (*D*-glucose, *D*-mannose and *D*-galactose) and **pentose** sugars (*D*-xylose and *L*-arabinose) that are linked by β -1,4 and β -1,3-glycosidic bonds usually and also exhibit branching and substitution with oligosaccharides, sugar acids (glucuronic acid and galacturonic acid), acetic acid and phenolic acids. The polysaccharide network is embedded in a matrix of **lignin**, an amorously polymerised polyphenol composed of monolignol monomers **p-coumaryl (H)**, **coniferyl (G)** and **sinapyl (S)**. Lignin permeates the **macrofibril** structure and reinforces the cell wall, contributing significantly to its durability (Rubin, 2008).

A wide array of plant biomass sources are being investigated for their utility as feedstocks – these are primarily agricultural by-products such as wheat straw and corn stover which do not compete with food production, as well as forestry by-products such as woodchips and grasses like *Miscanthus spp.* that can be grown on marginal land (Saini et al, 2015). Biorefineries that run on these non-edible, lignocellulosic feedstocks are called ‘advanced’ or ‘second generation’ biorefineries. ‘First generation’ biorefineries use feedstocks that directly compete with food production, such as starch from grains (maize or wheat), sugar (beetroot and sugar cane) or oil crops (rapeseed and palm) and are considered unsustainable (Yamakawa et al, 2018).

First generation feedstocks are currently used at a commercial scale to produce bioethanol or biodiesel. About 150 billion litres of biofuels were produced globally in 2018, with the majority produced in the United States and Brazil from maize and sugar cane, respectively (IEA). Second generation biorefineries have been successfully demonstrated on a pilot-scale for the production of biofuels, bio-based chemicals and materials but on the whole commercial-scale facilities still face an array of bottlenecks (Mossberg et al, 2018). The scalability of second generation bioprocesses is greatly limited by lignocellulose recalcitrance (Marriott et al, 2016). Due to its complex macromolecular structure, the crystallinity of the cellulose and the highly inert, amorphous nature of the surrounding lignin matrix, lignocellulose is extremely difficult to break down. A great deal of research is therefore being done to find economical and efficient ways of pre-processing lignocellulosic biomass in order to achieve viable sugar yields for use in biorefining (Jönsson & Martin, 2016).

Apart from lignocellulose recalcitrance, other process inefficiencies that limit the commercial viability of lignocellulosic biorefineries include inhibitor formation and fermentation (Yamakawa et al, 2018), as well as overhead costs for enzymes (Klein-Marcuschamer et al, 2012), pre-treatments and purification. These will require further research to overcome (Marriott et al, 2016; Pandey et al, 2015). Furthermore, the volatility of oil prices greatly influences the commercial viability of bio-based products as they deter investment into biorefineries, infrastructure and vehicles that run on biofuels (Uría-Martínez et al, 2018). Despite these limitations, companies around the world have started ventures in second generation biorefining. For example Dupont, Beta Renewables, Raizen, Poet/DSM, Abengoa and GranBio have invested heavily in cellulosic ethanol and are well

positioned to overcome major technological and technical challenges that currently constrain profitable commercial production at industrial scales (Yamakawa et al, 2018).

1.2.2 Pre-treatment

In order to liberate sugars from lignocellulosic biomass it must be subjected to harsh physical and/or chemical pre-treatments that make the lignocellulose more amenable to enzymatic degradation. Pre-processing increases the accessibility of lignocellulose for enzymes by reducing cellulose crystallinity, depolymerising hemicellulose and/or degrading lignin (Modenbach & Nokes, 2012). The type of pre-treatment used depends greatly on the feedstock. In general, the biomass is first subjected to physical disruption, such as milling, followed by a chemical or physicochemical treatment (Modenbach & Nokes, 2012). Chemical pre-treatments can include application of acids, bases, hot water or steam, ionic liquids (IL) or organic solvents (termed organosolv). Physicochemical pre-treatments include ammonia fibre explosion (AFEX), where biomass is exposed to liquid anhydrous ammonia at high temperature and pressure, hydrothermal processes such as liquid hot water pre-treatment, in which biomass is brought to high pressure and temperature, and steam explosion, which involves sudden depressurisation of liquid hot water pre-treated biomass. Treatment with microwaves, ultrasound or supercritical CO₂ can also be applied (Alvira et al, 2010).

Pre-treatments are generally costly and involve harsh conditions that can lead to the degradation and transformation of a wide range of compounds (**Figure 1.5**). If present at high concentrations many of these compounds can be inhibitory to enzymes and microorganisms employed later in the process. The most common and toxic degradation products include furan aldehydes, particularly 5-hydroxymethylfurfural (5-HMF) and furfural, which are formed under high temperatures from the degradation of hexoses and pentoses, respectively. These compounds inhibit microbial growth and can cause DNA damage. Some microorganisms, such as *Saccharomyces cerevisiae* (Brewer's yeast) can convert furfural and 5-HMF to less reactive alcohol derivatives, but growth and fermentation cease until this conversion process is complete, thereby reducing overall bioprocess productivity (Almeida et al, 2008; Almeida et al, 2009).

Other inhibitors include aliphatic organic acids, which can form from hydrolysis of acetyl groups derived from hemicellulose. Formic acid and levulinic acid can also form when

furfural and 5-HMF are hydrochemically degraded under very harsh conditions or extended pre-treatments (Jönsson & Martin, 2016). Aliphatic acids disrupt the pH gradient across microbial membranes, thereby inhibiting or killing the microorganism. For fermentative species like *S. cerevisiae* these acids are generally inhibitory at concentrations above 100 mM, with a toxicity hierarchy of acetic acid < levulinic acid < formic acid (Jönsson et al, 2013). Lignin degradation can lead to the formation of a diverse array of aromatic and phenolic compounds. These vary greatly between feedstocks and are difficult to identify and quantify, although common marker compounds include vanillin and cinnamaldehyde. The mechanism of toxicity is poorly understood, but it is postulated that phenols interfere with cell membrane integrity. Different phenols have also been shown to have a variety of cellular targets and mechanisms of inhibition (Adeboye et al, 2014). At μM to mM concentrations phenolics can also inhibit hydrolysis by inducing precipitation in enzymes (Ximenes et al, 2010).

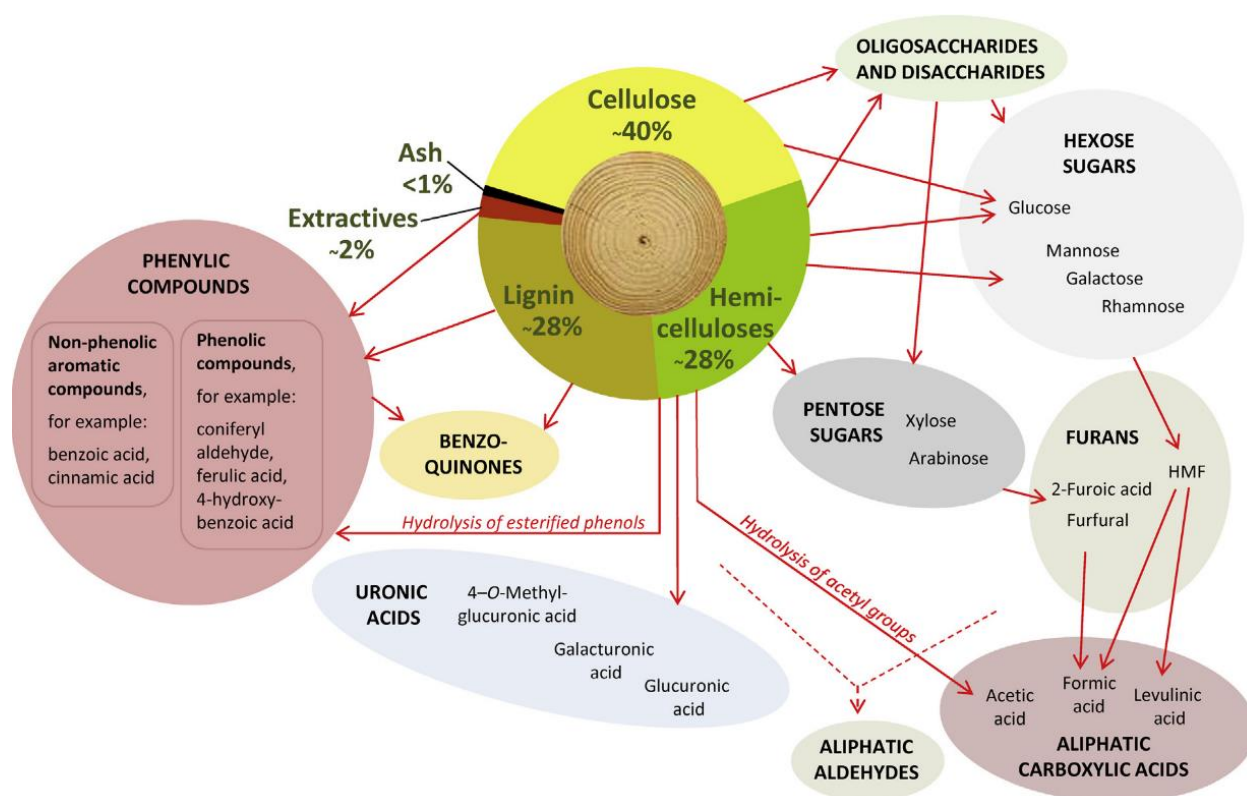


Figure 1.5: Common byproducts derived from lignocellulosic biomass during physicochemical pre-treatment
(Taken from Jönsson & Martin, 2016).

The types of inhibitors formed vary greatly between pre-treatments, with some methods producing fewer or lower concentrations of toxic compounds than others. Generally less harsh methods such as hydrothermal pre-treatments produce fewer inhibitors but are not effective for pre-treating all types of biomass. Approaches that are being taken to improve pre-treatment efficiency and reducing inhibitor formation include breeding and engineering less recalcitrant feedstocks, detoxifying feedstocks after pre-treatment using additives (reducing agents, alkali, polymers), extraction or enzymes, treatment with inhibitor degrading microorganisms (bioabatement), and also evolutionary or genetic engineering of fermentative microorganisms for superior inhibitor tolerance (Jönsson & Martin, 2016).

1.2.3 Enzymatic Hydrolysis

Pre-treatment is typically followed by hydrolysis, also termed saccharification, in which specialised enzymes, usually derived from fungi, are used to liberate sugars from the lignocellulose. To fully degrade cellulose and hemicellulose a wide range of enzymes (i.e. cellulases and hemicellulases) are required. Cellulose hydrolysis generally involves four major enzyme classes – lytic polysaccharide monooxygenases (LPMOs) which oxidise crystalline cellulose, introducing breaks into glucan chains and increasing accessibility for other cellulases; endoglucanases, which randomly hydrolyse internal covalent bonds between microfibrils, thereby creating free ends for other cellulases to act upon; exoglucanases (i.e. cellobiohydrolases) which produce free glucose and cellobiose molecules by cleaving glycosidic bonds from free reducing and non-reducing ends of cellulose chains; and β -glucosidases (i.e. cellobiases) which hydrolyse cellobiose and cellulooligosaccharides to liberate glucose molecules (**Figure 1.6**) (Andlar et al, 2018; Jorgensen et al, 2007; Van Dyk & Pletschke, 2012).

As described above (**Figure 1.4**), hemicellulose consists of a matrix of branched polysaccharides that are highly structurally and chemically diverse and closely associated with other cell wall components. A wide range of highly specific hemicellulolytic enzymes must therefore act synergistically to effectively hydrolyse all the distinct structural components of hemicellulose (Broeker et al, 2018; Van Dyk & Pletschke, 2012). Along with hemicellulases that degrade poly- and oligosaccharides, effective hemicellulose degradation requires the action of various esterases and furanosidases (Andlar et al, 2018).

Unlike cellulose and hemicellulose, lignin has a highly amorphous and non-repetitive structure, making it a difficult target for enzymes. However, to maximise polysaccharide accessibility, lignin must be degraded or modified. This can be achieved through the activity of free radicals, mediated by enzymes such as laccases and peroxidases (Have & Teunissen, 2001).

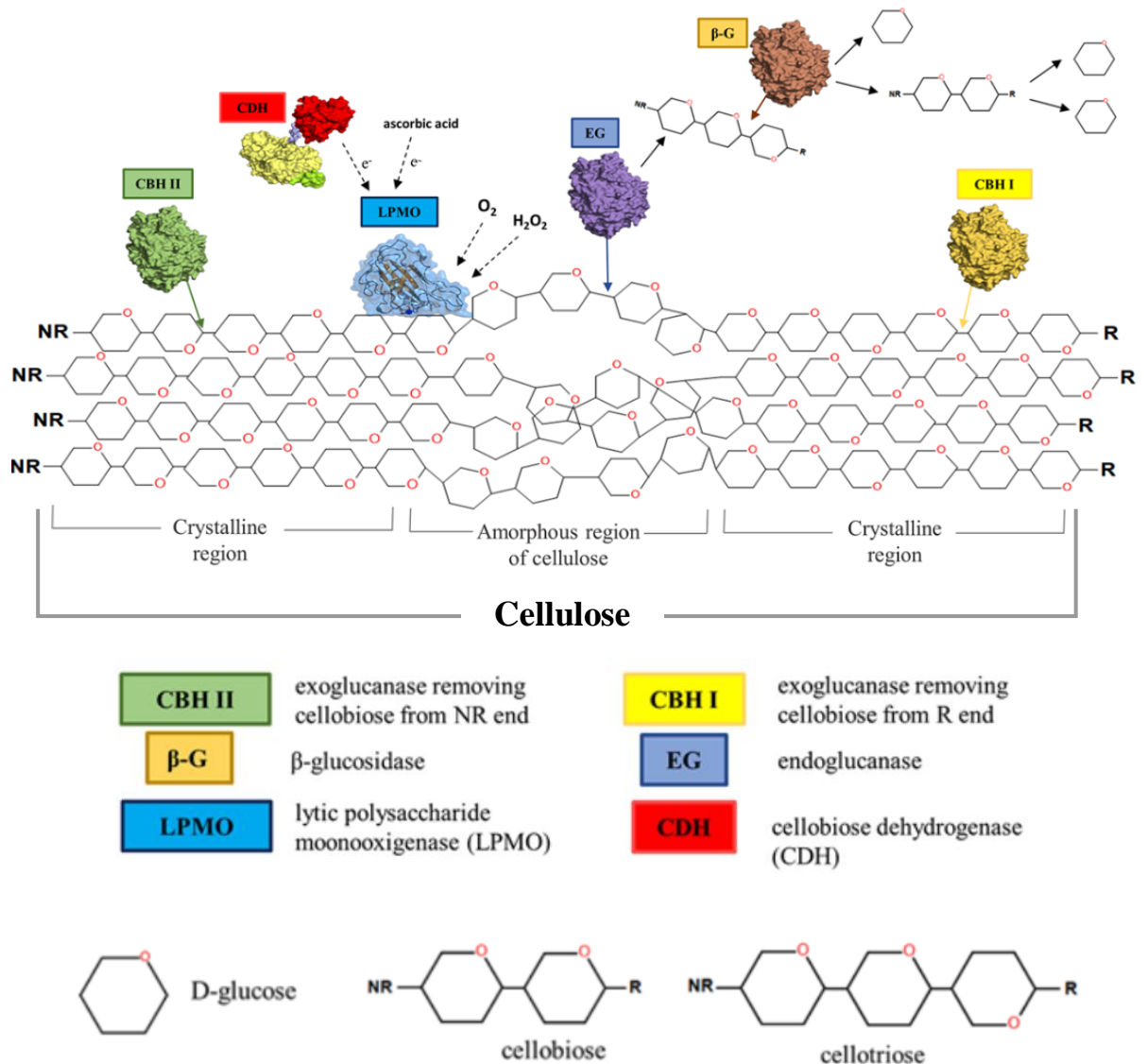


Figure 1.6: The enzymatic degradation of cellulose by endoglucanases, exoglucanases, β-glucosidases and LPMOs

(Adapted from Andlar et al, 2018).

NR = non-reducing end; R = reducing end;

Plant cell walls evolved to resist degradation, therefore these enzymes must all act synergistically to successfully break down the complex macromolecular structure of lignocellulose. Achieving effective hydrolysis on an industrial scale necessitates enzymes that have a high catalytic efficiency, thermal stability and are not prone to end-product inhibition. Specially formulated mixed enzyme cocktails have been developed specifically for biorefinery applications. These cocktails typically contain an assortment of cellulolytic and hemicellulolytic enzymes derived from crude cell lysate of filamentous fungi and can be attained in bulk quantities from specialist companies (Lopes et al, 2018). Enzymes have also been engineered to have superior properties that improve lignocellulose degradation, for example the cocktail Cellic[®] Ctec3 recently developed by Novozymes contains proprietary engineered enzymes with improved performance (Novozymes, 2019).

Enzyme efficiency is considered a major factor in facilitating viable industrial biorefining (Lopes et al, 2018). Large volumes of water are necessary to achieve efficient conversion to sugars as most pre-treatments and enzymatic processes rely on water to facilitate degradation (Zhao et al, 2012). However, to ensure that sugar levels in the final hydrolysate are concentrated enough for viable fermentation, biomass loadings must be as high as possible - ideally >15% w/v total solids (TS) (Modenbach & Nokes, 2012). This reduces the amount of available water and limits process efficiencies. Based on conversion yields and fermentation efficiencies reported in the scientific literature for ethanol production from corn stover, the cost contribution from enzymes would be \$1.47 per gallon. Assuming conversion at maximum theoretical yields, the cost of enzymes would contribute only \$0.68 to the price per gallon. Overall, the compounded cost of enzyme cocktails and inefficiencies of hydrolysis and other processing stages limit the potential for biorefineries to competitively produce bio-based products from lignocellulose (Klein-Marcuschamer et al, 2012).

1.2.4 Fermentation

The term fermentation has several meanings in different contexts. In the field of biochemistry fermentation refers specifically to metabolic processes in which an organic compound is broken down (catabolised) to generate energy under oxygen-free (anaerobic) conditions. Fermentation is believed to be an ancient method of energy production as it can occur without the tricarboxylic acid (TCA) cycle. Unlike other forms of metabolism, such

as aerobic or anaerobic respiration, fermentation produces the universal energy molecule adenosine triphosphate (ATP) through substrate-level phosphorylation without involving external electron acceptors, electron transport systems or membrane potential. At its most basic, fermentation can be described as the oxidation of a substrate to an oxidised intermediate, with some of the energy from oxidation contributing to the production of ATP (**Figure 1.7**). To restore the cellular redox balance, the oxidised intermediate is reduced to an end product, thereby regenerating nicotinamide adenine dinucleotide (NAD), the cofactor that was used in the initial oxidation (Todar, 2012).

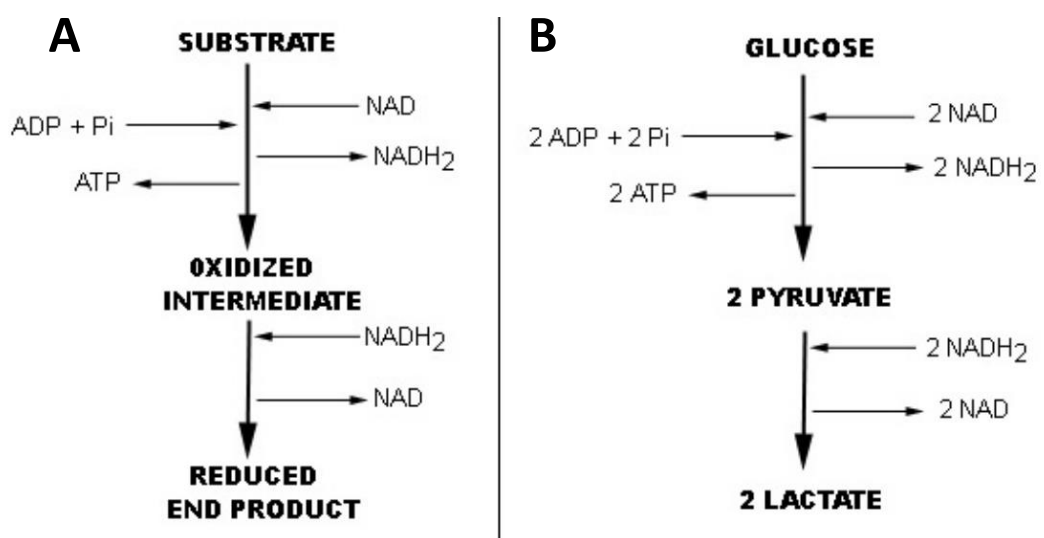


Figure 1.7: A model fermentation pathway

(Taken from Todar (2012))

- A. A basic fermentation involving the oxidation of a substrate by the oxidising agent nicotinamide adenine dinucleotide (NAD^+). Energy from this oxidation enables the generation of a molecule of adenosine triphosphate (ATP) from adenosine di-phosphate (ADP) and phosphate (P_i). To restore the cellular redox balance, the **oxidised intermediate** is reduced to an **end product**, thereby regenerating the oxidising agent NAD^+ from the reduced form, NADH_2 .
- B. A lactate fermentation, in which the substrate **D-glucose** is oxidised to two molecules of **pyruvate**, thereby generating two molecules of **ATP**. The two pyruvate molecules are then reduced to two molecules of the fermentation end product **lactate**.

In the context of industrial biotechnology, the definition of fermentation is broader, encompassing any microbial biomanufacturing process, independent of aerobicity (Salmond & Whittenbury, 1985). Modern industrial fermentation processes employ first generation feedstocks and are generally carried out in bioreactors via batch or fed-batch processes with a single species (monoculture) of bacteria or fungi that produce a product of commercial interest (Paulová & Brányik, 2013). A wide range of important and valuable commodity and specialty chemicals are produced by fermentation, such as antibiotics, bioethanol and citric acid (Salmond & Whittenbury, 1985). Other microbially derived products include enzymes, for example proteases used in laundry detergents, and biopharmaceuticals, such as human insulin, which is produced with a genetically engineered strain of the bacterium *Escherichia coli* (Jozala et al, 2016).

In biorefining, sugar-rich hydrolysates liberated from lignocellulosic biomass through saccharification can be used as carbon sources for microbial fermentations. Fermentations are generally carried out as an independent processing stage after hydrolysis, but fermentation and saccharification can also be combined in a process called simultaneous saccharification and fermentation (SSF). SSF enables sugars to be fermented as they are released by enzymes, relieving the product inhibition that limits enzyme efficiency. Furthermore, because SSF can be carried out in a single vessel the process uses less energy and saves processing time (Takkellapati et al, 2018). However, separate hydrolysis and fermentation (SHF) is more traditionally used as it allows for optimisation of each step independently to increase overall product yield. The method used is largely dependent upon the type of biomass and properties of the fermentative microorganism (Srivastava et al, 2015).

Along with the basic traits of a good industrial strain, such as rapid product synthesis and tolerance to the stressful conditions of an industrial bioreactor, a biorefining strain must also be able to grow efficiently and robustly on the lignocellulosic feedstock and utilise the full spectrum of available hexose and pentose sugars without suffering from product inhibition or inhibitor toxicity. In reality no strain naturally exhibits all the properties necessary for industrial production. Industrially viable strains are developed for a dedicated bioprocess by targeted selection and improvement through directed evolution and genetic engineering (Chen & Dou, 2015). Strains can be selected, evolved and engineered for a variety of desirable characteristics. For example, inhibitor and product

tolerance can be enhanced by improving stress response, increasing membrane integrity or raising efflux pump activity (Dunlop, 2011).

Productivity can also be increased by expanding the repertoire of sugars used by the microbe. Most microorganisms preferentially ferment D-glucose, but D-xylose, the second most common sugar in lignocellulosic hydrolysates, often cannot be fermented by industrially useful species. Species that do ferment D-xylose typically exhibit carbon catabolite repression (CCR), wherein one sugar (usually D-glucose) is used preferentially over other sugars, leading to sequential rather than simultaneous carbon source fermentation. Simultaneous mixed-sugar fermentation is crucial for an effective lignocellulosic bioprocess (Zhang et al, 2015). Introducing D-xylose fermentation is therefore a major engineering target and has been successfully achieved with numerous industrially useful microorganisms (Agrawal et al, 2010; Dien et al, 2003; Kim et al, 2013; Kurosawa et al, 2013; Lee et al, 2012; Smith et al, 2014).

The most well-established and robust species for industrial biorefining are the *S. cerevisiae* and *Zymomonas mobilis*. These two ethanol fermenting species (ethanologens) have been widely studied, adapted and engineered to produce bioethanol and other products. *S. cerevisiae* produces ethanol via the Embden-Meyerhof (EM) pathway (**Figure 1.8**), wherein D-glucose is sequentially oxidised to produce two molecules of pyruvic acid. Pyruvic acid is then reduced further to the end product ethanol and CO₂ (net reaction: Glucose + 2 ADP + 2 P_i → 2 Ethanol + 2 CO₂ + 2 ATP + 2 H₂O). The EM pathway is present in almost all living things and its end-product, pyruvic acid, is the precursor for the biosynthesis of many fermentation products, including alcohols, organic acids, fatty acids, and gasses (Todar, 2012).

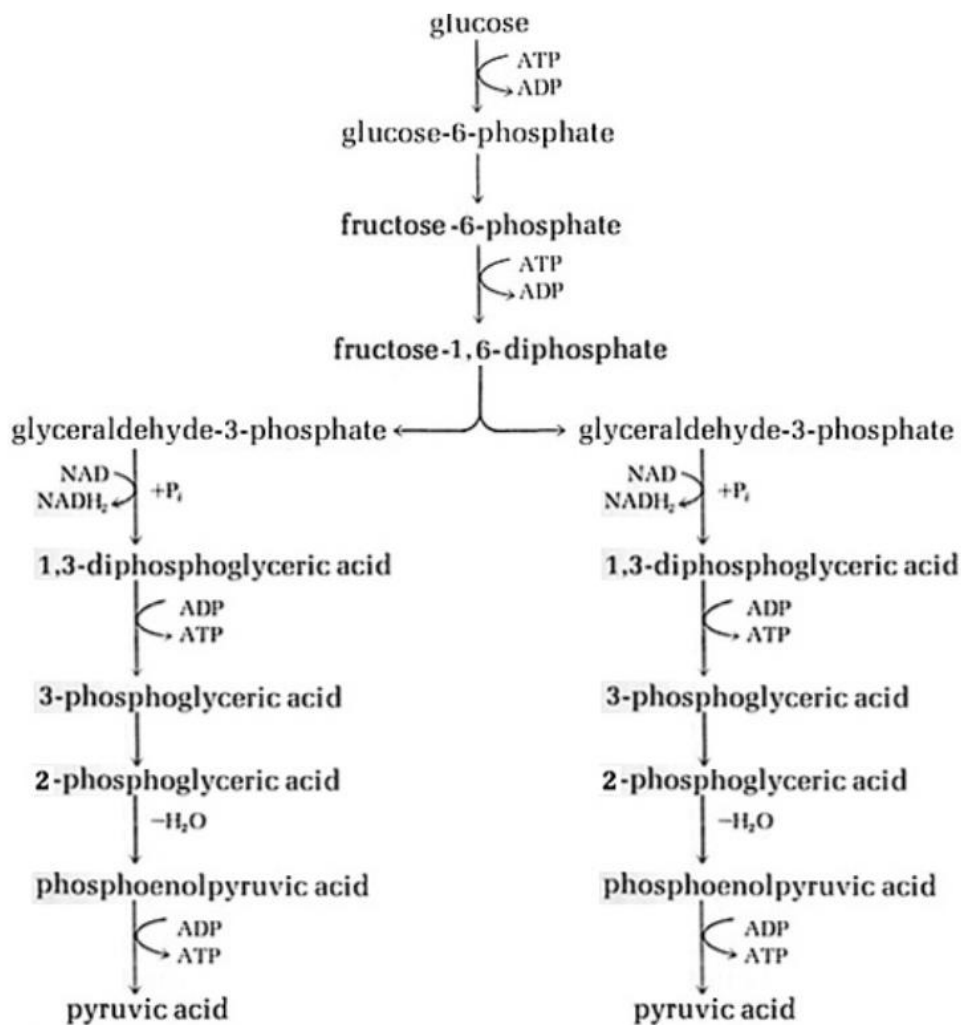


Figure 1.7: The Embden-Meyerhof Pathway

(Taken from Todar (2012)).

The Embden-Meyerhof (EM) pathway is the major pathway used for the dissimilation of *D*-glucose to pyruvic acid, a precursor that can be further converted to fermentation products such as alcohols, fatty acids, organic acids and gasses.

The bacterium *Z. mobilis* on the other hand produces ethanol via an alternative route called the Entner-Doudoroff (ED) pathway (**Figure 1.8**). Like the EM pathway, the ED pathway yields two pyruvate molecules, but via an asymmetrical sequence of oxidations that result in the production of only one molecule of glyceraldehyde-3-phosphate and the first pyruvic acid. Glyceraldehyde-3-phosphate is oxidised further via EM pathway reactions to form the second pyruvate. The two pyruvate molecules are then reduced to produce a net yield of two molecules of ethanol (Todar, 2012). Using the ED pathway for ethanol fermentation is unusual as this pathway is typically found in aerobic microorganisms.

However, by adapting the pathway for anaerobic fermentation *Z. mobilis* is able to produce ethanol with exceptional efficiency (Bucholz et al, 1987).

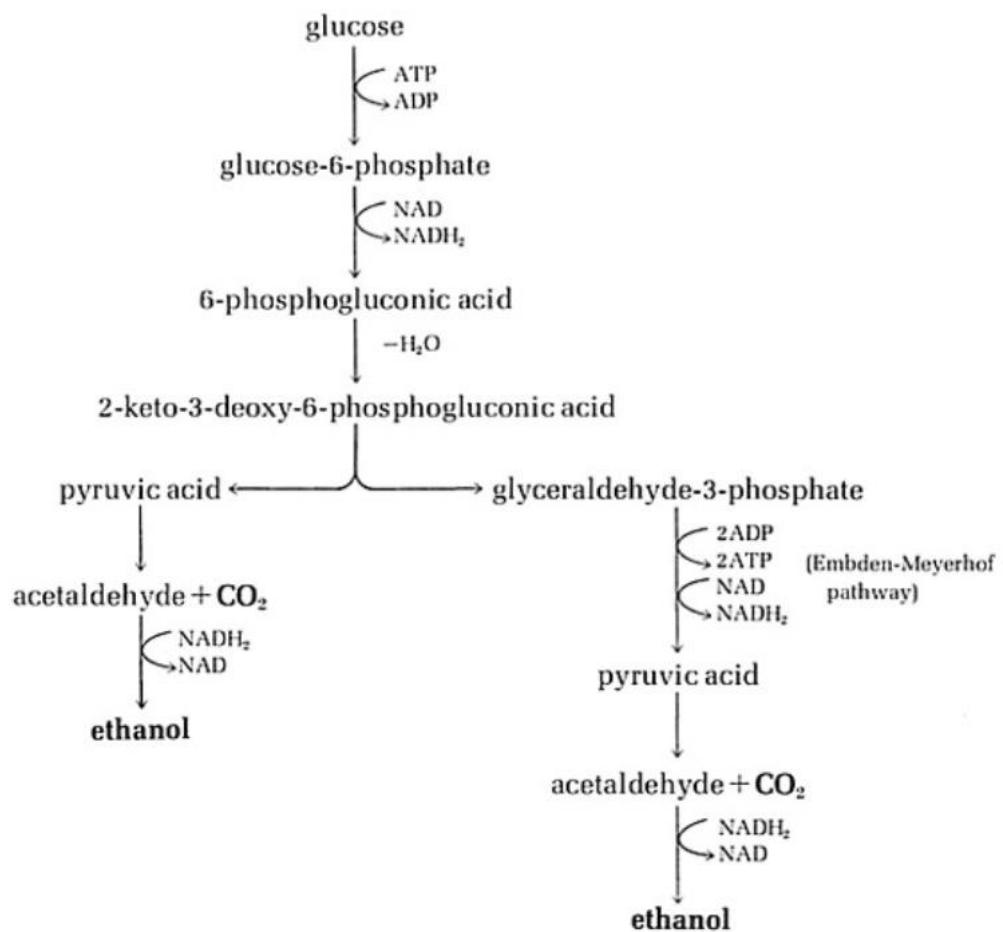


Figure 1.8: The Entner-Doudoroff Pathway

(Taken from Todar (2012)).

The Entner-Doudoroff (ED) pathway used by Zymomonas mobilis for ethanol fermentation. Net reaction: $\text{Glucose} + \text{ADP} + \text{P}_i \rightarrow 2 \text{ Ethanol} + \text{CO}_2 + 1 \text{ ATP} + 2 \text{ H}_2\text{O}$

Another important product that can be produced from renewable biomass is biodiesel, which is produced by oil-producing (oleaginous) microorganisms such as microalgae, some bacteria, yeasts and fungi (Meng et al, 2009). Microbial oils are stored intracellularly in the form of triacylglycerol (TAG) (**Figure 1.9-A**). TAG can be extracted from cell biomass and chemically transformed into biodiesel by transesterification (**Figure 1.9-B**) (Alvarez & Steinbüchel, 2002).

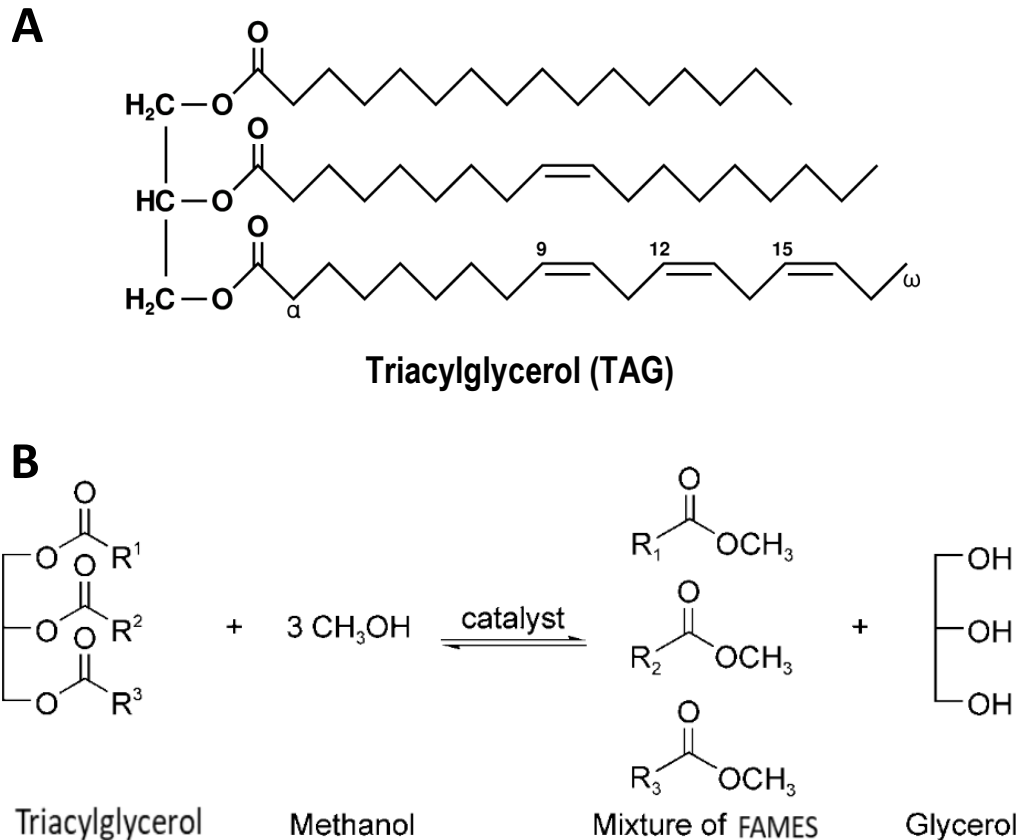


Figure 1.9: Triacylglycerol structure and mechanism of transesterification to Biodiesel
(Figure by author, with A. taken from Wikimedia commons (public domain) and B. adapted from Lestari et al, (2009)).

A: Structure of a **triacylglycerol (TAG)** molecule. TAG is made up of a glycerol molecule with three fatty acid (FA) chains attached. The FAs can be of varying length and functionality, but typically range between 14-20 carbons in nature.

FAs are named based on the number of carbon atoms and degree of saturation. Carbons are numbered from the first carbon of the carboxyl group (preceding the α -carbon) to indicate regions of unsaturation (double-bonds). The final carbon is always designated as the ω (omega) carbon. For example, the fatty acids in the TAG molecule shown above are (top to bottom): C:16:0 (Palmitic acid); C18:1(9) (Oleic acid); and C18:3(9,12,15) (α -linolenic acid).

B: Transesterification of **triacylglycerol (TAG)** in the presence of methanol to produce fatty acid methyl esters (**FAMES**) which can be used as **biodiesel**, and **glycerol**. R^n = various FAs

TAG is produced by similar pathways in both eukaryotes and prokaryotes but is rarer in bacteria – so far only heterotrophic aerobes (primarily in the order Actinomycetales) and cyanobacteria have been shown to synthesise TAG (Alvarez & Steinbüchel, 2002). TAG metabolism involves a series of complex anabolic and catabolic

pathways that occur under aerobic conditions (**Figure 1.10** and **Appendix IX**). Cells produce TAG as a means of storing carbon under conditions of nutrient limitation. TAG has a higher calorific value than proteins or carbohydrates, meaning it yields more energy when oxidised, enabling cells to live off their stores until environmental nutrients become available once more (Amara et al, 2016).

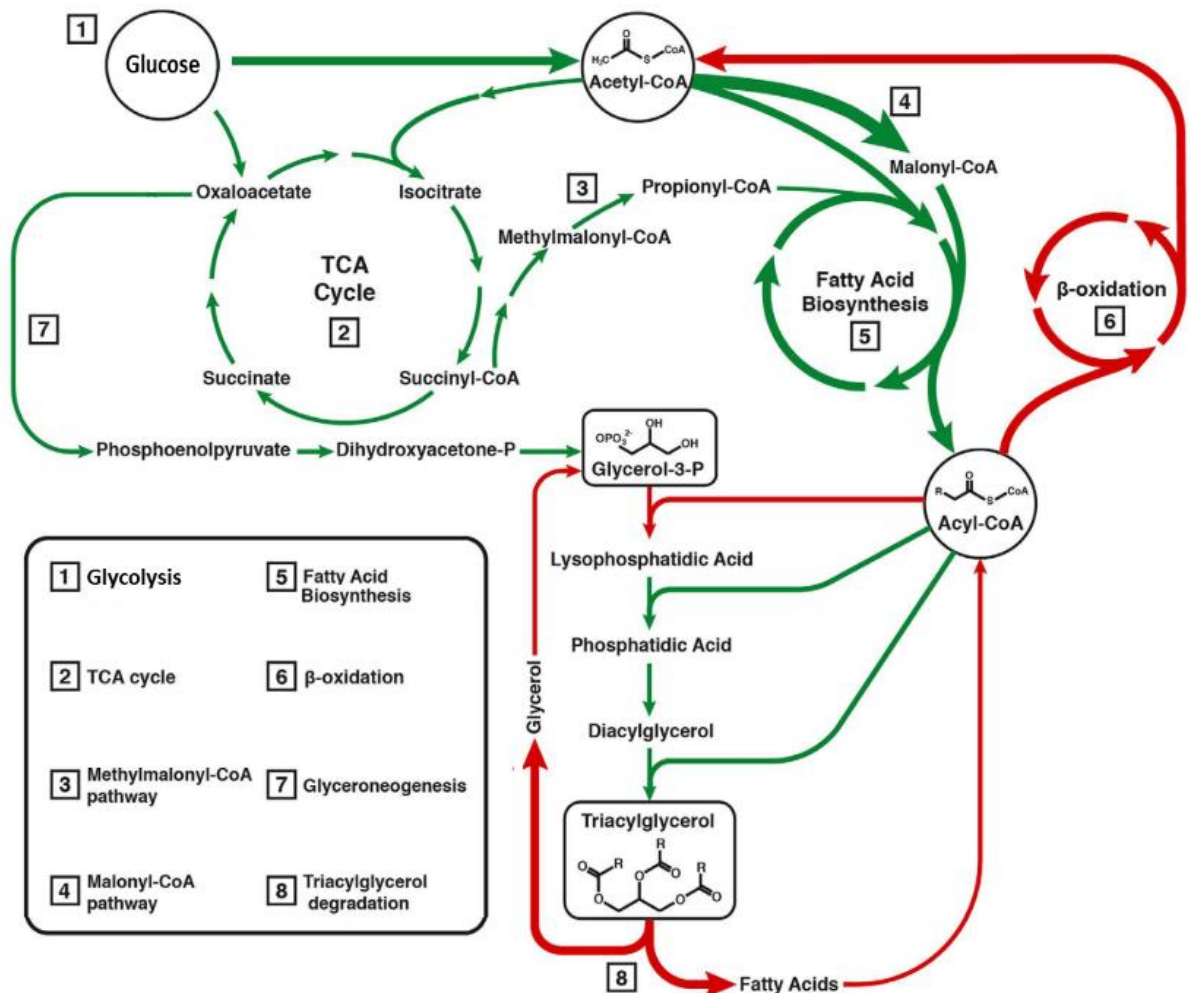


Figure 1.10: Triacylglycerol Metabolism

(Adapted from Amara et al, (2016)).

*Biosyntheses reactions are shown in green. Biodegradation reactions are shown in red. Metabolism is shown for D-glucose but can be substituted with any carbon source that the oleaginous organism can catabolise to the key precursors **acetyl-CoA**, **propionyl-CoA**, **malonyl-CoA** and **glycerol-3-Phosphate**.*

TAG can be synthesised from any carbon source that can be broken down by the microorganism to the key precursors acetyl-CoA, propionyl-CoA, malonyl-CoA and glycerol-3-phosphate. These precursors are sequentially condensed by dedicated fatty acid

synthases to varying carbon chain lengths and bond-saturation (**Figure 1.10-5**). At the same time, diacylglycerol is derived from glycerol-3-phosphate (**Figure 1.10-7**). To produce a molecule of TAG, diacylglycerol is condensed with three FA chains by diacylglycerol acyltransferase (DGAT). When the cell enters a state of starvation, TAG is broken down via a series of degradation pathways that involve splitting the TAG molecule into its constituent FAs and a glycerol (**Figure 1.10-8**). Glycerol is regenerated to glycerol-3-phosphate and the FAs are degraded via the β -oxidation pathway, thereby regenerating acetyl-CoA and cofactors which are fed back into the tricarboxylic acid (TCA) cycle and electron transport chain to produce energy (**Figure 1.10-6**) (Alvarez & Steinbüchel, 2002; Amara et al, 2016; Lestari et al, 2009).

TAG production is a slow process relative to secreted fermentation products such as ethanol due to the complexity of the physiology involved in transitioning between TAG synthesis and vegetative growth. TAG synthesis typically does not begin until late exponential phase when nutrients become limiting (Alvarez & Steinbüchel, 2002). It is therefore critical that the fermentation medium contains a balance of carbon and nitrogen that ensures optimal levels of biomass production before TAG synthesis begins. Cells must also be harvested at the point where TAG has reached peak concentrations to avoid cells catabolising their stores (Dong et al, 2016).

Another class of important bio-based products are platform chemicals, which are molecules that can be transformed into wide range of industrially valuable products via chemical conversion. An example is lactic acid (**Figure 1.11**). Lactic acid is produced at an annual rate of ~320,000 tonnes by industrial microbial fermentations and can be used as a building block to produce several useful chemicals. Lactic acid can be reduced and then dehydrated to produce propylene oxide, directly dehydrated to acrylic acid or hydrogenated to propanoic acid. Alternately it can be polymerised to polylactic acid, a biodegradable polymer with excellent properties for replacing plastics in packaging and textiles, or esterified to lactate esters, which are valuable solvents. Similarly, ethanol, although primarily used as a fuel, can be converted to acetaldehyde, acetic acid and other molecules used for polymer synthesis, including propylene, ethylene and butadiene (Takkellapati et al, 2018).

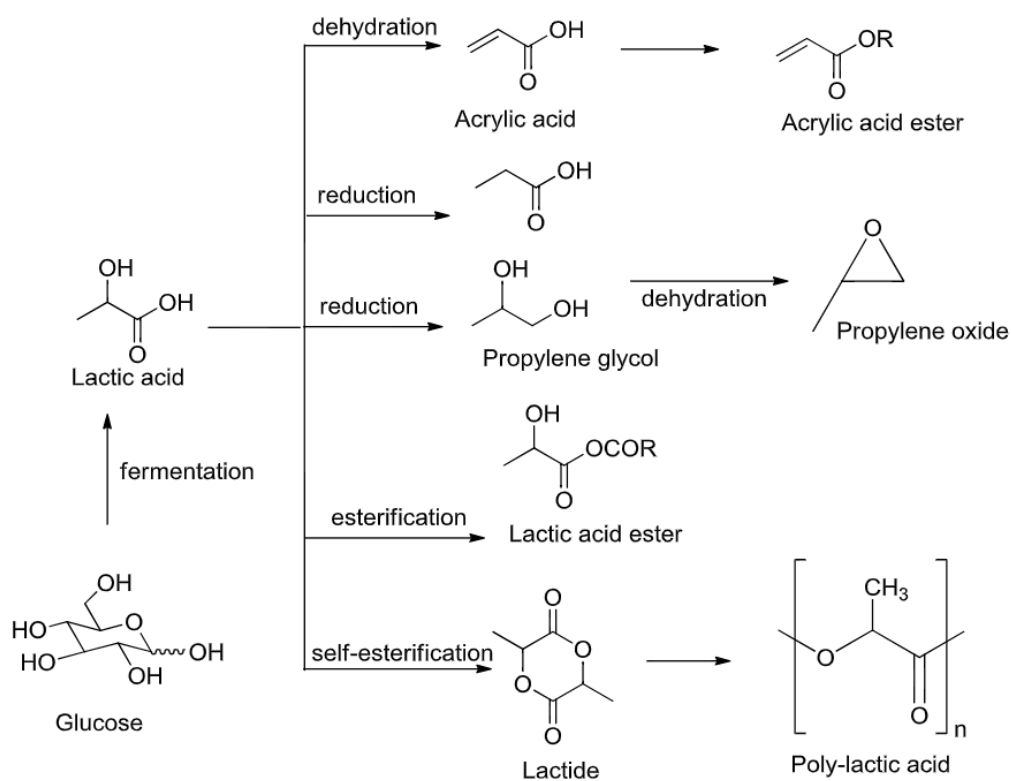


Figure 1.11: Value-added products synthesised from lactic acid

(Taken from Takkellapati et al, (2018)).

Other platform chemicals that can be produced biologically, are of industrial relevance and have been identified as being of high market attractiveness include 5-HMF, levulinic acid, methanol, 1,3-butanediol, 1,3-propanediol, 2,5-furandicarboxylic acid, 3-hydroxypropionic acid, acrylic acid, adipic acid, butadiene, D-mannitol, epichlorohydrin, L-lysine, levoglucosenone, glycerol, glucaric acid, fumaric acid, fatty alcohols, malic acid, methyl methacrylate, muconic acid, n-butanol, polyhydroxyalkanoates, propylene glycol, paraxylene, terpenoids, itaconic acid, succinic acid, furfural, xylitol, sorbitol and isoprene (LBNet, 2017).

Biorefining promises to transform the fuel and chemical sector and direct industry toward a more sustainable circular economic model. Although biorefining is a relatively recent development that still suffers from a range of technical challenges, many bio-based technologies and processes are coming of age. An increasing number of companies have begun to invest in the biorenewables sector and sales from bio-based products are growing at an annual rate of 8%. Overall the production of renewable bio-based chemicals is set to rise significantly in the coming decades, with predicted sales reaching between \$375 – 441 billion by 2020 (Takkellapati et al, 2018).

1.2.5 Other Outputs

Biorefineries are highly capital-intensive. Plants based around a single conversion technology are more sensitive to market volatility and have higher overheads, which raises product costs and lowers capacity for competing with petroleum-derived equivalents (Fernando et al, 2006). To develop a truly sustainable and circular biorefinery requires the integration and maximal valorisation of all waste streams resulting from a bioprocess, generally referred to as integrated biorefining (Cherubini et al, 2009). A biorefinery with several outputs can flexibly produce products to match market demands and supplement overhead costs by internally generating power. Major waste streams in biorefineries that can be used to produce energy and power include waste water from pre-treatment, lignin and other waste residues produced through hydrolysis, fermentation residues (spent cells and medium) as well as waste heat generated during fermentation or from cooling reactors after heat-based pre-treatments (Fernando et al, 2006).

A major avenue of investigation has been lignin valorisation. Lignin is the major residue left over after cellulose and hemicellulose have been saccharified and although it is a highly recalcitrant heteropolymer, a wide range of value-added products can be produced from it (**Figure 1.12**). The simplest method of valorising lignin is by producing syngas via gasification, however a variety of other pathways have also been demonstrated, such as conversion to hydrocarbons, oxidised products, phenols and macromolecules (IEA, 2013).

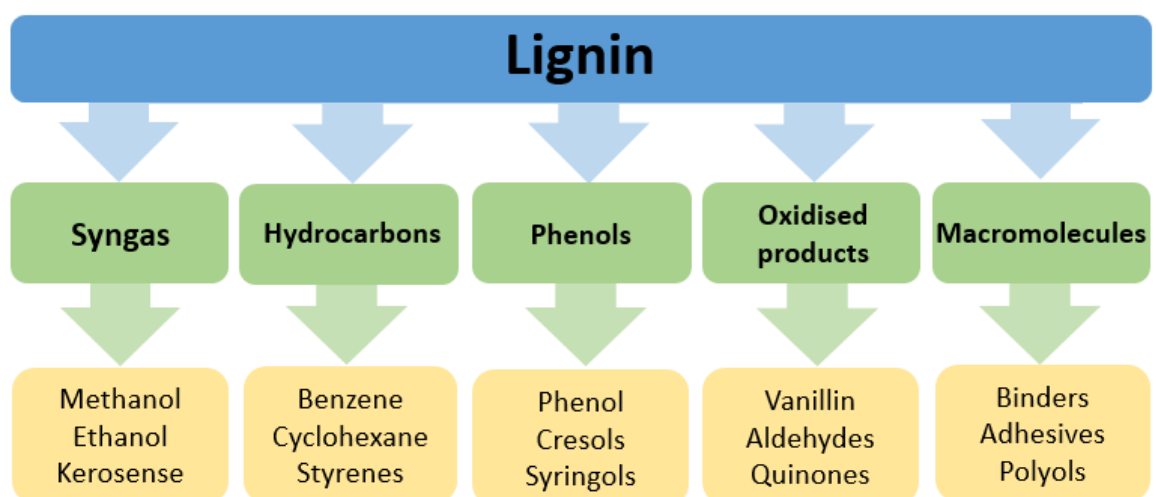


Figure 1.12: Value-added products synthesised from lignin
(Figure by author, based on IEA (2013))

Another major avenue for valorising biorefinery waste streams is anaerobic digestion (AD). AD is an established industrial process used around the world for treating waste water and solid waste. Although AD employs relatively simple technology, it is a highly multifunctional solution for treating a wide range of wastes, with over 30,000 industrial plants in operation worldwide, permanently producing 10,000 MW of power (Calusinska et al, 2018). Furthermore, AD outputs have numerous useful applications - biogas can be used for electricity, heat and fuel while the digestate, which contains spent cells and nutrient-rich organic matter, can be used as organic fertilizer (IEA, 2018). In a standard AD process (**Figure 1.13-A**) organic waste is fed to an anaerobic microbial community consisting of hundreds of diverse microorganisms that synergistically degrade biomass to biogas rich in methane (CH_4) (**Figure 1.13-B**).

Efficient methane production is largely dependent upon complex interactions between all species in the microbial community. The critical step of methane synthesis (methanogenesis) is carried out exclusively by archaea, but their productivity is dependent upon the availability of acetic acid, H_2 and CO_2 . These precursors can only be produced by other species specialised in carbon source degradation (hydrolysis), acidogenesis and acetogenesis, which generally belonging to the major phyla *Firmicutes*, *Bacteroidetes*, *Proteobacteria*, and *Chloroflexi* (Nelson et al, 2011). *Bacteroidetes* primarily carry out hydrolysis and fermentation of organic material to produce volatile fatty acids (VFAs), H_2 and CO_2 that can be utilised by other members of the community. *Proteobacteria* (particularly of the class *Deltaproteobacteria*) are vital due to their ability to degrade compounds like glucose, butyrate, propionate and acetate to H_2 and CO_2 . *Firmicutes* also play an important role as degraders of volatile fatty acids (VFAs) and producers of acetic acid used by archaea for methane production, whilst *Chloroflexi* are important for nutrient cycling as degraders of carbohydrates and cell material (Narihiro & Sekiguchi, 2007; Nelson et al, 2011).

Finally, the recapture of heat and integration of power is critical for biorefining as it provides an auxiliary source of energy to lower operational costs. Waste heat-to-power technologies are already implemented in other industries to collect and re-use heat lost during processing. Recovery is usually achieved with heat exchangers and heat recovery steam generators (Jouhara et al, 2018). In the context of a biorefinery, heat and CO_2 produced by fermenting microorganisms can be captured and used to power pre-

treatment and purification processes. Additional power can be generated by combusting waste residues (Nizami et al, 2017). Overall, valorising waste residues such as lignin, diverting waste water and residues to AD and recapturing heat for power recovery should be an integral part of any truly sustainable and circular biorefining platform (Cherubini et al, 2009).

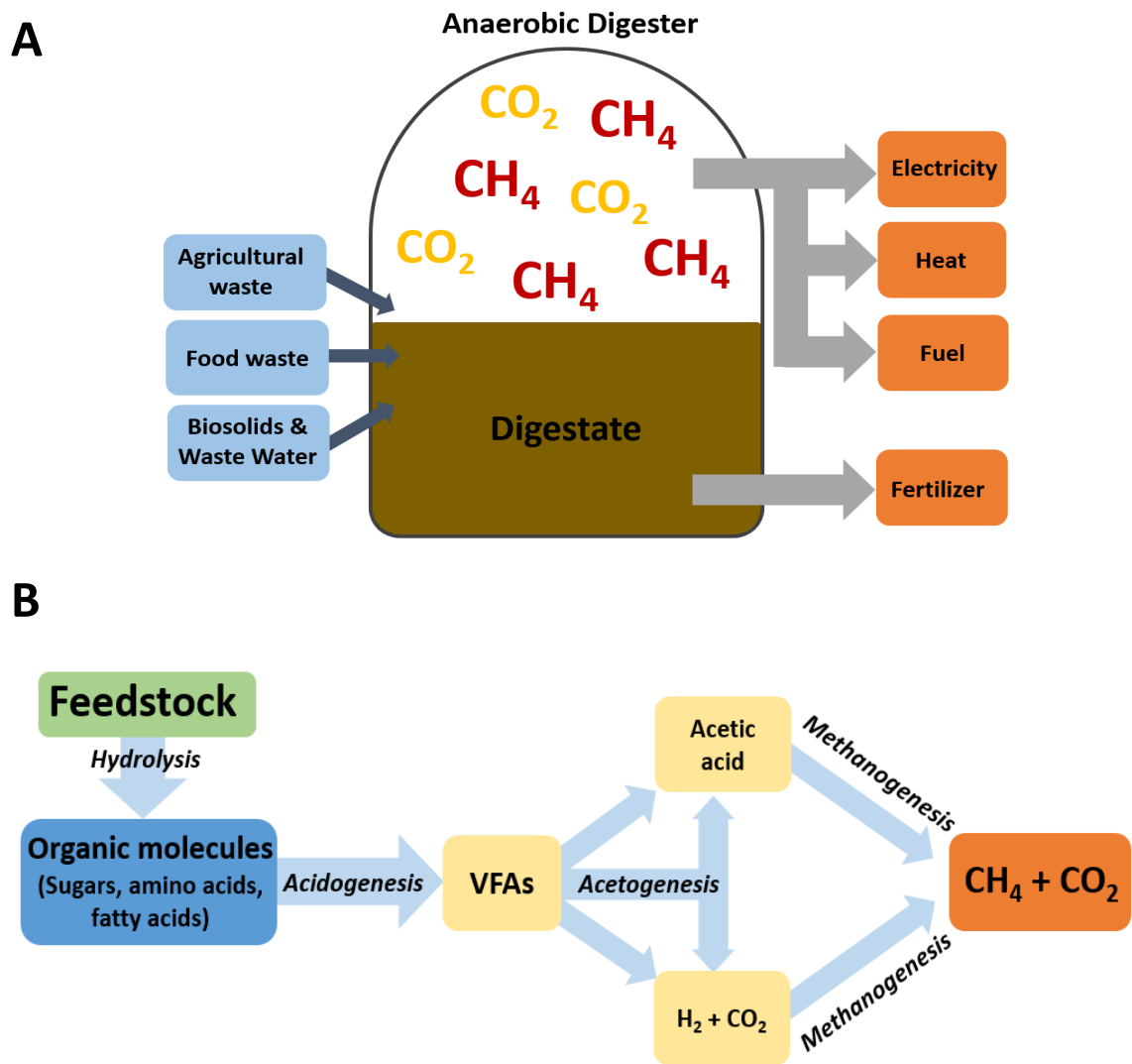


Figure 1.13: Overview of Anaerobic Digestion

(Figure by author, based on IEA (2018))

A: Anaerobic digestion plant inputs and outputs;

B: Biosynthetic pathways of biogas production. The major metabolic activities carried out by microbial communities inside an anaerobic digester include hydrolysis of the feedstock to organic molecules, which in turn are converted by acidogenesis to volatile fatty acids (VFAs). VFAs are converted by acetogenesis to acetic acid, H_2 and CO_2 , which are metabolised by methanogenic Archaea to CH_4 and CO_2 .

1.3 Municipal Solid Waste

The effective management of waste is a significant logistical and economic challenge that will become increasingly difficult to achieve as our planet becomes more urbanised and overpopulated. Municipal solid waste (MSW), which encompasses any non-industrial waste, including refuse from households, small businesses and public institutions, is of particular concern (DEFRA, 2015b). Just over 2 billion tonnes of MSW are currently generated by human beings yearly and volumes are projected to rise to 3.4 billion tonnes per year by 2050 (Kaza et al, 2018). This escalation is primarily attributed to increasing urbanisation and growing economic prosperity, particularly in lower and middle-income countries where waste generation is anticipated to increase 165-185%. Holistic and economical solutions are needed, not only to cope with the significant volumes of waste that will be generated, but also to mitigate the environmental burden of poor waste management and recover and recycle finite resources (Hoornweg, 2012).

1.3.1 Global Impact

The waste we generate has a considerable impact on the environment: the primary fate of MSW is to end up in landfills, where anoxic decomposition of the organic fraction leads to the release of methane, a potent greenhouse gas. Landfills are the third largest sources of anthropogenic methane emissions after animal husbandry and the energy sector, are projected to contribute substantially to the net global temperature rise over the next decade and will continue to be the leading cause of warming in 100 years (**Figure 1.14**) (Myhre, 2013).

Landfills are the most economical means for disposal of MSW and the most common method used globally, with over 90% of all MSW landfilled in many developing countries (Lamb et al, 2014). Another common disposal method is incineration, which can be used to generate energy in the form of heat, but at the cost of releasing greenhouse gasses (Lamb et al, 2014; UNEP, 2015). Less developed nations often lack the infrastructure necessary for effective MSW management, leading to MSW accumulating on roadsides, polluting air and water and creating unsanitary conditions that can spread disease (Hoornweg, 2012). Poorly managed MSW also clogs up waterways and makes its way out into the ocean. 80% of plastic polluting the marine environment originates from countries with large coastal

populations and poor waste management infrastructure, including China, Indonesia, the Philippines and Vietnam (Li et al, 2016).

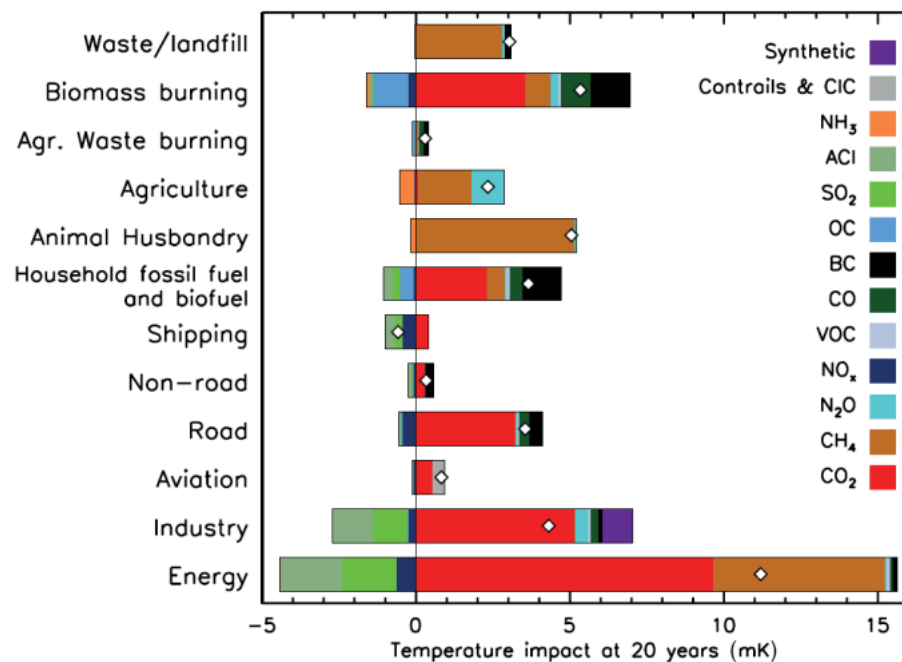


Figure 1.14: Contribution of different greenhouse gas emissions sectors to the net mean global temperature changes projected for the next 20 years

(Figure taken from Myhre, (2013)).

The major greenhouse gasses, methane (CH₄) and CO₂ are shown in brown and red, respectively; VOC = volatile organic compounds; CIC = contrail induced clouds.

Even amongst the worlds most developed nations, landfilling and incineration are still the fate of at least half of all MSW. In the United States of America 52.5% of all MSW is landfilled, 12.8% is incinerated and only approximately 25% is recycled. Less than 10% is composted. In the European Union (EU) a few member states have attained recycling rates of 50%, but landfilling and incineration are still widely implemented (Eurostat, 2017). **Figure 1.15** displays the trends of MSW treatment in the EU since 1995. Although landfilling has become less common overall, the amount of waste that is incinerated has risen by 100% since 1995, totalling 64 million tonnes in 2014 (Eurostat, 2016). Overall, it appears that countries that have successfully curbed landfilling over the last few decades, such as Germany, Sweden, Switzerland and Belgium, now have some of the highest rates of waste incineration (**Figure 1.16**). However, more sustainable practices such as recycling and composting have also seen some increase (Eurostat, 2017).

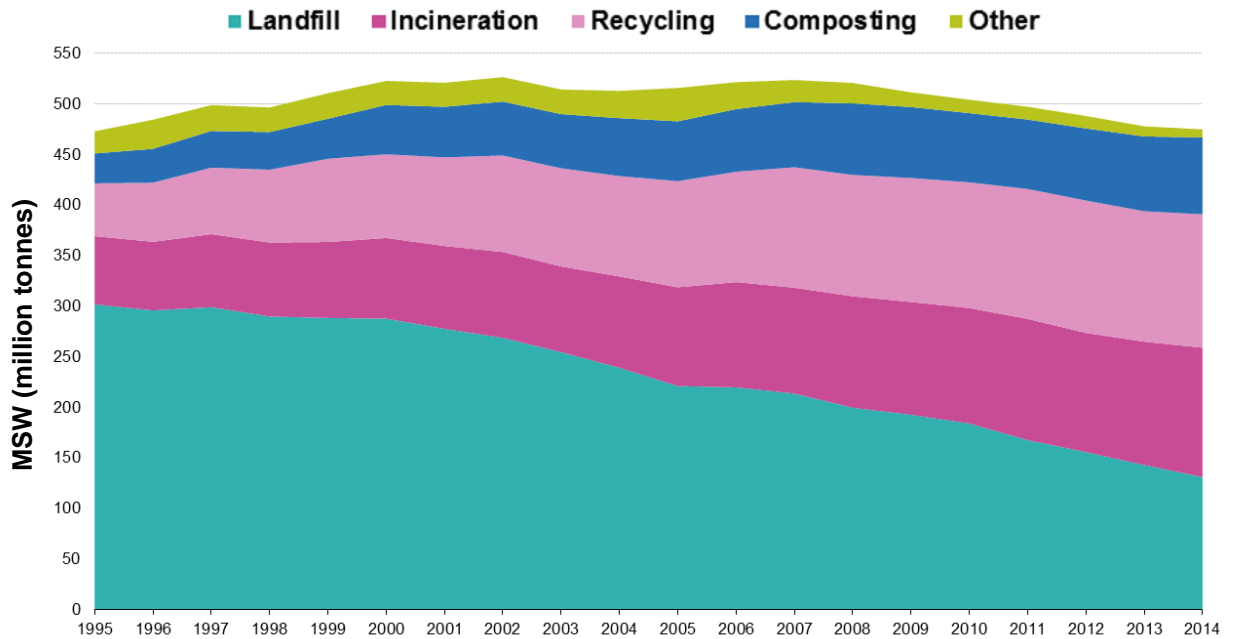


Figure 1.15: Management of municipal solid waste produced in European Union countries from 1995 to 2014. Taken from Eurostat (Eurostat, 2016).

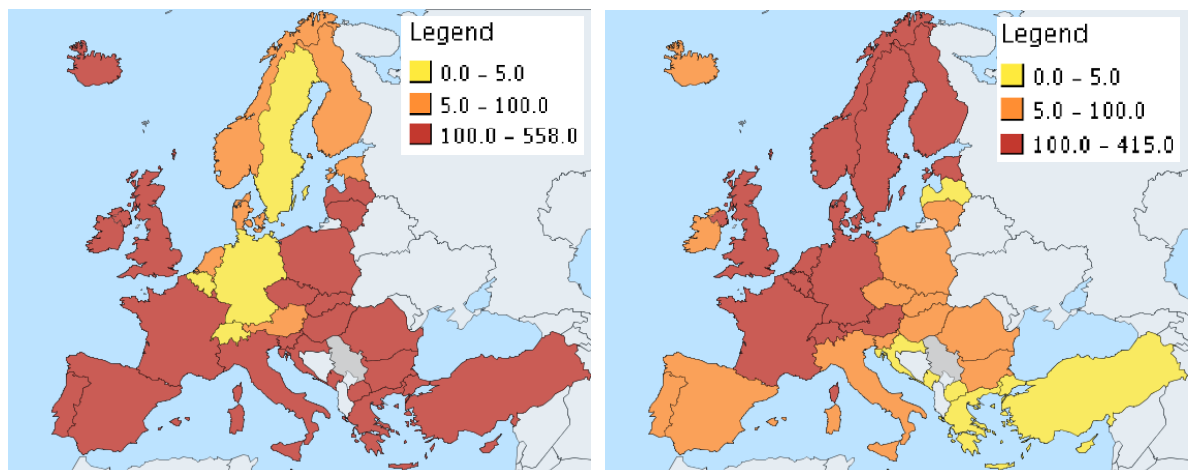


Figure 1.16: Prevalence of landfilling (left) and incineration (right) across European Union member states in 2015.

(Maps generated by author using data from Eurostat (2017)).

Legend shows kilograms of municipal solid waste disposed by each method per capita.

Incineration for energy capture has become widespread in the EU and is now used to dispose of 26% of all MSW, a 100% increase from 1995 levels (Eurostat, 2017b). Concurrently, landfilling has fallen by 58% since 1995 and is now the fate of 25% of MSW.

Incineration is more widespread than landfilling across Europe because it can be coupled to energy recapture for domestic heating. Despite this benefit however, incineration only represents the lesser of two evils as this process still generates significant CO₂ and NO emissions. It also requires more sophisticated infrastructure compared to landfilling, which hampers its implementation in less developed nations (Lamb et al, 2014). Overall, effective management of MSW is imperative if we are to ensure sustainable development on a global scale. There is a pressing need for economical and environmentally friendly methods to manage MSW that are logistically feasible for large urban populations and lower income nations (Hoorweg, 2013).

1.3.2 MSW Management in the United Kingdom

The total greenhouse gas emissions from wasted materials and waste management processes in the UK is over 200 million tonnes of CO₂, with a further 15 million tonnes of CO₂ equivalents annually emitted by landfills in the form of methane. Although these emission levels are significant, they are about 77% lower than 1995 levels due to reductions in the amount of biodegradable waste sent to landfill, enacted in compliance with European Commission Directive 99/31/EC (DEFRA, 2018). This directive dictates that the United Kingdom (UK) must reduce the volume of landfilled biodegradable material to 35% of 1995 levels by 2020 in order to reduce landfill-derived methane emissions, which it is reportedly on track to do (DEFRA, 2015b). Currently however about 15.7 million tonnes of MSW are still landfilled annually in (~23% of all MSW produced) of which ~7.7 million tonnes (49%) are biodegradable. A further 10 million tonnes are incinerated and the remainder is recycled, composted or subjected to anaerobic digestion (DEFRA, 2018).

Historically the UK has relied more heavily on landfills for waste disposal than other European nations. A key strategy for landfill mitigation was the introduction of a landfill tax in 2009 to disincentivise local authorities from landfilling biological MSW, the major cause of methane emissions (Gregson et al, 2015). Local councils subsequently outsourced waste management to integrated materials recovery facilities (MRFs), which are commercial facilities that mechanically and/or biologically process MSW using a variety of established technologies (**Figure 1.17**). There are over a hundred MRFs operational across the UK and they have become integral to the country's waste management (DEFRA, 2013). Anaerobic digestion facilities are also widespread, with 486 plants currently operating around the

country, 84 of which provide biomethane directly to the national grid (NNFCC, 2019). AD is primarily used for the treatment of domestic food and green waste, but also agricultural waste, manure and liquid waste (DEFRA, 2015a).

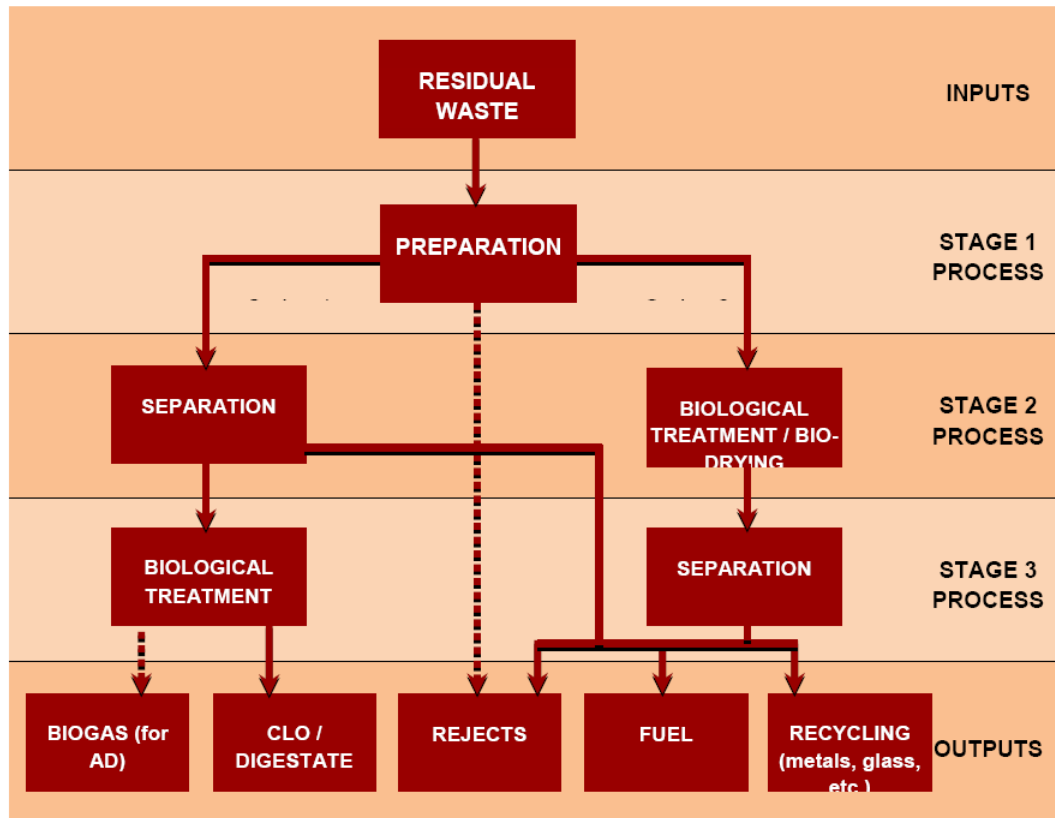


Figure 1.17: Overview of mechanical and biological processing stages operating within an integrated materials recovery facility (MRF)

(Taken from DEFRA (2013)).

AD = anaerobic digestion. CLO = compost-like output.

Fuel = energy recovered from incineration.

On average MSW produced in the UK is highly heterogeneous, consisting primarily of plastic (20%), food waste (15%) paper (11%) and card (8%). Minor components include garden waste, textiles, shoes, carpets, furniture, metal, glass, hazardous waste and waste electrical and electronic equipment (W.E.E.E) (**Figure 1.18**). Organic components such as card, paper, garden waste and discarded food make up approximately 40-50% of MSW (DEFRA, 2015b). These materials are primarily of plant origin are therefore rich in lignocellulose. Globally most MSW contains about 10-60% lignocellulose, although the

levels are highly dependent upon consumption patterns, geography and socioeconomics (Barampouti et al, 2019).

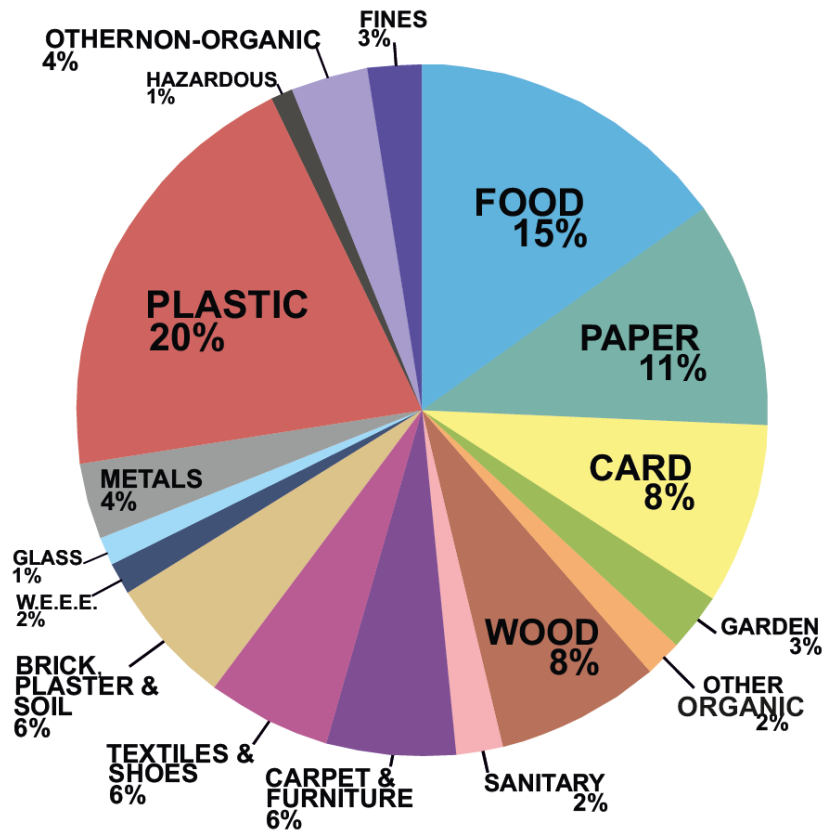


Figure 1.18: Major constituents of British MSW by percentage.

(Figure by author, using national estimates for 2011 from the Department for Environment, Fisheries and Rural Affairs (DEFRA) (DEFRA, 2015b)).

W.E.E.E = Waste Electrical and Electronic Equipment

1.3.3 Municipal Solid Waste as a Feedstock

Effective MSW management is central to developing a circular economy. The EC highlights key areas in this sector as follows: “Ensure energy recovery of non-recyclable waste; Reduce energy intensity of waste treatment; [and] increase use of biodegradable waste for bioenergy and bio-products,” (EC, 2011). Over half of the MSW generated in Europe is considered ‘non-recyclable’ but contains up to 60% lignocellulose-rich organic material. This organic fraction of MSW (OMSW) is estimated to have a similar energy potential to that which could be attained from available agricultural residues (Aracil et al,

2017). However, OMSW is considered a waste material and therefore has a limited number of permissible uses.

The application of any MSW-derived organic material onto agricultural land is currently not permitted within the EU because it is typically contaminated with heavy metals and organic pollutants that persist in the environment and are of ecotoxicological concern, such as polynuclear aromatic hydrocarbons (PAHs), polychlorinated biphenyls (PCBs), polychlorinated dibenzo-P-dioxins and furans (PCDD/Fs) and phthalates (Amlinger et al, 2004). Thus OMSW is typically incinerated for electricity production or subjected to anaerobic digestion. It can also be stabilised by drying and composting and then used as landfill capping material or applied onto marginal land, but these applications require special permits and are greatly dependent upon the degree of contamination (DEFRA, 2013). OMSW is generally considered an underutilised feedstock and is frequently highlighted as having good potential for biorefining applications (Aracil et al, 2017; Barampouti et al, 2019).

Several features make OMSW an attractive feedstock for biorefining – it is high in lignocellulose, abundant, continuously produced and does not compete with agriculture. Furthermore, the landfill taxes and gate fees that are legislated to disincentivise landfilling of OMSW can make it highly economical to source. For example, the gate fee and landfill tax rate in England for landfilling non-hazardous waste is between £88-169 per tonne (WRAP, 2018). Another benefit is that components such as paper and card have already been processed in a previous industrial manufacturing step, making them more amenable to enzymatic degradation than raw plant material (Jensen et al, 2011). However, there are also several inimitable challenges associated with valorising OMSW. Unlike other sources of lignocellulose, OMSW composition is extremely heterogeneous and inconsistent. It varies greatly across both temporal and geographical scales and components can originate from innumerable sources. The organic fraction also comes into close contact with a wide array of inorganic materials, many of which could introduce toxic compounds or metals into the biomass that may be inhibitory to enzymes and/or fermentative microorganisms (Aracil et al, 2017; Barampouti et al, 2019). Furthermore, there is a need for commercially viable separation technologies that can effectively segregate the organic fraction from inorganic materials to produce a useable feedstock.

So far OMSW has been widely studied in the literature as a feedstock for AD processes, composting and incineration (Adhikari et al, 2013; Clarke, 2018; Dang et al, 2017; Di Maria & Micale, 2015; Hartmann & Ahring, 2005; Lavagnolo et al, 2018; O’Callaghan, 2016; Razavi et al, 2019; Smith, 2009; Zhang et al, 2012). However, investigations into the amenability of OMSW for biorefining have been limited compared to other feedstocks (Barampouti et al, 2019; Matsakas et al, 2017). Progress made so far in the field of OMSW biorefining will be reviewed in detail in the forthcoming chapters.

1.3.4 Wilson Bio-Chemical and the Wilson System®

Wilson Bio-Chemical (<http://wilsonbio-chemical.co.uk/>) is a company based in Yorkshire, United Kingdom, that has developed a commercial autoclave-based process known as the Wilson System® for pre-treating mixed MSW (**Figure 1.19**). Autoclave treatment converts the organic fraction of MSW to a homogenous organic fibre known as Wilson Fibre®. Inorganic materials and plastics are sent for incineration while other valuable materials such as ferrous/non-ferrous metals, glass and textiles are recycled (WilsonBio-Chemical, 2018). The commercial autoclave vessels (**Figure 1.20**) are large, rotary, baffled vessels that can be loaded with up to 20 tonnes of MSW per 45 minute run. Each vessel can process up to 150,000 tonnes of MSW per annum, diverting 90% of waste from landfill (WilsonBio-Chemical, 2018).

Processing of inorganic material through the Wilson System® is a commercially viable process. However, the organic fraction makes up 40-60% of MSW and represents a large waste stream with few commercial-scale applications. In recent years Wilson Bio-Chemical have invested in research on potential commercial applications of Wilson Fibre® and have successfully attained ‘end-of-waste’ status for this biomass – end-of-waste status is granted by the EC to wastes that have undergone sufficient recovery to qualify as a product (i.e. secondary raw material) (EC, 2019). Having end-of-waste status eliminates the need for a waste plant operating licence, thereby lowering the cost of planning permissions and enabling any biorefinery developed around Wilson Fibre® to be classified as a bespoke production plant.

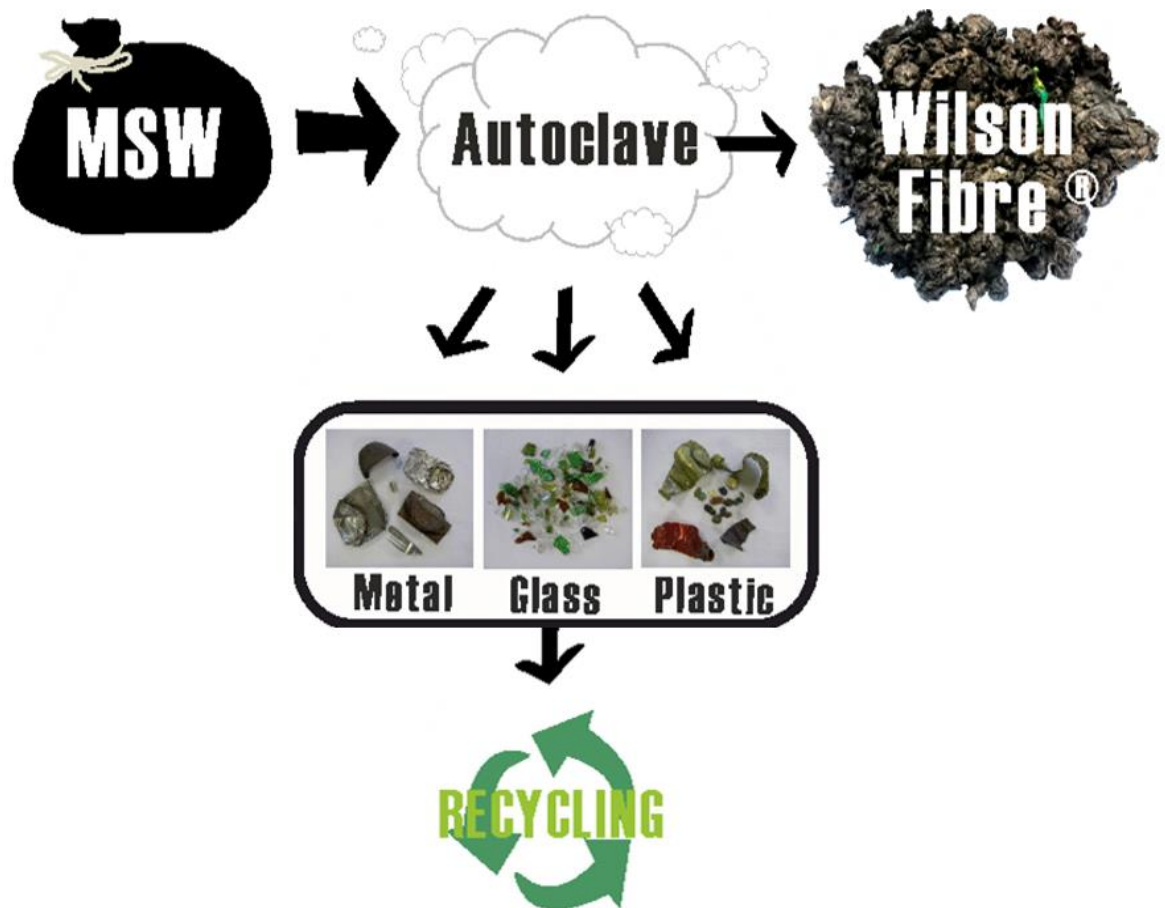


Figure 1.19: Overview of the Wilson System®
(Figure by author)

Mixed MSW is loaded into the autoclave vessel which is sealed and then treated at 160°C and 87 psi with dry steam. The vessel slowly rotates during treatment to agitate the MSW. As a result of the treatment the waste is sterile, homogenised and compacted, allowing the organic and inorganic fractions to be more easily separated. Materials are separated both manually and using automated vibrating screens of varying sizes. Inorganic materials such as metal and glass are recycled. Plastics are sent for incineration with heat recapture. The organic material that remains is called Wilson Fibre® and is high in lignocellulose (Wilson Bio-Chemical, 2018).



Figure 1.20: The Wilson System Autoclave

(Images printed with permission from Wilson Bio-Chemical Ltd.)

- A.** *Image of an industrial scale Wilson System Autoclave with capacity for 20 tonnes of mixed MSW per run.*
- B.** *Interior of the Wilson system autoclave filled with MSW, before autoclaving.*
- C.** *Interior of the Wilson System autoclave filled with MSW, post autoclaving. Compared to the image in B, it is evident that plastic and other organic materials have collapsed while organic material has become more homogenised.*

1.4 Aims and Objectives

This PhD project is a BBSRC Industrial Cooperative Award in Science and Engineering (iCASE) studentship carried out in partnership with Wilson Bio-Chemical. The primary aim of this study is to evaluate OMSW fibre as a feedstock for producing renewable biofuels or chemicals. To characterise this complex feedstock the OMSW fibre will be subjected to a comprehensive compositional analysis. This will be followed by enzymatic hydrolysis at high solids loading to produce an industrially relevant hydrolysate. The fermentability of the OMSW fibre hydrolysate will be evaluated by compositional analysis of nutrient levels, fermentation inhibitors and toxic metals. Additionally, the hydrolysis waste stream will be investigated as a feedstock for anaerobic digestion. Finally, eight microorganisms of biotechnological interest will be screened for the ability to robustly and efficiently ferment OMSW fibre hydrolysate. The most promising candidate species will be improved further for industrial applications through genetic engineering.

A critical challenge faced by researchers interested in studying OMSW is finding realistic and reproducible material for experiments. Using OMSW sampled from a single site in relatively small volumes does not fully capture the variability and heterogeneity of this feedstock at industrial scales and over time. Through collaboration with Wilson Bio-chemical we have developed a method for producing an industrially relevant and reproducible source of OMSW. A predetermined mixture of organic and inorganic materials was constructed according to the national statistics reported by DEFRA (2015b) (**Figure 1.18**) and subjected to autoclave pre-treatment in a pilot-scale Wilson System[®]. The resulting Wilson fibre[®] (henceforth termed OMSW fibre) is both reproducible and representative of OMSW produced across the UK.

Although the constructed OMSW fibre produced for this project is made up of a known and reproducible mixture of materials the feedstock itself is still highly heterogeneous, complex and uncharacterised. A comprehensive compositional analysis is therefore required in order to support further studies. **Chapter 2** provides a detailed summary of the structural and non-structural components of the constructed OMSW fibre, with the aim of determining the percentage abundance of lignocellulose and evaluating whether the cellulose and hemicellulose fractions are large enough to be practicable for bioprocessing. Other important components, including oils, proteins, metals and ash are also investigated and assessed in the context of developing a viable OMSW biorefinery.

Chapter 3 is concerned with the hydrolysis of OMSW fibre, with particular focus on the fate of metal species during the hydrolysis process. The fermentability of OMSW fibre hydrolysate is indirectly assessed based on the abundance and concentration of sugars and the presence of inhibitors, toxic metals and microbially accessible nutrients. Furthermore, the utility of a major waste stream, the residual material left over after hydrolysis, is investigated as a feedstock for biogas production through AD.

Chapter 4 aims to identify microorganisms of biotechnological utility that demonstrate robust and efficient growth on OMSW fibre hydrolysate. First the hydrolysate is evaluated for microbial toxicity and nutrient limitation using the model fermentative species *Escherichia coli*. Results are then presented for fermentation screens with eight different microbial species of biotechnological interest on nutrient-supplemented OMSW fibre hydrolysate. Each species' growth, productivity and robustness are evaluated and compared based on quantitative fermentation parameters. The most productive species, the oleaginous strain *Rhodococcus opacus* MITXM-61, is characterised in greater detail on OMSW fibre hydrolysate. Finally, with the aim of manipulating the FA profile of *R. opacus* to improve its industrial utility, results are presented from the heterologous expression of a plant-derived acyl-acyl carrier protein thioesterase in *R. opacus* grown on OMSW fibre hydrolysate.

Chapter 2: Compositional Analysis of Organic Municipal Solid Waste Fibre

2.1 Introduction

The organic fraction of MSW is an abundant, cheap and renewable source of lignocellulose but has been largely unexplored for biorefinery applications compared to other feedstocks. Harnessing OMSW for industrial bioprocessing involves a number of unique challenges, including (1) heterogeneous and inconsistent feedstock composition; (2) the need for efficient and industrially scalable methods of separating the organic fraction; and (3) the presence of residual metals and other pollutants in the feedstock that could have inhibitory effects on enzymes and/or fermentative microorganisms.

OMSW used for research purposes is typically acquired by manually sampling and sorting organic waste from local establishments such as restaurants (Adhikari et al, 2013; Aiello-Mazzarri et al, 2006; Lay et al, 1999). The compositional profiles of OMSW from these sources vary significantly depending on the type of establishment or the processing stage when it is intercepted, making them irreproducible and limiting comparability between studies. Some groups have tried to improve reproducibility by using materials such as newspaper (McCaskey et al, 1994), food waste (Ma et al, 2009) and even dog food (Dang et al, 2017) to represent OMSW. However, these substrates arguably fail to fully capture the heterogeneous nature of MSW-derived organic materials.

OMSW composition is largely dependent upon socioeconomic factors and the prevailing waste management practices. It also varies significantly over geographic and temporal scales (Kaza et al, 2018). The abundance of organic material in MSW ranges from 30-60% (Kaza et al, 2018) and reports of the lignocellulose fraction range between ~10-60% (Barampouti et al, 2019). Barampouti et al (2019) averaged the lignocellulose composition reported for OMSW across a wide range of published sources, encompassing data from countries all over the world, and found that the average lignocellulose composition in OMSW is $15.2 \pm 14.6\%$ cellulose, $7.4 \pm 4.6\%$ hemicellulose and $9.1 \pm 6.6\%$ lignin. OMSW also has a tendency to accumulate contaminants, especially metals, from contact with inorganic wastes which can further contribute to their complex composition. These metals are likely derived from MSW components such as batteries and have a tendency to be retained in the paper fraction of OMSW (Abdullah & Greetham, 2016). On average, the most common metals reported in analyses of OMSW, in order of abundance, are Ca, Na, K, As, Mg, Fe, Al,

Zn, Ba, Pd, Ti, Mn, Sn, Cr, Bo, Ni, Br, Mo, W, Co, Se, V, Ag and Cd, many of which can be highly toxic to life (Barampouti et al, 2019).

The complexity of OMSW contrasts starkly with agricultural and forestry by-products which generally exhibit relatively consistent compositional profiles (Marriott et al, 2016) and do not typically contain toxic metals. However, the fact that OMSW is widely available, rich in lignocellulose, does not compete with agriculture and currently has few high-value applications make it an appealing feedstock to investigate for sustainable biorefining (Barampouti et al, 2019; Haddadi et al, 2018; Meng et al, 2019). That said, the various pitfalls outlined above highlight the critical importance of using an industrially relevant source of OMSW to ensure the results of empirical studies are transferable. Industrially relevant sources of OMSW that have been used in published studies include OMSW collected directly from local MRFs or waste treatment plants (Farmanbordar et al, 2018b; Ghanavati et al, 2015; Hartmann & Ahring, 2005; Jensen et al, 2011; Lavagnolo et al, 2018) and autoclave pre-treated OMSW (Abdhulla, 2016; Ballesteros et al, 2010; Li et al, 2012b; Meng et al, 2019; Puri et al, 2013).

Autoclaving is an established industrial-scale process that is already employed in the waste industry to recover resources from MSW and enables rapid, hygienic and effective separation of organic and inorganic components (Quiros et al, 2015). Three studies that have reported compositional profiles for autoclave pre-treated OMSW: An MSW-derived paper pulp isolated by autoclaving contained 55% cellulose, 18% hemicellulose, 24% lignin and 3% ash (Puri et al, 2013). OMSW fibre produced on an industrial Wilson System® autoclave analysed by Abdel-Rahman et al (2013) contained 27.8% cellulose, 15.45% hemicellulose, 17.7% lignin, 11.2% lipids and 5.9% protein. Similarly, OMSW produced by autoclaving at 160°C for varying durations between 5 – 50 minutes was composed of between 37.5 – 43.9% cellulose, 5.0 – 5.8% xylose, 21.9 – 29.1% acid insoluble residue, 13.9 – 18.0% ash and 10.4 – 16.4% uncharacterised material (Ballesteros et al, 2002). All three studies report about 50% greater levels of polysaccharides than the averages calculated by Barampouti et al (2019) in their review, indicating that autoclaving is a relatively efficient strategy for isolating and concentrating organic materials in OMSW.

The presence of uncharacterisable material is a common feature in MSW-derived feedstocks, due to the fact that most compositional analyses for lignocellulose are designed for plant tissues and OMSW is incredibly heterogeneous. Puri et al (2013) also observed

that approximately 50% of material measured as lignin was actually unidentified organic matter of non-plant origin. A critical review of methods for compositional analysis of lignocellulosic materials concluded that routine analytical methods fail to accurately analyse MSW due to the high amounts of interfering extractives, lipids, protein and other contaminants. This continues to be a challenging limitation in this field and must be kept in mind when evaluating feedstock composition (Karimi & Taherzadeh, 2016).

2.1.1 Aims of this Chapter

The aim of this chapter was to undertake a comprehensive compositional analysis of the major structural and chemical components of OMSW fibre, to gain a better understanding of this heterogeneous feedstock and inform subsequent experimental work.

Key questions explored in this chapter:

- What percentage of the fibre is composed of lignocellulose?
- Are the cellulose and hemicellulose fractions high enough to be practicable for application in a bioprocess?
- Are any proteins or oils present that could provide nutrients to microorganisms in the fermentation step?
- What metal species are present in the fibre, what are their concentrations and are the levels of toxic species high enough to be inhibitory to microbial fermentation?
- How does the constructed OMSW fibre compare to industrial OMSW fibre and other sources of OMSW reported in the literature?

2.2 Materials & Methods

2.2.1 Production of the OMSW Fibre

The OMSW fibre used in this study was produced by Wilson Bio-Chemical on their pilot autoclave rig (**Figure 2.1**). The pilot rig is a scaled-down version of the commercial Wilson System® (WilsonBio-Chemical, 2018). An overview of the pilot rig process is given in **Figure 2.2**. The OMSW fibre was produced by combining a mixture of organic and inorganic materials that reflected the composition of MSW produced in an average British household, based on statistics reported by the Department of Environment, Food and Rural Affairs (DEFRA, 2015). The composition of the constructed MSW mixture is given in **Table 2.1** alongside the percentage composition reported by DEFRA.

Table 2.1: Composition of waste materials used for production of OMSW fibre on the Wilson Bio-Chemical Pilot Rig.

**Masses are based on the percentage composition of the major MSW components reported by DEFRA and adjusted to 100%.*

W.E.E.E. = Waste Electrical and Electronic Equipment.

| Type of waste | DEFRA reported composition (%) | Adjusted to 100% | Per 20 Kg batch (Kg)* |
|-----------------------------------|--------------------------------|------------------|-----------------------|
| Food | 15.0 | 20.80 | 4.16 |
| Plastic film | 8.9 | 12.34 | 2.47 |
| Dense plastic | 11.3 | 15.67 | 3.13 |
| Paper | 10.5 | 14.56 | 2.91 |
| Card | 8.4 | 11.65 | 2.33 |
| Wood | 7.6 | 10.54 | 2.11 |
| Metal | 3.5 | 4.85 | 0.97 |
| Garden | 2.7 | 3.74 | 0.75 |
| Other organic | 1.7 | 2.36 | 0.47 |
| W.E.E.E. | 1.5 | 2.08 | 0.42 |
| Hazardous/batteries | 1.0 | 1.39 | 0.28 |
| Carpet/underlay/furniture | 6.0 | - | - |
| Brick/plaster/soil | 5.9 | - | - |
| Textiles/shoes | 5.7 | - | - |
| Fines | 2.5 | - | - |
| Glass | 2.2 | - | - |
| Sanitary | 2.0 | - | - |
| Other non-combustible | 1.6 | - | - |
| Total | 100 | 100.00 | 20.00 |
| Estimated Biodegradability | 51.4 | 63.65 | 12.73 |

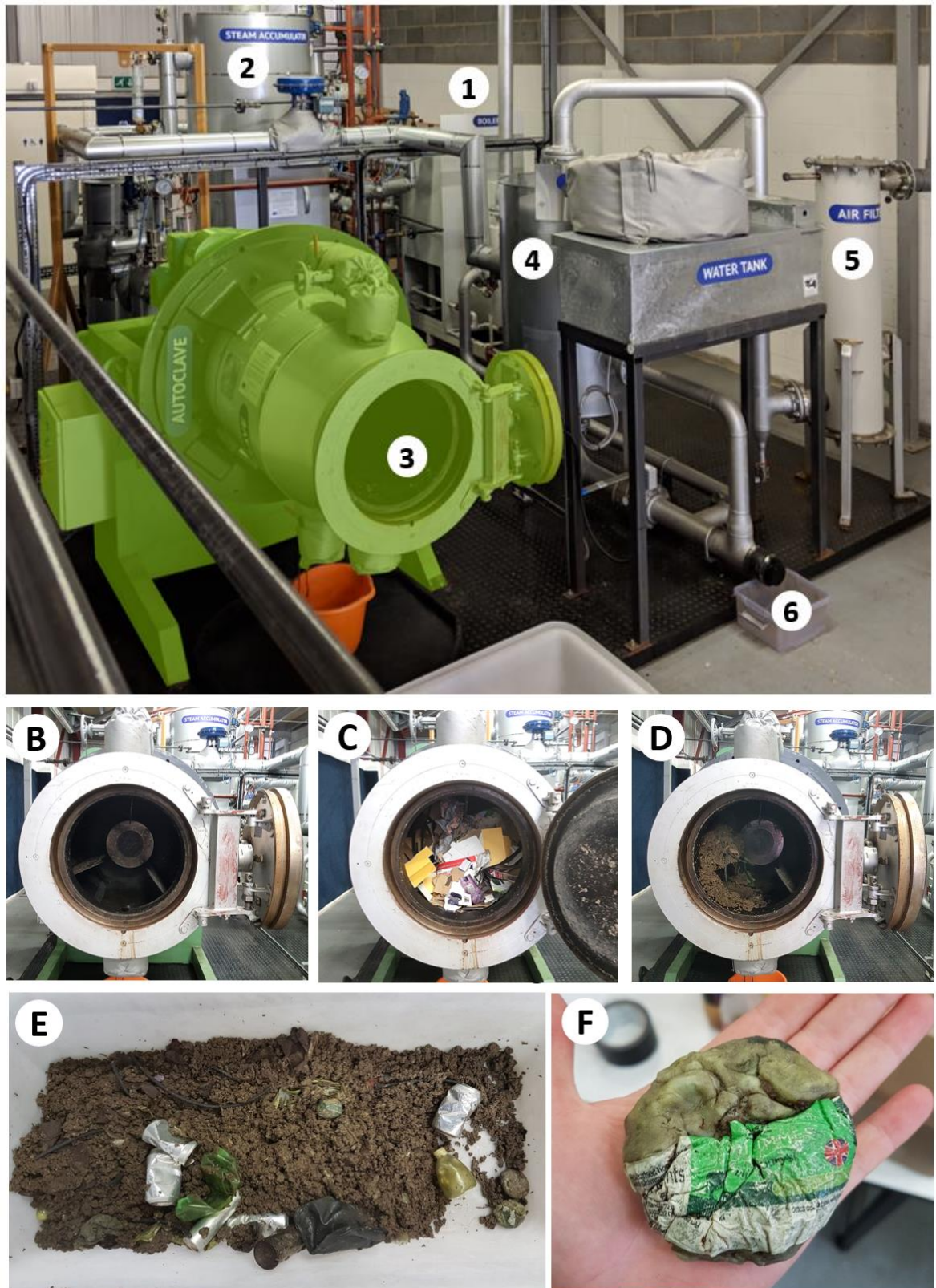


Figure 2.1: The Wilson Bio-Chemical Pilot Rig

Image courtesy of Wilson Bio-Chemical Ltd.

A: (1) Boiler; (2) Steam accumulator; (3) autoclave; (4) vent vessel & condenser; (5) air filter; (6) condenser outlet. **B:** Autoclave vessel before loading; **C:** Autoclave vessel loaded with constructed MSW mixture; **D:** Autoclave vessel after treatment; **E:** Constructed MSW before manual sorting; **F:** A 2.27 litre (4 pint) plastic milk bottle after autoclaving illustrates the effect of the treatment on plastics.

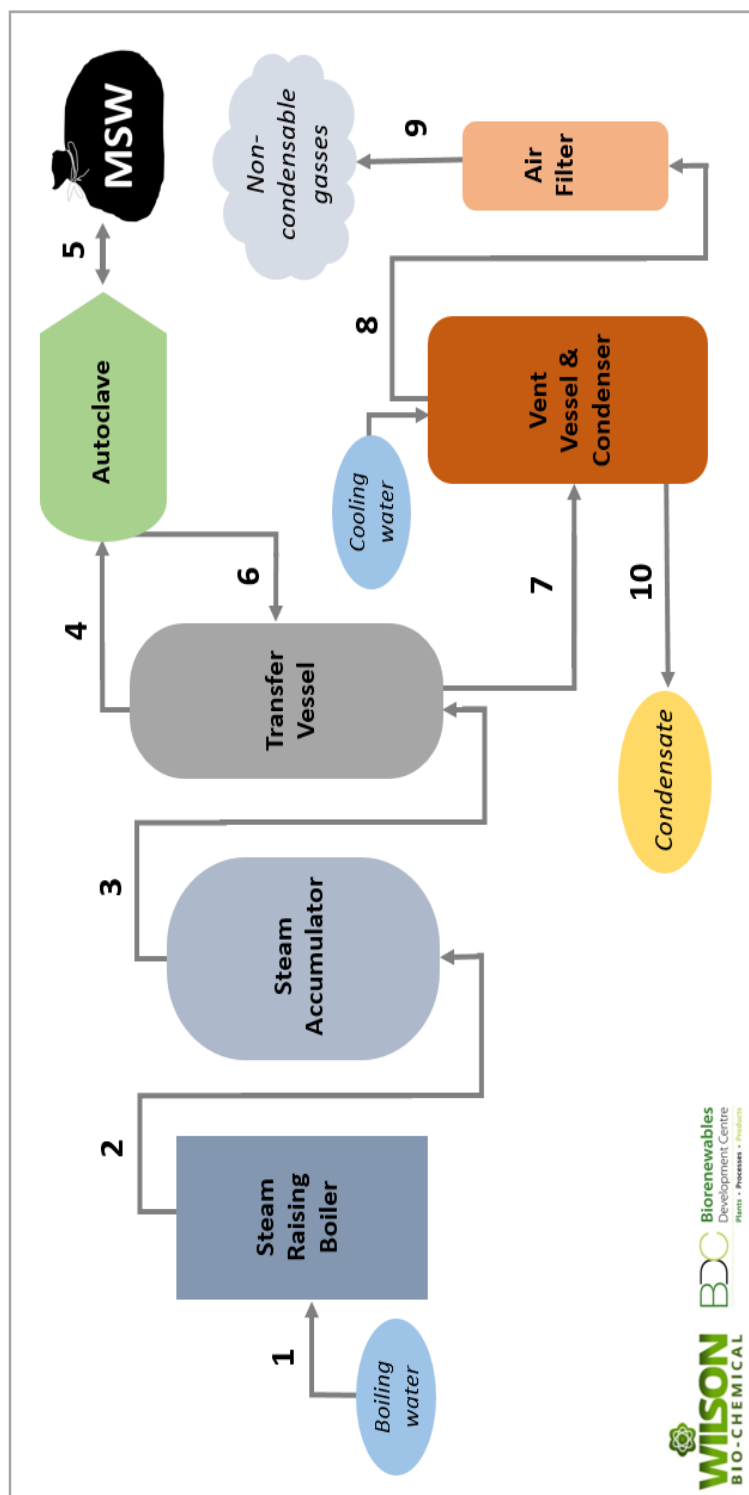


Figure 2.2: Schematic of Wilson Bio-Chemical Ltd. pilot rig
(Diagram by author, with permission from Wilson Bio-Chemical Ltd.)

Process overview: Boiling water is transferred to the **steam raising boiler (1)**. The boiler is heated to 247 psi then de-isolated from the **steam accumulator (2)** so that the two vessels can equilibrate to 116 psi. The steam is then directed through the **transfer vessel (3)** to the **autoclave vessel (4)** which has been pre-loaded with **MSW (5)**. The autoclave is run under standard conditions (160°C, 87 psi, 45 minutes with rotation at 4 rpm). Once the run is complete the steam is vented back through the **transfer vessel (6)** to the **vent vessel and condenser (7)**. Any non-condensable gases are directed through the **air filter (8)**, which scrubs out any malodorous compounds (9), while any liquid condensate is released through the bottom of the **condenser (10)**. Once the autoclave has cooled the pre-treated MSW is manually sorted to separate the organic and inorganic fractions.

2.2.2 Compositional Analysis

Compositional analysis of the OMSW fibre was carried out according to a range of standard protocols for analysis of lignocellulosic biomass. Unless otherwise specified, all analyses were performed in triplicate at minimum with fibre dried at 45°C and ball milled to a fine powder in a Retsch TissueLyser II (Qiagen).

2.2.3 Total Solids, Moisture & Ash content

Percentage moisture, total solids, pH and ash content were determined according to protocols established by the National Renewable Energy Laboratories (NREL) (Hames et al, 2008; Sluiter et al, 2008a; Sluiter et al, 2008b). Briefly, moisture content and total solids was determined by weighing out 10 g of OMSW fibre (as received) into pre-weighed crucibles and drying at 45°C until mass loss stabilised. Final dry masses were subtracted from the initial masses and the difference was used to calculate the percentage moisture and dry solids content of the feedstock. Ash (defined as any inorganic residue left after dry oxidation at 575°C by Sluiter et al (2008a)) was quantified by weighing out 1 g of dry fibre into pre-weighed ceramic crucibles and then heating these in a furnace (Carbolite, Type 301) at 600°C for 24 hours. The remaining material (ash) was weighed and percentage ash content calculated based on initial sample masses.

2.2.4 Lignin

Lignin content was analysed according to methods adapted from Fukushima & Hatfield (2001). 4.0 ± 0.1 mg of biomass was digested with 250 μ l freshly prepared acetyl bromide solution (25% v/v acetyl bromide, 75% v/v glacial acetic acid) in order to break the phenol bonds in the lignin. Samples were heated at 50°C for 3 hours and vortexed every 15 minutes for the final hour. Samples were cooled to room temperature (RT), then, working under a fume hood, the digested sample was transferred to a 5 ml volumetric flask. To ensure all sample liquid was transferred, tubes were rinsed with 1 ml 2 M NaOH. Next 175 μ l of 0.5 M hydroxylamine HCl was added, the flasks were stoppered and vortexed. Working quickly to avoid sample precipitation, the flasks were filled to final volume of 5 ml with glacial acetic acid, mixed several times by inversion, and 100 μ l transferred to an Eppendorf tube with 900 μ l glacial acetic acid. This diluted sample was transferred to a 1 ml quartz cuvette and the A_{280} was measured in a CaryWinUV spectrophotometer (blanked against glacial acetic acid). Absorbance values were converted to concentration of lignin using the Beer-Lambert law (**Equation 2.1**).

Equation 2.1: The Beer-Lambert Law

$$c = \frac{A}{\epsilon b}$$

Where:

c = lignin concentration in 5 ml sample (mol dm^{-3})

A = Absorbance at 280 nm

ϵ = the wavelength-dependent molar absorptivity coefficient ($\text{M}^{-1} \text{cm}^{-1}$)

b = the path length (1 cm).

The molar absorptivity coefficient of poplar ($\epsilon = 18.21$) was used to calculate the concentration of the MSW fibre-derived lignin. Concentration was converted from mol dm^{-3} to a percentage as described by **Equation 2.2**.

Equation 2.2: Calculating Percentage Lignin

$$\% \text{ Lignin} = c \left(\frac{v \cdot 100\%}{m} \right)$$

Where:

c = lignin concentration in 5 ml sample (mol dm^{-3})

v = volume of sample (5 ml)

m = initial mass of biomass sample (g)

2.2.5 Hemicellulose & Cellulose

Hemicellulose and cellulose were quantified by two consecutive methods, adapted from Foster et al (2010). First 4.0 ± 0.1 mg of biomass was weighed out into 2 ml screw-cap tubes and mixed with 0.5 ml trifluoroacetic acid (TFA). TFA digestion isolates all hemicellulosic sugars as monosaccharides but leaves behind crystalline cellulose and lignin. The tubes were flushed with argon gas to displace oxygen in the vial headspace as this interferes with hydrolysis. Samples were incubated in a 100°C heating block for 4 hours with mixing every 30 minutes, cooled to RT and then dried overnight in a centrifugal

evaporator with fume extraction. Pellets were re-suspended in 0.5 ml propan-2-ol and evaporated, twice, to ensure all TFA was removed.

Monosaccharides were solubilised from the dried pellet by adding 200 μ l dH₂O. The liquid fraction was carefully transferred to 1 ml syringes and filtered through 0.45 μ m PTFE filters into tapered HPAEC vials. Hemicellulosic sugars in the sample were analysed by high-performance anion exchange chromatography (HPAEC) on an ICS-3000 PAD system with an electrochemical gold electrode using a CarboPac PA20 analytical column (3x150 mm, Dionex) and guard column (3 x 30 mm, Dionex). Identification and quantification of monosaccharides was carried out by comparing retention times and integrated peak areas of the samples to an equimolar standard mixture of L-fucose, L-arabinose, L-rhamnose, D-galactose, D-glucose, D-xylose, D-mannose, D-galacturonic acid and D-glucuronic acid. Standards were analysed during the same run under the same conditions.

The pellet retained after the hemicellulose assay contains crystalline cellulose and lignin. The pellet was washed once in 1.5 ml water and twice with 1.5 ml acetone and then air-dried overnight. Cellulose was isolated using a modified Saeman hydrolysis (Saeman et al, 1945) involving a room temperature incubation for 4 hours with 90 μ l 72% sulphuric acid, followed by dilution to 3.2% sulphuric acid with 1890 μ l dH₂O and incubation for 4 hours at 120°C. Samples were cooled to RT and then centrifuged at top speed for 10 minutes. Lignin remains in the resulting pellet, while the crystalline cellulose has been solubilised to glucose and can be measured in the supernatant. Glucose concentration was quantification by colorimetric Anthrone assay (Viles & Silverman, 1949) alongside glucose standards ranging from 0-6.6 μ g of D-glucose. 40-60 μ l of sample supernatant or standard was diluted with water to give a final volume of 400 μ l. 800 μ l of freshly made Anthrone reagent (2 mg/ml Anthrone in concentrated sulphuric acid) was then added. Samples and standards were incubated at 80°C for 30 min. in a heating block. Glucose containing samples changed from yellow to blue-green. Samples and standards were cooled to RT and then 200 μ l was transferred to a 96-well flat bottom optical plate (NUNC) and absorbance at 620 nm was measured in a plate reader. The glucose concentrations were derived from the standard curve generated from the standards and converted to percentage cellulose based on the mass of the original biomass sample.

2.2.6 Oil

Oil (refers to any non-polar, hydrophobic and lipophilic substance) was extracted from dried OMSW fibre using a two-stage continuous extraction with ether. First the fibre was extracted continuously with ether and all extracted oil was dried and weighed. The residual solid material was collected and boiled with hydrochloric acid to release any remaining fats bound to the biomass. The solution was filtered through filter paper and then washed several times with water until a neutral pH was reached. The filter paper was dried and then extracted a second time with ether. Any liberated fats were again dried and weighed. The masses of oil collected from each extraction were summed and reported as percentage oil by dry mass. This analysis is a routine protocol carried out by Sciantec Analytical Ltd.

2.2.7 Protein

The Dumas method (also known as nitrogen combustion method) was used to determine the concentration of proteins in the OMSW fibre. Both organic and inorganic nitrogenous compounds in the sample were oxidised by combustion at 800-1000°C then reduced to gaseous form (N₂) and analysed by a thermal conductivity detector (Leco FP285 Nitrogen Analyser). This total nitrogen value was then converted to proteinaceous nitrogen (crude protein) using the conversion constant 6.25, the standard conversion factor used for compound feedstuffs and associated raw materials (Horwitz & Latimer, 2011; Jung et al, 2003). This analysis is a routine protocol carried out by Sciantec Analytical Ltd.

2.2.8 Metals

Metals present in the Wilson Fibre® were analysed as follows: Samples were digested with nitric and sulphuric acid (trace metal grade, 1:1 mixture) in a PTFE digestion vessel, treated in a microwave digestion system (Ethos Up) at 200°C for 15 minutes, cooled to ~25°C, transferred to a volumetric flasks (100 ml) and diluted to 100 ml with dH₂O. Samples were then diluted 100-fold with dH₂O and analysed on an Agilent 7700x inductively coupled plasma-mass spectrometer (ICP-MS). Results were quantified against calibration curves ($R^2 = \geq 0.998$) prepared from seven calibration standards of Agilent certified multi-element environmental reference standard no. 5183-4688. Metals in this standard include: Ag, Al, As, Ba, Be, Ca, Cd, Co, Cr, Cu, Fe, K, Mg, Mn, Mo, Na, Ni, Pb, Sb, Se, Tl, V, Zn, Th, U.

2.2.9 OMSW Washing

The OMSW fibre was subjected to washing with water in order to quantify the total soluble material and the solubility of metals. 25 g of dried fibre was placed in a pre-weighed centrifuge pot (600 ml) and washed with 500 ml of 95°C water. The pot was manually shaken for 1 minute and then incubated in a 95°C incubator for 4 minutes. Shaking and incubation were repeated for a total of 20 minutes. The sample was centrifuged (3000 xg for 15 minutes) and the wash water poured off through pre-weighed Miracloth (Merck) to catch any insoluble particulates. The washing was repeated a total of three times to ensure thorough removal of soluble material. The final fibre pellet was dried along with the Miracloth and the percentage mass loss was calculated. The dried washed fibre was subjected to metal analysis by ICP-MS as described in **2.2.2.6** in parallel with unwashed OMSW fibre in order to determine the degree of metal solubilisation. The calculated mass loss percentage was used to normalise calculations of the metal concentrations in the washed OMSW fibre to allow for more accurate comparison of washed and unwashed biomass.

2.2.10 Soxhlet Extraction & Extractives

Non-chemically bound components of biomass are defined as any non-chemically bound components of lignocellulose. To quantify non-structural components of the OMSW fibre, a Soxhlet extraction (described in **Figure 2.3**) was carried out according to methods established by Sluiter et al (2008b). This experiment was repeated twice. Briefly: 10 g MSW fibre (dried and milled) was washed under reflux (2-3 siphons/hour) with 250 ml water for 16 hours (note the apparatus was covered in cotton wool and wrapped in aluminium foil to aid in heat retention). The water in the distillation pot was then replaced with 250 ml ethanol and the same material was washed under reflux (5-6 siphons/hour) for a further 24 hours. The water and ethanol were collected after each run and stored in pre-weighed glass bottles (250 ml) at 4°C. To calculate the percentage of extractives per gram of fibre the water and ethanol samples from the Soxhlet extraction were dried down in a 45°C oven and the retained solids (extractives) were weighed. The cellulose, hemicellulose, lignin and ash content of the Soxhlet extracted fibre were quantified in parallel with non-extracted fibre as described in **2.2.2.1 - 2.2.2.3**.

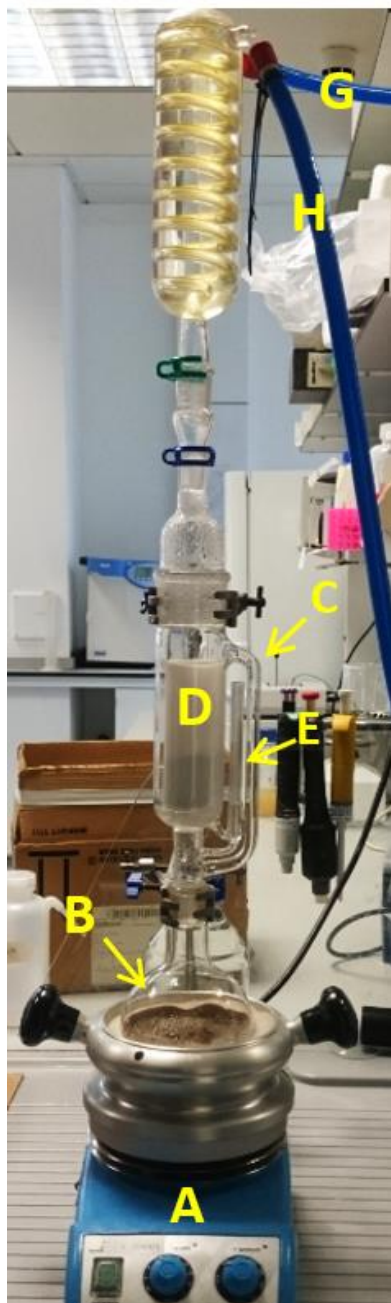


Figure 2.3: Anatomy of a Soxhlet extractor (image by author).

A = Electric heater

B = Distillation pot with boiling solvent

C = Distillation arm

D = Cellulose thimble containing biomass sample

E = Siphon

F = Condenser

G = Cooling water inlet

H = Cooling water outlet

The solvent (B) is boiled to the point of reflux by the electric heater (A). As the solvent enters the vapour phase it travels up through the distillation arm (C) into the upper half of the apparatus where the constant flow of cooling water (G & H) through the condenser (F) keeps conditions cool relative to the lower half of the apparatus. The solvent vapour condenses and runs down the sides of the apparatus into the central chamber where the sample is held in a thimble (D).

As the solvent accumulates in the central chamber the sample becomes immersed in solvent and any solvent-soluble components are extracted. Once the chamber is almost filled with solvent the siphon (E) drains the contents back down into the distillation pot. This cycle repeats several times an hour until all soluble, non-structural components are extracted from the biomass. All the extractables accumulate in the distillation pot and can be collected at the end of the experiment. The thimble can be dried and weighed to calculate the amount of biomass remaining after extraction.

2.3 Results

2.3.1 Composition of the Constructed OMSW Fibre

A pre-determined mixture of materials was used to produce OMSW fibre for this work (for a full list see 2.2.1 - Table 2.1), however, a wide range of complex and diverse materials had to be incorporated into the mixture to allow for a realistic feedstock to be generated. The constructed OMSW fibre was therefore still highly heterogeneous. Furthermore, the relatively harsh conditions produced by autoclave pre-treatment may have led to transfer or leaching of components from the inorganic fraction into the OMSW fibre fraction, adding further to the feedstock's compositional complexity. To gain a better understanding the composition of the OMSW fibre used throughout this project a range of relevant organic, inorganic, structural and non-structural components were characterised using a variety of well-established methods for the characterisation of lignocellulosic biomass.

2.3.2 Appearance and Moisture content

The OMSW fibre was dark brown in appearance and consisted largely of fibrous, spherical particles between 2 - 50 mm in size. **Figure 2.4-A** shows an image of the OMSW fibre taken immediately upon receipt (15 ml Falcon tube for scale). Some small plastic particles remained scattered throughout, as exemplified by the arrow in **Figure 2.4-B**.

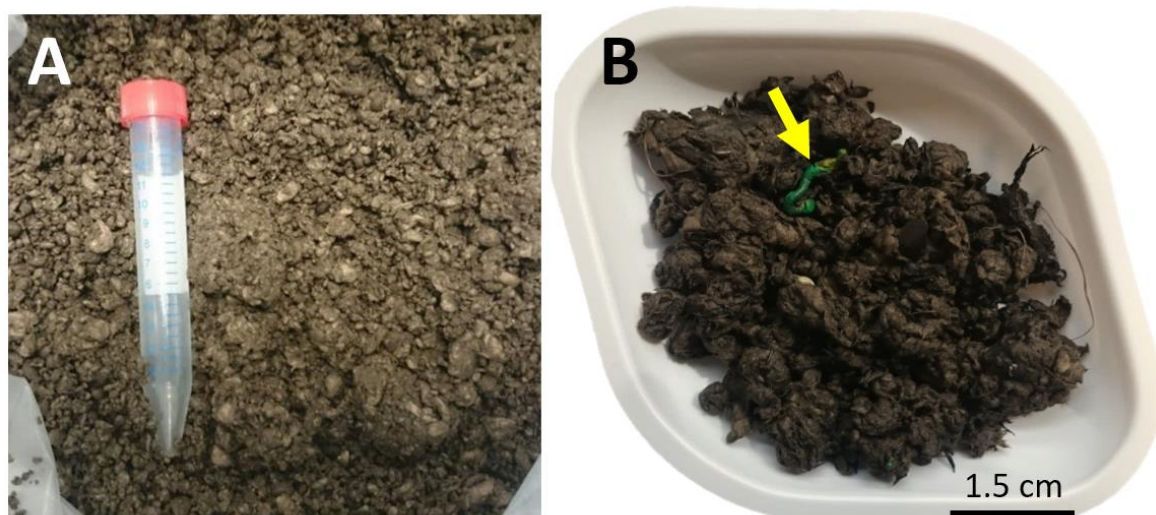


Figure 2.4: Appearance of the OMSW fibre

A: OMSW fibre with a 15 ml Falcon tube for scale. **B:** Representative sample of OMSW fibre (~10 grams) in a weighing boat.

Scale bar = 1.5 cm. The yellow arrow highlights a piece of residual plastic.

The OMSW fibre was immediately subjected to moisture and solids content analysis to accurately determine the amount of moisture retained from autoclaving. The fibre contained 70 ± 1 % moisture, however, the liquid did not drip unless forcefully squeezed, indicating a high absorption capacity.

2.3.3 Structural Components: Lignocellulose and Ash

Knowing the composition of the lignocellulose fraction and accurately quantifying the amount of cellulose and hemicellulose in a second-generation feedstock is critical for evaluating its valorisation potential and for informing subsequent experimental work. The lignocellulosic fraction of OMSW fibre was characterised using standard methods developed for compositional analysis of agricultural residues (for details see **2.1.5.3**). The OMSW fibre contained 57.7 ± 2.7 % (w/w) lignocellulose. The lignocellulose fraction was rich in cellulose, which comprised 65.2 ± 3.9 %. This equates to 37.6 ± 2.7 % of the total fibre dry mass. Lignin and hemicellulose made up 27.4 ± 2.8 % and 7.4 ± 2.9 % of the lignocellulose fraction, respectively (**Table 2.2**). Hemicellulose only made up a small portion of the total OMSW fibre (4.3 ± 0.1 %), but consisted of a wide range of monosaccharides, including D-fucose, L-arabinose, L-rhamnose, D-galactose, D-glucose, D-xylose, D-mannose, and D-galacturonic acid. A detailed breakdown of the monosaccharides present in the hemicellulose fraction is given in **Table 2.3**. D-xylose, D-glucose, D-mannose and D-galactose were the most abundant, comprising ~89% of the total hemicellulosic sugars. Overall the cellulose and hemicellulose fractions together made up 41.9 ± 2.7 % of the OMSW fibre. This is considered a reasonably large fraction of polysaccharides and compares favourably with previously published compositional analyses of OMSW which report anywhere between 7-50% lignocellulose (Barampouti et al, 2019; Mahmoodi et al, 2018b).

Inorganic structural components in lignocellulosic feedstocks are typically quantified as ash, which encompasses all mineral and inorganic structural materials that remain after biomass is oxidised above 575°C (Sluiter et al, 2008a). Ash content was measured as 14.74 ± 1.47 % w/w of the total OMSW fibre after dry oxidation at 600°C for 24 hours (for details see **2.2.2.1**). This is a considerably large fraction of ash compared to agricultural residues, which generally contain around 1-7% (Sorek et al, 2014). Due to the large paper fraction of OMSW, the majority of the ash fraction is likely to be composed of material from the inorganic filler and bulking agents used in paper manufacture. For example titanium oxide (TiO_2) and talc ($\text{Mg}_3\text{Si}_4\text{O}_{10}(\text{OH})_2$) are major components of paper

and are used as whiteners and/or fillers (Hubbe & Gill, 2016). Overall, structural materials in the form of lignocellulose and ash made up 62.44% of the total biomass.

Table 2.2: Composition of lignocellulose (cellulose, hemicellulose and lignin) in OMSW fibre

Results shown as percentage of total biomass and percentage of total lignocellulose. Hemicellulose and cellulose analysed by successive assays. Lignin analysed in a separate assay. For methods see 2.2.2.2 and 2.2.2.3.

$\pm SD$ = Standard deviation of minimum triplicate measurements.

| Component | % w/w Total Biomass | $\pm SD$ | % w/w Total Lignocellulose | $\pm SD$ |
|---------------|------------------------|-----------------------------|-------------------------------|-----------|
| Cellulose | 37.6 | ± 2.7 | 65.2 | ± 3.9 |
| Lignin | 15.8 | ± 0.4 | 27.4 | ± 2.8 |
| Hemicellulose | 4.3 | ± 0.1 | 7.4 | ± 2.9 |
| Total | 57.7 | ± 2.7 | - | - |

Table 2.3: Monosaccharide composition of the hemicellulose fraction of OMSW fibre.

Monosaccharides were isolated and analysed as described in 2.2.2.3.

$\pm SD$ = Standard deviation of triplicate measurements.

| Matrix Polysaccharide | % w/w Biomass | $\pm SD$ | % w/w Hemicellulose | $\pm SD$ |
|--------------------------|------------------|-------------------------------|------------------------|--------------------------------|
| L-Fucose | 0.016 | ± 0.002 | 0.372 | ± 0.049 |
| L-Arabinose | 0.272 | ± 0.016 | 6.401 | ± 3.862 |
| L-Rhamnose | 0.060 | ± 0.002 | 1.411 | ± 0.574 |
| D-Galactose | 0.405 | ± 0.023 | 9.533 | ± 5.406 |
| D-Glucose | 1.106 | ± 0.083 | 26.014 | ± 19.409 |
| D-Xylose | 1.336 | ± 0.032 | 31.419 | ± 7.473 |
| D-Mannose | 0.953 | ± 0.102 | 22.411 | ± 24.002 |
| D-Galacturonic Acid | 0.104 | ± 0.019 | 2.439 | ± 4.520 |
| Total | 4.251 | ± 0.139 | 100 | ± 32.765 |

In order to evaluate the reproducibility of the lignocellulosic fraction of OMSW fibre produced on the Wilson Bio-Chemical Pilot Rig, two further batches of OMSW fibre were produced using the same MSW mixture (for details see 2.2.1 – Table 1). The lignocellulose composition of these batches (hereafter called Batch 2 and Batch 3) was determined and is shown alongside the original batch of OMSW fibre (Batch 1) in Figure 2.5. Batch 1 and 2 were produced under the same conditions and were remarkably similar in composition, although hemicellulose levels were slightly lower in Batch 1. Batch 3 on the other hand was

treated under shorter, harsher conditions and contained a slightly larger cellulose fraction. These results may be skewed slightly however as there was large standard error between replicates. Overall the composition between batches is highly similar, demonstrating that the Wilson Bio-Chemical Pilot Rig can be used to reproducibly produce MSW fibre with a consistent lignocellulose fraction for use in empirical studies of OMSW valorisation.

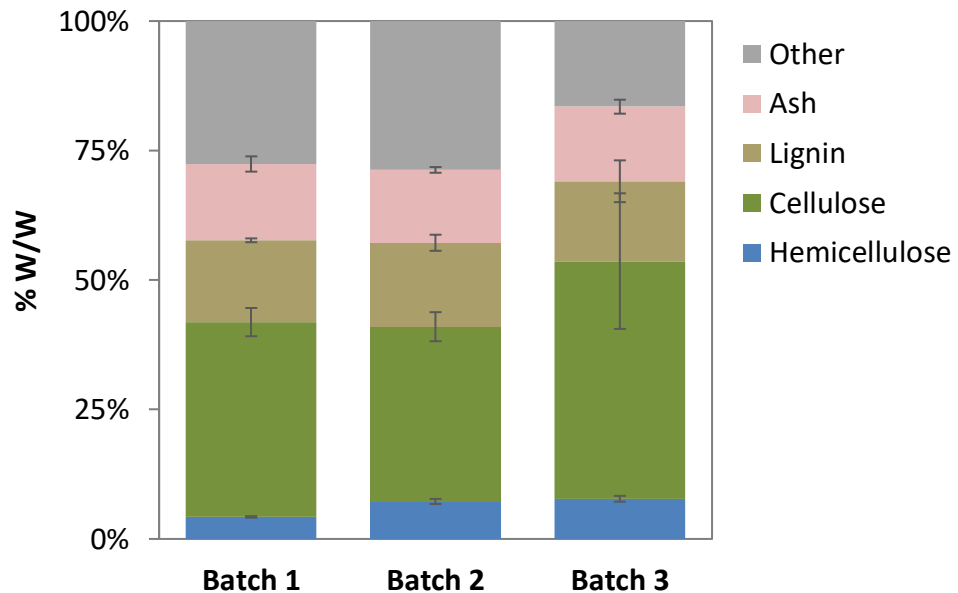


Figure 2.5: Composition of lignocellulose (cellulose, hemicellulose and lignin) in three batches of OMSW fibre

All three batches of OMSW fibre were produced on the Wilson Bio-Chemical pilot rig as described in 2.2.1. **Batch 1** and **Batch 2** were pre-treated at 6 bar and 160°C for 45 min. **Batch 3** was pre-treated at 9 bar and 180°C for 20 min. Note that **Batch 1** was used in all subsequent work throughout this project. Results are shown as percentage of the total sample dry weight (%w/w). Hemicellulose and cellulose analysed by successive assays. Lignin analysed in a separate assay. For methods see 2.2.2.2 and 2.2.2.3. Error bars show standard deviation of minimum triplicate measurements.

2.3.4 Non-Structural Components: Metals

After analysis of the structural materials in the OMSW fibre it was calculated that 37.56% of mass remained unaccounted. To characterise the outstanding components of the OMSW fibre, non-structural materials were analysed. Firstly, the levels of metals were measured as OMSW typically contains a wide range of metal contaminants that are leached from inorganic materials in MSW. To isolate the metals OMSW fibre was digested with concentrated nitric and sulphuric acid and treated in a microwave digestion system (for details see **2.2.2.6**). Metals were then measured by ionisation-coupled plasma mass spectrometry (ICP-MS). ICP-MS is a highly sensitive technique that can detect a wide array of metal species. A multi-element environmental reference standard was selected to analyse a broad range of environmentally relevant metal species including Silver (Ag), Aluminium (Al), Arsenic (As), Barium (Ba), Beryllium (Be), Calcium (Ca), Cadmium (Cd), Cobalt (Co), Chromium (Cr), Copper (Cu), Iron (Fe), Potassium (K), Magnesium (Mg), Manganese (Mn), Molybdenum (Mo), Sodium (Na), Nickel (Ni), Lead (Pb), Antimony (Sb), Selenium (Se), Tellurium (Tl), Vanadium (V), Zinc (Zn), Thorium (Th), and Uranium (U). Metals comprised 1.33 ± 0.26 % of the total dry weight and all metals except Th, Mo and Ag were detected in the OMSW fibre.

Metals can be toxic to microorganisms and may pose a major limitation in bioprocesses development. The type of damage inflicted is highly dependent on the metal species and environmental conditions. Some general examples of metal-dependent inhibition include electron transport chain inhibition, induction of free-radical chain reactions in the cytoplasm, competitive inhibition of transporters and mismetallation of enzymes (Lemire et al, 2013). A washing experiment was carried out to assess the solubility of the metals in OMSW fibre and evaluate the potential of using a washing step to eliminate metals prior to bioprocessing. OMSW fibre was washed three times with 95°C Milli-Q water to remove soluble material. The remaining solids were dried and subjected to metal analysis by ICP-MS (for details see **2.2.2.7**). The results of these analyses are given in **Table 2.4**, which lists the levels of each metal measured in the OMSW fibre (unwashed) and in washed OMSW fibre. Concentrations are presented in millimoles of metal per kilogram of OMSW fibre (mmol/Kg) and the percentage change in concentration after washing is given for each species (note that the mass loss to washing was accounted for when calculating percentage change).

Table 2.4: Metal levels in washed and unwashed OMSW fibre

OMSW fibre was washed three times with 95°C MilliQ water to remove all soluble material. The remaining solids were dried and subjected to metal analysis by Ionisation-Coupled Plasma Mass Spectrometry (ICP-MS) in parallel with samples of unwashed OMSW fibre. Mass loss to washing was accounted for when calculating the percentage change in metal concentration. For details see 2.2.2.7. Metals listed in order of abundance in unwashed OMSW fibre. \pm SD = Standard deviation of minimum triplicate measurements.

Metals shown in order of abundance in unwashed fibre. Ca= Calcium, Al = Aluminium, K = Potassium, Fe = Iron, Na = Sodium, Mg = Magnesium, Zn = Zinc, Mn = Manganese, Cu = Copper, Ni = Nickel, Ba = Barium, Cr = Chromium, V = Vanadium, Pb = Lead, Sb = Antimony, Co = Cobalt, As = Arsenic, Cd = Cadmium, U = Uranium, Tl = Tellurium, Ag = Silver, Mo = Molybdenum, Th = Thorium.

| Metal | Concentration (mmol/Kg) | | | | Change (%) |
|-------|-------------------------|---------------|----------|----------------|-----------------|
| | Unwashed | \pm SD | Washed | \pm SD | Increase |
| | | | | | Decrease |
| | | | | | Not Significant |
| Ca | 2,091.93 | \pm 184.75 | 2,066.03 | \pm 102.92 | -0.94 |
| Al | 166.90 | \pm 27.50 | 179.44 | \pm 30.98 | +5.70 |
| K | 66.53 | \pm 6.44 | 14.82 | \pm 2.83 | -58.96 |
| Fe | 62.44 | \pm 28.48 | 44.02 | \pm 5.45 | -22.38 |
| Na | 57.48 | \pm 5.43 | 3.36 | \pm 1.64 | -71.42 |
| Mg | 44.44 | \pm 6.00 | 40.00 | \pm 7.47 | -7.58 |
| Zn | 2.47 | \pm 1.65 | 1.60 | \pm 0.26 | -26.59 |
| Mn | 0.76 | \pm 0.06 | 0.69 | \pm 0.064 | -6.85 |
| Cu | 0.33 | \pm 0.06 | 0.30 | \pm 0.073 | -7.30 |
| Ni | 0.33 | \pm 0.25 | 0.12 | \pm 0.10 | -48.25 |
| Ba | 0.16 | \pm 0.02 | 0.18 | \pm 0.063 | +7.17 |
| Cr | 0.11 | \pm 0.01 | 0.15 | \pm 0.10 | +25.16 |
| V | 0.04 | \pm 0.01 | 0.035 | \pm 0.010 | -9.43 |
| Pb | 0.0138 | \pm 0.0031 | 0.016 | \pm 0.0055 | +13.78 |
| Sb | 0.0104 | \pm 0.0006 | 0.0061 | \pm 0.001 | -31.50 |
| Co | 0.0093 | \pm 0.0009 | 0.0090 | \pm 0.002 | -2.40 |
| As | 0.0012 | \pm 0.0007 | 0.0025 | \pm 0.0023 | +83.93 |
| Cd | 0.0003 | \pm 0.0001 | 0.00062 | \pm 0.00040 | +82.05 |
| U | 0.0005 | \pm 0.0001 | 0.00045 | \pm 0.000081 | -1.01 |
| Tl | 0.00003 | \pm 0.00002 | 0.000051 | \pm 0.000027 | +41.59 |
| Ag | - | - | 0.0047 | \pm 0.0066 | +100.00 |
| Mo | - | - | - | - | - |
| Th | - | - | - | - | - |

Calcium was by far the most abundant element detected. Present at just over 2 moles per Kg of fibre, Calcium was highly insoluble, showing no significant reduction after washing. As calcium carbonate (CaCO_3) is a major component of paper (Hubbe & Gill, 2016), the waste paper fraction of OMSW is the most likely source of the high calcium levels. Ca is often reported as the most abundant metal in OMSW (Barampouti et al, 2019). The other metal species were present at significantly lower levels, in the millimole to micromole per Kg range, and varied greatly in solubility. The most soluble species, in descending order, were Na (-71.42%), K (-58.96%), Ni (-48.35%), Sb (-31.50%), Zn (-26.59%), Fe (-22.38%), while the concentrations of V, Mg, Cu, Mn, As, Co, U, Ba and Al varied by less than $\pm 10\%$ and can be considered as remaining unchanged by washing.

A number of metal species increased in concentration, including As (+83.93%), Cd (+82.05%), Tl (+41.59%), Cr (+25.16%) and Pb (+13.78%). $24 \pm 4\%$ of the OMSW fibre was lost after the three successive washes. This soluble fraction was accounted for when calculating the percentage change and should have corrected for any resultant enrichment in metals. Furthermore, Ag was not detected at all in the original fibre, but trace amounts were found in the washed fibre samples. Overall this indicates that the metals are unevenly distributed throughout the fibre.

2.3.5 Non-Structural Components: Extractives

The metal washing experiment demonstrated that OMSW fibre contained a large fraction of soluble material (24%). Soxhlet extraction is a standard technique used for the removal of materials that are not chemically bound to the lignocellulose (i.e. non-structural components), including a variety of inorganic and organic materials such as phenols, aromatics, terpenes, waxes, oils and non-structural carbohydrates (Sluiter et al, 2008b). Soxhlet extraction involves rinsing biomass with water or ethanol under reflux in a Soxhlet apparatus. A Soxhlet apparatus consists of a distillation arm, a central chamber in which the biomass sample is held, and a condenser. The apparatus is attached on top of a distillation pot holding a solvent. When the solvent enters the vapour phase, it travels upwards through the distillation arm into the central chamber where the cooler conditions generated by the condenser cause the liquid to condense. Over time the sample becomes immersed in solvent and any soluble material is dissolved. Once the chamber is filled the solvent automatically drains back down into the distillation pot. Consequently only soluble components of the biomass are extracted and concentrated in the distillation pot while any

insoluble material remains in the chamber. The extraction cycle repeats several times an hour until all extractable material has been solubilised. The Soxhlet apparatus is described in greater detail in **Figure 2.3** (section **2.2.2.8**).

Solubles in the OMSW fibre were extracted, first with water and subsequently with ethanol. Soxhlet extraction with water leads to solubilisation of components such as non-structural sugars, nitrogenous/proteinaceous material and inorganic compounds. Extraction with ethanol solubilises components such as waxes, oils or chlorophyll (Sluiter et al, 2008). In total 17.10 ± 2.78 % of OMSW fibre was solubilised by Soxhlet extraction, with the water soluble and ethanol soluble fractions accounting for 9.15 ± 2.62 % and 7.95 ± 0.92 % of the total, respectively. Soxhlet extraction has also been demonstrated to improve the accuracy of methods used for lignocellulose compositional analysis as it removes interfering compounds (Sluiter et al, 2008b). Lignocellulose compositional analysis was therefore also carried out on the Soxhlet extracted OMSW fibre to evaluate any influence of non-structural components on compositional methods. Oil and protein were also measured in the OMSW fibre (for details see **2.2.2.4** and **2.2.2.5**) because these are non-structural components that can be used as a source of nutrients by microorganisms during fermentations. The results of all analyses of OMSW fibre composition are shown in **Table 2.5** alongside the composition of Soxhlet extracted OMSW fibre. The concentration of protein and oil are shown as a fraction of the ethanol and water extractable material, respectively, as they would have been solubilised in these steps.

The compositional profiles of the Soxhlet extracted and non-extracted MSW fibre were very similar. The levels of cellulose were closely comparable, with extracted fibre containing 36.85 ± 6.15 % cellulose on average compared to 37.61 ± 2.73 % measured in the original fibre. Lignin content decreased slightly after extraction, from 15.80 ± 0.37 % to 11.28 ± 0.33 %, indicating that soluble phenolic compounds such as tannins could have been contributing to the lignin concentrations measured in the original fibre. Ash content was also slightly lower, which may reflect the solubilisation of some organic compounds, but this variability is not significant when accounting for the standard deviation (14.74 ± 1.47 % ash in the original fibre versus 13.23 ± 0.44 % in extracted fibre). A 29.4% decrease in hemicellulose content was observed after Soxhlet extraction (**Figure 2.6**). The largest reduction was in D-glucose abundance, which decreased by 57%. This glucose is likely derived from starches as these are easily solubilised. Minor decreases were also observed

in the other sugars, which may have been hemicellulose-derived mono or disaccharides which are more readily washed out than polysaccharides.

Table 2.5: Composition of OMSW fibre and Soxhlet extracted OMSW fibre
Values reported as a percentage of the dry weight of OMSW fibre (%w/w).

| Component | Composition (% w/w) | | | |
|--------------------------------|---------------------|------------|-------------------------------|------------|
| | OMSW fibre | | Soxhlet extracted OMSW fibre* | |
| Cellulose | 37.61 | ± 2.73 | 36.85 | ± 6.15 |
| Hemicellulose | 4.25 | ± 0.14 | 3.00 | ± 0.01 |
| Lignin | 15.80 | ± 0.37 | 11.28 | ± 0.33 |
| Ash | 14.74 | ± 1.47 | 13.23 | ± 0.44 |
| Metals | 1.33 | ± 0.26 | - | - |
| Total extractives (water) | 9.15 | ± 2.62 | - | - |
| Protein | 3.23 | ± 0.40 | - | - |
| Other | 5.92 | <i>n/a</i> | - | - |
| Total Extractives (ethanol) | 7.95 | ± 0.92 | - | - |
| Oil | 1.72 | ± 0.92 | - | - |
| Other | 6.23 | <i>n/a</i> | - | - |
| Total unaccounted mass: | 9.17 | <i>n/a</i> | 35.64 | <i>n/a</i> |

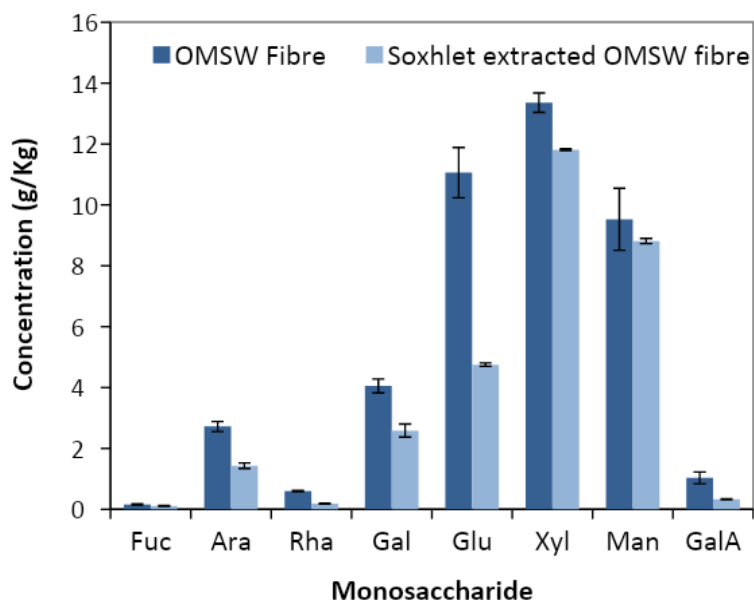


Figure 2.6: Concentration of hemicellulose-derived monosaccharides in OMSW fibre and Soxhlet extracted OMSW fibre

Fuc = Fucose; *Ara* = Arabinose; *Rha* = Rhamnose; *Gal* = Galactose; *Glu* = Glucose; *Xyl* = Xylose; *Man* = Mannose; *GalA* = Galacturonic acid.

2.3.6 Summative Composition

To give a clear overview of the total composition of OMSW fibre, a pie chart showing the collated percentage composition data is provided in **Figure 2.7**. Hemicellulose composition is shown separately to provide a summary of monosaccharide abundance. Mass closure was achieved to 90.83% when all compositional analyses were combined. Only 9.17% of total dry weight could not be accounted for.

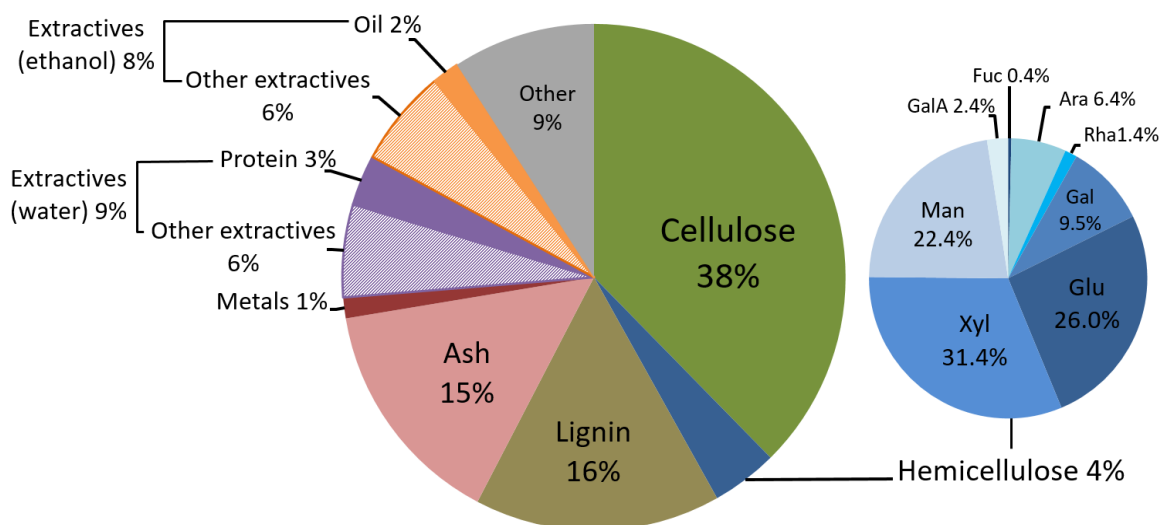


Figure 2.7: Percentage composition of OMSW fibre

All data are averages of at least triplicate measurements.

Appendix I provides all compositional data inclusive of standard deviations.

Appendix II provides a list of all metals and their respective concentrations and standard deviations.

Glu = Glucose; *Xyl* = Xylose; *Man* = Mannose; *Fuc* = Fucose; *Ara* = Arabinose;

Rha = Rhamnose; *Gal* = Galactose; *GalA* = Galacturonic acid.

Values are given as a percentage of the dry weight of OMSW fibre (%w/w).

Extractives (water) = % w/w of non-structural material extractable by Soxhlet extraction with water; *Extractives (ethanol)* = % w/w of non-structural material extractable by Soxhlet extraction with ethanol; Protein and oil were measured by separate analyses but are water and ethanol soluble, respectively, and are therefore reported as part of the extractable fractions. The

2.4 Discussion

OMSW is significantly heterogeneous and variable in composition compared to other lignocellulosic waste feedstocks. Agricultural and forestry by-products are generally highly homogeneous, compositionally consistent and inert, while the make-up of MSW differs considerably on both geographical and temporal scales. The abundance and composition of the organic fraction in particular are greatly influenced by prevailing socio-economic conditions and waste management systems (Kaza et al, 2018). Furthermore, OMSW comes into close contact with various inorganic wastes that may introduce toxic or inhibitory elements and compounds, adding further unpredictability to its composition. Collectively these factors make OMSW a challenging feedstock for empirical study and one that has consequently been underexplored for bio-manufacturing (Matsakas et al, 2017).

With the aim of tackling some of the challenges outlined above, the OMSW fibre used in this project was produced on a commercially proven autoclave pre-treatment system with a predetermined mixture of MSW, constructed according to national statistics on MSW composition in the UK. This novel approach enabled production of material that was representative of real-world OMSW as it would arise when homogenised at industrial volumes. OMSW fibre produced in this way also has a reproducible lignocellulose composition, as demonstrated by the consistent cellulose, hemicellulose and lignin fractions measured in three separately produced batches of OMSW fibre (**Figure 2.5**). Despite the benefits in reproducibility gained from this approach, the constructed fibre was still highly complex: ~41% was made up of non-structural components, ash and other material for which the composition is mostly indeterminable (**Table 2.5**). Such a large fraction of unknown material may make it challenging to disentangle the precise cause if growth inhibition arises when fermentation experiments are carried out.

Nevertheless, the compositional analysis revealed that the OMSW fibre contained a large polysaccharide fraction of approximately 42% (37.6 \pm 2.7 % cellulose, 4.3 \pm 0.1 % hemicellulose) (**Table 2.2**). Forestry and agricultural wastes generally contain 24–54% cellulose, 11–38% hemicellulose and 6–31% Lignin (Garrote et al, 1999; Klinke et al, 2001). The cellulose fraction in the OMSW fibre used in this study falls within the upper range of this, making it a potentially practicable fermentation feedstock. The fibre also contained small proportions of oil (1.7%) and protein (3.2%) which could be used as nutrients by microorganisms in the fermentation step. However, the hemicellulose fraction is far below

average of typical agricultural residues (Adhikari et al, 2018; Singh & Bihari Satapathy, 2018).

Compared to other reports of OMSW composition in the literature (**Figure 2.8**) the OMSW fibre used in this project had over twice the reported cellulose content, but hemicellulose levels were still in the lower range. Lignin levels were also above average, while the oil and protein levels measured in OMSW fibre were the lowest of any study (Barampouti et al, 2019). Interestingly, the cellulose content was similar to levels reported for other cities in the UK: 39.7% and 49% for Lester (Zhang et al, 2012) and Nottingham (Li et al, 2012a), respectively. That said, OMSW from Newtown, UK, contained only 5.5% cellulose, while the protein levels reported for this city were 25.8% - almost double those of the other UK regions (Barampouti et al, 2019). Significant regional differences in MSW composition can exist even within the same country because of local variation in socio-economic conditions and waste management practices (Barampouti et al, 2019; Kaza et al, 2018). Compositional variability is also evident across cities in Italy (**Figure 2.8, Padova, Treviso & Milan**). This has important ramifications for the development of an integrated MSW biorefinery as not all sources of OMSW will be viable for bioprocessing because the polysaccharide fraction may be impracticable.

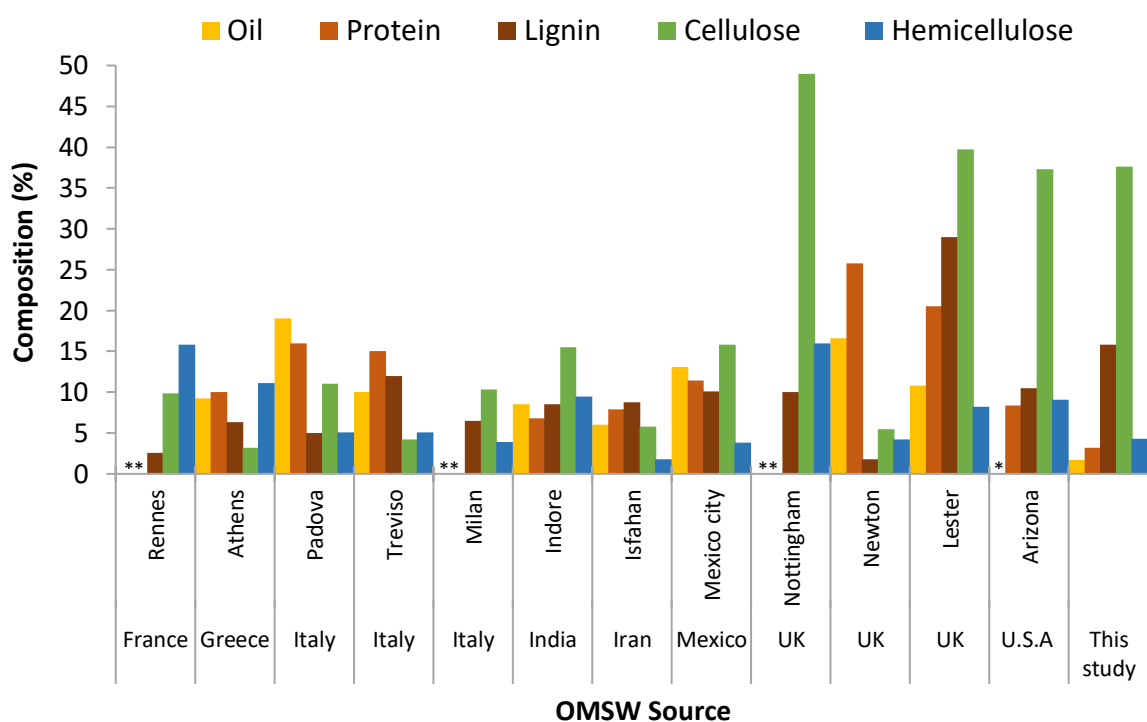


Figure 2.8: Percentage composition of OMSW reported for a range of cities and in this study

Figure by author, using data from Barampouti et al, (2019).

*Component not measured.

Another critical feature of OMSW is its metal content, due to the potential of various metal species for inhibiting or enhancing enzymatic hydrolysis and microbial fermentation processes. Pd, Ti, Sn, Bo, Br, and W were not tested for in the OMSW fibre, but the other metals reported to be most abundant OMSW by Barampouti et al (2019) were all detected with similar relative abundance (**Table 2.4**). The most toxic metals for microorganisms are non-essential metals (i.e. metals with no established function in biological systems, generally found at <1 µg/g in the environment). These species are highly inhibitory to biological systems even at extremely low levels (Lemire et al, 2013; Tchounwou et al, 2012; Wood & Wang, 1983). Worryingly, a wide range of non-essential metals were found in the OMSW fibre, including Al, Sb, As, Cd, Cr, Co, Ni, As, Pb and V. However, the chemistry of microbial metal toxicity is highly complex and dependent upon the metal species, its ionisation state, synergistic interactions with other metals, the environmental conditions (e.g. pH, redox potential) and the physiology of the fermentative microorganism (Bird et al, 2013; Chandrangu et al, 2017). Thus, the abundance of toxic metals in OMSW does not immediately rule out the possibility of developing a working bioprocess. Furthermore, metals with the greatest toxicity potential were not solubilised significantly after fibre was subjected to extensive washing and may therefore not cause a problem during fermentation. That said, metals could become mobilised under the conditions of enzymatic hydrolysis (between 50-55°C and pH 4-6, depending on the enzyme cocktail used). The behaviour of metals during hydrolysis is still unknown and will require further investigation.

A further consideration is that the maximum solid loading achievable for large scale hydrolysis of lignocellulosic biomass is generally ≤20% (Kristensen et al, 2009a; Modenbach & Nokes, 2012), therefore the final metal concentration in OMSW fibre hydrolysate will be at least five-fold more dilute. The theoretical concentration of each metal that would be released from OMSW fibre in a 20% total solids (TS) hydrolysis was calculated (**Table 2.6**). This shows that after hydrolysis the majority of metals would fall below the minimum inhibitory concentration (M.I.C.) of the model fermentative microorganism *Escherichia coli*, even when the highest values reported by Wilson Bio-Chemical for industrially produced OMSW fibre are applied. However, the calculated concentrations for Aluminium (Al) and Iron (Fe) in hydrolysate of the constructed OMSW fibre used in this project would be up to 15-fold over the M.I.C. for *E. coli* and could therefore potentially have a negative effect on microbial fitness in fermentation.

Table 2.6: Theoretical concentration of metals in hydrolysate of OMSW fibre after a 20% total solids hydrolysis.

(Data used with permission from Wilson Bio-Chemical Ltd.)

*M.I.C = Minimum inhibitory concentration for Escherichia coli. Concentrations of each metal were calculated assuming that 100% of the metals measured in the dry OMSW fibre would be solubilised in a 20% w/v total solids loading hydrolysis. Values for industrial OMSW fibre were calculated using the highest recorded measurement of each metal in a 32-month period. *Calculated using data for the highest recorded measurements of each metal.*

| Metal | Theoretical concentration in OMSW fibre hydrolysate (mM) | | M.I.C (<i>E. coli</i>) [mM] | Reference |
|-----------|--|--------------|-------------------------------|-----------------------|
| | Industrial (max.)* | This project | | |
| Calcium | - | 213.08 | <i>n/a</i> | - |
| Aluminium | - | 33.38 | 2.0 | (Nies, 1999) |
| Iron | - | 12.49 | 1.0 | (Kalantari, 2008) |
| Magnesium | - | 8.89 | <i>n/a</i> | - |
| Potassium | - | 13.31 | <i>n/a</i> | - |
| Sodium | - | 11.50 | <i>n/a</i> | - |
| Zinc | 1.54 | 0.49 | 2.0 | (Beard et al, 1997) |
| Manganese | - | 0.15 | 1.0 | (Nies, 1999) |
| Copper | 2.46 | 0.066 | 1.0 | (Nies, 1999) |
| Nickel | 0.25 | 0.066 | 20.0 | (Nies, 1999) |
| Chromium | 0.33 | 0.022 | 1.0 | (Nies, 1999) |
| Lead | 0.15 | 0.0028 | 5.0 | (Nies, 1999) |
| Vanadium | - | 0.0080 | 1.0 | (Nies, 1999) |
| Antimony | - | 0.0021 | 5.0 | (Nies, 1999) |
| Cobalt | - | 0.0019 | 1.0 | (Majtan et al, 2011) |
| Arsenic | 0.018 | 0.00024 | 3.0 | (Silver et al, 1981) |
| Cadmium | 0.004 | 0.000060 | 0.6 | (Hossain et al, 2012) |

A major limitation of the OMSW fibre used for this project is that it cannot capture the variability in metal levels observed on an industrial scale, which can fluctuate drastically, even within the same region. **Figure 2.9** below shows metal levels in OMSW fibre measured by Wilson Bio-Chemical Ltd. over 32 months on an industrial Wilson System® at a single site in the UK. While some elements such as Zn are consistent in abundance, others like Cu, F, As and Mo show occasional spikes and seasonal variability. Metal concentrations in the constructed fibre were also at least 50% below the average concentration measured in the industrial fibre. This is illustrated in **Table 2.7** below which compares the average and maximum levels of metals measured in the industrially produced Wilson Fibre® to the fibre used in this project. This highlights the fact that any bioprocess developed around OMSW

fibre will require a robust fermentative microorganism capable of tolerating fluctuations in a wide range of potentially toxic metal species.

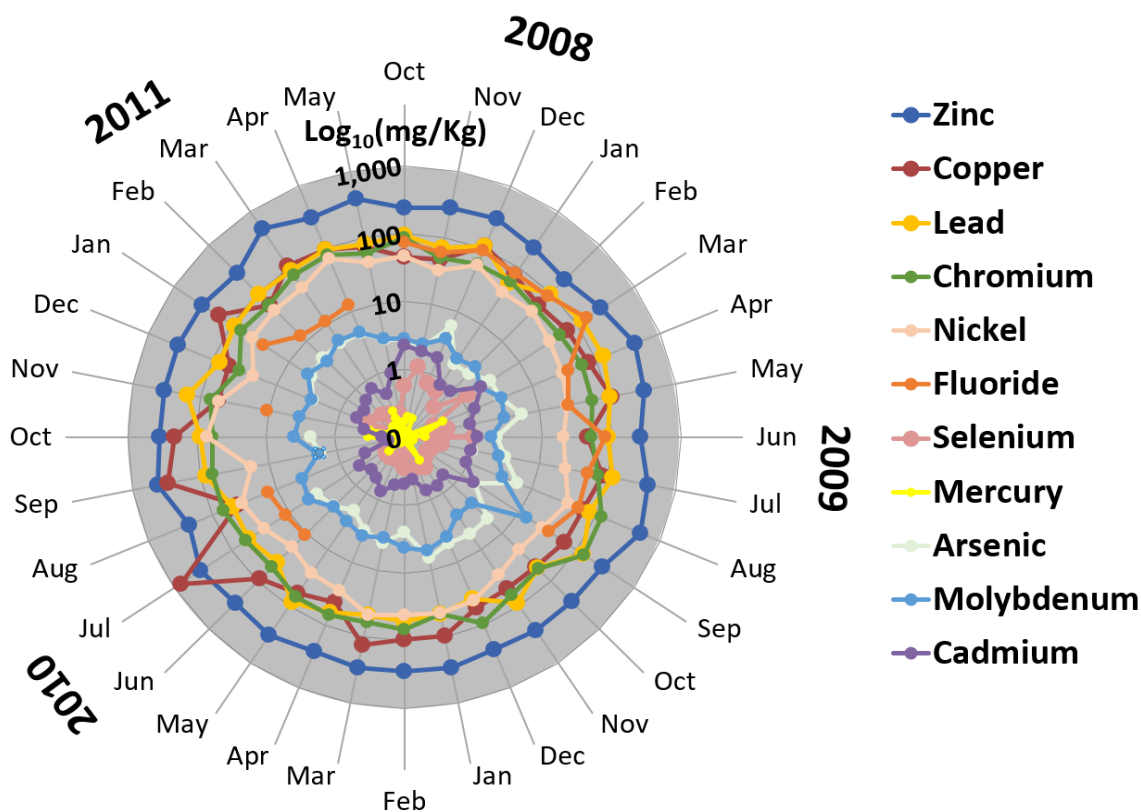


Figure 2.9: Abundance of metals in Wilson Fibre® produced on an industrial Wilson System® over 32 months

Data used with permission from Wilson Bio-Chemical Ltd. Concentration of metals shown as log₁₀ mg/Kg.

Overall the compositional analysis revealed that OMSW fibre has the potential to be a practicable feedstock for bioprocessing. It contains a large cellulose fraction and some nutrients such as oil and protein which may be beneficial to microorganisms during fermentation. The metal fraction poses a potential limitation as this could induce stress or inhibition of fermentative microorganisms. However, many of the metals that have the highest potential for microbial toxicity were also shown to be the least soluble, including Al, Ag, As, Pb and Cr. Further work is needed to test how metals will behave after hydrolysis and evaluate the extent to which they may affect microbial fermentation of OMSW fibre hydrolysate.

Table 2.7: Metal levels measured in industrial OMSW compared to metal levels in OMSW used in this project.

Note –Selenium and Molybdenum were measured in the industrial OMSW but not found in the constructed OMSW. Fluoride and Mercury were measured in the industrial OMSW but not in the constructed OMSW. For detailed methods see **2.2.2.6**.

$\pm SD$ = Standard deviation of minimum triplicate measurements.

| Metal | Concentration of OMSW fibre (mmol/Kg) | | | | |
|-----------------|---------------------------------------|-------------|---------|--------------|--------------|
| | Industrial* | | | This Project | |
| | Average | $\pm SD$ | Maximum | Average | $\pm SD$ |
| Zinc | 4.810 | ± 1.117 | 7.709 | 2.470 | ± 1.647 |
| Copper | 1.707 | ± 2.119 | 12.275 | 0.331 | ± 0.063 |
| Chromium | 1.273 | ± 0.382 | 1.646 | 0.112 | ± 0.012 |
| Nickel | 0.629 | ± 0.231 | 1.235 | 0.332 | ± 0.246 |
| Lead | 0.404 | ± 0.145 | 0.767 | 0.014 | ± 0.003 |
| Arsenic | 0.044 | ± 0.022 | 0.088 | 0.001 | ± 0.001 |
| Cadmium | 0.008 | ± 0.005 | 0.020 | 0.0030 | ± 0.0001 |

*Data used with permission from Wilson Bio-Chemical Ltd.

Chapter 3: Evaluating Hydrolysis, Fermentability and Biogas Production from OMSW Fibre

3.1 Introduction

Saccharification can be a significant barrier to the commercial viability of a bioprocess, requiring high titres of costly enzymes and large volumes of water to achieve efficient conversion of feedstock to sugars (Zhao et al, 2012). OMSW is largely composed of pre-processed lignocellulosic materials such as paper and card which are easier to hydrolyse than raw plant material, but typically also contains compounds that may be inhibitory to enzyme activity such as metals, calcium carbonate (CaCO_3), lignin and plastics. Optimising hydrolysis methods is therefore critical to developing a viable biorefining process around OMSW.

Several publications have investigated industrially relevant methods for enzymatic hydrolysis of OMSW. Jensen *et al.* (2010) demonstrated that organic material in mixed MSW could be solubilised using cellulases and the inorganic components isolated by sieving. This technique is economical, rapid and effective, resulting in solubilisation of 90% of the organic fraction and is currently used to isolate and saccharify OMSW for biogas production at the REnaissance power plant in Norwich, England (Novozymes, 2016). As part of her PhD thesis Puri (2014) investigated methods for hydrolysing paper pulp isolated from MSW using a more traditional SSF approach. The OMSW paper pulp was produced by Fiberight Ltd. on an industrial autoclave and washed to remove contaminants such as plastic, metals or minerals. The most effective hydrolysis yields were achieved using the industrial enzyme cocktail Cellic CTec3 in a two-stage hydrolysis involving an intermediary fermentation step with *S. cerevisiae* to alleviate product inhibition. Over four days 68% of available sugars were hydrolysed despite a relatively high solids content of $\geq 18.5\%$. The final D-glucose concentration was 8% (w/w), which is just within the industrially viable range (Puri et al, 2013).

Li *et al.* (2012a) also investigated saccharification of an OMSW fibre generated on an industrial autoclave for 45 minutes at 165°C and 100 psi. The fibre was dried, milled to varying particle sizes and hydrolysed. A 53% conversion of the cellulose and hemicellulose to sugars was achieved using 60 g/L fibre with 90 mg/g *Trichoderma reesei* cellulase. Based on their saccharification yields the authors calculated that industrial titres of ethanol (152

L per tonne of fibre) could potentially be produced, assuming efficient fermentation with *S. cerevisiae*.

Farmanbordar et al (2018b) tried to improve hydrolysis yields from OMSW by investigating different pre-treatment methods. OMSW was collected from an urban waste compost plant and subjected to pre-treatment with water or 0.5% w/w sulphuric acid at 140°C for 1 hour. Pre-treatment was carried out in a 500 ml high-pressure reactor with a total solids (TS) loading of 10% w/w using the commercial enzyme cocktail Cellic Ctec2. The highest sugar yields were attained with dilute acid pre-treated OMSW, which produced 21.33 g/L D-glucose and 1.85 g/L D-xylose. By comparison, liquid hot water pre-treated OMSW only yielded 14.07 g/L and 3.04 g/L D-glucose and D-xylose, respectively. Untreated OMSW had the poorest D-glucose yield, at 10 g/L, but a higher D-xylose yield (1.98 g/L) than the dilute acid treated samples because dilute acid treatments tend to solubilise hemicellulose (Farmanbordar et al, 2018b). Pre-treatment is a critical factor in improving biomass accessibility for enzymes so that efficient sugar yields can be attained, however, there is always a balance to be struck between the potential gains in hydrolysis efficiency and the cost of the pre-treatment. Pre-treatments often require expensive chemicals and significant energy for heating and cooling (Jönsson & Martin, 2016). In the context of MSW valorisation, autoclaving is a promising technology because it acts both to help separate and pre-treat OMSW in a single step (Li et al, 2012a; Meng et al, 2019).

Industrially relevant saccharification must be carried out at relatively high concentrations ($\geq 15\%$ total solids (TS)) as this is required to achieve sufficient sugar yields for viable fermentation (Larsen et al, 2008). However, higher TS concentrations have an inhibiting effect on substrate conversion. Increasing TS is not only technically challenging due to limitations in rheology, but also produces a drop in conversion efficiency, known as the solids effect (Kristensen et al, 2009a). The precise cause of this effect is still poorly understood. Although increasing the enzyme concentration reduces enzyme inhibition and can alleviate the effect to an extent, there is evidence that enzyme efficiency is also influenced by the associated increase in viscosity which slows enzyme diffusion. Furthermore, increasing diffusion by mechanical agitation only marginally improves yield (Wang et al, 2011a). Other factors contributing to enzyme inhibition include non-specific binding to lignin, which sequesters enzymes and causes them to lose functionality, and inhibition by metals (Berlin et al, 2006).

Non-ionic surfactants such as polyethylene glycol (PEG) can improve enzyme efficiencies by reducing unproductive enzyme adsorption to lignin or plastics (Borjesson et al, 2007). Although PEG did not improve saccharification in terms of viscosity or particle size distribution in the study by Jensen et al, (2011), work by Puri et al (2014) found that addition of PEG improved enzyme activity on OMSW. At the same time, tween, a surfactant which has been shown to potentiate enzymes in other studies, did not have a noticeable effect. Due to the highly heterogeneous composition of OMSW and the irreproducibility of material used in studies comparing effective hydrolysis methods across publications is challenging.

In a follow-up to their cellulase liquefaction study, Jensen et al. (2011) sought to increase hydrolysis yields by investigating how metals in waste water from MSW affect enzyme activity. The wastewater from this process contained several known inhibitors of cellulases (copper, mercury, lead, zinc, iron, chromium) and stimulators (calcium, magnesium, manganese), which could influence sugar yields. However, cellulase activity on filter paper was not significantly affected upon addition of MSW wastewater, indicating cellulases are relatively robust in the presence of MSW-derived metals (Jensen et al, 2011). That said, metals can be greatly inhibitory to fermentative microorganisms. Given the significant number of publications that have already investigated saccharification methods for OMSW, the development of hydrolysis methods for OMSW fibre is not a major objective of this thesis. Instead, this chapter focuses on producing an industrially relevant hydrolysate that contains realistic levels of inhibitors and metals and will examine the fate of metals during the hydrolysis process.

3.1.1 Aims of this Chapter

This chapter aims to investigate the saccharification potential of autoclave pre-treated OMSW fibre, evaluate OMSW fibre hydrolysate composition, assess its fermentability and investigate the possibility of biogas production from hydrolysis waste streams. Successful hydrolysis methods will be scaled-up to produce a large volume of high-sugar OMSW fibre hydrolysate, which will be used to screen a collection of fermentative microorganisms as part of **Chapter 4**. A methodological overview for this chapter is provided in **Figure 3.1**.

Key questions explored in this chapter include:

- Can OMSW fibre produced through commercial autoclave pre-treatment be converted to a viable hydrolysate using the commercial cellulase cocktail Cellic Ctec3?
- How do enzymatic hydrolysis conditions influence the solubility of metals in the OMSW fibre?
- Does the OMSW fibre hydrolysate contain any inhibitory compounds typically associated with lignocellulosic feedstocks?
- Does the OMSW fibre hydrolysate contain sufficient nutrients to support microbial growth?
- Can the residual solid material left over after OMSW fibre hydrolysis be valorised further by anaerobic digestion?

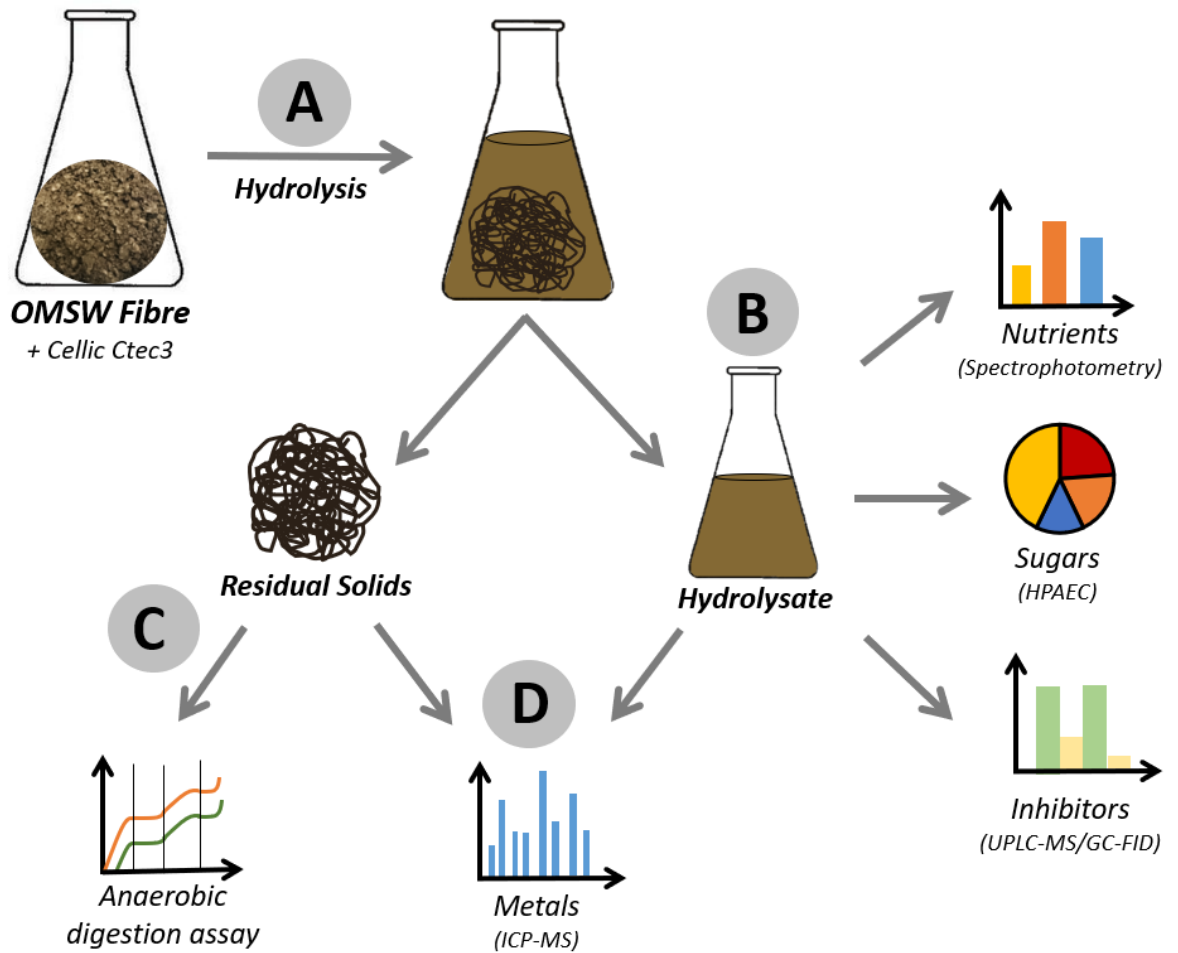


Figure 3.1: Methodological overview of experimental aims and approaches investigated in Chapter 3

A: Enzymatic hydrolysis of OMSW fibre with commercial enzyme cocktail Cellic Ctec3 will be evaluated and methods developed for production of a large, homogeneous batch of high-sugar hydrolysate for application in further experiments.

B: The hydrolysis liquid (**hydrolysate**) will be subjected to a compositional analysis. Key nutrients including sulphate, nitrogen and phosphate will be measured using standard **spectrophotometry**-based assays. Sugars will be analysed by high-pressure anion exchange chromatography (**HPAEC**) so that the hydrolysis yield can be calculated and sugar availability for fermentation determined. A range of common **inhibitors** will be tested by ultra-performance liquid chromatography with mass spectrometry (**UPLC-MS**) and gas chromatography (**GC-FID**).

C: Any un-hydrolysed material left over after hydrolysis (**residual solids**) will be evaluated for biogas production in a lab-scale anaerobic digestion set-up (**anaerobic digestion assay**).

D: Metals will be measured in both the residuals and hydrolysate to quantify how toxic species are solubilised through enzymatic hydrolysis and evaluate the potential effects on fermentation.

3.2 Materials and Methods

3.2.1 Determining Cellulase Activity as Filter Paper Units

Filter paper units (FPUs) are defined as the amount of enzyme capable of releasing 2 mg of sugar from 50 mg of cellulose filter paper within one hour. FPUs are a standard unit for quantifying cellulase activity and are used to determine enzyme loadings in lignocellulosic hydrolysis experiments (Adney & Baker, 2008). The amount of FPUs per millilitre of undiluted Cellic Ctec3 enzyme cocktail was determined using a standardised assay performed on an automated robotic platform (Tecan 200 Liquid Handling Robot). The assay was carried out by the robot as follows: 50 mg paper discs (Whatman No 1, Cole-Parmer Instrument Company) were loaded into 96 well plates (one disc per well). A standard curve was generated by adding enzyme cocktail (unfiltered) at 0, 25, 50, 75 and 100%, diluted with 25 mM sodium acetate buffer (pH 4.5) to a final volume of 550 μ l. The plate was incubated at 50°C for 2 hours and the sugar released from each reaction was quantified by an automated reducing sugar assay, as described in **3.2.7.1 (below)**. The standard curve was used to calculate the FPUs/g that release 2 mg of sugar within one hour. This value was used to calculate the volume of enzyme cocktail to be added to hydrolysis experiments described below.

3.2.2 Small-scale hydrolysis

Preliminary trials of OMSW fibre hydrolysis were carried in 100 ml conical flasks at 10% total solids loading. A range of enzyme loadings were trialled, including 0, 20, 30, 40, 50, 60 and 80 FPU/g solids. The hydrolysis slurry was prepared by mixing 10 g of OMSW fibre (equivalent to 3 g by dry mass or 10% total solids) with the required volume of Cellic Ctec3 enzyme cocktail (Novozymes) to achieve the required FPU/g concentration and then made up to 30 ml with sodium acetate buffer (200 mM, pH 4.5). Flasks were incubated in an orbital shaker at 52.5°C and 250 rpm. Samples were taken at regular intervals over 72 hours and analysed for total reducing sugar content by reducing sugar assay as described in **3.2.7.1**.

3.2.3 Large-scale hydrolysis

A single batch of hydrolysate was produced from 6 kg of OMSW fibre. To reduce contamination during hydrolysis, the fibre was re-sterilised by autoclaving at 120°C for 15 minutes in a laboratory grade autoclave. This was followed by incubation at room

temperature for 16 hours and then another autoclave step under the same conditions. This was done to eliminate any germinated microbial spores that could have contaminated the hydrolysis. The moisture content of the fibre was then reduced by manually squeezing through a synthetic cloth. The final moisture content of the dewatered fibre was determined as described in **2.2.2.1**. The fibre was then acidified to pH 5.0 by manually massaging concentrated H₂SO₄ into the biomass.

Hydrolysis reactions were set up in 2 Litre conical flasks. The fibre was mixed with water that was acidified to pH 5.0 with H₂SO₄ to give a final dry solid loading of 20% w/v. The lignocellulosic enzyme cocktail Cellic Ctec3 (Novozymes) was added to a concentration of 10% w/w of total available polysaccharides. Flasks were incubated for 48 hours at 52.5°C at 250 rpm and then the resulting slurry was centrifuged (3500 x g, 5 min.) in centrifuge pots (600 ml) to separate the hydrolysate liquid from the residual un-hydrolysed solids. All components were weighed throughout the experiment to ensure mass balance. Hydrolysis yields were calculated as described in **3.2.3**.

The supernatants were pooled and homogenised, adjusted to pH 6.5 with concentrated KOH and then the specific gravity of the liquid was measured with a Brannan Specific Gravity Hydrometer (S50, 190mm, Range: 1.000-1.050 SG) (**Figure 3.1**). The liquid hydrolysate was subjected to analysis for monosaccharides, metals and nutrients (sulphate, nitrogen and phosphate) as outlined in **3.2.5**. The remaining un-hydrolysed solid material was subjected to percentage moisture analysis, compositional analysis (lignocellulose and ash) and metal analysis as described in **2.2.2.1**, **2.2.2.2** and **2.2.2.3**. Hydrolysis liquid and residual solids were frozen in separate 1 L freezer bags and stored at -20°C.

3.2.4 Hydrolysate sterilisation

A sterile hydrolysate was produced as follows: hydrolysate was defrosted and centrifuged (27,000 x g, 30 min.) in a Sorval Evolution RC centrifuge with SLC-1500 (Sorvall) rotor to remove small insoluble particulates. The supernatant was filtered by vacuum through glass microfiber filter paper (Watman GF/C) in a Buchner funnel and then passed through a SteriCap Bottletop Filter Unit (0.22 µm PES membrane, 40cm² filtration area, 5-10L capacity, Merck-Millipore) under aseptic laminar flow. The sterile hydrolysate was then aliquoted into sterile tubes (50 ml) (Falcon) and stored at -20°C.

3.2.5 Calculating hydrolysis efficiency

Hydrolysis efficiency was calculated using the equation developed by Kristensen et al (2009b) for hydrolysis reactions with total solids loadings above 5% (**Equation 3.1**). To solve the equation the mass of the total reaction, total biomass and the insoluble solids left over after hydrolysis were accurately determined. This is done by pre-weighing all vessels and substrates throughout the hydrolysis. Other variables that need to be known include the concentration of monosaccharides and oligosaccharides (determined as described in **3.2.7.2**) and the specific gravity (determined as described in **3.2.6**) of the hydrolysate liquid.

Equation 3.1: Percentage yield for a high-solids hydrolysis (Kristensen et al, 2009b)

$$\% \text{ Hydrolysis} = \frac{\frac{m_{\text{reaction}} - m_{\text{insoluble}}}{SG_{\text{aq.phase}}} \times ([Glc] + 1.0526 \times [Cel])}{1.111 \times m_{\text{substrate}} \times F_{\text{cellulose}} \times DM} \times 100$$

| | |
|------------------------|--|
| m_{reaction} | mass of whole reaction (g) |
| $m_{\text{insoluble}}$ | mass of insoluble solids after hydrolysis (g) |
| $SG_{\text{aq.phase}}$ | specific gravity of aqueous phase (g/L) |
| $m_{\text{substrate}}$ | total mass of substrate (g) |
| $F_{\text{cellulose}}$ | fraction of cellulose in the substrate |
| DM | initial dry solids content (w/w) |
| $[Glc]$ | monosaccharide concentration in hydrolysate (g/L) |
| $[Cel]$ | oligosaccharide concentration in hydrolysate (g/L) |

3.2.6 Determining Specific Gravity

The ratio between the densities of two substances or fluids in a constant volume is called the specific gravity (SG), as described in **Equation 3.2**. SG is determined using a hydrometer (**Figure 3.2-A**). The hydrometer's functionality is based on Archimedes Principle, which states that "Any solid lighter than a fluid will, if placed in the fluid, be so far immersed that the weight of the solid will be equal to the weight of the fluid displaced" (Archimedes & Heath, 1897). When the hydrometer is placed into a fluid that has a specific gravity greater or lower than the fluid which it is calibrated against, its buoyancy will change. This difference can be read off the graduated scale of the hydrometer and thereby the relative SG is measured.

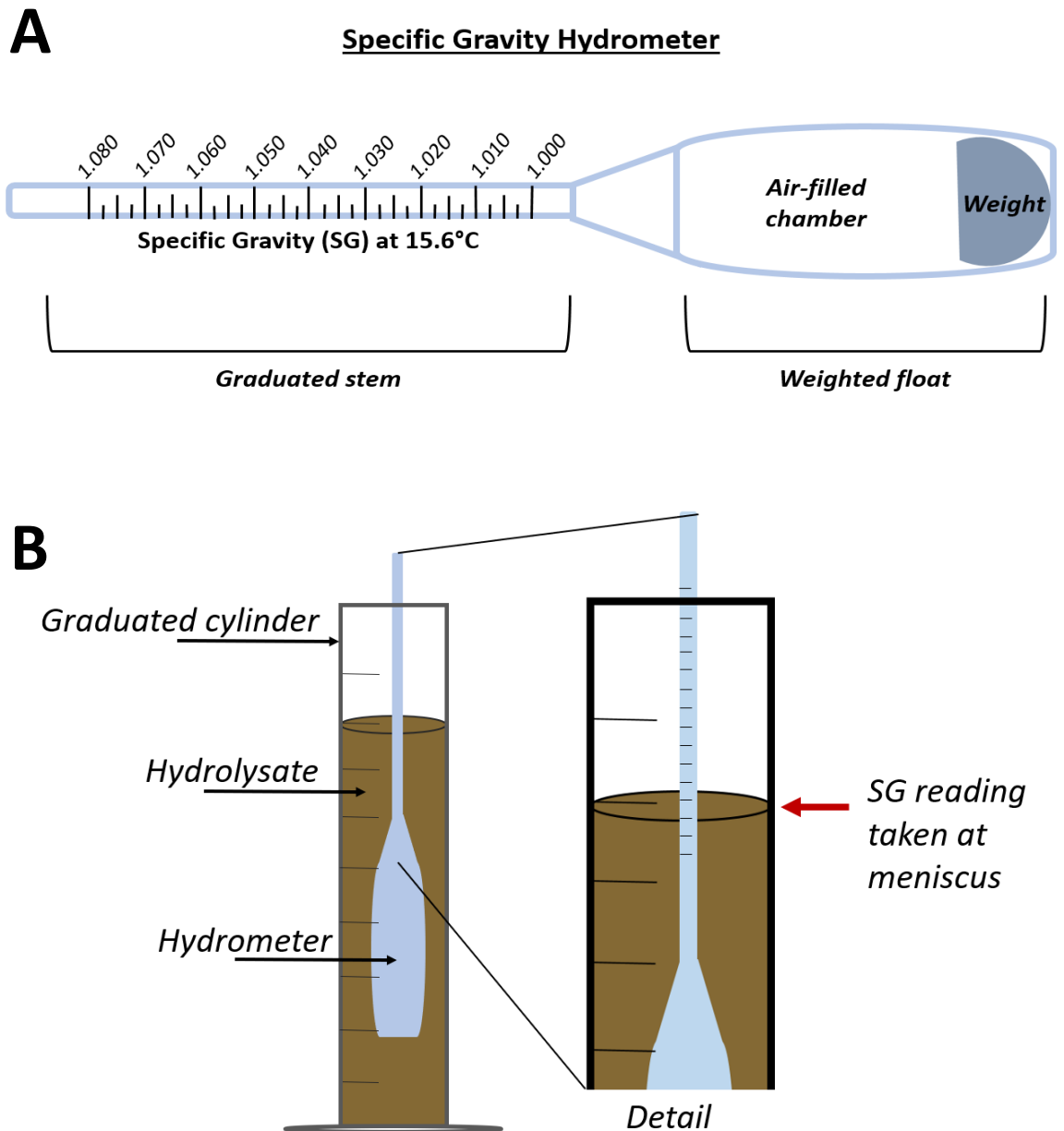


Figure 3.2: Measuring Specific Gravity (Schematics by author).

A: Schematic of a hydrometer.

The hydrometer consists of a hollow glass tube that is sealed so as to produce an **air-filled chamber**. The chamber acts as a float to enable buoyancy when immersed in a fluid. The float is weighted with a **counterweight** to ensure the hydrometer stays upright. The **graduated stem** is fitted with a scale that is calibrated to the density of a reference fluid.

B: Schematic of how specific gravity measurement in OMSW fibre hydrolysate

Liquid **hydrolysate** is poured into a **graduated cylinder** and allowed to equilibrate to the standard temperature to which the hydrometer is calibrated. The **hydrometer** is then carefully lowered into the hydrolysate and allowed to float freely. The **specific gravity** is read off the **graduated stem** by aligning the scale with the **meniscus** at eye level.

Equation 3.2: Definition of Specific Gravity (SG)

$$SG = \frac{\rho_{\text{substance}}}{\rho_{\text{water}}}$$

SG *Specific Gravity of the fluid or substance*

$\rho_{\text{substance}}$ *density of the fluid or substance, [kg/m³]*

ρ_{water} *density of water at a standard temperature (°C), [kg/m³]*

The SG of the OMSW fibre hydrolysate was measured using a Specific Gravity Hydrometer (Brannan S50, 190mm), with a range of 1.000-1.050, calibrated to the density of distilled water at the standard temperature of 15.6°C (60°F). To measure the specific gravity of the OMSW fibre hydrolysate, 250 ml of hydrolysate liquid was defrosted, poured into a 250 ml graduated cylinder and allowed to warm up to ~15.6°C (~10 minutes, also sufficient time to remove any air bubbles). The hydrometer was carefully dropped into the hydrolysate and the specific gravity reading was taken based on the level of the bottom of the meniscus, as illustrated in the diagram in **Figure 3.2-B**. The specific gravity reading was used to calculate the percentage hydrolysis yield using the equation described in **3.2.5**.

3.2.7 Hydrolysate analysis

3.2.7.1 Reducing sugars

Reducing sugars were measured using an automated robotic platform (Tecan 200 Liquid Handling Robot) using the high-throughput 3-methyl-2-benzothiazolinonehydrazone (MBTH) assay developed by Gomez et al., (2010). Briefly, a 96 well plate (1.2 ml, VWR) was set up with liquid samples (diluted in 25 mM sodium acetate buffer (pH 4.5)) alongside a series of standards containing 0-200 nmol D-glucose in 75 µl MilliQ water. Into a 96 well PCR plate the autosampler pipetted 75 µl of each sample and standard, 25 µl of NaOH (1 N), 50 µl MBTH reagent (0.21 mg/ml MBTH, 0.7 mg/ml DTT, freshly prepared), 100 µl oxidising reagent (0.5% FeNH₄(SO₄)₂, 0.5% Sulfamic acid and 0.25 N HCl) and 500 µl MilliQ water. Plates were incubated at 60°C for 20 minutes in a PCR machine and then left to cool and develop at RT for 24 hours. Samples were quantified by measuring absorbance at 620 nm. Absorbance readings were plotted for the standards and sugar concentrations of the samples were then calculated based on the line of best fit equation. Two replicate plates were prepared for each iteration of the assay.

3.2.7.2 Monosaccharides and oligosaccharides

The concentrations of monosaccharides and oligosaccharides in the hydrolysate were quantified by high-performance anion exchange chromatography (HPAEC) as follows: The sterile filtered hydrolysate described in 3.2.2 was serially diluted (1:1500 for monosaccharide analysis and 1:200 for oligosaccharide analysis) in Milli-Q H₂O and then 200 µl was filtered through a 0.45 µm filter into tapered HPAEC vials (Dionex). Samples were analysed by HPAEC on an ICS-3000 PAD system with an electrochemical gold electrode using a CarboPac PA20 analytical column (3x150 mm, Dionex) and guard column (3x30 mm, Dionex). Identification and quantification of monosaccharides and oligosaccharides was carried out by comparing retention times and integrated peak areas of the samples to equimolar standard mixtures analysed during the same run under the same conditions. The monosaccharide standard mixture contained: L-fucose, L-arabinose, L-rhamnose, D-galactose, D-glucose, D-xylose, D-mannose, D-galacturonic acid and D-glucuronic acid. The oligosaccharide standard mixture contained: glucose, cellobiose, cellotriose, cellotetraose, cellopentaose and cellohexaose.

3.2.7.3 Metals

Metal levels in the hydrolysate and the residual solids left over after hydrolysis were analysed in triplicate by ICP-MS as described in 2.2.2.6. Note that the residual solids were dried and ground to powder with a mortar and pestle before digestion. The digestion step was not required for the aqueous hydrolysate samples as the metals were already soluble.

3.2.7.4 Marker inhibitors

Inhibitory compounds commonly found in lignocellulosic hydrolysates were analysed in the OMSW fibre hydrolysate. Furfural, 5-hydroxymethylfurfural (5-HMF), vanillin and levulinic acid were measured by ultra-performance liquid chromatography (UPLC) with mass spectrometric detection (MS). Samples were chromatographically separated on a Waters Acquity I-Class System with VanGuard pre-column with C18 frit (Waters) and a BEH C18 column (100x2.1 mm, 1.7 µm, Waters). All runs were carried out with a gradient (min/%B = 0/16, 2.5/16, 2.8/100, 2.9/100, 3.3/16, 4/16) of solvent A (5% MeOH, 0.1% acetic acid) and solvent B (0.1% acetic acid in MeOH). Injection volume was 2 µl with a flow rate of 0.5 ml/min at 45°C. MS was carried out on a Thermo Endura Triple Quad with HESI positive ion source and single reaction monitoring (SRM) with one transition for each compound (compound, precursor *m/z*/product *m/z*: levulinic acid, 99.12/71.22; HMF,

109.09/81.15; furfural, 97.12/69.22; vanillin, 153.05/93.11). Data was analysed with Thermo Xcalibur 4.0.27.10 software.

A range of organic acids, including acetic, butyric, formic, heptanoic, hexanoic, isobutyric isovaleric, 4-methylvaleric, propionic and valeric acid were measured in the OMSW fibre hydrolysate by gas chromatography (GC) with flame-ionization detection (FID). OMSW fibre hydrolysate was prepared for analysis in triplicate by acidifying 1 ml with 7.5 µl concentrated orthophosphoric acid (Sigma-Aldrich) and run on the GC-FID in parallel alongside a volatile free acid standard (CRM46975, Sigma-Aldrich). The GC-FID set up consisted of a Nukol column (30 m x 0.25 mm, I.D 0.25 µm (24107)) with a helium carrier (30 psi) and liquid injection. Detectors and injectors were operated at 200°C. Temperature was increased from 75-150°C (10°C/min), 150-200°C (20°C/min) and held for 10 minutes.

3.2.7.5 Nutrients

Essential nutrients (nitrogen, phosphate and sulphate) were analysed using commercial testing kits that rely on enzymatic or chemical reactions followed by quantification by spectrophotometry.

Phosphate and sulphate were quantified using standard Hach-Lange Kits designed for water quality testing, in conjunction with a Hach-Lange HT200S High Temperature Thermostat (used to heat samples according to manufacturer's instructions) and a Hach-Lange DR3900 Spectrophotometer (for automatic test quantification). Total Phosphate and orthophosphate were measured by Hach-Lange LCK350 Phosphate Kit (detection range: 60-60 mg/L PO_4^{3-} and 2-20 mg/L $\text{PO}_4\text{-P}$), based on the phosphomolybdenum blue assay in which phosphate reacts with Mo^{6+} under acidic conditions to produce a blue product that is colorimetrically quantified. Sulphate was measured by Hach-Lange LCK153 Sulphate Kit (detection range: 40-150 mg/L SO_4^{2-}), based on the reaction of barium chloride ions with sulphate to produce insoluble barium sulphate which can be quantified as a change in turbidity.

Nitrogenous compounds were quantified using enzymatic assay kits by Megazyme. First Ammonia, Urea and L-Arginine (L-Arg) were measured according to manufacturer's instructions by L-Arginine/Urea/Ammonia Kit (K-LARGE), then primary amino nitrogen (PAN) was measured by Primary Amino Nitrogen Kit (K-PANOPA) according to manufacturer's instructions. Results from both kits were used to calculate the total Yeast Available Nitrogen (YAN), defined as the total concentration of nitrogen in a fermentation

that is accessible to the Brewer's Yeast *Saccharomyces cerevisiae*. YAN is calculated from total ammonia, urea, L-arginine and PAN, as shown in **Equation 3.3**.

Equation 3.3: Calculating Yeast Available Nitrogen (YAN)

$$YAN_{total} = 1000 \times \left[\frac{Ammonia \times 14.01}{17.03} + \frac{Urea \times 28.02}{60.06} + \frac{L-Arg \times 28.02}{174.21} \right] + PAN$$

Total YAN (YAN_{total}) is calculated as mg of nitrogen per Litre (mg/L) and the values of each nitrogenous compound (ammonia, urea, L-Arg) are given in g/L. PAN is given in mg/L. Note that each ammonium ion contributes one nitrogen atom (14.01 g/mol), each urea ion contributes two, and each L-arginine contributes three. However, only two nitrogen atoms are counted for L-arginine because its primary amino group is already accounted for as part of the PAN (measured separately).

3.2.8 Anaerobic Digestion Assays

3.2.8.1 Small-scale Anaerobic Digestion Assay

To investigate the biogas production potential of residual material from OMSW fibre hydrolysis a small-scale anaerobic digestion assay was set up as shown in **Figure 3.3**. Glass serum bottles (100 ml) were set up in triplicate with either low (20 g) or high (40 g) loadings of residual material from OMSW fibre hydrolysis. As a positive control three bottles were set up with 15 g of OMSW fibre. As a negative control three bottles were set up without any biomass added. Each sample was inoculated with 40 g of sludge (digestate) from an active industrial anaerobic digester operated by Yorkshire Water Ltd. All samples were sealed with rubber bungs and vortexed thoroughly before being connected to the small-scale anaerobic digestion apparatus (**Figure 3.3**). Samples were allowed to degas over the first 5 days to eliminate intrinsic gasses. Methane levels were then recorded over the next 41 days, with measurements taken every day for 20 days then every 2-3 days.

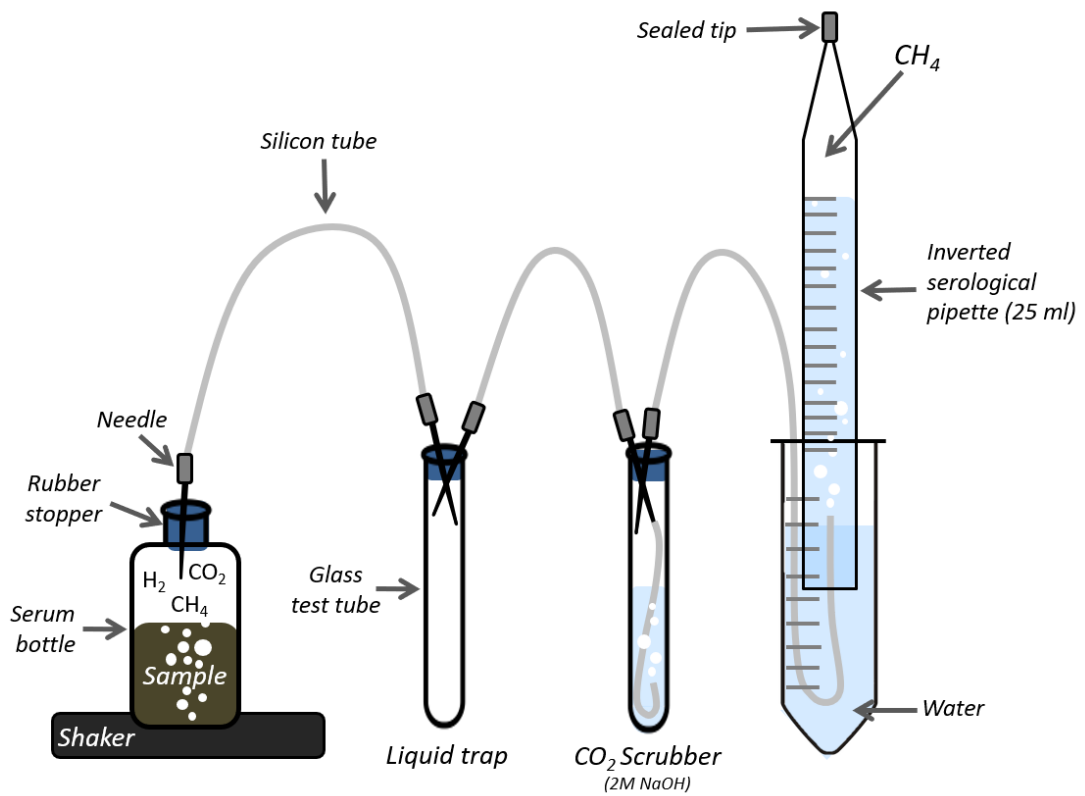


Figure 3.3: Schematic of the small-scale anaerobic digestion apparatus

(Schematic by author, experimental design developed by James F. Robson (University of York) as part of his PhD thesis).

Biomass is combined with sludge from an anaerobic digester in a glass serum bottle. The bottle is sealed with a rubber bung to prevent gas exchange and secured on an orbital shaker that agitates the sample. The rubber bung of the serum bottle is pierced with a needle attached to a silicon tube. Any gas produced by the anaerobic digestion culture can only escape through the needle. Biogas first passes through the **liquid trap** (catches moisture & particulates), then through the **CO₂ scrubber** (2M NaOH, eliminates CO₂ & H₂) so that only **methane (CH₄)** remains. The CH₄ bubbles up through an inverted 25 ml **serological pipette** that is sealed at the tip and placed in a tube of water. Water in the pipette is displaced by biogas and the volume of gas in the headspace can be read off the scale. Once 20 cm³ of headspace had been displaced the serological pipette is reset by refilling with water.

3.2.9 Automated Biomethane Potential Assay

A custom automated anaerobic digestion system was used to determine the biomethane potential of OMSW fibre and residual solids from OMSW fibre hydrolysis. The system consisted of eleven glass mini-bioreactors (**Figure 3.4-A**). Each mini-reactor was fitted with impellers attached to powered stirring rods anchored to a gas tight reactor lid with two sampling ports - gas-out and feed-in/sample-out (**Figure 3.4-B**). The full mini-bioreactor set-up is shown and described in **Figure 3.5-Left**. Total gas and percentage methane were measured continuously in real time as described in **Figure 3.5-Right**.

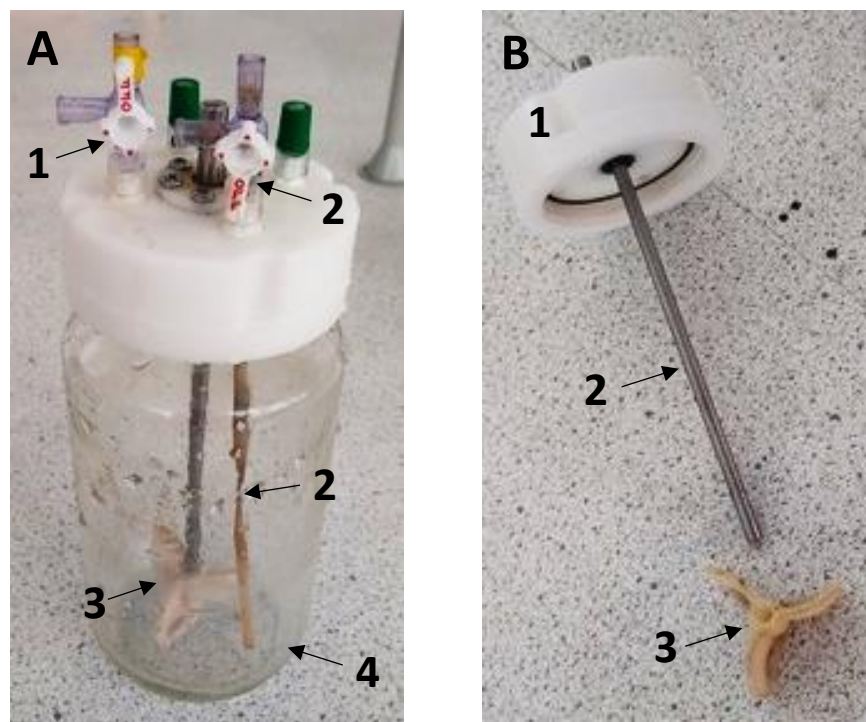


Figure 3.4: Anaerobic Digestion Mini-bioreactor Assembly

(Images courtesy of James F. Robson, University of York)

A: Mini-bioreactor:

(1) Gas outlet port; (2a) Sampling port (feed-in, sample-out); (2b) Sampling/feeding tube; (3) Impeller (detail in B); (3) Glass vessel (1 L);

B: Mini-bioreactor stirring mechanism:

(1) Bioreactor lid (gas sealed); (2) Powered stirring rod; (3) Impeller.



Figure 3.5: Automated Lab-Scale Anaerobic Digestion System

(Image courtesy of James F. Robson (University of York) who developed this system as part of his PhD thesis).

Left: Bottom - Temperature controlled water bath containing 11 mini-bioreactors (as depicted in **Figure 3.4**). Set to 35°C. Top - The bioreactor tops are attached to a powered pulley system which is connected to a single motor. Gas outlets from each mini-bioreactor are attached to gas impermeable silicon-based tubes that lead to gas the detection apparatuses (**Right**).

Right: Top - Gas outlets from the bioreactor system are connected to an array of infrared (IR) methane sensors (Dynament, certified mining grade, 0-100% detection range). The IR sensors emit an analogue signal recorded by an Arduino computing platform running custom software that converts this signal to a methane percentage. Bottom - A tipping bucket mechanism with temperature and pressure compensation enables total gas yield to be recorded continuously in real time at standard temperature and pressure.

3.2.9.1 Set-up, Sampling and Feeding

OMSW fibre and residual material from MSW fibre hydrolysis were defrosted and dewatered by manual squeezing through synthetic cloth. Moisture content was analysed as described previously (2.2.2.1.). OMSW fibre and hydrolysis residuals were prepared as suspensions of 1.25% w/v, respectively. Each suspension was blended in a food blender for 10 minutes to homogenise the biomass and make the material small enough to pass through the 3 mm diameter tube (C-flex) used to feed the mini-bioreactors. Suspensions were stored in 1 litre Duran bottles at 4°C for the duration of the experiment.

At regular intervals 50 ml of digestate was non-invasively sampled from each digester with a 60 ml capacity syringe (BD Plastipak) with attached tube. Each sample was transferred to Falcon tubes and the pH was measured with pH strips (Fisher Brand). After each sampling the reactors were fed with 50 ml of either the OMSW fibre or residuals suspension. The two negative control reactors were also sampled and fed with 50 ml water. Sampling was carried out over 43 days at the same time of day. Sampling intervals were every 7 days (days 0, 7, 14, 21 and 28), then every 3 days (days 31, 34 and 37) and finally every 2 days (days 39, 41 and 42).

A 1 ml aliquot of each sample was transferred to a dried, pre-weighed Eppendorf tube (1.5 ml) and spun down. The supernatant was discarded, and the pellet was weighed to calculate total dry solids. Remaining sample material was frozen at -20°C for use in further analyses as described in **3.2.9.2.3** and **3.2.9.2.4**.

3.2.9.2 Chemical Oxygen Demand

A 15 ml aliquot of each digestate sample was centrifuged at 3,500 xg for 20 minutes and the supernatants separated from the pellets. Chemical oxygen demand (COD) of the supernatants was measured using a Hach Lange COD Kit (LCK514) with a detection range of 100-2000 mg/L O₂ according to manufacturer's instructions. Samples were analysed by adding 2 ml of supernatant to the test vials provided in the kit. Vials were mixed and transferred to a Hach-Lange HT200S High Temperature Thermostat (used to heat samples according to manufacturer's instructions) and the colour change was then quantified with a Hach-Lange DR3900 Spectrophotometer to quantify the COD.

3.2.9.3 Microbial Community Characterisation

The microbial communities in AD reactors fed with fibre or residuals were characterised using phylogenetic 16S rRNA amplicon sequencing. Digestate from the final sample point of two reactors was analysed from each condition (fed with OMSW fibre or fed with residuals). DNA was extracted from each sample and the v3-v4 region of 16s rRNA was amplified with commonly used v3v4 primers (Klindworth et al, 2013) with a Quick-16s NGS Library Prep Kit (Zymo Research) according to manufacturer's instructions. Sequencing was carried out via Illumina MiSeq 2 x 300 bp by the genomics facility at Leeds University. The bioinformatics pipeline was performed according to the Quantitative Insights Into Microbial Ecology (QIIME) bioinformatics platform (Caporaso et al, 2010) default parameters and primers were trimmed using a DADA2 software package (Callahan et al,

2016) using a cut length of 25 bp. Reads were clustered into operational taxonomic units (OTUs) using the UCLUST algorithm based on a 97% sequence identity threshold. Taxonomic annotation of OTUs was performed using the GreenGenes (DeSantis et al, 2006) rRNA database.

3.3 Results

3.3.1 Hydrolysis of OMSW fibre

Small-scale hydrolysis experiments were initially used to assess the amenability of autoclave pre-treated OMSW fibre to hydrolysis with Cellic Ctec3. Optimal conditions for Cellic Ctec3 are 50 – 55°C and a pH between 4.5 - 5.5, therefore the mean conditions (pH 5.0 and 52.5°C) were chosen. OMSW fibre was added at a medium solids loading (10% w/v TS) with enzyme concentrations ranging from medium to high (20-80 FPU/g). These conditions led to a polysaccharide conversion of between 40-80%, with higher enzyme loadings releasing more sugars (**Figure 3.6**). The most rapid hydrolysis occurred within in the first 12 hours for all enzyme loadings, followed by a more gradual rate of sugar release up to 72 hours when the reaction was stopped.

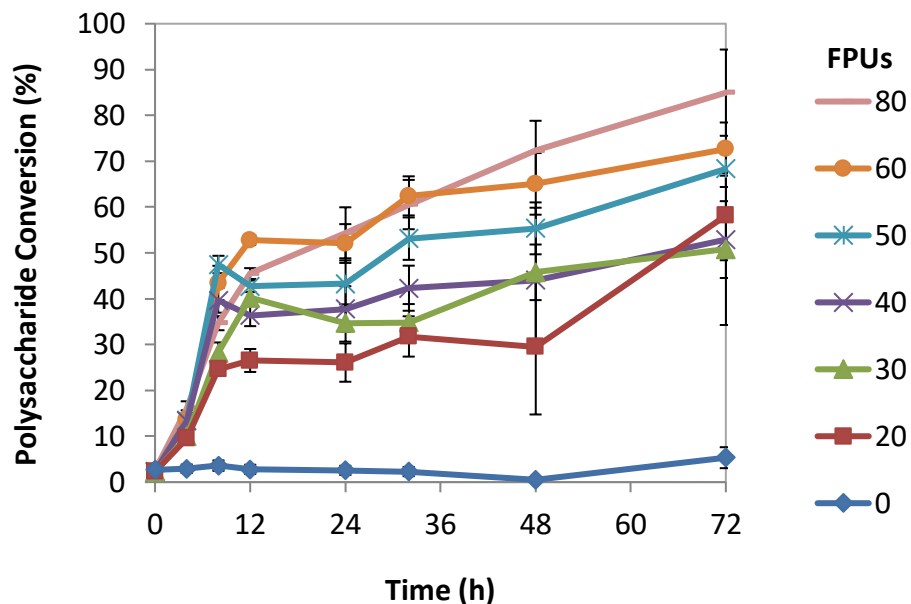


Figure 3.6: Preliminary trial of OMSW fibre hydrolysis using a range of enzyme loadings

It is typical for enzymatic hydrolysis of lignocellulose to initially progress at a rapid rate and then slow into a plateau phase, often ending with incomplete hydrolysis of the substrate (Arantes & Saddler, 2011). This phenomenon can be overcome by dosing more enzyme, but the relationship between enzyme loading and sugar release efficiency is generally non-linear, especially at higher enzyme loadings. For example, in **Figure 3.6** the 60 and 80 FPU/g enzyme loadings had similar sugar yields for the first 30 hours and the final polysaccharide conversion for the 80 FPU/g reactions was only about 10% greater compared to the 60 FPU/g reactions. Similarly, the sugar release was very similar for the

30 and 40 FPU/g loadings. The large error bars between replicates and inconsistent sugar release observed between the enzyme loadings may also be due to mixing limitations that are inherent to small-scale laboratory hydrolysis set-ups (Neubauer et al, 2013). It was concluded that autoclave pre-treatment was sufficiently harsh to make the lignocellulose in the OMSW fibre accessible to hydrolysis by Cellic Ctec3 and consequently no further pre-treatments would be necessary to produce a hydrolysate with enough sugar for fermentation experiments.

Next, a large-scale hydrolysis process was developed for OMSW fibre at the industrially relevant solids loading of 20%. An excess concentration of the commercial enzyme cocktail Cellic Ctec3 (10% enzyme by weight of total available polysaccharide) was used to ensure the enzymes would liberate enough sugars to sustain microbial fermentations and the final hydrolysate would contain industrially realistic concentrations of inhibitors and metals. The hydrolysis methodology used for preliminary experiments involved acidifying the biomass with glacial acetic acid and then buffering the slurry with 200 mM sodium acetate buffer (see **3.2.2**). Acetate is very inhibitory to facultative anaerobes (Koh et al, 1992). For example, *E. coli* is completely inhibited by 425 mM acetate (Zaldivar & Ingram, 1999). To produce a hydrolysate more suitable for fermentation applications glacial acetic acid was exchanged for concentrated H₂SO₄. H₂SO₄ was manually massaged into the fibre until the pH dropped to 5.0 and then a slurry was prepared using distilled water adjusted to pH 5.0 with H₂SO₄ (for full method see **3.2.3**). Although no buffer was employed, the combination of the acidified fibre and water maintained the pH effectively until the end of hydrolysis without adding compounds inhibitory to fermentative microbes.

The hydrolysis slurry was distributed across eight 2 litre conical flasks as shown in **Figure 3.7-A**. To facilitate mixing in the absence of an impeller, shake flasks were only filled to ~25% of capacity and agitated nonstop throughout hydrolysis at 250 rpm in an orbital shaker. Due to the high viscosity of the 20% TS slurry, the set-up did not produce any agitation at first. However, after 3-6 hours as the enzymes began to break down some of the polysaccharides, adequate agitation was achieved. Within 48 hours a liquefied hydrolysate was produced (**Figure 3.7-B**). After hydrolysis all un-hydrolysable solids were separated by centrifugation from the liquid fraction. The two fractions are shown in the image in **Figure 3.7-C**.

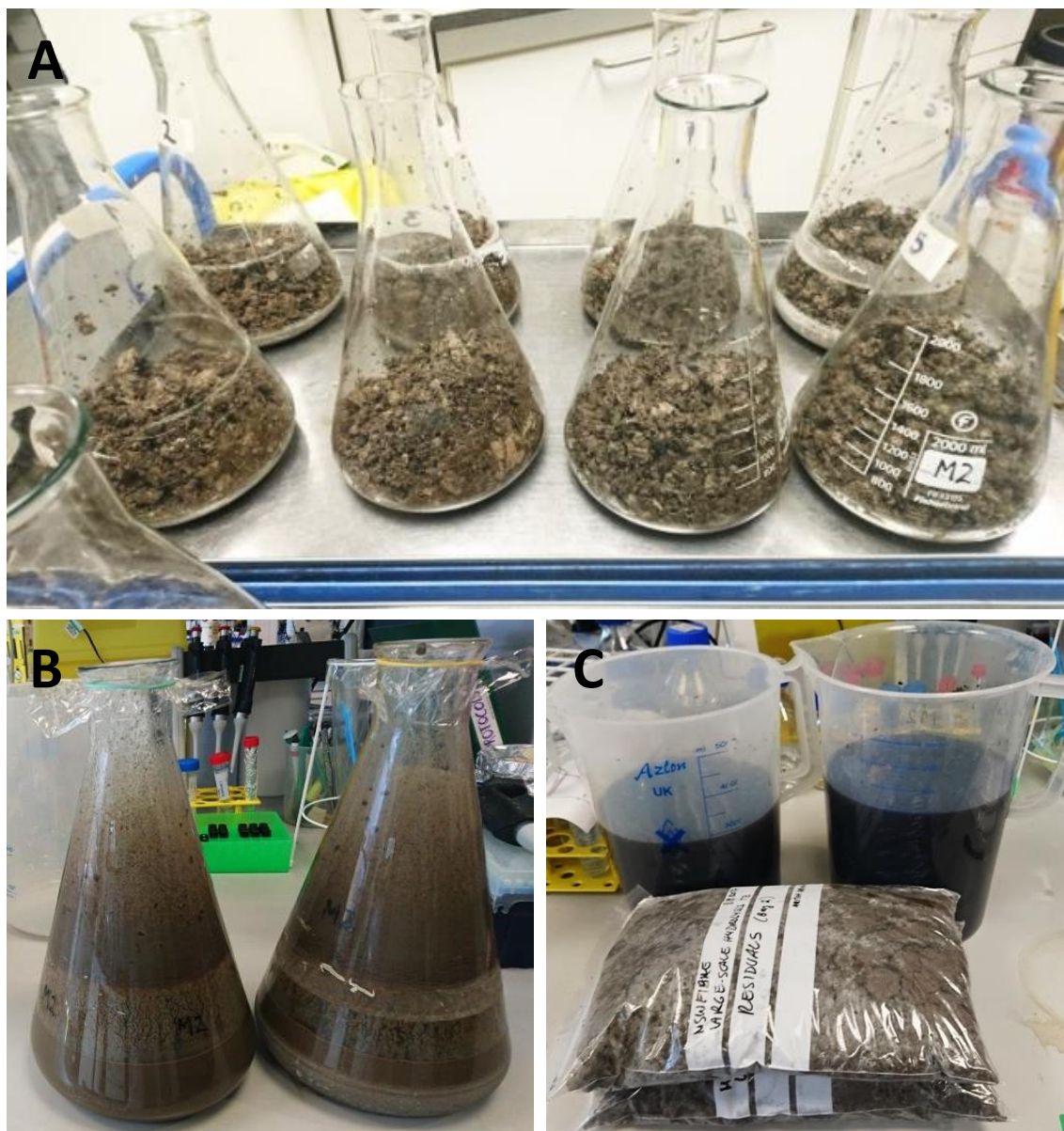


Figure 3.7: Images of the key stages in the large-scale hydrolysis of OMSW fibre
(Images by author)

- A. *Image of the large-scale hydrolysis set up: Eight 2L conical flasks were set up with MSW fibre (20% dry weight by volume), Cellic Ctec3 (10% weight by weight of available polysaccharides) and 400 ml liquid.*
- B. *Appearance of the hydrolysate slurry after 48 hours of hydrolysis.*
- C. *Hydrolysis liquid and residual solids after centrifugal separation.*

The final concentration of monosaccharides in the liquid fraction was 78.13 ± 1.93 g/L (7.8% w/v). D-glucose, D-xylose and D-mannose were the most abundant sugars overall, present at concentrations of 54.69 ± 1.31 , 17.54 ± 1.10 and 4.25 ± 0.61 g/L, respectively, and making up 98% of the total sugars in the OMSW fibre hydrolysate. L-fucose, L-arabinose, L-rhamnose and D-galactose were also detected in small quantities (**Figure 3.8**). The total hydrolysis yield was calculated as 75.29%, equivalent to 61.19% of available cellulose and about 59% of available hemicellulose. The final sugar concentration attained in the OMSW fibre hydrolysate was 7.8% w/v, which is just below the minimum sugar concentration needed for a hydrolysate to be economically viable for bioethanol production ($\geq 8\%$ w/w (Chen & Liu, 2017)). No doubt hydrolysis yields could be improved by using a dedicated hydrolysis vessel with powered mixing capabilities. Nevertheless, the hydrolysate was deemed to contain enough sugars to be practicable for assessing the suitability of OMSW fibre for fermentation.

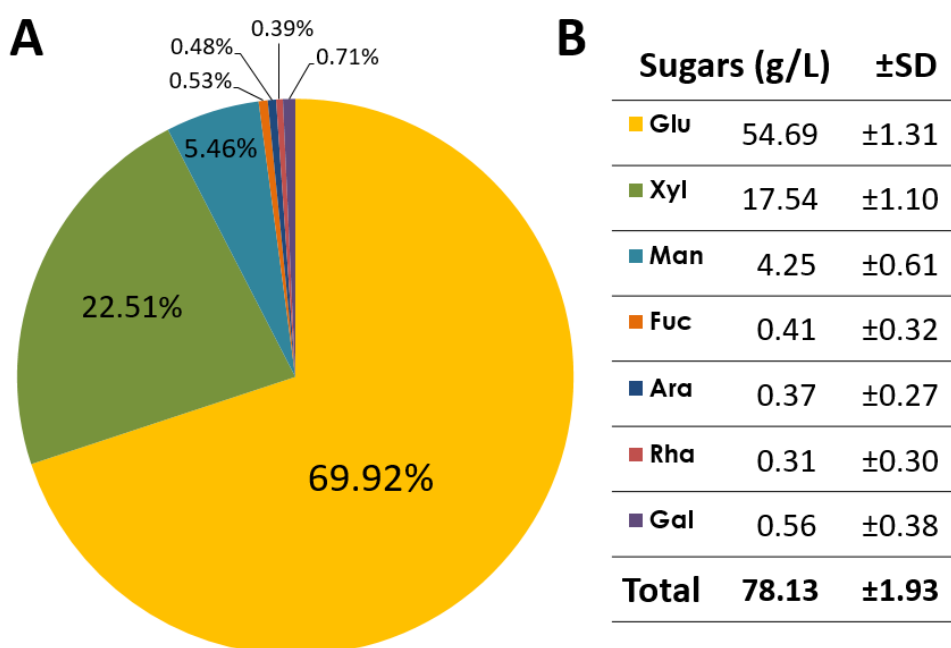


Figure 3.8: Concentration and abundance of monosaccharides measured in hydrolysate of OMSW fibre

±SD= standard deviation of triplicate measurements.

Colours in A correspond to the colours marked for each sugar in B.

Glu = D-Glucose; Xyl = D-Xylose; Man = D-Mannose; Fuc = L-Fucose;

Ara = L-Arabinose; Rha = L-Rhamnose; Gal = L-Galactose.

A: Total percentage abundance of monosaccharides in OMSW fibre hydrolysate.

B: Concentration of monosaccharides in OMSW fibre hydrolysate in g/L.

It should also be noted that there are some caveats involved in calculating hydrolysis yields for solids loadings above 5% that must be considered when developing scalable hydrolysis methods. Hydrolysis is carried out using water as the primary solvent, but as sugars are solubilised from the insoluble lignocellulosic fraction the density of the liquid increases. This change in density can be accounted for in calculations by measuring the specific gravity (SG) of the final hydrolysate. SG is defined as the ratio between the densities of two substances, where one substance is used as a reference substance (in this case the density of distilled water at 15.6°C) and the volume of the two substances is equivalent.

For hydrolysis reactions with low solids loadings ($\leq 5\%$) usually employed in laboratory scale experiments, the differences in specific gravity of the different components are so minor that they can be considered equal and are disregarded when calculating hydrolysis yields. However, as Kristensen et al (2009b) have demonstrated, as the solids loadings increase over 5% this no longer holds true and knowing the specific gravity of the final hydrolysate becomes critical for accurate calculation of hydrolysis yield. If a standard method for calculating hydrolysis yield is used, for example the standard equation used by the National Renewable Energy Laboratories (NREL), the hydrolysis yields are up to 36% greater (Kristensen et al, 2009b). Due to the industrial nature of this project and the high solids loading employed, I chose to apply the more comprehensive hydrolysis yield equation put forward by Kristensen et al (**Equation 3.1**) for calculating hydrolysis yields.

3.3.1.1 Inhibitor and metal content

The OMSW fibre hydrolysate was analysed for potential fermentation inhibitors, including metals and common inhibitory compounds, to assess any potential toxicity to fermentative microbes and evaluate the degree of metal solubilisation caused by hydrolysis (**Table 3.3**). A wide range of organic acids were detected in the hydrolysate, including levulinic, acetic, propionic, butyric and hexanoic acid. The most abundant acids were levulinic and acetic acid at 29.64 ± 0.37 mM and 5.77 ± 0.09 mM, respectively. The other organic acids were present at <0.3 mM. The inhibitory aldehydes vanillin, 5-hydroxymethylfurfural (5-HMF) and furfural were also measured, but only vanillin was detected at 2.10 ± 0.10 mM.

All metals originally detected in the OMSW fibre (**Chapter 2, Table 2.4**) were also found in the hydrolysate, except cadmium which was absent in the hydrolysate. Again, calcium was the most abundant element at 119.20 mM. Other metals present in the mM

range were highly soluble species including potassium, sodium and magnesium. All other metal species were present at relatively low levels, in the μM to nM range. To better understand how inhibitory compounds and metals might affect microbial fermentation, the levels measured in the OMSW fibre hydrolysate were compared to the minimum inhibitory concentrations (M.I.C) reported in the literature for the model fermentative microorganism *Escherichia coli*. These are given in **Table 3.1** alongside their respective references.

The concentration of all inhibitory compounds and potentially toxic metals were below the M.I.C reported for *E. coli*. No studies reporting magnesium or calcium inhibition in *E. coli* were found in the literature, although evidence suggests that high cation levels can disrupt intracellular pH, thereby increasing sensitivity to organic acids (Warnecke & Gill, 2005). Sodium and potassium are physiologically important cations present at μM levels in the hydrolysate, but evidence suggests growth inhibition requires concentrations around 1 M (Wu et al, 2014). The inhibitory effects of many metals are highly dependent on pH, redox and microbial physiology, therefore the potential effects on fermentative microorganisms are difficult to predict. Based on the M.I.C values presented in **Table 3.1**, the most potentially problematic species are iron and aluminium, as their concentrations are closest to the M.I.C. and therefore could potentially affect microbial fitness.

To gain a better understanding of how metals are solubilised during enzymatic hydrolysis, the metal levels in the residual solids were analysed and compared to the concentrations in the hydrolysate (**Figure 3.9**). For comparison, the metal levels originally measured in the OMSW fibre (described in **Chapter 2, Table 2.7**) were used to calculate the concentration of metals that would theoretically be released in a 20% TS hydrolysis, assuming 100% solubilisation (**Figure 3.9, 'fibre'**). Interestingly, except for highly water-soluble species (potassium and sodium), most metals in the system were retained in the residual solids fraction (**Figure 3.9, 'residuals'**). Metals in the liquid fraction (**Figure 3.9, 'hydrolysate'**) made up $\leq 30\%$ of the total metal concentration.

Overall, the theoretically calculated metal levels were lower than the total metal levels measured in the hydrolysate liquid and residual solids combined. This is possibly because a much greater volume of OMSW fibre was homogenised to make the hydrolysate compared to the 5-10 g used for ICP-MS analysis, highlighting the limitations of representative sample taking in compositional analysis. It also indicates that metals are heterogeneously distributed within the OMSW fibre. Some metals were absent in the hydrolysate and the OMSW fibre but were detected in the residual material, including

selenium, arsenic and thallium. However, these were present at very low levels (<3.0 μM). The hydrolysate contained approximately 6-fold more metals by dry weight than the OMSW fibre, thus less abundant metal species were probably more easily detected by ICP-MS.

Table 3.1: Organic acids, aldehydes and metals measured in OMSW fibre hydrolysate and the minimum inhibitory concentration (M.I.C) of each analyte for the model fermentative microorganism *Escherichia coli*

±SD = standard deviation of triplicate analyses; n/d = not detected; n/a = not applicable.

| Analyte | Concentration | | M.I.C (<i>E. coli</i>) [mM] | Reference |
|------------------|---------------|----------------|----------------------------------|-----------------------------|
| | [mM] | $\pm SD$ | | |
| Acids | | | | |
| Levulinic | 29.64 | ± 0.37 | 345 | (Zaldivar & Ingram, 1999) |
| Acetic | 5.77 | ± 0.09 | 416 | (Zaldivar & Ingram, 1999) |
| Propionic | 0.24 | ± 0.08 | 570 | (Chun et al, 2014) |
| Butyric | 0.11 | ± 0.0027 | 460 | (Chun et al, 2014) |
| Hexanoic | 0.11 | ± 0.02 | 12 | (Hou et al, 2017) |
| Aldehydes | | | | |
| Vanillin | 2.10 | ± 0.10 | 10 | (Zaldivar et al, 1999) |
| 5-HMF | | n/d | 32 | (Zaldivar et al, 1999) |
| Furfural | | n/d | 36 | (Zaldivar et al, 1999) |
| Metals | | | | |
| Calcium | 119.20 | ± 0.000032 | n/a | - |
| Sodium | 15.26 | ± 0.00014 | 910 | (Wu et al, 2014) |
| Potassium | 7.67 | ± 0.000030 | 1,100 | (Wu et al, 2014) |
| Magnesium | 3.65 | ± 0.00099 | n/a | - |
| Iron | 0.70 | ± 0.000028 | 1 | (Kalantari, 2008) |
| Aluminium | 0.58 | ± 0.00014 | 2 | (Nies, 1999) |
| Zinc | 0.12 | ± 0.000020 | 2 | (Beard et al, 1997) |
| Manganese | 0.050 | ± 0.000056 | 1 | (Nies, 1999) |
| Nickel | 0.0061 | ± 0.000090 | 20 | (Nies, 1999) |
| Chromium | 0.0011 | ± 0.00013 | 1 | (Nies, 1999) |
| Copper | 0.00082 | ± 0.00031 | 1 | (Nies, 1999) |
| Antimony | 0.00078 | ± 0.000053 | 5 | (Nies, 1999) |
| Vanadium | 0.00072 | ± 0.00015 | 1 | (Nies, 1999) |
| Cobalt | 0.00055 | ± 0.00019 | 1 | (Majtan et al, 2011) |
| Molybdenum | 0.00019 | ± 0.00035 | >10 | (Stewart & Macgregor, 1982) |
| Lead | 0.000049 | ± 0.000031 | 5 | (Nies, 1999) |

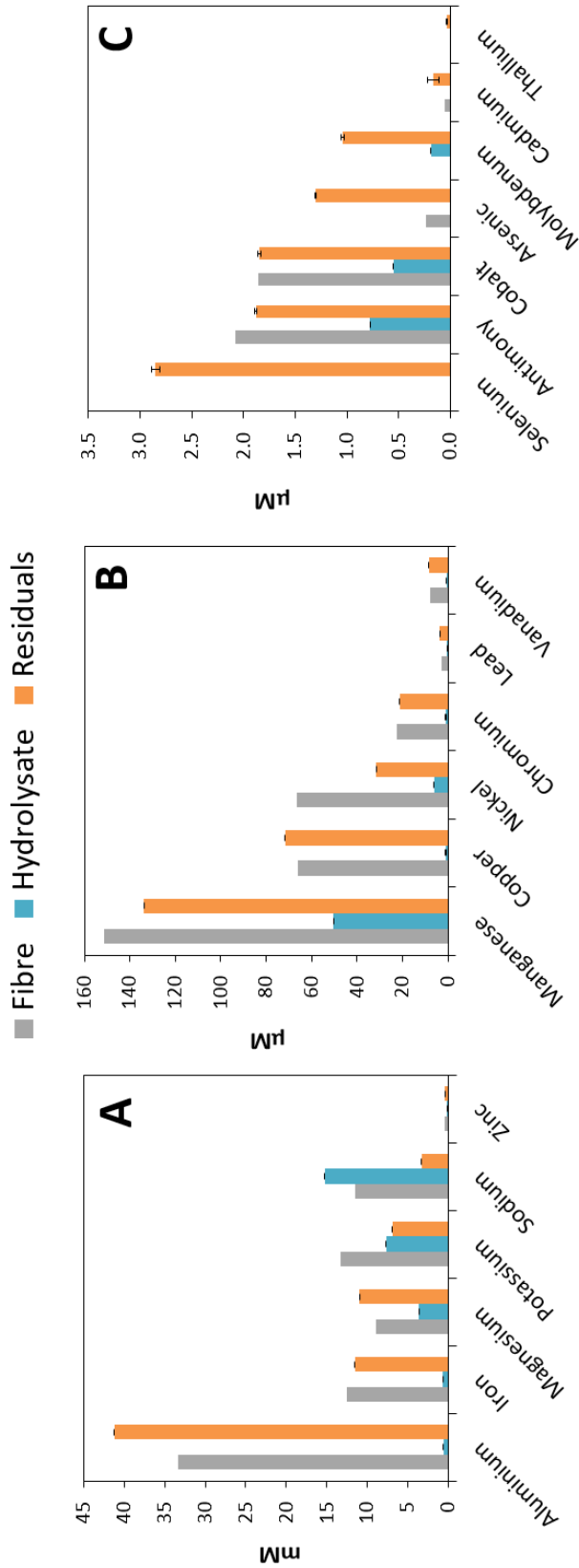


Figure 3.9: Fractionation of metals in the liquid and solid fractions produced after OMSW fibre hydrolysis

Measurements of liquid and solid fraction metals carried out by ionisation coupled plasma mass spectrometry (ICP-MS) as described in 3.2.5.2.

Error bars show standard deviation of triplicate measurements.

Fibre: The theoretical concentration of metals that would be released from the OMSW fibre into the hydrolysate by enzymatic hydrolysis, assuming 100% solubilisation of all metals present. These values are based on the metal levels measured in the OMSW fibre prior to hydrolysis and account for a five-fold dilution in a 20% total solids hydrolysis reaction.

Hydrolysate: The concentration of metals measured in the liquid fraction of the OMSW fibre hydrolysate.

Residuals: The concentration of metals measured in the residual solid material left over after OMSW fibre hydrolysis. Calculations account for a 5-fold dilution in a 20% total solids hydrolysis reaction.

3.3.1.2 Nutrient analysis

To get a full picture of the nutrient profile of OMSW fibre hydrolysate key nutrients required for microbial growth were measured, including phosphate, sulphate and various nitrogen sources (**Table 3.2**). Phosphate was measured as orthophosphate (a measure of free PO_4^{3-} in the sample) and total phosphorus (also called orthophosphate as phosphorus ($\text{PO}_4\text{-P}$) because all phosphorus must be converted to PO_4 before it can be quantified). The hydrolysate contained 0.44 ± 0.003 mM of phosphorus, of which only 0.11 ± 0.001 mM was orthophosphate. Sulphate was present in the highest abundance overall, at 15.24 ± 1.21 mM. A typical method for measuring availability of microbially accessible nitrogen in industrial fermentations is to calculate Yeast Available Nitrogen (YAN) (see **3.2.7.5**) (Boudreau et al, 2018). YAN combines measures of ammonia, urea, L-arginine and primary amino nitrogen (nitrogen derived from peptides and amino acids) to calculate the total concentration of nitrogen sources that can be accessed by Brewer's Yeast (*Saccharomyces cerevisiae*) in a typical fermentation. Total YAN in the hydrolysate was 4.85 ± 0.14 mM, primarily comprising ammonia (2.27 ± 0.09 mM), with some primary amino nitrogen (PAN) (0.32 ± 0.01 mM) and low levels of L-Arginine (0.03 ± 0.01 mM). Urea levels were insignificant. Overall, the level of microbially accessible nitrogen and phosphate measured in the OMSW fibre hydrolysate was at least 50% below the levels that would be used in a typical defined medium for *E. coli*. For example, MOPS minimal medium contains 10 mM ammonia and 0.4 mM Phosphate (Neidhardt et al, 1974). The hydrolysate may therefore require supplementation with nutrients to be viable for fermentation.

Table 3.2: Levels phosphorus, orthophosphate, sulphate, nitrogenous compounds and calculated yeast available nitrogen (YAN) in OMSW fibre hydrolysate

**For details on methods and calculating YAN see 3.2.7.5.*

| | | |
|---|-------|-------------|
| Of which: Ammonia (NH_3) | 2.27 | ± 0.09 |
| L-Arginine | 0.03 | ± 0.01 |
| Primary Amino Nitrogen (PAN) | 0.32 | ± 0.01 |
| Total Phosphorus ($\text{PO}_4\text{-P}$) | 0.440 | ± 0.003 |
| Orthophosphate (PO_4^{3-}) | 0.11 | ± 0.001 |
| Sulphate (SO_4^{2-}) | 15.24 | ± 1.21 |

3.3.2 Methane production from residual solids of OMSW fibre hydrolysis

A total of 2.25 kg (by dry weight) of OMSW fibre was used for large scale hydrolysis, of which 1.63 kg or 72.5% (by dry weight) was recovered. This residual material had a moisture content of $58.9 \pm 0.3\%$, which constituted the ~ 2.3 Litres of liquid hydrolysate that could not be recovered after centrifugal separation. Furthermore, based on the hydrolysis yields calculated in section 3.3.1, it was estimated that 14.7% cellulose and 1.6% hemicellulose remained in the residual solids fraction. The relatively large fraction of polysaccharides and soluble sugars retained in this waste stream indicated it could potentially be used as a feedstock for anaerobic digestion (AD). The biomethane potential (BMP) of the residual solids was therefore assessed through two lab-scale AD experiments.

3.3.2.1 Small-scale anaerobic digestion assay

Using a small lab-scale AD apparatus (detailed in 3.2.8.1), methane production was measured over 46 days with a high (20% TS) and low (13% TS) loading of residuals and an 8% TS loading of OMSW fibre (**Figure 3.10**). OMSW fibre was used as a positive control because it has been widely demonstrated to be a good AD feedstock (Tyagi et al, 2018). To control for any lingering activity of the microbial community, the methane production of the inoculum (sludge from an industrial AD plant) was also measured.

For the first five days the samples equilibrated, rapidly releasing inherent gasses. The methane levels were therefore scaled to zero from day 5. Once the reactors equilibrated, very little gas production was observed from the samples for two weeks. However, the negative control steadily released methane throughout the duration of the experiment as the sludge still contained 2.5% solids for the microbial community to degrade. After a total of ~ 20 days the samples began producing methane in bursts with high variability between replicates. This is likely due to gasses becoming trapped because of the high solids content of the samples. However, the averaged data indicates that overall the residual material had a greater biomethane yield than the OMSW fibre. The samples containing residual material produced a total of 131.3 ± 79.3 biomethane for the high solids loading (**Figure 3.10, 'residuals (high)'**) and 121.5 ± 93.5 ml of biomethane for the low solids loading (**Figure 3.10, 'residuals (low)'**), or 2.5 and 2.2 times more than the negative control, respectively. The samples containing OMSW fibre produced the least methane overall, 45.7 ± 28.9 ml total, or 9.6% less than the control.

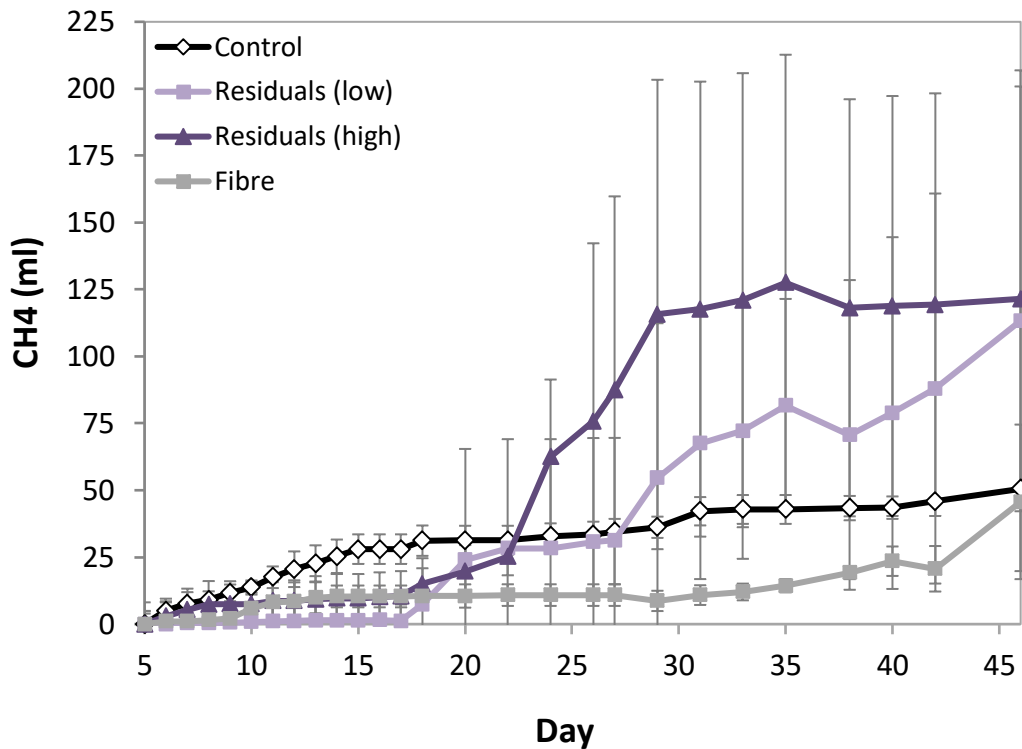


Figure 3.10: Cumulative biomethane yield from anaerobic digestion of OMSW fibre hydrolysis residual material over 46 days.

CH_4 = methane (ml); **Residuals (low)** = 20 g residual material (13% TS); **Residuals (high)** = 40 g residual material (20% TS); **Fibre (positive control)** = 15 g OMSW fibre (8% TS); **Control** = 40 g digestate only (2.5% TS);

Three assays were set up per feedstock. 40 g of digestate sludge was added to each sample. Measurement of methane production was started at day 5 to account for initial sample degassing. Error bars show standard deviation of triplicates. For details see 3.2.8.1.

AD of OMSW at high solids (>10% TS) has been demonstrated to be more efficient and economical than at low solids, but powered mixing is necessary to achieve sufficient agitation (Rivard et al, 1993). It was not possible to get consistent methane yield data over the short duration of this AD experiment, probably due to the inadequate agitation achieved by the small-scale anaerobic digestion apparatus with the high solids loadings. Nevertheless, the residual material showed good methane production potential and was therefore trialled at much lower (1.25%) solids loading using an automated lab-scale AD apparatus.

3.3.2.2 Automated lab-scale anaerobic digestion assay

To more accurately assess the BMP of OMSW fibre hydrolysis residuals an AD reactor feeding experiment was carried out with an automated lab-scale AD apparatus that measured biogas and methane yield in real time (outlined in **3.2.8.1**). The AD reactors were fed at regular intervals over 43 days with 50 ml of a 1.25% w/v suspension containing residuals or OMSW fibre. Volumetrically equivalent samples were removed before each feeding and analysed for total solids and COD.

The total solids content was similar for all reactors ($\sim 15 \pm 5$ g/L) and relatively stable over the course of the experiment, with a slight decreasing trend for the fibre ($R^2 = 0.49$) and residuals samples ($R^2 = 0.34$), while the negative control stayed relatively stable throughout ($R^2 = 0.05$) (**Figure 3.11**). This indicated that the microbial communities were efficiently utilising the carbon source after each feeding and the feedstock was not accumulating over time.

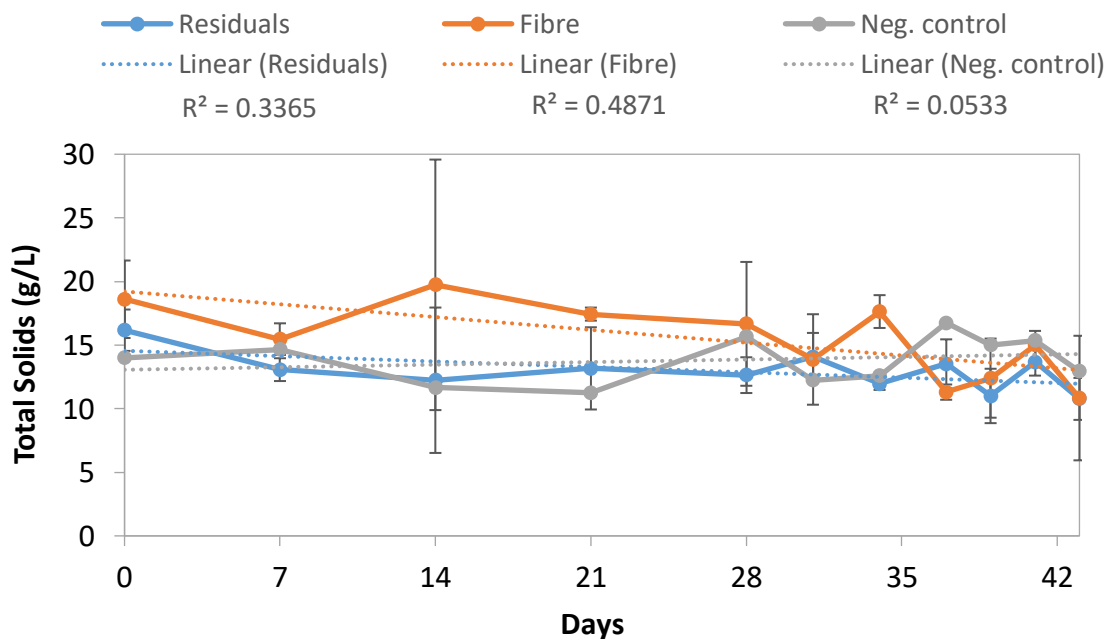


Figure 3.11: Total solids content of digestate from anaerobic digestion of OMSW fibre and residuals

Total dry solids were measured at regular intervals over 43 days in digestate samples from AD reactors fed with OMSW fibre (**Fibre**), residuals solids from OMSW fibre hydrolysis (**Residuals**) or water (**Neg. control**). Error bars show standard deviation of triplicates for Fibre and Residuals and duplicates for Neg. control.

This is supported further by the COD data (**Figure 3.12**). The COD of the feedstock suspensions was $46,733 \pm 416$ mg/L O₂ for the residuals and $1,199 \pm 58$ mg/L O₂ for the fibre, therefore the COD of the digestate would have increased over time if the AD community was not active. However, COD levels fluctuated in the range of 250-350 mg/L O₂ but did not increase, demonstrating that the AD community was efficiently utilising the carbon introduced at each feeding and the feedstock was not causing dysbiosis. There was no significant change in COD for residuals and fibre samples over the course of the experiment ($R^2 = 0.19$ and 0.09 , respectively) whereas COD decreased in the negative control samples ($R^2 = 0.72$), which were being starved of carbon over the course of the experiment.

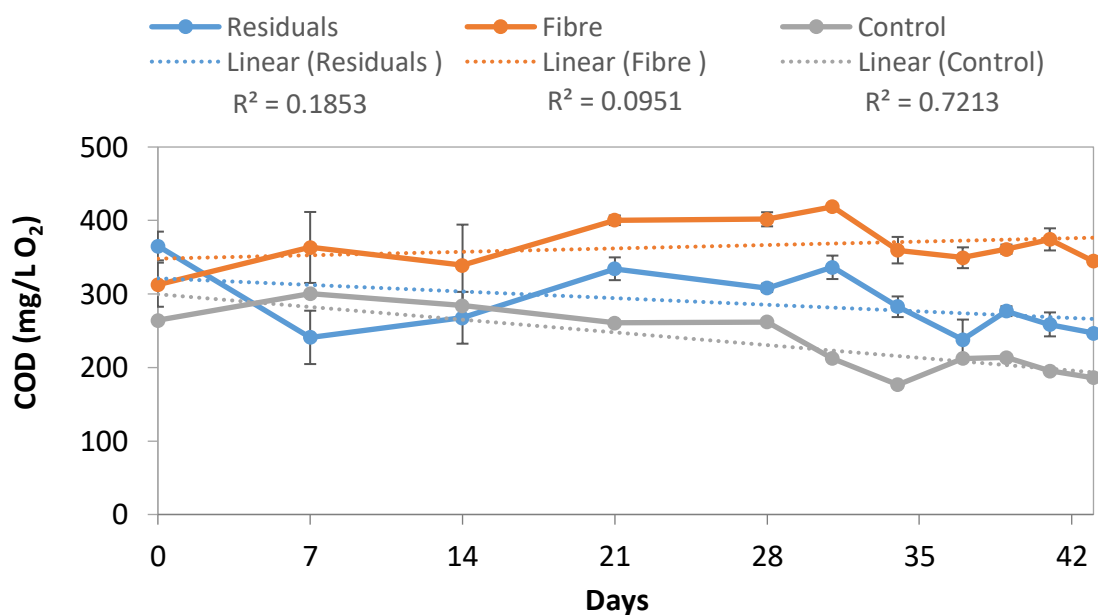


Figure 3.12: Chemical oxygen demand of digestate from anaerobic digestion of OMSW fibre and residuals

Chemical oxygen demand (COD, mg/L O₂) was measured at regular intervals over 43 days in digestate samples from AD reactors fed with OMSW fibre (**Fibre**), residuals solids from OMSW fibre hydrolysis (**Residuals**) or water (**Neg. control**). Error bars show standard deviation of triplicates for Fibre and Residuals and duplicates for Neg. control.

The total biogas yield and proportion of methane produced by each reactor was measured in real time over 43 days as detailed in **3.2.8.2**. Note that three reactors were trialled with each feedstock, but one fibre-fed reactor became faulty over the course of the experiment making biogas measurements inaccurate. Biogas and methane data from this reactor were therefore disregarded in all analyses presented in **Figure 3.13**.

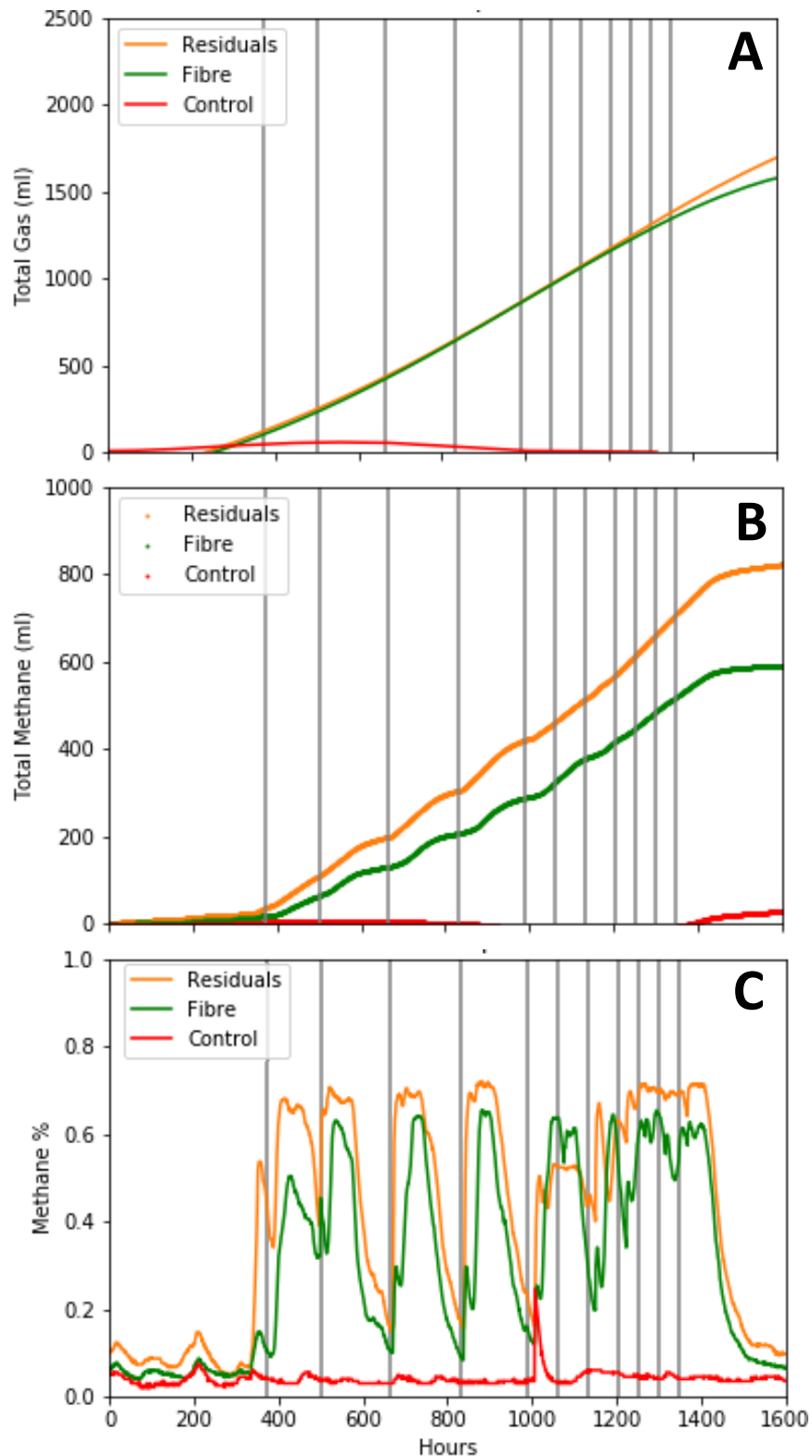


Figure 3.13: Cumulative biogas and methane production from anaerobic digestion of OMSW fibre and residuals

(A) Total gas (ml), **(B)** total methane (ml) and **(C)** percentage methane (%) produced over 1600 hours by AD reactors fed with OMSW fibre (**green**), residuals from OMSW fibre hydrolysis (**orange**) or water (**red**). Feeding days demarcated by vertical **grey lines**. First feeding at ~350 h and final feeding at ~1350 h (43 days). Residuals = averages of three AD reactors. Fibre = averages of two AD reactors. Control = averages of two AD reactors fed with water only.

There was no significant difference in the total biogas yield produced from the residuals compared to the fibre (**Figure 3.13-A**). Reactors fed with fibre and residuals produced a total of 1,532 ml and 1,753 ml of biogas, respectively. Although total biogas production was nearly identical for most of the experiment, the proportion of methane was significantly greater throughout for reactors fed with residuals, which produced 831 ml of methane (47.4% of total biogas), while fibre-fed reactors only produced 593 ml of methane (38.7% of total biogas) (**Figure 3.13-B**).

The rate of methane production rapidly increased after each feeding (demarcated by grey lines), but in reactors fed with residuals the high methane production was sustained for about 100 hours before dropping off (**Figure 3.13-C, 'Residuals'**), while in fibre-fed reactors there was a small spike in methane production after feeding followed by a second, larger peak that rapidly declined (**Figure 3.13-C, 'Fibre'**). Importantly, biogas production remained relatively stable once feedings increased in frequency (after 1000 h), indicating that the microbial communities could cope with more frequent nutrient and carbon source influx and still maintain efficient methane production. After feeding was stopped (after 1350 h) the methane levels declined in all reactors, although biogas production continued (**Figure 3.13-A and C, 1400 - 1600 h**).

The 33.4% greater methane yield attained from residuals could indicate that the microbial community present in these reactors was more efficient at methane production or that the feedstock was more easily converted to methane. To get a better understanding of the microbial community composition DNA was extracted from the final digestate samples and subjected to 16s rRNA sequencing. Between 197,697 and 250,036 reads were matched to 308 OTUs. Sequencing depth was sufficient to draw conclusions of taxonomic abundance as a stable measure of the Shannon Index, which quantifies species richness and evenness, was observed above 2,500 reads (**Appendix III**).

Species identified by phylogenetic amplicon analysis were grouped by their taxonomic affiliations at the phylum level to get an overview of the microbial community structure (**Figure 3.14**). Surprisingly, community composition was highly similar in reactors fed with residuals and reactors fed with OMSW fibre. The most abundant taxonomic groups were Bacteria of the phyla *Bacteroidetes*, *Firmicutes* and *Chloroflexi*. The *Spirochaetae*, *Proteobacteria* and Archaea in the phylum *Euryarchaeota* (for a comprehensive taxonomic table with all annotations see **Appendix IV**). These results are consistent with previous studies, which showed that *Firmicutes*, *Bacteroidetes*, *Proteobacteria*, *Chloroflexi*,

Spirochaetes and *Actinobacteria* are the dominant phyla found in industrial biogas reactors digesting municipal solid and liquid wastes and are generally associated with a healthy methanogenic community (Guo et al, 2015; Sundberg et al, 2013).

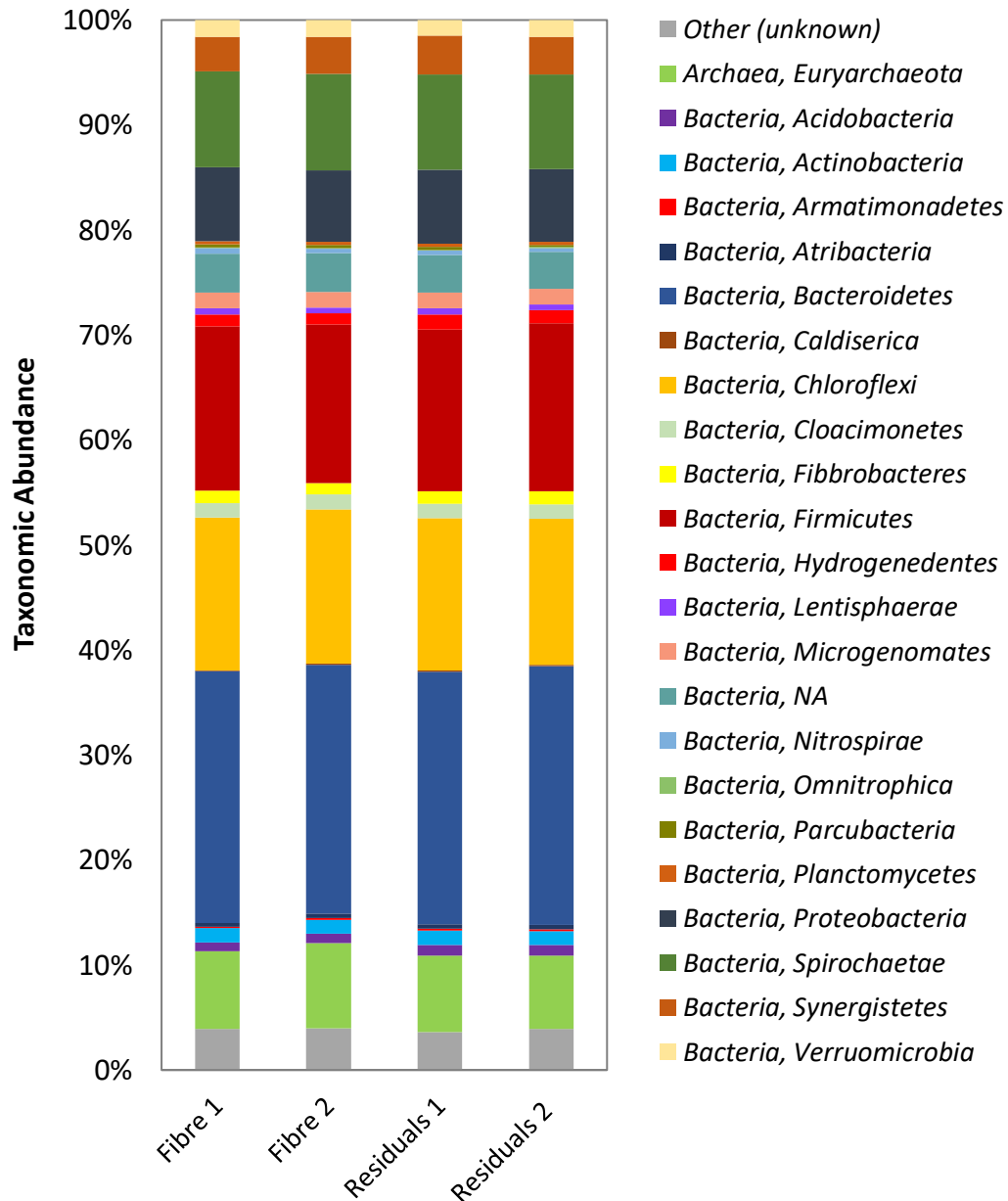


Figure 3.14: Taxonomic abundance of microbial communities after 43 days of anaerobic digestion with OMSW fibre or residuals, based on groupings of 16s rRNA sequences

The 16s rRNA amplicon profiles were assigned taxonomy in Greengenes (DeSantis et al, (2006)) and then grouped by Phylum to provide an overview of the taxonomic abundance within the digestate. A comprehensive table of all taxonomic annotations is provided in **Appendix IV**.

3.4 Discussion

A primary objective of this project was to produce a large, consistent volume of OMSW fibre hydrolysate for substrate-oriented screening of microbial species in subsequent work. Method development was therefore focused on producing a hydrolysate with enough sugars for fermentation and industrially realistic levels of inhibitors and metals. Although hydrolysis optimisation was outside the scope of this project, some observations were made while developing the hydrolysis methodology that would be pertinent to future bioprocess development for OMSW fibre.

Maintaining the pH of the slurry was a major challenge in preliminary experiments - the OMSW fibre demonstrated a strong buffering capacity which caused the pH to rise to ~6.5 over the course of hydrolysis, leading to inefficient and inconsistent saccharification between samples and thus significant variability between replicates. Calcium originating from CaCO_3 paper filler was present at high levels in the feedstock (~2 mol per Kg) and its alkalisng qualities probably greatly contributed to the high buffering capacity. CaCO_3 dissolution not only elevates pH beyond the optimal range for cellulases, but cellulases have also been shown to preferentially bind to CaCO_3 in the presence of hardwood pulp (Chen et al, 2012).

Previous studies with waste paper showed that removal of CaCO_3 by acid washing significantly improved hydrolysis efficiency (Wang et al, 2011b). However, the cost of adding large volumes of acid and water to solubilise CaCO_3 could be expensive at industrial scales. It is also important to consider that unlike waste paper, OMSW fibre contains high levels of toxic metals that could become solubilised into the wash water and would require specialised disposal, incurring additional costs. Furthermore, work by (Puri, 2014) on MSW-derived paper pulp found that washing out CaCO_3 with neutral detergent or H_2SO_4 had no effect on hydrolysis yields, whereas the addition of polyethylene glycol (PEG 6000) improved enzyme activity and availability, affording a 40% reduction in Cellic Ctec3 loading. The hydrolysis protocol developed for this project involved manual massaging of concentrated H_2SO_4 into the biomass until the optimal pH was reached, thereby avoiding the need for a washing step. This method was very labour-intensive on a lab scale but could have potential on an industrial scale as bioreactors can maintain pH by in-line monitoring and automatic dosing of acid while the biomass is agitated. Further work will be needed to evaluate the viability of this approach in conjunction with hydrolysis enhancers such as PEG 6000.

This chapter was largely focused on characterising the lignocellulosic hydrolysate produced from OMSW fibre and evaluating its potential for fermentation. Lignocellulosic hydrolysates are known to contain close to one hundred compounds, many of which inhibit microbial growth (Fenske et al, 1998; Heer & Sauer, 2008; Klinke et al, 2001). Due to its heterogeneous nature, OMSW is likely to contain even more diverse chemicals that would not be found in agricultural feedstocks. There are currently no published studies that report concentrations of common lignocellulose-derived inhibitors in OMSW hydrolysate. Two studies by Farmbordar et al (2018a; 2018b) reported total phenolics and tannins in dilute acid and organosolv pre-treated OMSW but did not provide details of specific compounds, while Ghanavati et al (2015) reported levels of 5-HMF and furfural in sulphuric acid pre-treated OMSW hydrolysate that had undergone detoxification by over-liming. This is the first time a comprehensive analysis of key fermentation inhibitors has been carried out on an enzymatic hydrolysate of OMSW.

The absence of furfural and 5-HMF in the OMSW fibre hydrolysate (**3.3.1.1, Table 3.1**) is promising as these inhibitors are the most prevalent source of toxicity-dependent growth inhibition in lignocellulosic hydrolysates, especially when present in combination (Almeida et al, 2009; Feldman et al, 2015; Heer & Sauer, 2008). Although unusual, an absence of furfural and 5-HMF has been reported for a range of feedstocks and pre-treatments, for example wet oxidised wheat straw (Klinke et al, 2003) acid steam pre-treated willow (Jönsson et al, 1998), and dilute acid pre-treated poplar, switchgrass and corn stover (Fenske et al, 1998). However, as levulinate is a breakdown product of 5-HMF the presence of 29.64 mM levulinate in the hydrolysate indicates that some 5-HMF was present but was degraded. Typically some residual 5-HMF would be expected in the sample, and its absence is peculiar. Unfortunately, it was not possible to measure formic acid to determine if furfural degradation also occurred, but very little would be expected as there is very little hemicellulose in the OMSW fibre. Similarly, the low level of organic acids in the hydrolysate is unsurprising as these are also derived from hemicellulose (Kim, 2018).

A notable finding from the hydrolysate analysis was that most metals from the OMSW fibre were retained in the residual solids fraction and only about a third of the total concentration of each metal was solubilised (**Figure 3.9**). On an industrial scale this phenomenon could buffer the fluctuation of metals and reduce some of the risk of metal toxicity in fermentations. The fact that the final concentrations of metals and inhibitors measured in the hydrolysate were all below the MICs reported for *E. coli* is also promising

(**Table 3.2**). That said, comparing M.I.C.s is only useful as a general assessment of OMSW fibre fermentability as these values are highly dependent upon the strains and conditions used and can vary greatly between studies. As discussed in **Chapter 2**, predicting how toxic different metal species will be to microorganism under fermentation conditions is challenging because metal toxicity is so dependent on environmental conditions and microbial physiology. Furthermore, although a wide range of marker inhibitors was measured, it is possible that other, less common inhibitory compounds could be present. The hydrolysate may also require nutrient supplementation to enable effective growth as YAN and phosphate levels were suboptimal (**Table 3.2**). Overall, to holistically evaluate the fermentability of OMSW fibre hydrolysate further assessment with growth and fermentation assays is necessary.

It was calculated that the metal concentration in the residual solids fraction was six times greater (by dry weight) than in the OMSW fibre. Disposing of this hazardous waste would require off-site transportation which incurs further operational costs. The fact that methane production from hydrolysis residuals was greater than from OMSW fibre (**Figure 3.13**) demonstrates that AD may be a viable option for further on-site valorisation of hydrolysis waste and potentially also metal immobilisation. The metal levels in the residual solids fraction did not inhibit the development of a robust methanogenic community (**Figure 3.14**), however in an industrial reactor toxicity could occur over time as metals accumulate in the digestate. Other studies have shown that anaerobic digestion can reduce the bioavailability of metals (Dong et al, 2013) and that metals can be immobilised further if necessary by subjecting the digestate to composting (Smith, 2009). These possibilities should be investigated for OMSW fibre biorefinery waste streams.

Both AD reactors fed with OMSW fibre and residuals produced almost identical microbial communities containing phyla closely associated with methanogenesis (**Figure 3.14**). The reactors fed with residual material produced more methane than those fed with OMSW fibre as the carbon in the residuals was probably more easily and rapidly accessible to the microbial community. As a by-product of saccharification, the residuals contained hydrolysed monosaccharides, cellobiose, partially degraded cellulose and also spent enzymes which could have provided nitrogen. The un-hydrolysed OMSW fibre on the other hand contained more recalcitrant polysaccharides that would require degradation before they could be used for methanogenesis and, based on the compositional analysis, only minor amounts of protein. This would explain why the reactors fed with residuals produced

more methane yields for a longer duration while a slower methanogenesis rate was observed from fibre-fed communities (**Figure 3.13-C**). The sudden spike in methane production observed in fibre-fed reactors after each feeding indicates a small amount of easily accessible carbon was present in the fibre but was quickly used up before the cellulose could be hydrolysed. A recent study by Mahmoodi et al, (2018a) also trialled anaerobic digestion of residual solids from hydrolysis of dilute acid pre-treated OMSW but found that the un-hydrolysed OMSW produced greater methane yields than the residuals. This is likely because 96% saccharification was achieved from the OMSW after dilute acid pre-treatment, so almost no sugars were left in the residuals. On an industrial scale the residuals waste stream may need to be combined with the spent cells and fermentation residues to ensure adequate carbon and nutrients for effective AD.

Chapter 4: Identifying Microorganisms for Optimal OMSW Fibre Hydrolysate Fermentation

4.1 Introduction

The compositional profile of OMSW fibre hydrolysate presented in **Chapter 4** showed that a wide range of toxic metals and inhibitors are present in OMSW fibre that may negatively impact fermentation efficiency and productivity. Past studies have primarily dealt with the inherent complexity and toxicity of OMSW by relying on the intrinsic robustness of mixed microbial communities or co-cultures. This approach has been successfully used to produce biogas (Anyaoaku & Baroutian, 2018; Lavagnolo et al, 2018; Razavi et al, 2019; Yuan et al, 2014; Zhang et al, 2012), hydrogen (Lay et al, 1999; Shah et al, 2016; Sharma & Melkania, 2018; Zhen et al, 2016) and acids (Aiello-Mazzarri et al, 2006; McCaskey et al, 1994) from a variety of OMSW sources. The few bioproducts that have been produced from OMSW through monoculture fermentations include ethanol, cellulases and TAG, as well as solventogenic fermentation products (acetone, butanol, ethanol, butyric acid and acetic acid).

A few studies have demonstrated ethanol fermentation from OMSW produced by autoclave pre-treatment using *S. cerevisiae* (Ballesteros et al, 2010; Puri et al, 2013). Ballesteros et al (2010) used autoclave pre-treated OMSW in a fed batch SSF process with *S. cerevisiae* at 20% TS and attained yields of 30 g/L ethanol (3% w/v) over 96 hours, equivalent to 60% of maximum theoretical yield. The authors calculated that 160 L of ethanol could be produced per tonne of OMSW via this process. Similarly, Puri et al (2013) carried out a two-stage fermentation of OMSW pulp in with an intermediate fermentation step using *S. cerevisiae*. This approach increased glucan conversion by 9% and produced a total ethanol yield of 5.5% w/v over the entire 6-day (144 h) SSF process. Overall these studies suggest that SSF is a promising route for converting autoclave pre-treated OMSW to ethanol.

Efficient ethanol production by SHF has also been demonstrated with OMSW obtained from a landfill site. *Mucor indicus*, a highly inhibitor tolerant fungus, produced ~0.8% ethanol from OMSW hydrothermally pre-treated at 160°C for up to 60 minutes in a lab-scale, autoclave-like process (Mahmoodi et al, 2018b). In a related study (Mahmoodi et al, 2018a), dilute acid pre-treated OMSW was fermented with the same fungus and ~1.9% ethanol was attained after 72 h. These yields are significantly lower than those achieved by Ballesteros et al, (2010) and Puri et al, (2013) with *S. cerevisiae*, likely because *M. indicus* is

not an established industrial strain. However, its high inhibitor tolerance makes it an intriguing species for OMSW biorefining and it could be improved further by selection and adaptive evolution for industrial applications.

Butanol has also been produced from OMSW sampled from an MSW composting plant with *Clostridium acetobutylicum*. Although *C. acetobutylicum* was initially inhibited by tannins in the OMSW hydrolysate, tannin extraction with ethanol alleviated inhibition and enabled production of 83.9 g butanol (71 g gasoline equivalents) and 20.8 g ethanol (13 g gasoline equivalents) per kg OMSW. The platform chemicals acetone (36.6 g/kg), acetic acid (14.6 g/kg) and butyric acid (41.8 g/kg) were also produced (Farmanbordar et al, 2018b). In a follow-up study, butanol was produced to even higher levels after the OMSW was detoxified with organosolv pre-treatment, yielding 102.4 g/kg butanol (85.3 g gasoline equivalents), 13.14 g/kg ethanol (8.2 g gasoline equivalents) and also 40.16 g/kg acetone, 19.72 g/kg acetic acid, and 47.21 g/kg butyric acid (Farmanbordar et al, 2018a). These results are promising as butanol and other ABE fermentation products are valuable fuels and platform chemicals, however, the economics of an additional detoxification step must be assessed by life cycle and techno-economic analysis.

Abdhulla et al, (2016) explored the production of cellulases from MSW fibre isolated through industrial-scale autoclaving by solid-state fermentation with the filamentous fungi *Aspergillus niger* and *Trichoderma reesei*. Crude enzymes isolated from *T. reesei* produced the best results, with a cellulase activity of 26.10 FPU/g at 30°C. The enzymes were evaluated for their ability to hydrolyse MSW and released 24.7% of available glucose. By comparison the commercial enzyme control, Cellic Ctec2, released 32.8% of available glucose over the same timeframe. This study showed that OMSW could potentially be used as a renewable, low-cost feedstock for producing cellulolytic enzymes that could be used in other biorefinery processes.

Finally, TAG was produced with the oleaginous yeast *Cryptococcus aerius* using OMSW from a commercial compost plant pre-treated with sulphuric acid. The yeast initially grew poorly on the hydrolysate due to the presence of metals and the inhibitors 5-HMF and furfural, therefore the feedstock was detoxified by over-liming. This process also reduce the nitrogen content, which was beneficial for improving TAG yields. The highest yields attained were 8.19 g/L FAs, primarily between C:14 – C:18, equivalent to 39.6 g of TAG per Kg of OMSW (Ghanavati et al, 2015). This study is the only example of microbial lipid production from OMSW.

The heterogeneous nature of OMSW is the main feature that may preclude its viability as a biorefining feedstock. As demonstrated in many of the studies outlined above, there are a number of unknown components present in OMSW that can be inhibitory to microorganisms, such as tannins, metals and chemical inhibitors. Furthermore, the diversity of sources from which OMSW is acquired for empirical studies, along with the inherent heterogeneity and variability of the feedstock, preclude the possibility of drawing conclusions about which species would be the best choice for developing an OMSW fibre biorefining platform. As such, this chapter examines the fermentation potential of eight different biotechnologically useful microorganisms using a substrate-oriented screening approach and presents several robust species with desirable characteristics for producing renewable fuels and chemicals from OMSW.

4.1.1 Aims of the Chapter

The primary aim of this chapter is to identify industrially useful microorganisms that are intrinsically well suited to growth on OMSW fibre hydrolysate and then optimise the best performing species for biomanufacturing. First, OMSW fibre hydrolysate fermentability will be holistically assessed through growth assays with the model fermentative microorganism *Escherichia coli* to evaluate hydrolysate toxicity and nutrient limitation. Next, a collection of eight biotechnologically useful microorganisms are assessed for their ability to grow on OMSW fibre hydrolysate and produce bioproducts. The most promising species will be further characterised and developed for industrial fermentation applications.

Key questions explored in this chapter include:

- Can OMSW fibre hydrolysate support the growth of the model fermentative microorganism *Escherichia coli*?
- Do nutrient deficiencies or substrate inhibition limit the growth of *E. coli* on OMSW fibre hydrolysate?
- Can OMSW fibre hydrolysate support the growth of other industrially valuable microorganisms?
- Can the most promising fermentative species be improved further for OMSW fibre bioprocessing?

4.2 Materials and Methods

4.2.1 Microorganisms, Chemicals and Media

All microorganisms used in this study, their respective culture conditions, routine culture media and fermentation products of interest are listed in **Table 4.1**. Note that facultative anaerobes were always pre-cultured aerobically but grown microaerobically in fermentations assays.

Table 4.1: Microorganisms, media and culture conditions used in this study.

**Rich medium used for routine culture maintenance, see details in text below;*

T= Optimum growth temperature (°C); TAG = Triacylglycerol;

| Species | Strain | T (°C) | Conditions | Maintenance Medium* | Product of interest |
|---|------------|--------|--------------------------|---------------------|---------------------|
| <i>Clostridium saccharoperbutylacetonicum</i> | DSM14923 | 30 | Anaerobic | RCM | Butanol |
| <i>Escherichia coli</i> | LW06 | 37 | Aerobic/ Microaerobic | LB | Ethanol |
| <i>Geobacillus thermoglucosidasius</i> | DSM2542 | 55 | Aerobic/ Microaerobic | TSB | Ethanol |
| <i>Pseudomonas putida</i> | NCIMB8249 | 30 | Aerobic | LB | <i>n/a</i> |
| <i>Rhodococcus opacus</i> | MITXM-61 | 30 | Aerobic | LB | TAG |
| <i>Saccharomyces cerevisiae</i> | ATCC200062 | 30 | Aerobic/ Microaerobic | YPD | Ethanol |
| <i>Schizosaccharomyces pombe</i> | JB953 | 32 | Aerobic/ Microaerobic | YES | Ethanol |
| <i>Zymomonas mobilis</i> | DSM424 | 30 | Aerobic/ Anaerobic | RM | Ethanol |

Reinforced Clostridial Medium (RCM), Luria-Bertani (LB) medium and Tryptic Soy broth (TSB) were purchased from Thermo Scientific (Oxoid). Rich Medium (RM) contained (per Litre) D-glucose (20 g), Yeast extract (10 g) and K₂HPO₄ (2 g). Yeast extract Peptone Dextrose (YPD) contained (per Litre) D-glucose (20 g), Yeast extract (5 g) and Bacto peptone (10 g). Yeast extract with supplements (YES) contained (per Litre) Yeast extract (5 g), D-glucose (30 g) and supplements (225 mg adenine, histidine, leucine, uracil and lysine hydrochloride). All components were purchased from Sigma-Aldrich.

Microorganisms were stored in their respective maintenance medium with glycerol (25%) at -80°C. Stock cultures were streaked onto 15% agar plates of their respective media to produce colonies. Plates were stored at 4°C for no more than 2 weeks. Note that *E. coli* LW06 was always grown with 100 µg/ml Ampicillin. In some experiments *E. coli* LW06 was grown on MOPS minimal medium, a defined medium developed by Niedhardt et al, (1974). The medium was prepared using the concentrations listed in **Table 4.2**. D-glucose was added as a carbon source at 5% w/v.

Table 4.2: Composition of MOPS minimal medium
Based on recipe by Neidhardt et al (1974).
Supplemented with carbon source as needed.

| Component | Concentration (mM) |
|--|----------------------|
| K ₂ HPO ₄ | 0.50 |
| NH ₄ Cl | 10.0 |
| MgCl ₂ | 0.523 |
| K ₂ SO ₄ | 0.276 |
| FeSO ₄ | 0.010 |
| CaCl ₂ | 5 x 10 ⁻⁴ |
| NaCl | 50.0 |
| MOPS | 40.0 |
| Tricine | 4.0 |
| (NH ₄) ₆ (MO ₇) ₂₄ | 3 x 10 ⁻⁶ |
| H ₃ BO ₃ | 4 x 10 ⁻⁴ |
| CoCl ₂ | 3 x 10 ⁻⁶ |
| CuSO ₄ | 10 ⁻⁵ |
| MnCl ₂ | 8 x 10 ⁻⁵ |
| ZnSO ₄ | 10 ⁻⁵ |

4.2.2 Seed Cultures

Seed cultures of each species were always prepared in triplicate on their respective maintenance media and grown up under the conditions listed in **Table 4.1**. Each replicate was grown up from a single colony taken from a fresh agar plate. To aerobically culture *E. coli*, *G. thermoglucosidasius*, *P. putida*, *R. opacus* and *S. cerevisiae* a loop of cells from a single colony was inoculated to 20 ml of rich medium in sterile tubes (50 ml, Falcon) and incubated with shaking at 200 rpm. Cultures of *C. saccharoperbutylacetonicum*, *Z. mobilis* and (where specified) *E. coli* were prepared in an anaerobic chamber and cultured according to the Hungate Method (Hungate, 1969). A loop of cells from a single colony grown on agar plates was suspended in sterile, anaerobic Milli-Q H₂O and transferred by

syringe to 100 ml serum bottles containing 20 ml of anaerobic maintenance medium supplemented with Resazurin indicator (1 mg/L) (Sigma-Aldrich). Note that for *C. saccharoperbutylacetonicum* 100 µl of defrosted glycerol stock was used as inoculum instead of plated colonies. Serum bottles were incubated with agitation at 100 rpm.

4.2.3 Nutrient Growth Assays with *E. coli*

4.2.3.1 Assays with Chemical Nutrients

Sterile OMSW fibre hydrolysate (described in **Chapter 3, 3.2.2**) was supplemented with essential nutrients (phosphorus (K_2HPO_4), sulphur (H_2SO_4) and nitrogen (NH_4Cl_2)) to determine which nutrients, if any, were limiting microbial growth. In all experiments 9 ml of OMSW fibre hydrolysate was buffered with MOPS (40 mM) and supplemented with different nutrient sources to a final volume of 10 ml. Nutrients were always supplemented at the following concentrations, either individually or in combination: 0.5 mM K_2HPO_4 , 0.3 mM H_2SO_4 , 10 mM NH_4Cl_2 . Control cultures were set up in parallel and are described in the relevant figure legends.

Nutrient-supplemented hydrolysates were transferred to sterile conical flasks (100 ml) with foam bungs and inoculated with *E. coli* LW06 from seed cultures. Seed cultures (set up as described in **4.2.2**) were harvested in mid-exponential phase, washed twice in Milli-Q H_2O and re-suspended in 1ml of Milli-Q H_2O to give a final optical density at 600 nm (OD_{600}) of 0.4. 250 µl of this suspension was transferred to a culture flask with 10 ml culture medium to give a starting OD_{600} of 0.01. Cultures were grown aerobically over 48 hours with aeration at 160 rpm. In some instances, MOPS minimal medium (recipe **Table 4.2**) was used as a control medium. 100 µl of culture medium was sampled at regular intervals for spectrophotometric measurement of optical density at 600 nm (OD_{600}). All experiments were carried out in biological triplicate with a single negative control flask for each condition. Media from negative control flasks was used to blank the spectrophotometer. All samples contained 100 µg/ml Ampicillin.

4.2.3.2 Assays with Nutritional Adjuncts

Hydrolysate growth assays were carried out as described above in **4.2.3.2** but, instead of supplementing the OMSW fibre hydrolysate with chemical nutrients, the hydrolysate was mixed with complex nutrients in the form vitamin-enriched yeast extract (VYE) (Sigma-Aldrich) or Corn Steep Liquor (CSL) (British Aqua Feeds). CSL and VYE were respectively prepared as 25% w/v stock solutions in Milli-Q H_2O and dissolved with heating in a 60°C

water bath before sterile filtration through a 0.22 µm syringe filter (Millex®). 9 ml of OMSW fibre hydrolysate was buffered with 40 mM MOPS and then supplemented with CSL or VYE to a final concentration of 1% v/v and made up a final volume of 10 ml with Milli-Q H₂O.

4.2.4 Fermentations

4.2.4.1 Fermentation Medium

Fermentation medium was prepared the same way for each fermentation: 9.4 ml of sterile OMSW fibre hydrolysate (prepared as described in **Chapter 3, 3.2.4**) was supplemented with 1% v/v sterile VYE and 40 mM MOPS buffer to give a final volume of 10 ml. For aerobic and microaerobic fermentations the medium was transferred to sterile conical flasks (100 ml). For anaerobic fermentations the medium was prepared in sterile wide-mouth conical flasks (250 ml) with foam bungs and allowed to deoxygenate in an anaerobic chamber for four days. Cysteine-HCl was then added to scavenge any residual oxygen. Serum bottles (100 ml) were deoxygenated in the anaerobic chambers for one week, sealed with rubber stoppers and crimp-tops and autoclaved. 10 ml of fermentation medium was aliquoted into the sterile anaerobic serum bottles by syringe. Fermentation medium was pre-heated to each species' optimal temperature before inoculation.

4.2.4.2 Fermentation Assays

Fermentations were set up with each species in triplicate using 10 ml fermentation medium (described in **4.2.4.1**). Two negative controls (fermentation medium only, no inoculum) were also prepared for each incubation temperature. For microaerobic fermentations with *S. cerevisiae*, *G. thermoglucosidasius* and *E. coli* cultures were grown in conical flasks (100 ml) sealed with one-way airlocks, depicted in **Figure 4.1**. Airlocks were cleaned with 70% propan-2-ol and filled with sterile water before insertion under sterile laminar flow. For aerobic fermentations with *R. opacus* and *P. putida* conical flasks with sterile foam bungs were used to promote aeration. For strictly anaerobic fermentations with *Z. mobilis* and *C. saccharoperbutylacetonicum* cultures were grown in serum bottles (100 ml) prepared under anaerobic conditions as described in **4.2.4.1**.

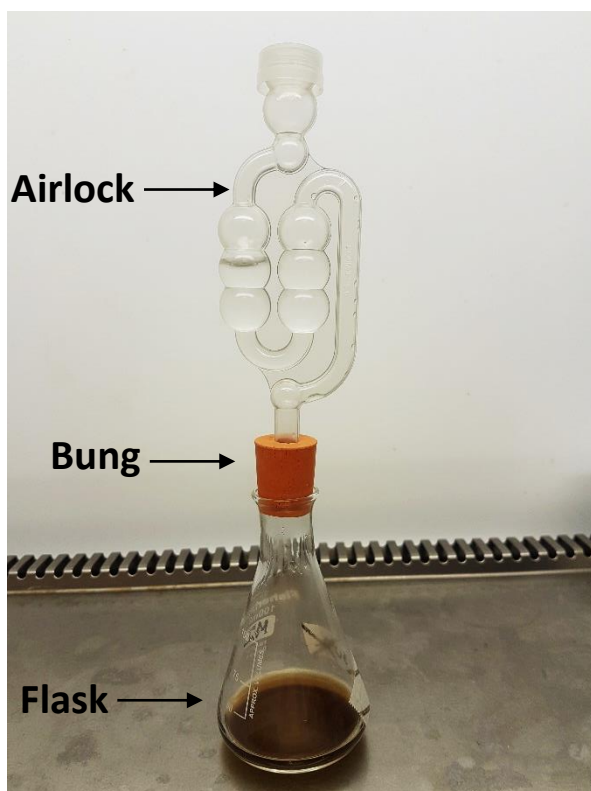


Figure 4.1:
Microaerobic fermentation set-up
(Image by Author).

A 100 ml conical flask containing 10 ml fermentation medium is fitted with a plastic airlock to simulate the microaerobic conditions of a batch fermentation. The airlock is inserted through a rubber bung and then sterilised with 70% propan-2-ol under sterile laminar flow. The rubber bung is used to tightly seal the flask, so any gasses produced during fermentation can only escape through the airlock. The airlock is filled with sterile water to prevent incursion of oxygen and contaminants from the environment.

Seed cultures of each species were set up as described in 4.2.2. Cells from seed cultures were harvested in mid-exponential phase and washed twice in Milli-Q H₂O before re-suspending in 1 ml of fermentation medium. The re-suspended cells were added back to each flask to give a starting OD₆₀₀ of 0.05. Cultures were incubated at each species' optimal temperature (see Table 4.1) with shaking at 160 rpm. 300 µl was sampled from fermentations and negative controls at regular intervals over 48 hours, or 72 hours for *R. opacus* and *P. putida*. A maximum of 100 µl of sample was diluted in Milli-Q H₂O and used for OD₆₀₀ measurement. The remaining 200 µl was stored in Safe-Lock Microtubes (0.5 ml, Eppendorf) at -20°C for use in further analyses. The final pH of each sample was also recorded at the end of each fermentation using pH strips (Fisherbrand) and the final cell dry weight (CDW) was determined with the remaining culture as described in 4.2.6.3

The dry cell material from *R. opacus* cultures was used to analyse fatty acid content and total TAG levels as described in 4.2.6.6. Fermentation samples were later defrosted, spun down (3,500 x g, 5 min) and 10 µl was used to analyse the levels of D-glucose and D-xylose (as described in 4.2.6.1). A further 10 µl of samples from *C. saccharoperbutylacetonicum*, *E. coli* (IPTG-induced), *S. cerevisiae*, *S. pombe* and *Z. mobilis* fermentations were subjected to acetone, ethanol and butanol analysis as described in 4.2.6.2.

4.2.4.3. TAG Production Time Courses

Fermentation time courses were carried out with *R. opacus* to better characterise TAG production over time. Aerobic fermentations were set up in triplicate as described in 4.2.4.2 but this time with 40 ml fermentation medium in 250 ml conical flasks. Seed cultures were prepared as described in 4.2.2, grown to mid-exponential phase and inoculated to the fermentation medium at an OD₆₀₀ of 0.05. Samples were incubated at 30°C with shaking at 250 rpm instead of 160 rpm to ensure enough aeration in the greater culture volume. Fermentations samples were taken over 6 days and stored in dry, pre-weighed 2 ml tubes (Eppendorf). 2 ml of medium was taken for time points at 0, 24, 48 hours, and 1 ml of medium taken for time points at 72, 96, 120 and 144 hours. Samples were defrosted and spun down (3,400 x g, 10 min) and then supernatants were taken into separate tubes. Pellets were dried and used to measure CDW at each time point as described in 4.2.6.3. Supernatants were used to measure D-glucose and D-xylose as described in 4.2.6.1 and YAN levels as previously described in Chapter 3, 3.2.7.5. Dry cell material from CDW measurement was used for fatty acid analysis as outlined in 4.2.6.6 below.

4.2.5 Light Microscopy

Rhodococcus opacus cells sampled over the course of fermentation (methods outlined in 4.2.4.2) were imaged using a light microscope. Cells from time points 24, 48 and 72 were defrosted and gently resuspended by pipetting. 5 µl of each sample was transferred to a glass microscope slide and mixed with 10 µl of Milli-Q H₂O. The suspension was mixed, spread evenly across the bottom two-thirds of the glass slide using the side of a pipette tip, and then fixed with a Bunsen Burner flame. Fixed cells were stained using a Gram staining kit (Remel) and left to dry at room temperature. Slides were examined under the light microscope at 100x magnification with oil immersion (no cover slip). At least three images were taken of each sample. Images were cropped and edited in Microsoft Office Power Point. Scale bars were calculated for each image based on the standard dimensions of 4164 x 3120 pixels per image and 0.0211 µm per pixel.

4.2.6 Biochemical Analytical Methods and Calculations

4.2.6.1 Glucose and Xylose

Frozen fermentation time course samples were thawed and centrifuged (4000 x g, 5 minutes). 10 µl of supernatant was serially diluted with dH₂O (1:1500 dilution for hydrolysates and fermentation time points 0, 12, 24, and 48; 1:1000 dilution for samples from all subsequent time points). Diluted samples were analysed by high-performance anion exchange chromatography (HPAEC) on an ICS-3000 PAD system with an electrochemical gold electrode using a Dionex CarboPac PA20 analytical column (3x150 mm) and guard column (3x30 mm). Identification and quantification of the major sugars in the hydrolysate (D-glucose and D-xylose) was carried out by comparing retention times and integrated peak areas of the samples to an equimolar standard mixture of D-glucose and D-xylose during the same run under the same conditions.

4.2.6.2 Ethanol, Butanol and Acetone

Ethanol, acetone and butanol were measured over as follows: 10 µl of each fermentation time-course sample was transferred to 2ml crimp-top flat-bottom GC vials and mixed with 500 µl of 1M NaCl containing 0.0004% propan-1-ol as an internal standard. Standards of ethanol, acetone and butanol were prepared at concentrations between 0.1-4.0% v/v, respectively. All samples were analysed on an Agilent 6890 Gas Chromatograph (GC) fitted with a Gerstel Multi-purpose 2 (MPS2) autosampler with SPME pink fibre (23-Gauge, 65µm, PDMS/DVB, SUPELCO) linked to a LECO Pegasus IV Time of Flight (TOF) Mass Spectrometer (MS). The GC was fitted with a glass injector liner (Ultra Intert, Straight 0.75 mm ID 5pk, Restek) Rxi5Sil Column with Integra guard (Restek) and was operated with an initial temperature of 70°C (2.5 min. hold) then ramped at 65°C/min. to 200°C and held for 1 minute before cooling at 70°C/min. to 70°C (1 min. hold). The MS mass range was 10-300 with an electron energy of -70V. The autosampler was run for 10 minutes, including cooling time (1-minute extraction, 0.1 minute desorb and 7 minutes fibre bakeout). Results were quantified against the propanol internal standard and standard curves. Results were converted from %v/v to g/L using the density of ethanol (0.789 g/cm³), butanol (0.810 g/cm³) or acetone (0.784 g/cm³) as described in **Equation 4.1**.

Equation 4.1: Converting from %v/v to g/L

$$A_{g/L} = \frac{(A_{\%}/100)}{D} \times 1000$$

Where:

- $A_{g/L}$ = concentration of the analyte in g/L
 $A_{\%}$ = percentage of analyte measured by GC-MS (acetone, butanol or ethanol)
 D = density of analyte (g/cm³)

4.2.6.3 Final Cell Dry Weight

At the end of fermentation 1 ml of each fermentation culture and negative control fermentation was transferred to dry, pre-weighed Microtubes (1.5 ml, Eppendorf). Samples were centrifuged (4,000 x g, 5 minutes) and washed twice in dH₂O to remove any soluble material. The pellets were frozen at -20°C and then lyophilised in a freeze dryer (Heto PowerDry LL3000). The final weight of the samples was subtracted from the initial tube weight to calculate the final mass of cell dry weight (CDW) per ml of fermentation broth. The final masses of the negative control fermentations were used to calculate the mass of insoluble solids (precipitate) formed in the fermentation medium after 1% VYE addition. The weight of precipitate was averaged for each pair of negative controls and subtracted from the final CDW of each associated fermentation to correct for the mass added by the precipitate. Note that for *R. opacus* MITXM-61 the entire remaining culture volume was transferred to dry, pre-weighed 15 ml conical tubes (Falcon), recorded and then subjected to centrifugation, washing, drying and weighing as described above. The dry *R. opacus* cells were also used for fatty acid profiling as described in 4.2.6.6.

4.2.6.4 Calculating Fermentation Yield Parameters

To quantitatively evaluate the fermentation efficiency of each species key yield parameters were calculated for each fermentation, including the percentage of total fermentable sugars consumed over the course of fermentation (**Equation 4.2**), the product to substrate ratio (i.e. specific yield) (**Equation 4.3**), the total product yield expressed as a percentage of the theoretical maximum (**Equation 4.4**) and the overall productivity in g/L.h⁻¹ (i.e. process productivity) (**Equation 4.5**).

Equation 4.2: Percentage of total fermentable sugars catabolised

$$\Delta \text{Sugars}_{total} (\%) = \frac{(Glu_i + Xyl_i) - (Glu_f + Xyl_f)}{(Glu_i + Xyl_i)} \times 100$$

Where:

$\Delta \text{Sugars}_{total}$ = Change in sugar concentration after fermentation as a percentage of the total available D-glucose and D-xylose (equivalent to the percentage of total fermentable sugars used). Sugars not fermented by the microorganism are disregarded.

Glu_i = Concentration of D-glucose at the start of the fermentation (g/L).

Xyl_i = Concentration of D-xylose at the start of the fermentation (g/L).

Glu_f = Concentration of D-glucose at the time of maximum product concentration (g/L)

Xyl_f = Concentration of D-xylose at the time of maximum product concentration (g/L)

Equation 4.3: The product to substrate ratio

$$P/S = \frac{P_{max}}{(Glu_i + Xyl_i) - (Glu_f + Xyl_f)}$$

Where:

P/S = The Product to Substrate ratio, also known as specific yield

P_{max} = The maximum concentration of product (g/L)

Glu_i = Concentration of D-glucose at the start of the fermentation (g/L)

Xyl_i = Concentration of D-xylose at the start of the fermentation (g/L)

Glu_f = Concentration of D-glucose at the time of maximum product concentration (g/L)

Xyl_f = Concentration of D-xylose at the time of maximum product concentration (g/L)

Equation 4.4: Percentage yield (product yield attained by fermentation, given as a percentage of the theoretical maximum yield from sugars)

$$\text{Yield} (\%) = \frac{P/S}{Y_{max}} \times 100$$

Where:

% Theoretical Yield = The product yield as a percentage of the theoretically calculated maximum yield for that fermentation product.

P/S = The Product to Substrate ratio (determined from **Equation 4.3**)

Y_{max} = The maximum theoretical yield, determined from the literature.
(Y_{max} ethanol = 0.511; Y_{max} Triacylglycerol = 0.316)

Equation 4.5: Fermentation productivity

$$\text{Productivity (g/L.h}^{-1}\text{)} = \frac{P_{max}}{T_{max}}$$

Where:

- Productivity* = The amount of product produced per litre of fermentation medium per hour, also known as process productivity, (g/L.h⁻¹)
- P_{max}* = The maximum concentration of product (g/L)
- T_{max}* = Time taken to produce the maximum concentration of product (*P_{max}*) in h

Equation 4.6: Yield per tonne

$$\text{Yield (Kg/t)} = S \times (P/S)$$

Where:

- Yield* = The amount of product that could be produced from one tonne of OMSW fibre, based on observed sugar conversion efficiencies, (Kg/t).
- S* = Total substrate (i.e. sugars) available in the feedstock (g/Kg)
- P/S* = The Product to Substrate ratio (g/g) (determined from **Equation 4.3**)

4.2.6.5 Calculating the Carbon to Nitrogen Ratio

The carbon to nitrogen ratio of the fermentation medium (OMSW fibre hydrolysate supplemented with 1% VYE) was determined using the **Equation 4.6**. The equation assumes that the major sugars in the hydrolysate (D-glucose and D-xylose) contain 40.001 % carbon atoms in the total mass and that all nitrogen in YAN (determined as described in **Chapter 3, 3.2.7.5**) is accessible to the fermentative microorganism.

Equation 4.6: Calculating the carbon to nitrogen ratio of fermentation media

$$C/N = \frac{\text{Sugars}_{total} \times \%C}{YAN \times M_{nitrogen}}$$

Where:

- C/N* = Carbon to Nitrogen Ratio
- Sugars_{total}* = Total concentration of microbially accessible sugars (g/L)
- YAN* = Total concentration of yeast available nitrogen (M)
- %C* = Percentage of carbon atoms in the sugar molecules
- M_{nitrogen}* = Molar mass of nitrogen (14.00643 g/mol)

4.2.6.6 Fatty Acid Profiling and Triacylglycerol Quantification

Fatty acid (FA) composition of triacylglycerols extracted from *R. opacus* MITXM-61 was determined by taking 5-10 mg of lyophilised (i.e. freeze-dried) cells into 2 ml screw cap GC vials and adding 10 µl of 25 mg/ml Heneicosanoic acid (21:0) internal standard (part no. H5149, Sigma). The samples were then transmethylated to fatty acid methyl esters (FAMES) by adding 500 µl 1N Methanolic HCl and 200 µl Hexane and heating at 85°C for 24 hours. The samples were cooled to RT, mixed with 250 µl 0.9% KCl and 600 µl Hexane, vortexed and left to rest for 5 minutes to allow for phase separation. Next, 100 µl of the upper (hexane) layer was transferred to a tapered GC vial with crimp-cap lid. 100 µl of hexane was prepared as a negative control and two vials with 50 µl external standard (37 Component FAMES mix, Certified Reference Material, Supelco). All samples were analysed on a Thermo Trace GC Ultra GC-FID (Gas Chromatograph with Flame Ionisation Detector) with an SGE BPX70 column (10M x 0.1 mm, part no. 054600). The FA levels measured in each sample were converted to mg of FA per mg of sample described in **Equation 4.7**. The mg/mg FA levels were summed for each time point and the grams of TAG per litre of fermentation broth were calculated as described in **Equation 4.8**.

Equation 4.7: Converting GC-FAMES peak areas to milligrams of fatty acid per sample

$$FA_{sample} \text{ (mg/mg)} = \frac{\left(\frac{A_{sample}}{A_{standard}} \times 250,000 \right) \times 10^{-6}}{Sample}$$

Where:

FA_{sample} = mg of fatty acid per mg of sample used in GC-FAMES analysis

A_{sample} = Peak area of the fatty acid methyl ester ($mV \cdot s^{-1}$)

$A_{standard}$ = Peak area of the C21:00 internal standard ($mV \cdot s^{-1}$)

250,000 = The nanograms (ng) of internal standard added to each sample

Sample = Mass of lyophilised cells used for analysis (mg)

Equation 4.8: Concentration of TAG per litre of fermentation medium

$$TAG \text{ (g/L)} = \left(\sum_i FA_i \right) \times CDW$$

Where:

TAG = mass of triacylglycerol (TAG) per litre of fermentation medium, g/L

$\sum FA_i$ = summation of each fatty acid in the sample, calculated in **Equation 4.7**

CDW = concentration of cells per litre of fermentation medium (cell dry weight), in mg/ml

4.2.6.7 Calculating the Cetane Number

To evaluate the ignition and combustibility potential TAG-derived FAs the cetane number (CN) was calculated using equations developed by Klopfenstein (1982) for a mixture of neat FAMES. The CN is a dimensionless number used to measure the quality of a fuel in terms of ignition and combustibility. The CN is scaled relative to cetane (n-hexadecane, C₁₆H₃₄) which is a completely straight (saturated) hydrocarbon (i.e. ignites easily under compression) and has thus been assigned a CN of 100. The CN of biodiesel usually falls between 35 and 65. A cetane index (CN_{*i*}) was calculated for each individual FAME using **Equation 4.9** and then the CN for the total FAME mixture extracted from *R. opacus* was calculated using **Equation 4.10**.

Equation 4.9: Calculating the cetane index for each FAME

$$CN_i = 58.1 + 2.8 \times \left(\frac{n_i - 8}{2} \right) - 15.9 \times db_i$$

Where:

*CN_{*i*}* = The cetane number index of the FAME, dimensionless.

*n_{*i*}* = The number of carbon bonds in the FAME molecule (between 8 – 24)

*db_{*i*}* = The number of double bonds in the FAME molecule, dependent upon saturation

58.1 = The cetane index for the shortest FAME within the scope of the equation (C8:00)

2.8 = Cetane index increment when the FAME chain is increased by two carbon atoms

15.9 = Cetane index increment when a double bond is present within the FAME molecule

Equation 4.10: Calculating the cetane number for a FAME mixture

$$CN = \sum_i w_i CN_i$$

Where:

CN = The cetane number for the total mixture of FAMES, dimensionless.

CN_i = The cetane index of an individual FAME, calculated with **Equation 4.9**

W_i = The mass percentage of an individual FAME within the FAME mixture, %w/w

4.2.7 Molecular Biology**4.2.7.1 Plasmids**

Plasmid pTip-QC1, used throughout this work, was developed by Nakashima and Tamura (2004a) as an inducible shuttle vector for cloning and protein expression in *E. coli* and *Rhodococcus* species (**Figure 4.2**). pTip-QC1 is 8,384 base pairs (bp) in length and contains ampicillin and chloramphenicol resistance genes for selection in *E. coli* and *Rhodococcus spp.*, respectively. To ensure maintenance and replication in *Rhodococcus* the *RepAB* region is required. *RepAB* contains a putative origin of replication and codes for two replication initiation proteins. The exact replication mechanism is unknown, but Θ -type is suspected based on homology to Rep proteins of ColE2 plasmids (Nakashima and Tamura, 2004b).

Expression at the multiple cloning site (MCS) is induced in the presence of 1 $\mu\text{g/ml}$ of thiostrepton, a cyclic oligopeptide antibiotic. Transcription is regulated by the formation of a complex between thiostrepton and the constitutively expressed regulator TipAL. This complex greatly increasing the affinity of RNA polymerase for the *tipA promoter* (P_{tipA}). Thiostrepton resistance is conferred by the *tsr* gene (*ThioR*) from *Streptomyces azureus* (Nakashima & Tamura, 2004b). The MCS contains an N-formylmethionine start codon (ATG), two hexa-histidine sequences for C- and/or N-terminal protein tagging and a range of unique cut sites for restriction cloning (*NdeI*, *EcoRI*, *SnaBI*, *NotI*, *BamHI*, *HindIII*, *BglII* and *XhoI*); Upstream of the MCS is the ribosome binding site (RBS) LG10, derived from gene 10 of T7 bacteriophage (Nakashima & Tamura, 2004a) (**Figure 4.2-MCS detail**).

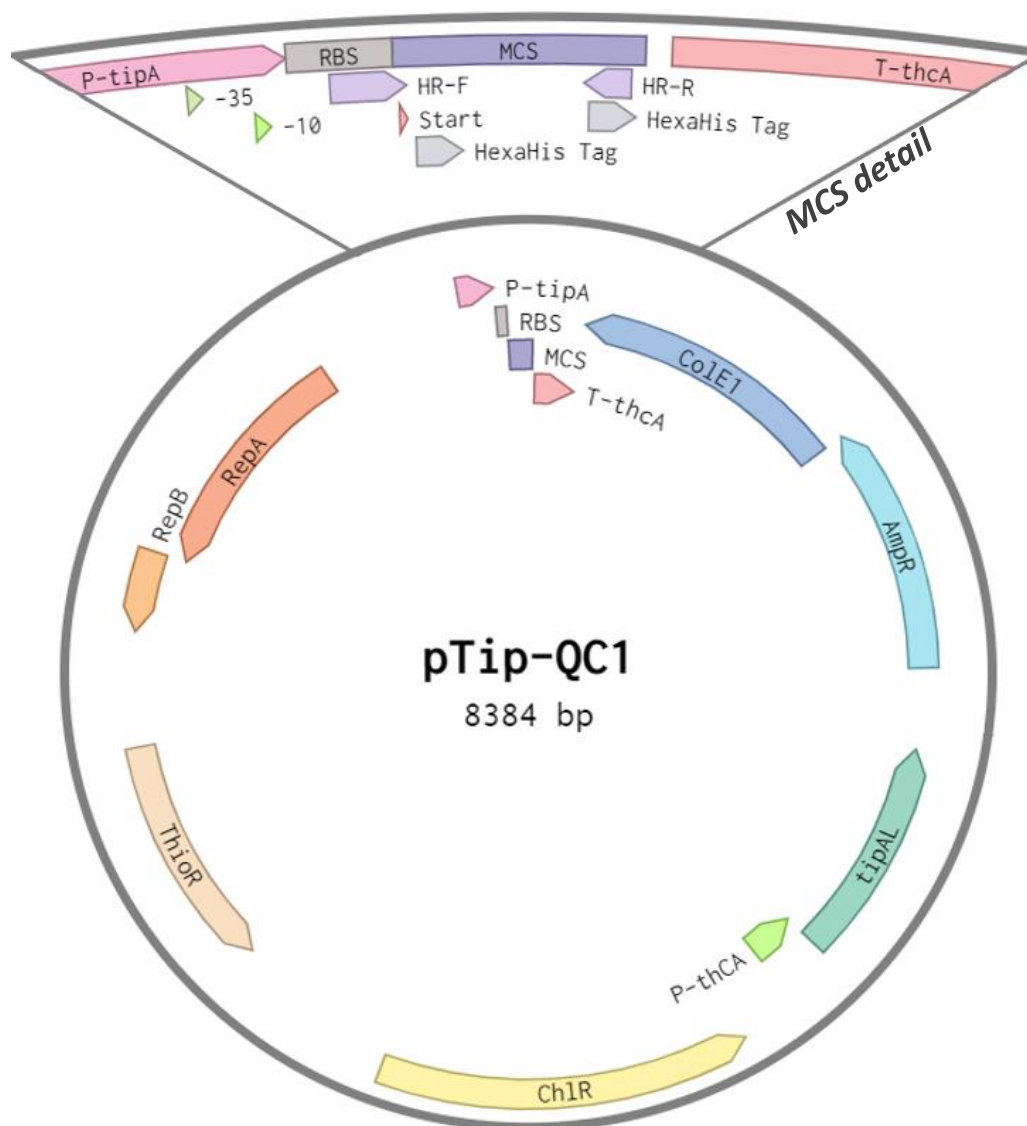


Figure 4.2: Map of plasmid pTip-QC1 with close-up of MCS
(Image generated by author using Benchling Informatics Platform)

Plasmid pTip-QC1 is an 8,384 bp Rhodococcus – E. coli shuttle vector designed for thiostrepton-inducible protein expression by Nakashima and Tamura (2004b).

P-tipA: Thiostrepton-inducible promoter *tipA*; **RBS:** Ribosome Binding Site; **MCS:** Multiple Cloning Site; **T-thcA:** Terminator *thcA*; **ColE1:** Replication origin for *E. coli*; **AmpR:** *Bla* for ampicillin resistance; **tipAL:** Transcriptional regulator of thiostrepton inducible transcription from P_{tipA} ; **P-thCA:** Constitutive promoter of the aldehyde dehydrogenase gene in *Rhodococcus erythropolis*, used for constitutive expression of *tipAL*; **ChlR:** Chloramphenicol resistance gene, from *R. erythropolis*; **ThioR:** Thiostrepton resistance gene; **RepA & RepB:** Region required for autonomous replication in *Rhodococcus spp.* **MCS detail (top):** -35 & -10: Shine-Dalgarno sequence; **Start:** Transcription Start codon; **HexaHis Tag:** Hexa-histidine sequence; **HR-F & HR-R:** Homologous regions selected for In-Fusion cloning, as detailed in 4.2.7.5 below.

4.2.7.2 Primers, PCR and Sequencing

Primers used for DNA sequence amplification by PCR and/or sequencing throughout this project are listed, along with their specific application, in **Table 4.3**. PCR was always carried out in a SimpliAmp Thermal Cycler using Phusion High Fidelity PCR Kit (Thermo Fisher Scientific). PCR reaction components are given in **Table 4.4** and the PCR protocol, based on manufacturer's instructions, is given in **Table 4.5**.

Sequencing of PCR products and plasmids was always carried out using a custom sequencing service provided by Eurofins Genomics (<https://www.eurofinsgenomics.eu>) using the Light Run Tube Barcode service. This service uses dideoxychain sequencing, a modified version of Sanger sequencing that generates high quality reads of ~500-2000 bp.

Table 4.3: PCR primers used throughout this project and their respective applications.

T_m = primer pair melting temperature (optimised for PCR conditions listed in **Table 4.5** and **4.6**.)

F/R = Forward or Reverse strand primer.

| Primer name | F/R | Sequence (5'-3') | T_m | Application |
|-------------|-----|-------------------------------|-------|--|
| MCS-f | F | CATGGTATATCTCCTTCTTAAAGTTAAAC | 60 | Linearisation of vector pTip-QC1 from target MCS |
| MCS-r | R | GAGCATCACCATCACCATC | | |
| 6097-6118_f | F | TCCGTGTTTGTGCAGGTTTC | 62 | PCR amplification and linearization of construct ACP-BTE |
| 6604-6625_r | R | GTTGTTCACTCTTCTGCTGGC | | |
| Seq-FWD | F | GCGTGGACGGCGTCTAGAAATAATTTT | 60 | Sequencing across pTip-QC1 MCS |
| Seq-RVS | R | TAAAAGGAGATATACCATGGCCACCACCT | | |

Table 4.4: PCR reaction components

*Adjust volume of H₂O to account for volume of template added.

| Component | Volume per 50 µl reaction (µl) |
|--------------------------------|--------------------------------|
| Nuclease free H ₂ O | 37.5 |
| 5x Phusion HF Buffer | 10.0 |
| 10 mM dNTPs | 1.0 |
| 10 µM Forward Primer stock | 0.5 |
| 10 µM Reverse Primer stock | 0.5 |
| Phusion Polymerase | 0.5 |
| Template DNA | At least 20 ng per reaction* |

Table 4.5: PCR protocol*See **Table 4.4** for details.

**At least 30 seconds per 1 kbp of DNA to be amplified.

| Step | Temperature (°C) | Duration (min:sec) | Cycles |
|----------------------|------------------------|----------------------|--------|
| Initial denaturation | 98 | 10:00 | X1 |
| Denaturation | 98 | 00:30 | |
| Annealing | Primer pair dependent* | 00:10 | X35-42 |
| Extension | 72 | Template dependent** | |
| Final extension | 72 | 00:10 | X1 |
| Hold | 4 | ∞ | ∞ |

4.2.7.3 Agarose Gel Electrophoresis

Agarose gel electrophoresis was carried out to visualise DNA products from PCR reactions. Agarose gels were prepared by dissolving 1% agarose in 0.5 x Tris-Borate-EDTA (TBE) buffer (recipe detailed in **Table 4.6**) by microwaving. Ethidium bromide was then added to a final concentration of 0.5 µg/ml. The gel mixture was poured into an electrophoresis gel cast (Bio-Rad) fitted with a 12-well comb and allowed to set at room temperature. The gel was submerged into a horizontal electrophoresis cell (MiniSub Cell CT, Bio-Rad) filled with 0.5 x TBE. PCR samples were mixed with 6 x purple gel loading dye (New England Biolabs) and loaded into the wells by pipetting. At least one well was always loaded with 10 µl of DNA Ladder (either: 1 Kb DNA Ladder (New England Biolabs) or 1 Kb Plus GeneRuler (Thermo Scientific)). Gels were run at 80-100 V until the lowest marker band progressed ~80% of the way down the gel. Gels were visualised and photographed on a UV gel doc (UVITEC Essential). Sizes of DNA bands were quantified against the standard bands of the DNA ladder.

Table 4.6: 10x Tris-Borate-EDTA Buffer Recipe*Working concentration = 0.5x*

| Component | Quantity | Concentration (M) |
|----------------------------|----------|-------------------|
| Tris | 121.1 g | 1.00 |
| Boric Acid | 61.8 g | 1.00 |
| EDTA (disodium salt) | 7.4 g | 0.02 |
| Distilled H ₂ O | to 1 L | - |

4.2.7.4 Synthetic DNA Design and Synthesis

The protein sequence of Acyl-acyl Carrier Protein Thioesterase BTE (referred to throughout this work as ACP-BTE) (NCBI accession no. Q41635.1, shown in **Figure 4.3**) was codon optimised for *Rhodococcus opacus* using JCat (Java Codon Adaptation Tool), an online codon adaptation tool developed by Grote et al, (2005). The DNA sequence was adapted to the codon usage of *Rhodococcus jostii* RHA1 (GC content = 66.98%) which was the closest related species available for codon optimisation in the JCat database.

| | |
|---|------------|
| MATTSLASAFCSMKAVMLARDGRGMKPRSSDLQLRAGNAPTSCLKMINGTK | 50 |
| FSYTESLKRLPDWSMLFAVITTFISAAEKQWTNLEWKPKPKLPQLDDHF | 100 |
| GLHGLVFRRTFAIRSYEVGPDRSTSILAVMNHMQEATLNHAKSVGILGDG | 150 |
| FGTTLEMSKRDLMWVVRRTHVAVERYPTWGDTEVECEWIGASGNNGMRRD | 200 |
| FLVRDCKTGEILTRCTSLSVLMNTRRLSTIPDEVRGEIGPAFIDNVAV | 250 |
| KDDEIKKLQKLNSTADYIQGGLTPRWNDLDVNQHVNNLKYVAWVFETVP | 300 |
| DSIFESHHSFTLEYRRECTRDSVLRSLTTVSGGSSEAGLVCDHLLQLE | 350 |
| GGSEVLRARTEWRPKLTDSFRGISVIPAEPRV | 382 |

Figure 4.3: Published protein sequence of Acyl-acyl Carrier Protein Thioesterase BTE from *Umbellularia californica*

Length: 382 amino acids; Molecular mass: 42.92 kDa
GenBank accession number: Q41635.1

To enable fusion cloning of ACP-BTE into expression plasmid pTip-QC1, the codon optimised sequence was modified to contain two sequences flanking the target insertion site in the MCS. The homologous sequences were placed at the start and end of the gene as shown in **Figure 4.4** and then synthesised using the Fisher Scientific GeneArt Gene Synthesis service. Fisher Scientific assembled the sequence from synthetic oligonucleotides and/or PCR products and inserted it into a pMK-RQ plasmid with Kanamycin resistance. The final construct was verified by sequencing and certified with 100% sequence identity by Fisher Scientific.

To isolate and amplify the construct DNA the plasmid was handled according to manufacturer's instructions as follows: the 5 µg of plasmid DNA provided was resuspended in the appropriate volume of Milli-Q H₂O and incubated for 1 hour at RT. The liquid was gently pipetted up and down to resuspend the DNA and then the sample was stored at -20°C). The construct was isolated from the pMK-RQ plasmid by PCR using primers 6097-6118_f and 6604-6625_r, as detailed in **4.2.7.2**. The amplified construct was confirmed by

DNA gel electrophoresis as described in 4.2.7.3 and then cloned into the target vector (pTip-QC1) as outlined in 4.2.7.5 below.

```

GTTTAACTTTAAGAAGGAGATATACCATG GCCACCACCTCCCTCGCCTCC 50
GCCTTCTGCTCCATGAAGGCCGTATGCTCGCCCGCGACGGCCGCGGCAT 100
GAAGCCCCGCTCCTCCGACCTCCAGCTCCGCGCCGGCAACGCCCCACCT 150
CCCTCAAGATGATCAACGGCACCAAGTTCTCTACACCGAGTCCCTCAAG 200
CGCCTCCCCGACTGGTCCATGCTCTTCGCCGTATCACCACCATCTTCTC 250
CGCCGCCGAGAAGCAGTGGACCAACCTCGAGTGGAAAGCCCAAGCCCAAG 300
TCCCCAGCTCCTCGACGACCACTTCGGCCTCCACGGCCTCGTCTTCCGC 350
CGCACCTTCGCATCCGCTCTACGAGGTCGGCCCCGACCGCTCCACCTC 400
CATCTCGCCGTCATGAACCACATGCAGGAGGCCACCCTCAACCACGCCA 450
AGTCCGTCGGCATCCTCGGCGACGGCTTCGGCACCACCCTCGAGATGTCC 500
AAGCGCGACCTCATGTGGGTCGTCCGCCGACCCACGTCGCCGTCGAGCG 550
CTACCCACCTGGGGCGACACCGTCGAGGTCGAGTGCTGGATCGGCGCCT 600
CCGGCAACAACGGCATGCGCCGCGACTTCTCGTCCGCGACTGCAAGACC 650
GGCGAGATCCTCACCCGCTGCACCTCCCTCTCCGTCTCATGAACACCCG 700
CACCCGCCGCTCTCCACCATCCCCGACGAGGTCCGCGGCGAGATCGGCC 750
CCGCTTCATCGACAACGTCGCCGTCGAAGGACGACGAGATCAAGAAGCTC 800
CAGAAGCTCAACGACTCCACCGCCGACTACATCCAGGGCGGCCTACCCC 850
CCGCTGGAACGACCTCGACGTCAACCAGCACGTCAACAACCTCAAGTACG 900
TCGCCTGGGTCTTCGAGACCGTCCCCGACTCCATCTTCGAGTCCCACCAC 950
ATCTCCTCCTCACCCTCGAGTACCGCCGCGAGTGCACCCGCGACTCCGT 1000
CCTCCGCTCCCTACCACCGTCTCCGGCGGCTCCTCCGAGGCCGGCCTCG 1050
TCTGCGACCACCTCCTCCAGCTCGAGGGCGGCTCCGAGTCTCCGCGCC 1100
CGCACCGAGTGGCGCCCCAAGCTCACCGACTCCTTCGCGGCATCTCCGT 1150
CATCCCCGCGAGCCCCGCGTCGAGCATCACCATCACCATC 1191
    
```

Figure 4.4: DNA sequence synthesised using GeneArt Synthesis Service

Total sequence length = 1,191 bp.

Grey = Codon optimised DNA sequence of acyl-acyl carrier protein Thioesterase BTE (ACP-BTE) from Umbellularia californica.

Blue = Homologous sequences of target cloning site in the pTip-QC1 MCS, to enable fusion cloning as described in 4.2.7.5 below.

4.2.7.5 In-Fusion Cloning

In-Fusion cloning is a rapid, efficient and directional cloning method in which a PCR fragment containing the gene of interest is enzymatically fused with a target site in a DNA vector. Unlike traditional restriction enzyme-mediate cloning, In-Fusion cloning does not require restriction or ligation enzymes. Although the precise mechanism of action is proprietary, the basic methodology and principle is described in **Figure 4.5**. Fusion cloning works rapidly and seamlessly so long as there is a 15-20 bp homology between the ends of the PCR product and the target site.

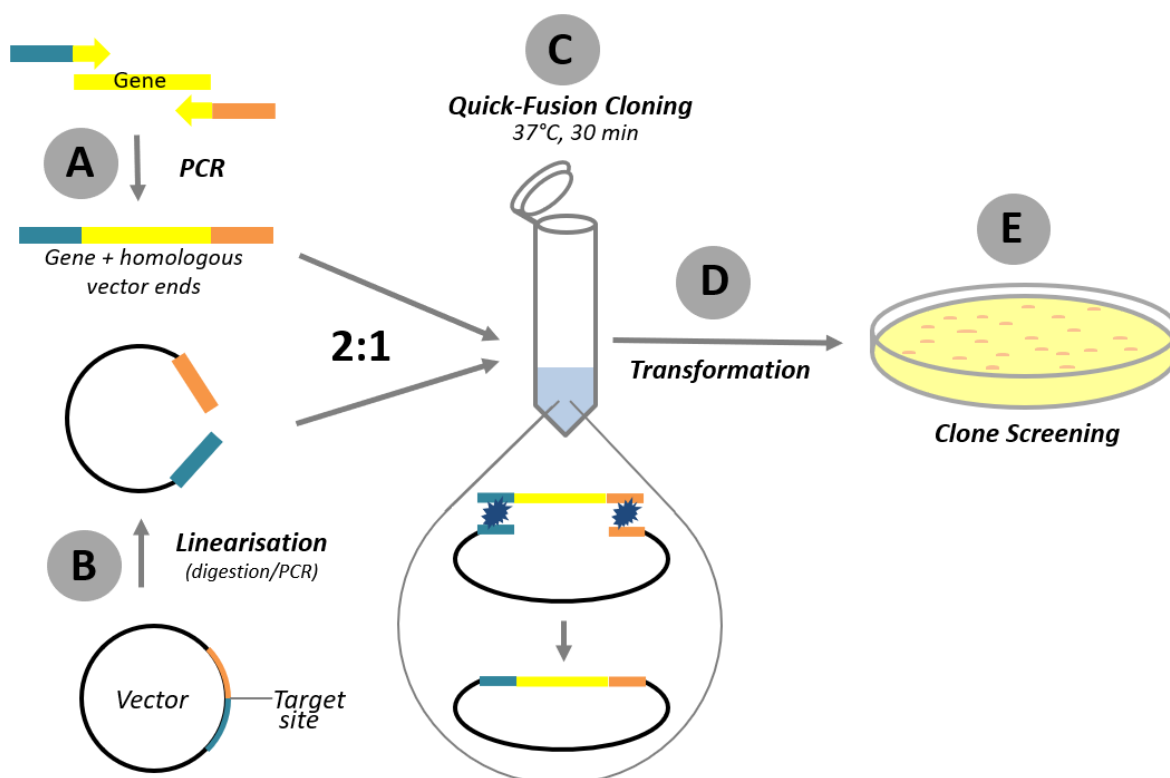


Figure 4.5: Overview of Quick-Fusion Cloning Protocol
(Schematic by author based on BioTool One-Step Cloning Kit Manual)

A: The gene of interest is amplified by PCR using gene-specific primers with a ~15 bp overhang homologous to the target cloning site of the vector. This produces a linear insert with ~15 bp of directional homology to the target cloning site on either end.

B: The vector is linearised by PCR or restriction enzyme digestion at the target cloning site.

C: Linearised vector and insert are mixed at a 2:1 (insert:vector) molar ratio in a tube and combined with the components of the Quick-Fusion Cloning Kit. The mixture is then incubated at 37°C for 30 mins so the components can react.

D: High efficiency competent cells are transformed directly with the Quick-Fusion reaction mixture.

E: Clones are screened by plasmid purification followed by sequencing or PCR amplification of the target cloning site to confirm successful integration of the insert.

In-Fusion cloning was carried out using a One-Step Quick-Fusion Cloning Kit (BioTool), according to manufacturer's instructions. Because the target gene was synthesised (detailed in 4.2.7.4), the construct was designed to already contain ends with homology to the target cloning site. This eliminated the need for PCR amplification with overhang primers as described in Figure 4.5-A. Instead the insert was prepared from the synthesised construct. Vector pTip-QC1 (described in 4.2.7.1) was linearised by PCR using

primers MCS_f and MCS_r (detailed in 4.2.7.2). The Quick-Fusion reaction was set up in a total volume of 10 µl with a 2:1 molar ratio of insert:vector, 1 µl Fusion Enzyme and 2 µl 5x Fusion Buffer and then made up to volume with nuclease free H₂O. A negative control reaction was also set up without the addition of Fusion Enzyme. After 30 minutes incubation at 37°C 2 µl of reaction mixture was directly used to transform *E. coli* as described in 4.2.7.6 below. At least three successful clones were grown up in 5 ml LB with ampicillin (100 µg/ml) and plasmids were purified as described in 4.2.7.7 below. Presence of the insert was confirmed by sequencing as outlined in 4.2.7.2.

4.2.7.6 Transformation by Heat Shock

Transformation of plasmids into *E. coli* SoloPack® Gold Competent Cells (Stratagene) were carried out according to manufacturer's instructions. Briefly: Competent cells stored at -80°C were defrosted on ice. 1 µl of plasmid (~25-50 ng) was added to the cells and incubated on ice for a further 30 mins. As a negative control, 1 µl of nuclease free water was added to one tube of competent cells. As a positive control, 1 µl of manufacturer provided plasmid (pUC18 with ampicillin resistance) was added to one tube of competent cells. The competent cells were heat shocked for 60 seconds exactly in a water bath pre-heated to exactly 42°C. Immediately after heat shock, 175 µl of LB pre-heated to 37°C was added and tubes were incubated horizontally at 37°C with shaking at 200 rpm for 1 hour. The entire contents of each tube (200 µl) were plated directly onto LB agar selection plates with 100 µg/ml ampicillin, respectively. Plates were incubated overnight at 37°C and colonies were checked the following day.

4.2.7.7 Purifying Plasmids from *E. coli*

Cultures of *E. coli* carrying the plasmid of interest were grown up overnight in 5-10 ml of LB with Ampicillin (100 µg/ml). Plasmids were purified using a Wizard® Plus SV Miniprep Kit (Promega) according to manufacturer's instructions. The concentration of purified plasmids was quantified using a NanoDrop Microvolume Spectrophotometer (ThermoFisher). To produce plasmid at ≥1 µg/µl concentration necessary for transforming *R. opacus* (detailed in 4.2.7.8 below), cultures of *E. coli* carrying the plasmid of interest were grown up over 24 hours in ~200 ml LB with Ampicillin (100 µg/ml). Plasmids were then purified from the full culture volume using a Plasmid Maxi Kit (QUIAGEN) according to the low-copy number plasmid purification protocol provided by the manufacturer. When the

concentration of purified plasmid was too low samples were concentrated using a Savant DNA120 Speed-Vac Concentrator. Plasmids were verified by sequencing as described in and/or by PCR amplification of the MCS as described in **4.2.7.2**.

4.2.7.8 *Rhodococcus opacus* Competent Cell Production

Competent *Rhodococcus opacus* MITXM-61 cells were produced using the protocol reported by Kurosawa et al, (2013). *R. opacus* was grown overnight on 10 ml LB. 0.5 ml of the overnight culture was transferred to a 250 ml conical flask with 100 ml MB + 1.5% glycine (recipe **Table 4.7**). The culture was grown up at 30°C with shaking at 250 rpm for ~16 hours (to an OD₆₀₀ of ~0.25). The culture was transferred to two 50 ml Falcon tubes and centrifuged (3,500 xg, 10 min). Cell pellets were washed twice in 15 ml of EPB1 (20 mM 4-(2-hydroxyethyl)-1-piperazineethanesulfonic acid (HEPES) with 5% glycerol, adjusted pH to 7.2 with KOH and filter sterilised) and EPB2 (5 mM HEPES with 15% glycerol, adjust to pH 7.2 with KOH and filter sterilised). The final cell pellet was resuspended in 0.5 ml of EPB2 and 100 µl aliquots were transferred to sterile Eppendorf tubes (1.5 ml). Tubes were flash frozen in liquid nitrogen and stored at -80°C.

Table 4.7: Recipe for MB + 1.5% glycine

| Component | Concentration (g/L) |
|------------------|----------------------------|
| Yeast extract | 5.0 |
| Bacto Tryptone | 15.0 |
| Bacto Soytone | 5.0 |
| NaCl | 5.0 |
| Glycine | 15.0 |

4.2.7.9 Transformation by Electroporation

Plasmids were transformed to *Rhodococcus opacus* MITXM-61 by electroporation according to the protocol reported by Shao et al, (1995). Competent *R. opacus* MITXM-61 cells (prepared as described in **4.2.7.8**) were slowly defrosted on ice and then mixed with 2-3 µl of highly concentrated plasmid DNA (for efficient transformation at least 1 µg/µl is needed). As a negative control 2 µl of nuclease free water was added to one tube of competent cells. All cells, including the negative control, were transferred to 2 mm electroporation cuvettes (Molecular BioProducts, cat. #5520) and electroporated in an electroporator (BioRad Gene Pulser). Electroporation conditions were 2.5 kV, 25 µF and 400 Ω.

Immediately after electroporation cells were gently mixed with 600 μ l of pre-warmed LB (30°C) and transferred to 2 ml Eppendorf tubes. Cells were recovered for 3 hours by horizontal incubation in a 30°C incubator with shaking at 400 rpm. After incubation cells were gently spun down (3,000 x g, 10 mins), resuspended in 200 μ l LB, and the entire volume was plated onto LB agar selection plates with 34 μ g/ml chloramphenicol. Note that due to the lack of a suitable positive control plasmid 100 μ l of the negative control cells were plated onto a LB plate without selection antibiotic (to check competent cell viability) and the remaining 100 μ l were plated onto a normal selection plate. All plates were incubated at 30°C for a maximum of 5 days. Where electroporation was successful colonies appeared within 3-5 days.

4.2.7.10 Purifying Plasmids from *R. opacus*

To confirm plasmid identity in *R. opacus* at least three transformants were respectively grown up over ~48 hours in a 500 ml shake flask containing 200 ml LB with chloramphenicol (34 μ g/ml) for selection. Two hours before harvest 50 μ g/ml ampicillin was added to reduce membrane integrity and facilitate cell disruption during plasmid purification. Plasmids were purified from the full culture volume using a Plasmid Maxi Kit (QUIAGEN) according to the low-copy number plasmid purification protocol provided by the manufacturer. If the concentration of purified plasmid was below the requirement for sequencing samples were concentrated using a Savant DNA120 Speed-Vac Concentrator. Plasmids were verified by sequencing and/or by PCR amplification of the MCS as described in 4.2.7.2.

4.2.8 Recombinant Gene Expression

4.2.8.1 SDS-PAGE

R. opacus carrying pTip-QC1_ACP-BTE was grown up in triplicate on 10 ml LB with 20 μ g/ml chloramphenicol at 30°C with shaking at 250 rpm. After 16 hours cultures were induced with 1 μ g/ml thiostrepton and incubated for a further 24 hours. As a negative control a culture of *R. opacus* carrying pTip-QC1 (empty vector) was grown in parallel, induced with thiostrepton and treated like samples as described below. For the final 2 hours of growth 50 μ g/ml ampicillin was added to reduce membrane integrity and facilitate cell lysis. Cells were spun down (3,000 x g, 10 min), washed once in phosphate-buffered saline (PBS) (Sigma-Aldrich) re-suspended in 5 ml PBS and sonicated for a total of 15 min (3 seconds on, 7 seconds off, output 3.5).

Sonicated cultures were centrifuged (5,000 x g, 5 min) and 40 µl of the supernatant was taken into an Eppendorf tube. The pellet was washed once and resuspended in 5 ml PBS and then 40 µl was taken into an Eppendorf tube. Both supernatant (soluble protein) and pellet (insoluble protein) samples were mixed with 10 µl 4x loading dye (3 µl β-mercaptoethanol + 100 µl bromophenol blue) and boiled for 10 minutes in a heating block. Sodium dodecyl sulphate polyacrylamide gel electrophoresis (SDS-PAGE) was then carried out as follows: SDS-PAGE gels were prepared according to **Table 4.8** and set up in a Mini PROTEAN Tetra Vertical Electrophoresis cell (Bio-Rad). 20 µl of each sample was loaded onto the gel along with 5 µl of PageRule 10-180 kDa protein ladder (Thermo Fisher) and run for approximately 1 hour. The gel was stained for 6 hours in Coomassie blue and then de-stained overnight in a mixture of 10% acetic acid, 50% methanol and 40% H₂O.

Table 4.8: Recipe for preparation of SDS-PAGE resolving and stacking gel

Note: 10% APS to be prepared fresh every time. TEMED induces polymerisation and should be added last.

| Component | 12% resolving gel (ml) | 4% stacking gel (ml) |
|--------------------------|---------------------------|-------------------------|
| 30% w/v acrylamide | 4.00 | 0.65 |
| 1.5M Tris pH 6.8 | 2.50 | - |
| 0.5 M Tris pH 6.8 | - | 1.25 |
| 10% SDS | 0.10 | 0.05 |
| Milli-Q H ₂ O | 3.40 | 3.05 |
| 10% APS | 0.10 | 0.05 |
| TEMED | 0.01 | 0.005 |

4.2.8.2 Expression Time-Course

R. opacus^{pTip-QC1_ACP-BTE} and *R. opacus*^{pTip-QC1} were grown in a TAG time-course growth assay as described in **4.2.4.3**. This time however cultures were induced with 1 µg/ml thiostrepton after 48 hours in order to evaluate any changes in CDW, TAG production or FA profile in response to plasmid expression. Samples were taken every 24 hours for 6 days. Pellets were used to measure CDW at each time point as described in **4.2.6.3** and for total TAG quantification and fatty acid profile analysis as outlined in **4.2.6.6**.

4.3 Result

4.3.1 Evaluation of OMSW Fibre Hydrolysate Fermentability

Initial experiments demonstrated that *E. coli* could not be cultured under aerobic conditions on pure OMSW fibre hydrolysate. Growth limitation could have been caused by a variety of factors, including insufficient nutrients, nutrient inaccessibility, metal toxicity and/or the presence of unknown organic compounds. To assess the degree to which these factors were affecting growth a series of growth assays were carried out. OMSW fibre hydrolysate was supplemented with a source of nitrogen, sulphate or phosphate, either individually or in combination, and inoculated with *E. coli* LW06. OD₆₀₀ was measured over 48 hours as a proxy for growth. Positive control cultures included cells grown on MOPS minimal medium with 5% w/v D-glucose and cells grown on OMSW fibre hydrolysate supplemented with all components of MOPS minimal medium (except a carbon source) to the same final concentration (for detailed methods see 4.2.3.2).

The first series of assays (**Figure 4.6-A**) showed that OMSW hydrolysate supplemented with all chemical components necessary for growth (i.e. MOPS minimal medium) enabled *E. coli* to reach an OD₆₀₀ of ~5.5 (**Figure 4.6-A, 'Hydrolysate + Min. med.'**). Cells grown on the positive control medium (MOPS minimal medium + 5% D-glucose) produced ~40% less biomass (**Figure 4.6-A, 'Min. med. + 5% glucose'**) and no growth occurred on neat hydrolysate (**Figure 4.6-A, 'Hydrolysate (neat)'**). This indicated that growth on neat hydrolysate was primarily constrained by nutrient limitation rather than substrate inhibition.

Growth of *E. coli* on the OMSW fibre hydrolysate was investigated further by supplementing with a source of sulphate (K₂SO₄), ammonium (NH₄Cl) and phosphate (K₂HPO₄) at the same concentrations used in MOPS defined medium (**Figure 4.6-B**). In this series of assays cells grew to a slightly lower OD₆₀₀ overall, likely due to variations in seed cultures or a difference in the shaker model used. However, when compared to the positive control, the results showed that growth was not significantly increased by the addition of phosphate or sulphate (**Figure 4.6-B, 'Hydrolysate + S', 'Hydrolysate + P'**). In contrast, ammonium supplementation led to growth comparable with the MOPS minimal medium positive control (**Figure 4.6-B, 'Hydrolysate + N'**), although it did not restore growth to the level of hydrolysate supplemented with all components of MOPS minimal medium (**Figure 4.6-B, 'Hydrolysate + Min. med.'**). It was concluded that one or more nutrients were limiting growth, therefore another series of assays were carried out in which the

hydrolysate was supplemented with sulphate, ammonium and phosphate combinatorically (**Figure 4.6-C**).

Supplementation with both ammonium and phosphate (**Figure 4.6-C, 'Hydrolysate N & P'**) led to growth equivalent to the hydrolysate with minimal medium and hydrolysate supplemented with all three nutrients (sulphate, ammonium and phosphate). Overall this demonstrated that the OMSW fibre hydrolysate was primarily limited in nitrogen, with a secondary deficiency in phosphate but no significant limitation in sulphate. Nutritional supplements employed in industrial fermentations are typically derived from waste products from other industries, such as corn steep liquor, yeast autolysate or casein hydrolysate, because they are abundant and low cost (Kampen, 2014). Two industrially relevant nutrient supplements were therefore trialled with OMSW fibre hydrolysate: Corn steep liquor (CSL) (a by-product of corn wet-milling) (Liggett & Koffler, 1948) and vitamin-enriched yeast extract (VYE) (a substitute for yeast autolysate, a by-product of the brewing industry)(Kerby & Vriesekoop, 2017). Unfortunately, addition of 1% CSL led to immediate and irreversible precipitation of the hydrolysate which made OD₆₀₀ measurements impossible. Addition of 1% VYE only produced minimal precipitate formation, therefore this was trialled as an industrial nutrient adjunct.

Nutrients were measured in hydrolysate supplemented with 1% VYE as described in **Chapter 3 (3.2.7.5)** and are shown in **Table 4.9** alongside the nutrient levels measured in neat OMSW fibre (originally presented in **Chapter 3, Table 3.4**). Addition of 1% VYE increased the microbially available nitrogen (shown as YAN) and total phosphorus approximately 10-fold, while sulphate levels stayed similar, with a slight decrease due to the dilution effect from VYE addition. When *E. coli* was grown on OMSW fibre hydrolysate supplemented with 1% VYE cells entered exponential phase more rapidly (**Figure 4.6-D, 'Hydrolysate + 1% VYE'**) and produced almost twice as much biomass as cells cultured on hydrolysate supplemented with phosphate and ammonium (**Figure 4.6-D, 'Hydrolysate + N & P'**).

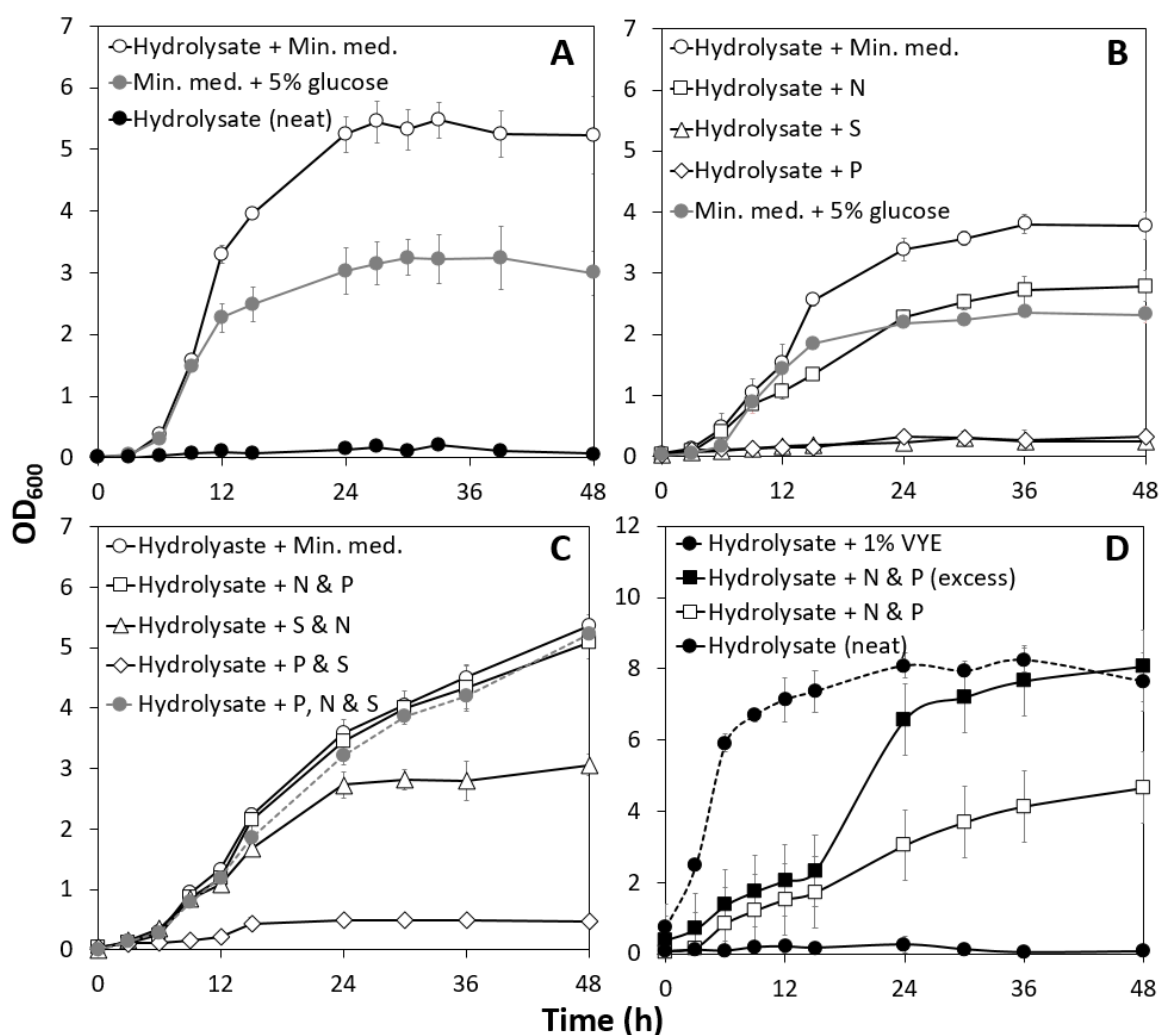


Figure 4.6: Growth of *Escherichia coli* LW06 on OMSW fibre hydrolysate supplemented with nutrients

All growth curves are averages of three biological replicates. Each plot represents a separate experiment. Error bars show standard deviation from the mean for triplicate fermentations.

A: OMSW fibre hydrolysate supplemented with MOPS minimal medium components ('Hydrolysate + Min. med.') or 40 mM MOPS buffer ('Hydrolysate (neat)'). Positive control fermentation: MOPS defined medium with 5% D-glucose ('Min. med. + 5% glucose').

B: OMSW fibre hydrolysate supplemented with 0.3 mM K₂SO₄ ('Hydrolysate + S'), 10 mM NH₄Cl ('Hydrolysate + N') or 0.5 mM K₂HPO₄ ('Hydrolysate + P'). 'Hydrolysate + Min. med.' and 'Min. med. + 5% glucose' as in A.

C: OMSW fibre hydrolysate supplemented with 10 mM NH₄Cl and 0.5 mM K₂HPO₄ ('Hydrolysate + N & P'), 0.5 mM K₂HPO₄ and 0.3 mM K₂SO₄ ('Hydrolysate + P & S'), or 0.5 mM K₂HPO₄, 10 mM NH₄Cl and 0.3 mM K₂SO₄ ('Hydrolysate + P, N & S'). 'Hydrolysate + Min. med.' as in A.

D: OMSW fibre hydrolysate supplemented with 1% vitamin-enriched yeast extract ('Hydrolysate + 1% VYE') or excess ammonium and phosphate (20 mM NH₄Cl and 1 mM K₂HPO₄) ('Hydrolysate + N & P (excess)'). 'Hydrolysate + N & P' as in C and 'Hydrolysate (neat)' as in A.

Table 4.9: Levels of phosphorus, orthophosphate, sulphate, nitrogenous compounds and calculated yeast available nitrogen (YAN) in OMSW fibre hydrolysate and OMSW fibre hydrolysate supplemented with 1% vitamin-enriched yeast extract (VYE).

*For details on methods and calculating YAN see Chapter 3, 3.2.7.5.

| Nutrient | Concentration (mM) | | | |
|---|--------------------|--------|---------------------|-------|
| | Neat Hydrolysate | | Hydrolysate +1% VYE | |
| | mM | ±SD | mM | ±SD |
| Yeast Available Nitrogen (YAN)* | 4.85 | ±0.14 | 46.63 | ±4.06 |
| Of which: Ammonia (NH ₃) | 2.27 | ±0.09 | 3.48 | ±0.10 |
| L-Arginine | 0.03 | ±0.01 | 0.82 | ±0.03 |
| Primary Amino Nitrogen (PAN) | 0.32 | ±0.01 | 5.28 | ±0.51 |
| Phosphate (PO₄ as phosphorus) | 0.44 | ±0.003 | 3.83 | ±0.17 |
| Orthophosphate (PO₄³⁻) | 0.11 | ±0.001 | 0.63 | ±0.01 |
| Sulphate (SO₄²⁻) | 15.24 | ±1.21 | 14.85 | ±0.52 |

E. coli attained a final OD₆₀₀ of ~8.0 on hydrolysate with 1% VYE, which contains approximately 7% w/v D-glucose and D-xylose (the major metabolically accessible sugars for *E. coli*). This level of biomass production is proportional to cultures grown on MOPS minimal medium containing 5% D-glucose, which entered stationary phase at an OD₆₀₀ of ~5.5 (**Figure 4.5-A, 'Min. med. + 5% glucose'**). It is also greater than the average growth of *E. coli* on the standard rich medium LB, which usually culminates at an OD₆₀₀ of ~7.0 (Sezonov et al, 2007). In fact, the high level of growth observed with VYE could only be recapitulated by culturing *E. coli* on hydrolysate supplemented with an excess of ammonium and phosphate (20 mM NH₄Cl₂ and 1 mM K₂HPO₄, respectively) (**Figure 4.5-D, 'Hydrolysate + N & P (excess)'**). However, these cells exhibited a longer lag phase compared to cells grown with VYE. This was surprising as ammonia is the preferred nitrogen source of *E. coli* and amino acids (the primary nitrogen source in VYE) are used less efficiently so slower growth would be expected (Wang et al, 2016).

Overall, the model fermentative microorganism *E. coli* demonstrated efficient and unrestricted growth on nutrient-supplemented OMSW fibre hydrolysate. The biomass levels attained were commensurate with the available sugars and no notable substrate inhibition from metals or inhibitors was evident. Furthermore, VYE was shown to have potential as an industrially relevant adjunct for supplementing microbially accessible nitrogen and phosphate in OMSW fibre hydrolysate fermentations.

4.3.2 Time-Course Kinetics of Eight Species Grown on OMSW Fibre Hydrolysate

Eight biotechnologically useful microorganisms were screened in a series of fermentation assays with OMSW fibre hydrolysate to identify species that are intrinsically well suited for biofuel or chemical production from this complex feedstock. Growth of each species was characterised on 10 ml of OMSW fibre hydrolysate supplemented with 1% VYE under optimal growth conditions (for strains and conditions see **Table 4.1**). Samples were taken at regular intervals over the course of the fermentation for a maximum of 72 hours and used to determine OD₆₀₀, sugar consumption and product accumulation. This data was plotted for each species, providing an overview of the fermentation dynamics with respect to growth, product synthesis and carbon utilisation. Fermentation kinetics are presented below for each species in alphabetical order.

4.3.2.1 *Clostridium saccharoperbutylacetonicum*

Clostridium saccharoperbutylacetonicum DSM14923 (also N1-4) is a Gram-positive, spore forming, strictly anaerobic solventogenic bacterium that produces n-butanol, an industrially valuable fuel and chemical, through the acetone, butanol and ethanol (ABE) fermentation pathway (Noguchi et al, 2013). The ABE fermentation process is biphasic, involving an initial acidogenic phase wherein acetate and butyrate are synthesised from sugars until the pH drops to around 4.5, at which point metabolism shifts more toward solventogenesis where organic acids are re-assimilated and fermented to butanol and ethanol (Buehler & Mesbah, 2016). *C. saccharoperbutylacetonicum* is closely related to the well-studied solventogen *Clostridium acetobutylicum* (Jang et al, 2012) and is of industrial interest because, unlike *C. acetobutylicum*, it can ferment both D-glucose and D-xylose simultaneously without carbon catabolite repression (CCR) (Noguchi et al, 2013).

C. saccharoperbutylacetonicum grew very poorly on OMSW fibre hydrolysate (**Figure 4.7**). Only 4% of available D-glucose was used and no significant change in D-xylose levels were detected. The cells had a ~12 hour lag phase and only reached a maximum OD₆₀₀ of 1.72 ±0.65. Furthermore, no ethanol, acetone or butanol were detected in the fermentation medium at any time point analysed. The final pH of the cultures was around 5.0-5.5, indicating that acidogenesis was interrupted. Overall, it appears that some component of the OMSW fibre hydrolysate was significantly inhibitory to *C. saccharoperbutylacetonicum*.

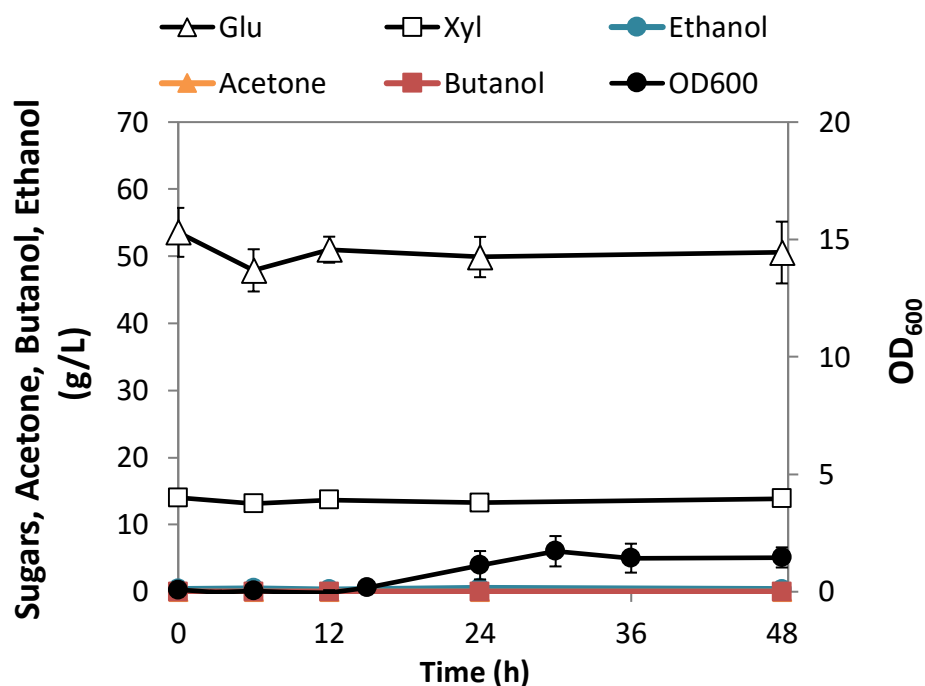


Figure 4.7: Fermentation kinetics of *Clostridium saccharoperbutylacetonicum* grown on OMSW fibre hydrolysate

C. saccharoperbutylacetonicum was grown anaerobically in 100 ml serum bottles on 10 ml OMSW fibre hydrolysate supplemented with 1% VYE and 40 mM MOPS buffer. Starting OD_{600} was 0.05. Samples were taken over 48 hours. For details see 4.2.4.2. Accumulation of products (ethanol, butanol, and acetone) and consumption of D-glucose (Δ Glu) and D-xylose (\square Xyl) are plotted on the primary Y-axis in g/L. Optical density at 600 nm (secondary Y axis) was used as a proxy for biomass production.

4.3.2.1 *Escherichia coli*

E. coli, the model organism of bacteriology, is of interest for biorefining applications because it is an established industrial microorganism, highly amenable to genetic manipulation and capable of using a wide range of lignocellulose-derived sugars, including D-glucose, L-arabinose and D-xylose (Huffer et al, 2012). *E. coli* is a Gram-negative facultative anaerobe that can produce ethanol in small quantities along with acetate, lactate and formate via mixed-acid fermentation (Valle et al, 2015). The strain used throughout this project, *E. coli* LW06, was engineered to more efficiently produce ethanol via an IPTG-inducible Entner-Doudoroff (ED) pathway (detailed in 1.2.4, Figure 1.8) derived from *Zymomonas mobilis* (Woodruff et al, 2013).

In preliminary nutrient supplementation assays with OMSW fibre hydrolysate (see 4.3.1) LW06 grew to a high OD_{600} of ~ 8.0 . However, these experiments were conducted under aerobic conditions without induction of the heterologous ethanol pathway. In the fermentation shown in **Figure 4.8**, *E. coli* was grown micro-aerobically to simulate batch conditions and ethanol production was induced with IPTG. Surprisingly, LW06 attained even higher biomass levels than in previous assays, reaching an OD_{600} of 18.1 ± 1.6 . D-glucose was depleted within 24 hours and used preferentially over D-xylose, as is typical of the sugar utilisation hierarchy in *E. coli* and most other hexose and pentose sugar fermenters (Aidelberg et al, 2014). The highest ethanol yield was attained after 24 hours, at 10.9 ± 0.5 g/L of ethanol (34 ± 2 % of maximum theoretical yield), coinciding with glucose depletion and entry into stationary phase.

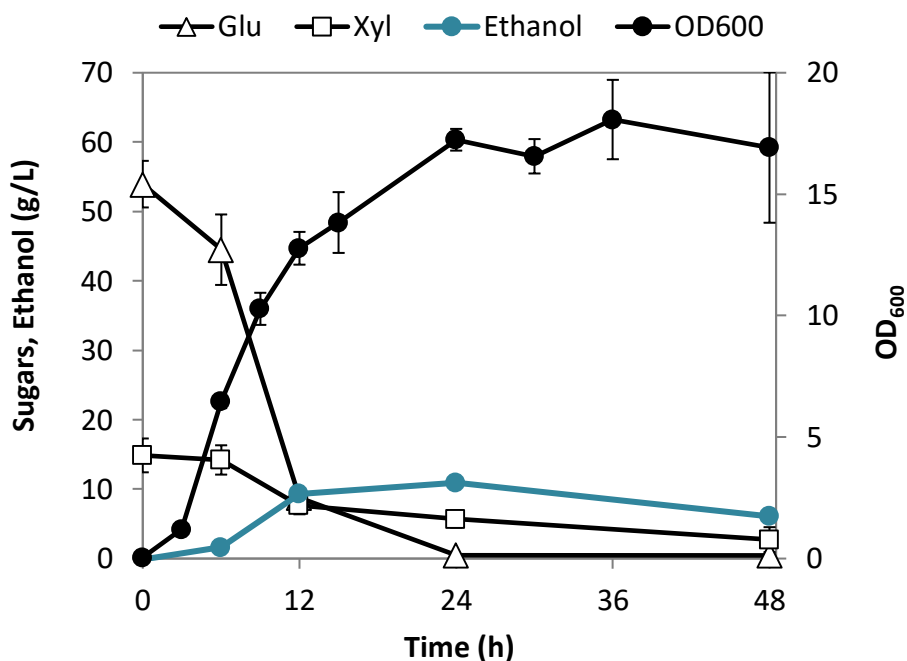


Figure 4.8: Fermentation kinetics of *Escherichia coli* grown on OMSW fibre hydrolysate

E. coli was grown micro-aerobically in 100 ml shake flasks with airlocks on 10 ml OMSW fibre hydrolysate supplemented with 1% VYE, 40 mM MOPS buffer and 1 mM IPTG to induce ethanol production. Starting OD_{600} was 0.05. Samples were taken over 48 hours. For details see 4.2.4.2. Accumulation of products (ethanol, butanol, and acetone) and consumption of D-glucose (Δ Glu) and D-xylose (\square Xyl) are plotted on the primary Y-axis in g/L. Optical density at 600 nm (secondary Y axis) was used as a proxy for biomass production.

4.3.2.2 *Geobacillus thermoglucosidasius*

Geobacillus thermoglucosidasius is a thermophilic, endospore-forming, Gram-positive facultative anaerobe that produces ethanol as part of a mixed-acid fermentation (Zeigler, 2014). Thermophilic bacteria are useful for bioprocessing as fermentations at high temperatures reduce cooling costs, increase biomass conversion efficiency and ethanol recovery and reduce the potential of contamination (Turner et al, 2007). Previous studies have shown that *G. thermoglucosidasius* can be engineered (Cripps et al, 2009) and evolved (Zhou et al, 2016) to produce greater ethanol yields, however, the strain used in this project is the type strain DSM2542 which has not been genetically modified.

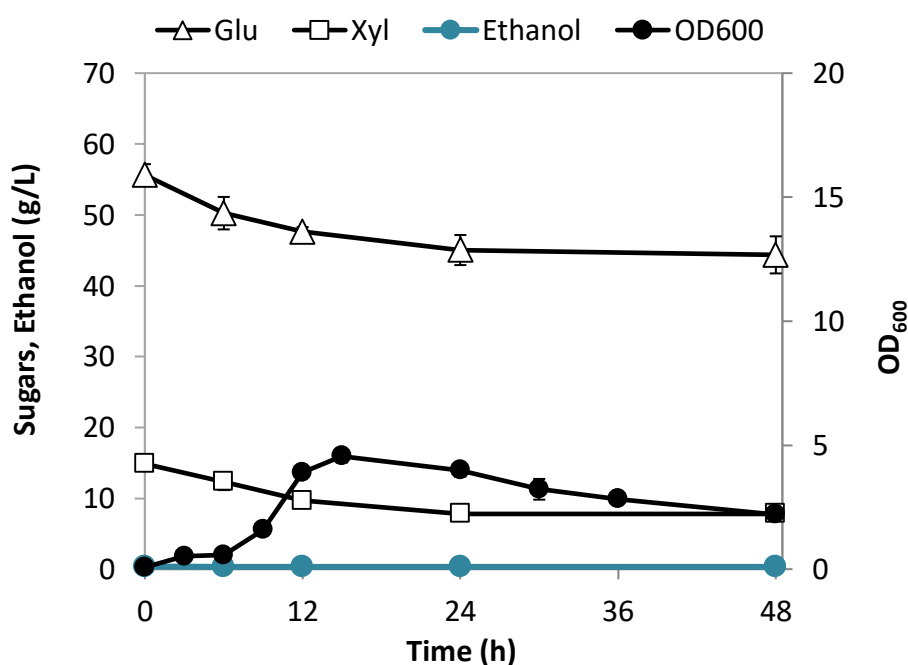


Figure 4.9: Fermentation kinetics of *Geobacillus thermoglucosidasius* grown on OMSW fibre hydrolysate

G. thermoglucosidasius was grown micro-aerobically in 100 ml shake flasks with airlocks on 10 ml OMSW fibre hydrolysate supplemented with 1% VYE and 40 mM MOPS buffer. Starting OD₆₀₀ was 0.05. Samples were taken over 48 hours. For details see 4.2.4.2. Accumulation of products (ethanol, butanol, and acetone) and consumption of D-glucose (Δ Glu) and D-xylose (\square Xyl) are plotted on the primary Y-axis in g/L. Optical density at 600 nm (secondary Y axis) was used as a proxy for biomass production.

Within the first 15 hours of fermentation on OMSW fibre hydrolysate *G. thermoglucosidasius* rapidly grew to an OD₆₀₀ of 4.55 ±0.38 while metabolising D-glucose and D-xylose simultaneously (**Figure 4.9**). Growth then stopped abruptly despite 61% of sugars remaining in the medium. Furthermore, no ethanol was detected in the medium at any time point analysed. During mixed-acid fermentation ethanol is produced along with acetate, lactate and formate (Zhou et al, 2016), therefore high ethanol yields were not expected. However, the complete absence of ethanol in conjunction with the premature growth cessation indicates that inhibition was caused by some component of the hydrolysate.

4.3.2.3 *Pseudomonas putida*

Pseudomonas putida is a Gram-negative aerobe known for its versatile metabolism and extensive resistance to xenobiotics and lignocellulosic inhibitors (Belda et al, 2016; Loeschcke & Thies, 2015). This species was chosen for this project as the extent of the toxicity of OMSW fibre was initially unknown. Although the strain used in this project, NCIMB 8249, does not produce an industrially useful product, previous work (Nikel & de Lorenzo, 2014) has shown that *P. putida* can be metabolically engineered to produce ethanol and has a greater ethanol tolerance than *E. coli*. *P. putida* has also been engineered to co-utilise cellobiose, D-glucose and D-xylose (Dvořák & de Lorenzo, 2018).

P. putida attained a final OD₆₀₀ of 13.6 ±0.1 on OMSW fibre hydrolysate but only managed to use 68.8% of the available D-glucose (**Figure 4.10**). Growth was somewhat biphasic, slowing after 12 hours to what could be a brief lag or possibly a detoxification phase and then increasing again after 36 hours. Stationary phase was reached at 48 hours, around the same time glucose metabolism stopped. Premature growth cessation indicates that something in the hydrolysate was inhibitory to the cells. One of the major limitations for *P. putida* as a biomanufacturing chassis is that it is very neutrophilic and does not possess all acid stress response pathways present in other Enterobacteria (Belda et al, 2016). The final pH of the fermentation medium was measured at around 3.0 for all three replicate cultures, indicating that growth may have been inhibited by autoacidification.

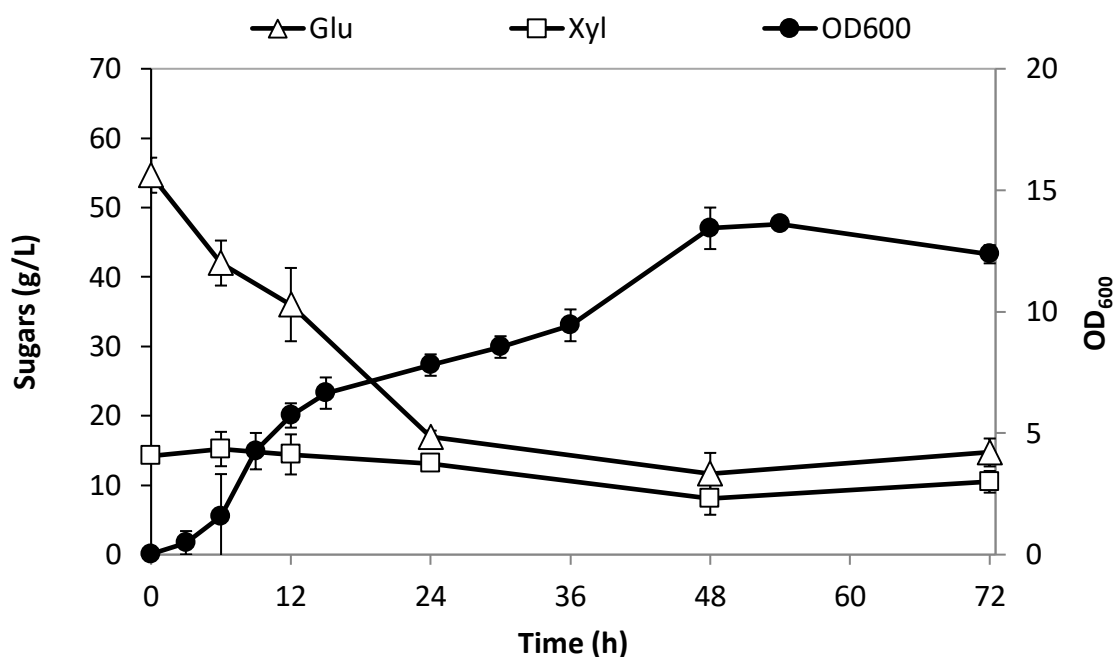


Figure 4.10: Fermentation kinetics of *Pseudomonas putida* grown on OMSW fibre hydrolysate

P. putida was grown aerobically in 100 ml shake flasks on 10 ml OMSW fibre hydrolysate supplemented with 1% VYE and 40 mM MOPS buffer. Starting OD₆₀₀ was 0.05. Samples were taken over 72 hours. For details see 4.2.4.2. Consumption of D-glucose (Δ Glu) and D-xylose (\square Xyl) are plotted on the primary Y-axis in g/L. Optical density at 600 nm (OD₆₀₀, secondary Y axis) was used as a proxy for biomass production. **Note this strain does not metabolise D-xylose.**

4.3.2.4 *Rhodococcus opacus*

Rhodococcus opacus is an aerobic, Gram-positive, soil-dwelling Actinomycete. Uniquely for a bacterium, *R. opacus* can produce and intracellularly accumulate triacylglycerol (TAG) from a wide range of carbon sources (Alvarez et al, 1996). A detailed overview of TAG biosynthesis is given in **Appendix IX**. TAG can be used as a precursor for the production of biodiesel, aviation fuel, plastics, surfactants and polymers. The highest reported volume of TAG accumulation by an *R. opacus* strain is 76% of CDW after growth on gluconate (Wältermann et al, 2000). *R. opacus* MITXM-61, used throughout this project, was evolutionarily engineered by Anthony J. Sinskey's group at the Massachusetts Institute of Technology (MIT) to co-utilise D-xylose with D-glucose (Kurosawa et al, 2014). The industrial potential of *R. opacus* for biorefining is well established and it has been grown with high productivity on numerous industrially useful substrates, including glycerol

(Kurosawa et al, 2015c) and hydrolysates of corn stover, wheat straw and hardwood pulp (Kurosawa et al, 2015a; Kurosawa et al, 2013; Kurosawa et al, 2014).

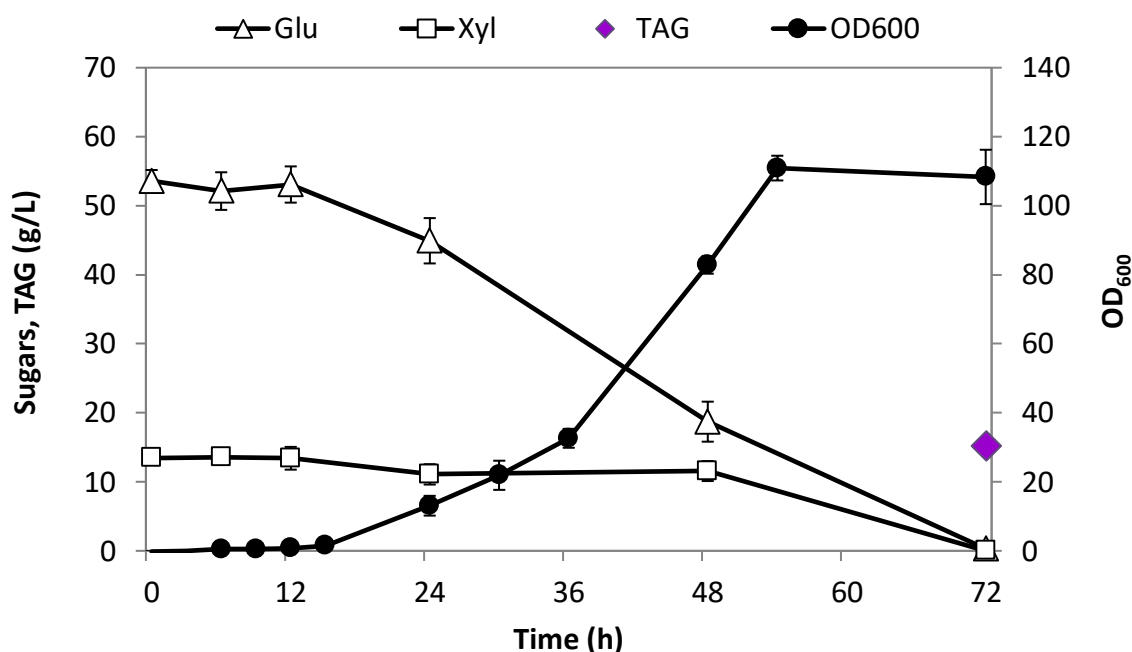


Figure 4.11: Fermentation kinetics of *Rhodococcus opacus* grown on OMSW fibre hydrolysate

R. opacus was grown aerobically in 100 ml shake flasks on 10 ml OMSW fibre hydrolysate supplemented with 1% VYE and 40 mM MOPS buffer. Starting OD_{600} was 0.05. Samples were taken over 72 hours. For details see 4.2.4.2. Accumulation of triacylglycerol (TAG) and consumption of D-glucose (Δ Glu) and D-xylose (\square Xyl) are plotted on the primary Y-axis in g/L. Optical density at 600 nm (OD_{600} , secondary Y axis) was used as a proxy for biomass production.

R. opacus MITXM-61 grew exceptionally well on OMSW fibre hydrolysate, attaining a high OD_{600} of 110.91 ± 3.58 (Figure 4.11). Growth started after a ~12-hour lag phase and D-glucose and D-xylose were concurrently depleted over 60 hours. Biomass production stopped after 54 hours although sugars were not yet depleted. This was not due to substrate inhibition however, because the stationary phase cells continued to use the remaining D-glucose and D-xylose. In *R. opacus* TAG synthesis typically occurs at the end of exponential phase and in early stationary phase when nutrients are limiting but carbon source is still abundant. Attaining high TAG yield therefore requires a carefully balanced carbon to nitrogen (C/N) ratio to ensure there is a high cell density at stationary phase but also sufficient residual carbon to store as TAG (Alvarez et al, 2013; Kurosawa et al, 2010). The addition of 1% VYE to OMSW fibre hydrolysate provided an C/N ratio of 44 (for

calculations see 4.2.5.3), enabling a TAG yield of 15.2 ± 1.1 g/L after 72 hours, equivalent to 48.91 ± 1.42 % of CDW or 72 ± 5 % of theoretical yield (note that TAG could only be quantified at the end of fermentation as at least 5 mg of cells were required for GC-FAMES, see 4.2.5.4.). It was concluded from these results that *R. opacus* is well adapted for efficient and robust growth on OMSW fibre hydrolysate.

4.3.2.5 *Saccharomyces cerevisiae*

Saccharomyces cerevisiae is the model organism for industrial biotechnology and has been studied extensively for lignocellulosic biorefining applications (Petrovič, 2015). *S. cerevisiae* is also one of the few microorganisms that has been used to ferment hydrolysates of OMSW (Ballesteros et al, 2010; Puri et al, 2013). Strain ATCC 200062 (also NREL D5A) is genetically derived from Red Star® baker's yeast and was used for this project because it has repeatedly been shown to robustly ferment lignocellulosic feedstocks (Nguyen et al, 2017; Spindler et al, 1989).

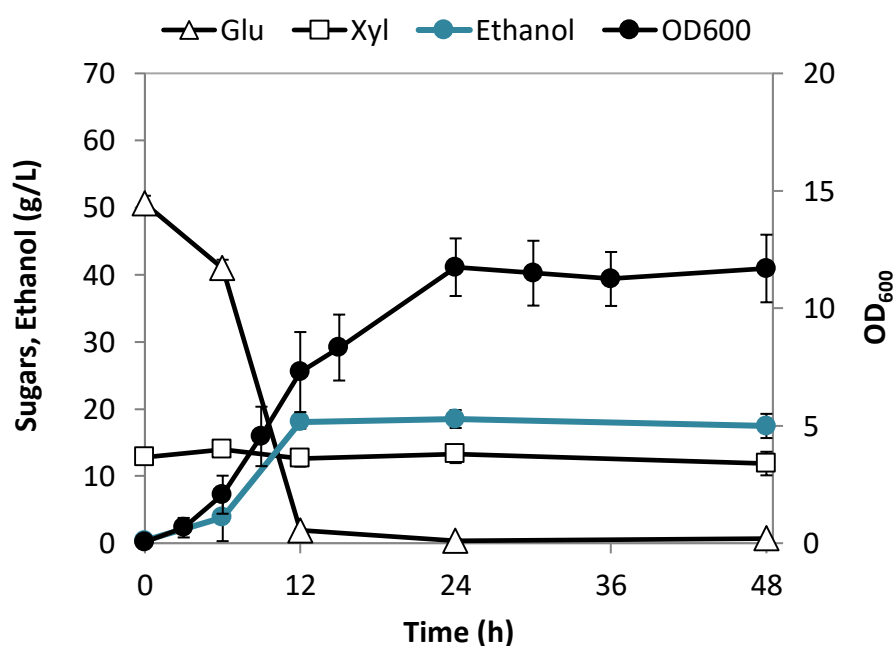


Figure 4.12: Fermentation kinetics of *Saccharomyces cerevisiae* grown on OMSW fibre hydrolysate

S. cerevisiae was grown micro-aerobically in 100 ml shake flasks with airlocks on 10 ml OMSW fibre hydrolysate supplemented with 1% VYE and 40 mM MOPS buffer. Starting OD₆₀₀ was 0.05. Samples were taken over 48 hours. For details see 4.2.4.2. Accumulation of ethanol and consumption of D-glucose (Δ Glu) and D-xylose (\square Xyl) are plotted on the primary Y-axis in g/L. Optical density at 600 nm (OD₆₀₀, secondary Y axis) was used as a proxy for biomass production. **Note this strain does not metabolise D-xylose.**

S. cerevisiae ATCC 20062 grew efficiently on OMSW fibre hydrolysate, depleting most of the D-glucose within 12 hours (**Figure 4.12**). Maximum biomass and ethanol yields were attained after 24 hours upon D-glucose depletion. Ethanol yield was 18.0 ± 1.3 g/L, equating to 70 ± 2 % of maximum theoretical yield. *S. cerevisiae* had the highest productivity of any organism trialled in this project, producing ethanol at 0.36 ± 0.03 g/L.h⁻¹ over 24 hours without any notable product or substrate inhibition. This strain could therefore have very good potential for OMSW fibre bioprocessing, although its efficiency was limited by the inability to ferment D-xylose.

4.3.2.6 *Schizosaccharomyces pombe*

The fission yeast *Schizosaccharomyces pombe* is a model organism used extensively in molecular genetic studies, but is understudied as a bioethanol producer despite the fact that it was originally isolated from palm wine (Hayles & Nurse, 1992). This yeast shares many industrially useful characteristics with *S. cerevisiae*, including tolerance to osmotic stress and ethanol, flocculability, generally regarded as safe (GRAS) status and genetic tractability. *S. pombe* JB953 is a wild strain isolated in Australia (Jeffares, 2018; Jeffares et al, 2015) that produced the highest ethanol titre in a preliminary plate reader screen of eight *S. pombe* isolates grown with OMSW fibre hydrolysate for 24 hours (See **Appendix V** for details).

Figure 4.13 shows that in the shake flask fermentation assay *S. pombe* JB953 grew on OMSW fibre hydrolysate relatively efficiently, using all available D-glucose within 24 hours and producing 14.9 ± 1.9 g/L of ethanol, or 51 ± 7 % of the theoretical maximum with a productivity over 24 hours of 0.31 ± 0.04 g/L.h⁻¹. A decrease in D-xylose levels was also measured although *S. pombe* is not reported to ferment D-xylose. This strain may however be capable of D-xylose uptake for xylitol production, as has been reported for some yeasts (Jeffries & Kurtzman, 1994). Overall, *S. pombe* grew well on OMSW fibre hydrolysate, without showing any obvious signs of substrate or product inhibition. However, only half the theoretically possible ethanol titre was produced because most carbon was allocated to biomass production. This could potentially be improved through further optimisation of the fermentation conditions.

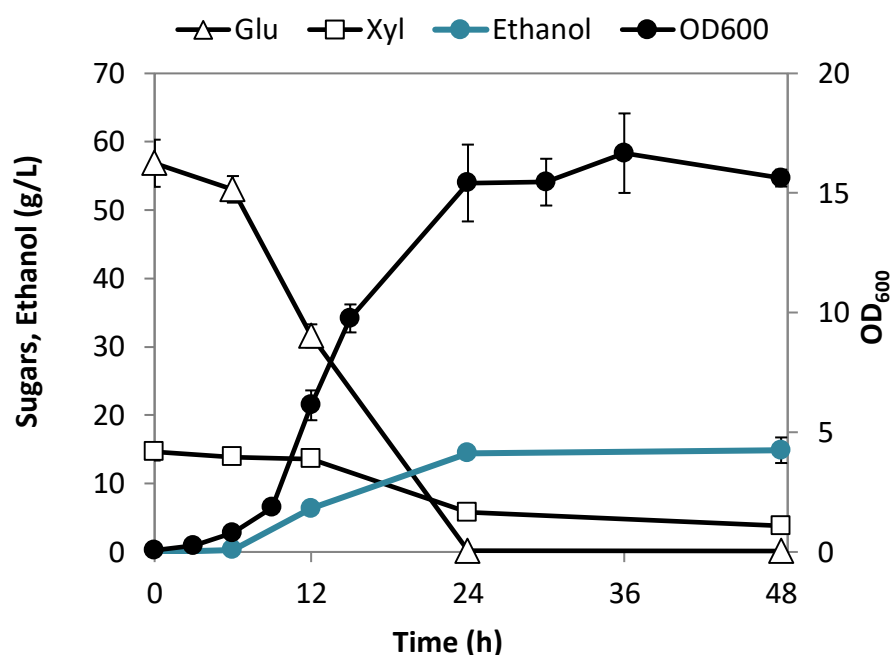


Figure 4.13: Fermentation kinetics of *Schizosaccharomyces pombe* grown on OMSW fibre hydrolysate

S. pombe was grown micro-aerobically in 100 ml shake flasks with airlocks on 10 ml OMSW fibre hydrolysate supplemented with 1% VYE and 40 mM MOPS buffer. Starting OD_{600} was 0.05. Samples were taken over 48 hours. For details see 4.2.4.2. Accumulation of ethanol and consumption of D-glucose (Δ Glu) and D-xylose (\square Xyl) are plotted on the primary Y-axis in g/L. Optical density at 600 nm (OD_{600} , secondary Y axis) was used as a proxy for biomass production. **Note this strain can metabolise but not ferment D-xylose.**

4.3.2.7 *Zymomonas mobilis*

Zymomonas mobilis is a Gram-negative, facultatively aerobic species that is extensively studied for bioethanol production due to its high ethanol tolerance, volumetric productivity and rapid glucose uptake rate (Yang et al, 2016). *Z. mobilis* is one of few anaerobes that can catabolise glucose via the Entner-Doudoroff (ED) pathway (detailed in 1.2.4, Figure 1.8), which is typically found in strict aerobes (Swings & De Lay, 1977). The ED pathway forms the core of *Z. mobilis* metabolism and is its only available route for carbon catabolism. Anaerobic fermentation via the ED pathway produces just 1 mol of ATP per mol of glucose, consequently, *Z. mobilis* has the lowest molar growth yield of any known microorganism and must maintain a high level of metabolic flux to guarantee enough energy for survival. To achieve this, ethanologenic enzymes are expressed to 50% of soluble cell protein and sugars are imported via high-velocity facilitated diffusion, resulting in highly direct and efficient ethanol production (Conway, 1992). Despite its overall

effectiveness, *Z. mobilis* is limited for bioprocessing applications because it exclusively ferments D-glucose, D-fructose and sucrose (Yang et al, 2016).

Z. mobilis subsp. mobilis DSM424 (also ZM1) is a well-studied strain originally isolated from a fermentation of Pulque, a traditional Mexican alcoholic beverage made from sap of the Agave plant (*Agave americana*) (Pappas et al, 2011). During growth on OMSW fibre hydrolysate, *Z. mobilis* DSM 424 rapidly used all available D-glucose within 24 hours and produced 17.5 ± 0.03 g/L ethanol, equivalent to a productivity of 0.73 ± 0.01 g/L.h⁻¹ (Figure 4.14). On the whole *Z. mobilis* appears to be a promising species for bioethanol production from OMSW fibre hydrolysate, but as with *S. cerevisiae*, the inability to utilise D-xylose limits the efficacy of this strain for fermentation of lignocellulosic biomass.

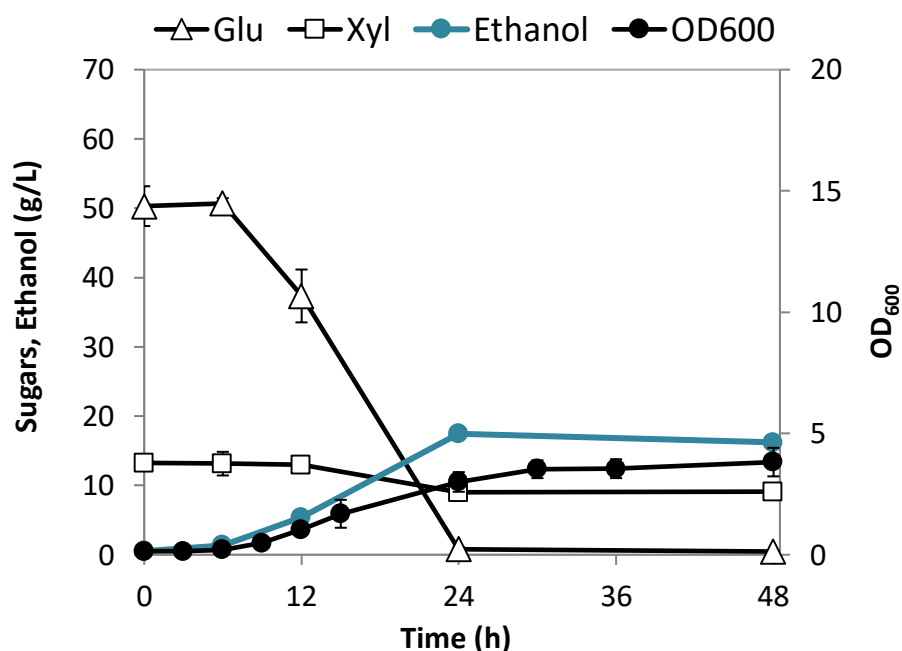


Figure 4.14: Fermentation kinetics of *Zymomonas mobilis* grown on OMSW fibre hydrolysate

Z. mobilis was grown anaerobically in 100 ml serum bottles on 10 ml OMSW fibre hydrolysate supplemented with 1% VYE and 40 mM MOPS buffer. Starting OD₆₀₀ was 0.05. Samples were taken over 48 hours. For details see 4.2.4.2. Accumulation of products (ethanol, butanol, and acetone) and consumption of D-glucose (Δ Glu) and D-xylose (\square Xyl) are plotted on the primary Y-axis in g/L. Optical density at 600 nm (secondary Y axis) was used as a proxy for biomass production. **Note this strain does not metabolise D-xylose.**

4.3.3 Evaluating Relative Fermentation Efficiency between Species

All eight species trialled on OMSW fibre hydrolysate varied greatly in their fermentation kinetics and relative efficiencies. Each species exhibited unique carbon consumption, growth and product synthesis dynamics. To provide an overview of the fermentation dynamics and compare each species relative performance, the time course fermentations are presented side by side in **Figure 4.15**. Furthermore, to compare the species more quantitatively, key yield parameters were calculated for each fermentation. These values are summarised in **Table 4.10**, including the total percentage of fermentable sugars consumed by each species over the course of fermentation, the final dry weight of cell biomass recovered per litre of fermentation broth, the gram per gram ratio of product to sugar consumed, the maximum product yield (in g/L and as a percentage of the theoretical maximum yield) and the overall productivity in g/L.h⁻¹. Additionally, the amount of product that could be produced from one tonne of OMSW fibre (kg/t) was calculated and a maximum theoretical yield per tonne was estimated assuming complete sugar conversion during hydrolysis.

To evaluate the performance of the species relative to one another the fermentation kinetics were compared in conjunction with the calculated yield parameters, thereby enabling the most promising candidates to be identified. The poorest performing strains utilised less than 50% of the sugars metabolically available to them and did not produce the product of interest. This included *C. saccharoperbutylacetonicum* (**Figure 4.15-F**) and *G. thermoglucosidasius* (**Figure 4.15-C**). Both these microorganisms were sensitive to some component of the hydrolysate that did not significantly affect the other species, making them less desirable candidates for application in an OMSW fibre bioprocess.

Species that performed moderately well include *P. putida* (**Figure 4.15-G**), *E. coli* (**Figure 4.15-D**) and *S. pombe* (**Figure 4.15-B**). These species used most or all the sugars metabolically available to them but primarily allocated carbon to biomass production. *S. pombe* and *E. coli* only produced ethanol to 51 ±7 % and 34 ±2 % of the theoretical maximum, respectively, therefore most of the catabolised carbon was directed toward growth (**Table 4.10**). Their performance could likely be improved by further optimising culture conditions to promote fermentative metabolism. In the case of *P. putida* autoacidification could be prevented by using a stronger buffer or pH control system, however, significant genetic engineering would be necessary to develop this species into a platform for OMSW fibre bioprocessing.

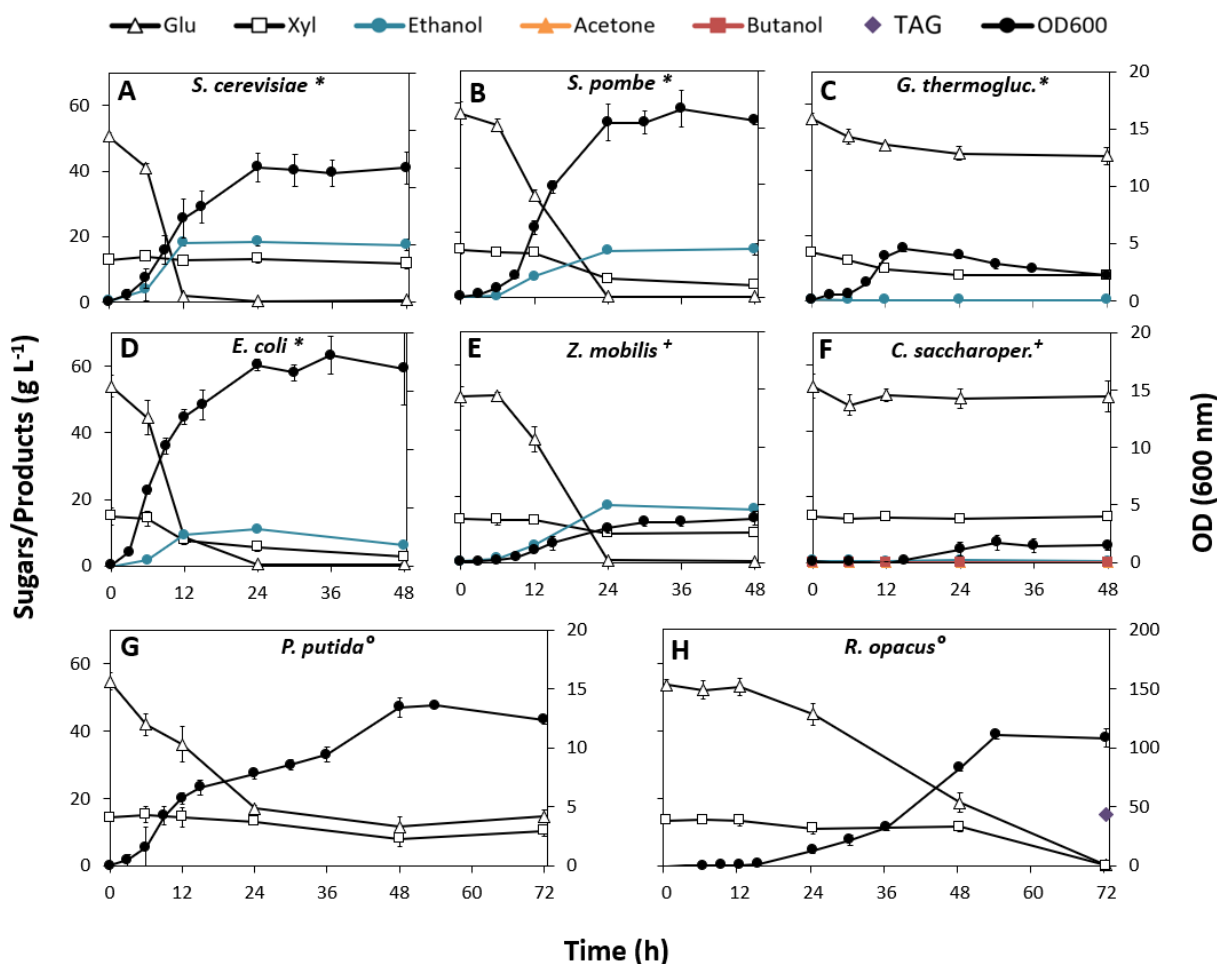


Figure 4.15: Fermentation kinetics of eight different microorganisms grown on OMSW fibre hydrolysate.

(A) *Saccharomyces cerevisiae**; (B) *Schizosaccharomyces pombe**;
 (C) *Geobacillus thermoglucosidasius**; (D) *Escherichia coli**; (E) *Zymomonas mobilis*⁺;
 (F) *Clostridium saccharoperbutylacetonicum*⁺; (G) *Pseudomonas putida*[°] and
 (H) *Rhodococcus opacus*[°];

Culture conditions: *Micro-aerobic (shake flasks with airlocks);
⁺Anaerobic (serum bottles); [°]Aerobic (shake flasks with foam bungs).

Accumulation of products (ethanol, butanol, acetone or triacylglycerol (TAG)) and consumption of D-glucose (Δ) and D-xylose (\square) are plotted on the primary Y-axis. Optical density at 600 nm (secondary Y axis) was used as a proxy for biomass production. All species were inoculated to a starting OD₆₀₀ of 0.05. Each species was grown on 10 ml OMSW fibre hydrolysate supplemented with 1% VYE and 40 mM MOPS buffer. Starting OD₆₀₀ was always 0.05. Note that TAG yield could only be measured at the end of fermentation (see 4.2.4.2 for details).

Table 4.10: Key fermentation yield parameters for eight species grown on OMSW fibre hydrolysate

TAG = Triacylglycerol; n/a = not applicable; n/d= not detected; \pm SD = standard deviation of triplicate measurements. The equations used to calculate these variables are given in 4.2.6.4.

| Species | Strain | Product | Time (h) | Glucose used (%) | | Xylose used (%) | | Total Sugars used (%) ^a | Mean \pm SD | | | | Yield per tonne (Kg/t) ^e | Theoretical max. yield (Kg/t) ^f |
|--------------------------------------|------------|---------|----------|------------------|-------------|-----------------|---------------------|------------------------------------|--|------------------------|-----------------------------------|-----|-------------------------------------|--|
| | | | | Product | Yield (g/L) | Final CDW (g/L) | Product Yield (g/L) | | Productivity (g/L.h ⁻¹) ^b | P/S (g/g) ^c | Percentage yield (%) ^d | | | |
| <i>P. putida</i> | NCIMB8249 | None | 72 | 73.1 | n/a | 63.4 | 2.5 \pm 0.4 | n/a | n/a | n/a | n/a | n/a | n/a | n/a |
| <i>C. saccharoperbutylacetonicum</i> | DSM14923 | Butanol | 48 | 5.6 | 0.0 | 4.4 | 0.7 \pm 0.1 | n/d | n/a | n/a | n/a | n/a | n/a | n/a |
| <i>G. thermoglucosidasius</i> | DSM2542 | Ethanol | 48 | 20.3 | 47.5 | 26.0 | 0.4 \pm 0.1 | n/d | n/a | n/a | n/a | n/a | n/a | n/a |
| <i>E. coli</i> | LW06 | Ethanol | 48 | 99.1 | 61.6 | 91.0 | 9.0 \pm 0.8 | 10.9 \pm 0.5 | 0.46 \pm 0.02 | 0.17 \pm 0.01 | 34 \pm 2 | 55 | 70 | |
| <i>S. pombe</i> | JB953 | Ethanol | 48 | 99.8 | n/a | 99.8 | 3.3 \pm 0.1 | 14.9 \pm 1.9 | 0.31 \pm 0.04 | 0.26 \pm 0.03 | 51 \pm 7 | 74 | 101 | |
| <i>Z. mobilis</i> | DSM424 | Ethanol | 24 | 98.4 | n/a | 98.4 | 1.3 \pm 0.2 | 17.5 \pm 0.3 | 0.73 \pm 0.01 | 0.35 \pm 0.01 | 69 \pm 1 | 87 | 136 | |
| <i>S. cerevisiae</i> | ATCC200062 | Ethanol | 24 | 99.3 | n/a | 99.3 | 2.5 \pm 0.1 | 18.0 \pm 1.3 | 0.75 \pm 0.06 | 0.36 \pm 0.03 | 70 \pm 5 | 90 | 139 | |
| <i>R. opacus</i> | MITXM-61 | TAG | 72 | 99.5 | 100.0 | 99.6 | 32.7 \pm 0.4 | 15.2 \pm 1.1 | 0.21 \pm 0.02 | 0.23 \pm 0.02 | 72 \pm 5 | 76 | 91 | |

^a Percentage of metabolically available sugars consumed based on initial D-glucose and D-xylose concentrations shown in Appendix VI.

^b Grams of product produced per litre of fermentation medium per hour, also known as process productivity, (g/L.h-1)

^c Product to substrate yield ratio (grams of product per gram of sugar fermented).

^d Product yield attained by fermentation, given as a percentage of the theoretical maximum yield from sugars. Assuming theoretical maxima of 0.316 g/g sugar for triacylglycerol and 0.511 g/g for ethanol. Note that these figures may be overestimates as only the major carbon sources D-glucose and D-xylose were accounted for. A range of less abundant sugars or other carbon sources could be metabolised by the microorganism, contributing to product yield.

^e Kg of product that could be produced from one tonne of OMSW fibre, based on observed conversion efficiencies.

^f Kg of product that could be produced from one tonne of OMSW fibre, assuming complete conversion of sugars in hydrolysis.

The species that showed the most promise for production of biofuels and chemicals from OMSW fibre were *S. cerevisiae* (**Figure 4.15-A**), *Z. mobilis* (**Figure 4.15-E**) and *R. opacus* (**Figure 4.15-H**). *S. cerevisiae* and *Z. mobilis* achieved comparable ethanol yields (69 ± 1 % vs. 79 ± 5 % of theoretical yield, respectively), productivities (0.73 ± 0.01 and 0.74 ± 0.06 g/L.h⁻¹) and product to substrate (P/S) ratios (0.35 ± 0.01 and 0.36 ± 0.03 g/g) when accounting for the standard deviation. Interestingly, despite this parity, the final CDW of *Z. mobilis* was 46% lower than *S. cerevisiae* (**Table 4.10**). The high volumetric productivity of this bacterium relative to *S. cerevisiae* is well established (Bucholz et al, 1987) and is further supported by these results. It was calculated that per tonne of OMSW fibre processed under the conditions trialled in this work, about 90 Kg of ethanol could be produced with *S. cerevisiae* and 87 Kg of ethanol with *Z. mobilis*. If all available cellulose could be isolated from OMSW fibre through hydrolysis, these yields could rise to 139 and 136 Kg/t, respectively (**Table 4.10**).

Although both ethanologens attained very high yields, neither could ferment D-xylose, thus limiting their overall productivity. By comparison, *R. opacus* accessed both the D-glucose and D-xylose in the hydrolysate and produced 15.2 ± 1.1 g/L TAG, the highest yield of product relative to the theoretical maximum attained by any species trialled in this study. At the same time however, *R. opacus* only had a productivity of 0.21 ± 0.02 g/L.h⁻¹, the lowest overall (**Table 4.10**). This was due to a lag phase of about 12 hours bringing the total fermentation time to 72 hours (**Figure 4.15-H**). Despite its high product yield, *R. opacus* would only produce 76 Kg of TAG per tonne of OMSW fibre, significantly less than the amount of ethanol produced by *Z. mobilis* and *S. cerevisiae*. Even under perfect hydrolysis conditions TAG yield would only increase to 91 Kg/t. However, as discussed in the introduction, TAG biosynthesis is metabolically and physiologically very different from ethanol fermentation. TAG also has a different market value as it competes primarily with palm oil for biodiesel production. It is therefore difficult to make direct comparisons between ethanologenic and oleaginous species.

It should also be noted that the calculations presented in **Table 4.10** are only broad estimates of fermentation performance. They exclusively accounted for the major carbon sources D-glucose and D-xylose and discount the contributions to product yield from other less abundant sugars or carbon sources not measured in the compositional analysis. For example, D-mannose, the third most abundant sugar in OMSW fibre hydrolysate (5.46% w/v) can also be fermented by *R. opacus* (Holder et al, 2011) and *S. cerevisiae* (Li et al,

2015), but not *Z. mobilis*. These yield calculations should therefore be treated with caution as they do not account for all carbon available in the system and may therefore be overestimates. Overall however, robust growth and near theoretical yields were core features of *E. coli*, *Z. mobilis* and *R. opacus*, making all three excellent candidate strains for further development in an OMSW fibre-based bioprocess.

4.3.4 Characterising OMSW Fibre Hydrolysate Fermentation by *R. opacus*

R. opacus MITXM-61 was chosen as the primary candidate strain to be developed further for application in an OMSW fibre biorefinery because of its ability to efficiently and concurrently use D-glucose and D-xylose and produce near-theoretical yields of TAG from OMSW fibre hydrolysate. The fact that there are no prior publications investigating the usefulness of *R. opacus* for OMSW bioprocessing also make it an interesting microorganism to study. As such, the physiology and TAG production kinetics of *R. opacus* grown on OMSW fibre hydrolysate were investigated in greater detail.

GC-FID can be used to measure the total yield of TAG but also enables the individual fatty acids (FAs) that make up the TAG molecules to be identified and quantified. This is important because fatty acid length has a significant impact on their application. Long-chain fatty acids (LCFAs, between 13-21 carbon atoms in length) are optimal for biodiesel production, while medium-chain fatty acids (MCSAs, between 6-12 carbons in length) are more useful for producing aviation fuel (i.e. kerosene) and for deriving ingredients used in cosmetics (Jimenez-Diaz et al, 2017; Lestari et al, 2009). A list of all FAs detected in *R. opacus* cells grown on OMSW fibre hydrolysate for 72 hours is given in **Table 4.11**. The most abundant FAs were Palmitic (C16:0), Heptadecanoic (C17:0), Cis-10-Heptadecenoic (C17:1n-7) and Cis-9-Octadecenoic (C18:1n-7c), which is consistent with previous analyses of FA composition in *R. opacus* (Alvarez & Steinbüchel, 2002).

To evaluate the viability of FAs derived from *R. opacus* for biodiesel production the cetane number (CN) was calculated as described in **4.2.6.7**. The CN is used as a measure of the combustion and ignition potential of a biodiesel relative to cetane (n-hexadecane), a straight chain hydrocarbon with very high ignitability (Giakoumis, 2013). To determine the CN of a mixture of FAMES a cetane index (CN_i) is calculated for each individual FAME. According to EU specifications, a biodiesel must have a minimum CN of 51 with a minimum CN_i of 46 (CEN, 2009). The CN_i for each individual FAME extracted from *R. opacus* is listed in **Table 4.11**.

Table 4.11: Fatty acid composition profile of *Rhodococcus opacus* MITXM-61 growth on OMSW fibre hydrolysate for 72 hours and the calculated cetane index of each fatty acid

Yields are given as the percentage (w/w) of total fatty acids (FA) with standard deviation (\pm SD) of triplicate measurements. Common names are given where available.

C:D = Lipid number, expressed as the number of Carbon atoms to Double bonds.

CN_i = Cetane index, measures the combustibility and ignitability of individual FAMES.

CN = Cetane number, measures the combustibility and ignitability of biodiesel mixture.

| FA | C:D | % | \pm SD | CN _i |
|---|---------------------|---------------|-----------------------------|-----------------|
| Capric | C10:0 | 0.04 | \pm 0.02 | 60.9 |
| Undecyclic | C11:0 | 0.12 | \pm 0.00 | 62.3 |
| Lauric | C12:0 | 0.14 | \pm 0.02 | 63.7 |
| Tridecyclic | C13:0 | 0.03 | \pm 0.00 | 65.1 |
| Myristic | C14:0 | 2.17 | \pm 0.16 | 66.5 |
| Myristoleic | C14:1(9) | 0.03 | \pm 0.00 | 50.6 |
| Pentadecanoic | C15:0 | 5.96 | \pm 0.41 | 67.9 |
| Cis-10-pentadecenoic | C15:1(5) | 0.45 | \pm 0.03 | 52.0 |
| Palmitic | C16:0 | 28.84 | \pm 1.96 | 69.3 |
| Hypogeic | C16:1(7) | 9.06 | \pm 0.72 | 53.4 |
| Heptadecanoic | C17:0 | 10.88 | \pm 0.78 | 70.7 |
| Cis-10-Heptadecenoic | C17:1(10) | 13.65 | \pm 0.96 | 54.8 |
| Stearic | C18:0 | 5.28 | \pm 0.36 | 72.1 |
| Trans-9-Octadecenoic | C18:1(9) | 1.93 | \pm 0.18 | 56.2 |
| Cis-9-Octadecenoic | C18:1(9) | 18.65 | \pm 1.49 | 56.2 |
| Cis-11-Octadecenoic | C18:1(11) | 0.45 | \pm 0.09 | 56.2 |
| 9-trans, 12-trans-Octadecadienoic | C18:2(9,12) | 0.02 | \pm 0.02 | 40.3 |
| 9-cis, 12-cis-octadecadienoic | C18:2(9,12) | 0.07 | \pm 0.01 | 40.3 |
| γ -Linoleic | C18:3(6,9,12) | 1.18 | \pm 0.09 | 24.4 |
| Stearidonic | C18:4(6,9,12,15) | 0.03 | \pm 0.00 | 8.5 |
| Arachidic | C20:0 | 0.23 | \pm 0.02 | 74.9 |
| Gondoic | C20:1(11) | 0.06 | \pm 0.00 | 59.0 |
| Cis-13-Eicosenoic | C20:1(13) | 0.04 | \pm 0.04 | 59.0 |
| Homo- γ -Linolenic | C20:3(8,11,14) | 0.06 | \pm 0.03 | 27.2 |
| Arachidonic | C20:4(5,8,11,14) | 0.04 | \pm 0.02 | 11.3 |
| Eicosapentanoic | C20:5(5,8,11,14,17) | 0.07 | \pm 0.01 | -4.6 |
| Behenic | C22:0 | 0.14 | \pm 0.03 | 77.7 |
| Erucic | C22:1(13) | 0.10 | \pm 0.02 | 61.8 |
| Docosadienoic | C22:2(13,16) | 0.21 | \pm 0.02 | 45.9 |
| Nervonic | C24:1(15) | 0.07 | \pm 0.01 | 64.6 |
| FA (total): | | 100.00 | \pm2.91 | |
| FA (as a percentage of cell dry weight): | | 48.91 | \pm1.42 | |
| CN (total): | | | | 62.5 |

Only eight of the thirty FAs detected had a CN below 46 and these made up just 1.67% of the total FA profile. It was calculated that the total mixture of TAG-derived FAMES isolated from *R. opacus* had a CN of 62.5. This indicates that TAGs from *R. opacus* grown on OMSW fibre could be converted directly to high-quality biodiesel, on par with oil-crop derived biodiesels currently produced from jatropha and palm (Jiménez-Díaz et al, 2016). These results are also consistent with work by Fei et al, (2015) who calculated a CN value of ~60 for *R. opacus* MITXM-61 grown on a mixture of D-glucose and D-xylose.

To gain further insight into TAG production during growth on OMSW fibre hydrolysate, light microscopy was used to visualise *R. opacus* cells sampled at 24, 48 and 72 hours (**Figure 4.16**). The microscopy revealed that there was a noticeable change in cellular morphology between the early and later stages of fermentation. 24 hours into fermentation *R. opacus* cells had a long, rod shape (**Figure 4.16-A & B**) but as the fermentation progressed morphology shifted toward shorter, rounder rods and clear regions began to appear within the cell interior (**Figure 4.16-C & D**). It is known from electron microscopy studies of *R. opacus* PD630 that TAG accumulates within the cell in lipid inclusions that are visible within the cytoplasm (Alvarez et al, 1996). These lipid inclusions were just visible under the light microscope as clear regions surrounded by the more electron-dense, stained membrane and compacted intracellular material (**Figure 4.16-E & F**).

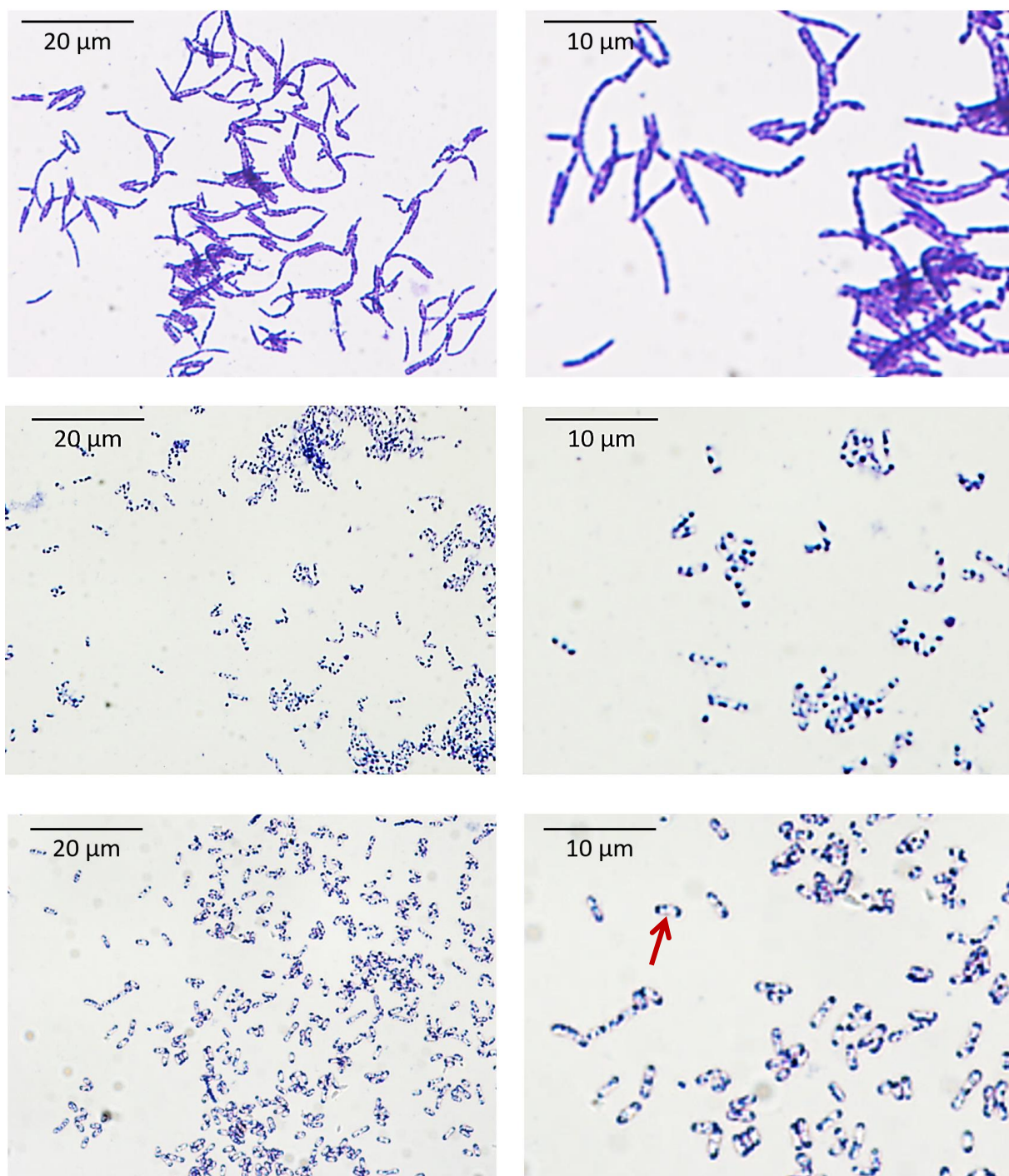


Figure 4.16: Light microscopy images of *Rhodococcus opacus* cells after 24, 48 and 72 hours of growth on OMSW fibre hydrolysate

(Images taken by author with help from University of York Imaging and Cytometry Laboratory).

Cells from the experiment shown in **Figure 4.11** were fixed and stained with crystal violet and imaged using a light microscope at 100x magnification with oil immersion (for details see **4.2.5**). Scale bars for **A**, **C** and **E** represent 20 µm; Scale bars for **B**, **D** and **F** represent 10 µm.

Images **A**, **C** and **E** show *R. opacus* after 24, 48 and 72 hours of growth on OMSW fibre hydrolysate, respectively. Images **B**, **D** and **F** show regions of interest within images **A**, **C** and **E**, enhanced with 50% digital zoom. **Red arrow** in **F** highlights an example of lipid inclusions (clear regions) within the cell where triacylglycerol has accumulated.

The light microscopy studies indicated that TAG accumulation was at or near the maximum yield after 72 hours. To gain a more quantitative understanding of the time course kinetics of TAG production from OMSW fibre hydrolysate a fermentation assay was carried out in a larger volume (40 ml) and TAG levels were measured at regular intervals over six days along with the levels of sugars, YAN and CDW (**Figure 4.17**). Unfortunately, the larger culture volume used in this assay had a negative effect on the growth and productivity of *R. opacus*. Although the dynamics corresponded to those originally presented in **Figure 4.12**, the lag phase lasted 12 hours longer and growth rate was slower overall, leading to a 14% lower CDW upon entry into stationary phase. Cells were still in mid exponential phase at 72 hours whereas stationary phase was reached after 54 hours in the initial fermentation trial. Furthermore, the peak TAG yield was lower, reaching only 64 ± 4 % of the theoretical maximum, compared to 72 ± 5 % attained previously.

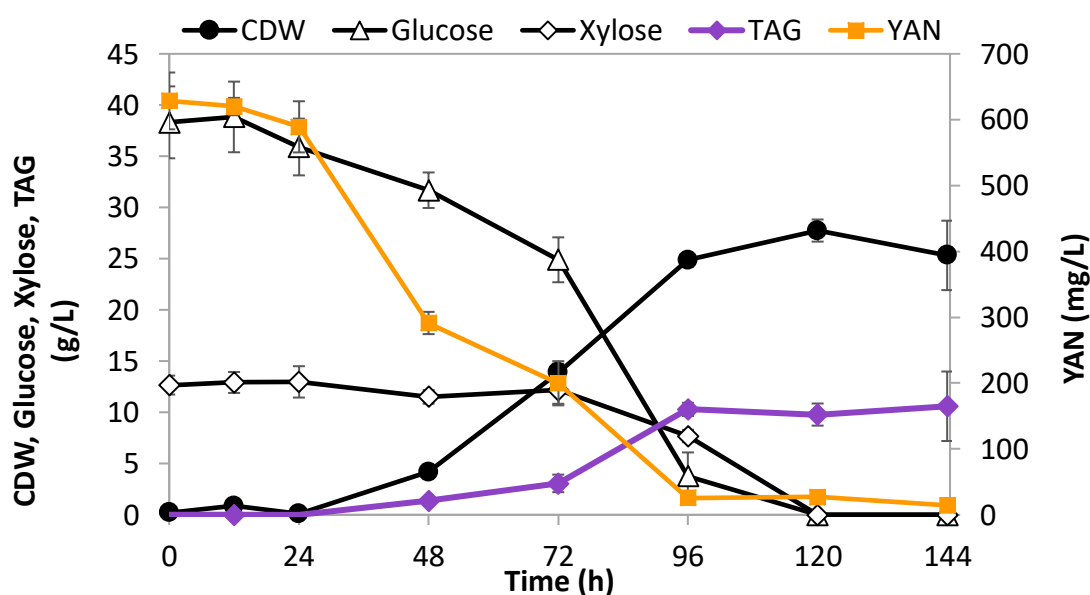


Figure 4.17: Comprehensive TAG production kinetics of *R. opacus* grown on OMSW fibre hydrolysate

R. opacus was grown aerobically in 250 ml shake flasks on 40 ml OMSW fibre hydrolysate supplemented with 1% VYE and 40 mM MOPS buffer. Starting OD_{600} was 0.05. Samples were taken over 144 hours and used to analyse the levels of TAG, YAN, sugars and CDW (for detailed methods see 4.2.4.3). Accumulation of TAG, consumption of D-glucose (Δ Glu) and D-xylose (\square Xyl) and CDW are plotted on the primary Y-axis in g/L. YAN is plotted on the secondary Y axis in mg/L.

The productivity of *R. opacus* in this assay was 0.11 ± 0.01 g/L.h⁻¹ over 96 hours, 50% lower than before (**Table 4.10**). Growth was likely slowed due to under-aeration as this species has a very high oxygen demand, requiring at least 60% dissolved oxygen for optimal growth in stirred tank bioreactors (Kurosawa et al, 2014) . The shaking rate was increased to 250 rpm for this assay to accommodate for the greater culture volume but determining effective oxygen transfer rates in shake flasks is challenging without in-line monitoring (Büchs, 2001).

Despite exhibiting more delayed growth overall, the results presented in **Figure 4.16** still provide an overview of the relationship between sugar uptake, nitrogen catabolism and biomass production in *R. opacus* grown on OMSW fibre hydrolysate. TAG levels reached a maximum of 10.09 ± 0.65 g/L at 96 hours, just when nitrogen uptake stopped. Approximately 26 mg/L or 4% of YAN remained in the hydrolysate between 96-144 hours, indicating that some of the nitrogenous compounds in the VYE were inaccessible to *R. opacus*. D-glucose was co-utilised with D-xylose, although D-glucose was taken up more rapidly. 3.77 ± 2.32 g/L D-glucose and 7.69 ± 0.60 g/L D-xylose remained in the medium at 96 hours when TAG levels reached their peak, but both sugars were fully depleted after 120 hours.

R. opacus PD630, the parent strain of MITXM-61, has the most diverse repertoire of nitrogenous compound catabolism genes of any TAG producing bacterium (Holder et al, 2011) but generally prefers using ammonium over amino acids or urea (Fei et al, 2015). It grows poorly L-glutamic acid, N-acetyl-L-glutamic acid, L-proline, hydroxy-L-proline, glycine, N-glycyl-L-proline, L-alaninamide, L-phenylalanine and L-threonine and not at all on L-histidine (Holder et al, 2011). These peptides and amino acids may have made up the residual 4% of nitrogenous compounds remaining in the medium at the end of the OMSW fibre fermentation. Overall the fermentation dynamics coincide well with studies published by other groups on the kinetics of *R. opacus* grown on sugars (Kurosawa et al, 2015c; Kurosawa et al, 2013; Kurosawa et al, 2014) and the FA profile (presented in **Appendix VI**) coincided closely with the profile from the initial fermentation trial (**Table 4.11**).

4.3.5 Engineering Lauric Acid Production in *Rhodococcus opacus*

R. opacus can produce a wide range of FAs but, as mentioned above, the most abundant molecules are 16-18 carbons long. Previous work by Voelker and Davies (1994) showed that *E. coli* could be engineered to produce higher yields of MCFAs (primarily lauric

acid (C12:00)) by expressing the plant enzyme acyl-acyl carrier protein (ACP) thioesterase BTE (ACP-BTE). ACP-BTE is predominantly expressed in the seeds of the California Bay (*Umbellularia californica*), which are rich in laurate. Its role in FA biosynthesis is to terminate elongation of the fatty acid chain once it is 12 carbons long by hydrolysing the terminal acyl-ACP thioester, leading to release of the FA from the FA synthase machinery (Voelker et al, 1992). However, to significantly increasing lauric acid production and attenuate LCFA synthesis, ACP-BTE had to be expressed in an *E. coli* strain deficient in the β -oxidation pathway responsible for FA degradation, thereby preventing premature degradation of lauric acid (Voelker & Davies, 1994).

We set out to investigate whether FA biosynthesis could be manipulated in *R. opacus* by expressing ACP-BTE during growth on OMSW fibre hydrolysate. A transcriptomic analysis of *R. opacus* RHA1 under nitrogen-limiting conditions showed that genes involved in TAG degradation such as lipases were ten- to sixteen-fold less abundant during transition-phase, when most TAG synthesis occurs (Amara et al, 2016). It is possible that this down-regulation of the β -oxidation pathway during TAG storage conditions would enable MCFAs produced by ACP-BTE to accumulate in *R. opacus*.

First the ACP-BTE gene was codon optimised for *Rhodococcus* and synthesised as described in 4.2.7.4. The synthetic ACP-BTE gene was successfully cloned into pTip-QC1, an inducible *E. coli* – *Rhodococcus* shuttle vector, downstream of the thiostrepton inducible promoter *TipA* (for details see 4.2.7.1 and 4.2.7.5). pTip-QC1_ACP-BTE was then transformed to *R. opacus* as described in 4.2.7.9. The presence of the insert was confirmed by sequencing, both in *E. coli* after cloning and in successful transformants of *R. opacus*. Results from each of these steps are presented in **Appendix VIII**. Expression of ACP-BTE was assayed by SDS-PAGE of crude cell lysate from *R. opacus* cells carrying the ACP-BTE gene (*R. opacus*^{pTip-QC1_ACP-BTE}) that were induced with thiostrepton during growth on LB. An enriched band was present at the expected mass (43.74 kDa) in both the soluble and insoluble protein fractions but was absent in the empty vector control (*R. opacus*^{pTip-QC1}) (**Figure 4.18**). The enriched band was more intense in the insoluble fraction of the induced cultures, indicating that a large fraction of the protein may be misfolded due to overexpression. However, the same band was present in the soluble fraction (**Figure 4.18, arrow**), indicating that some of the protein may have been in a soluble form.

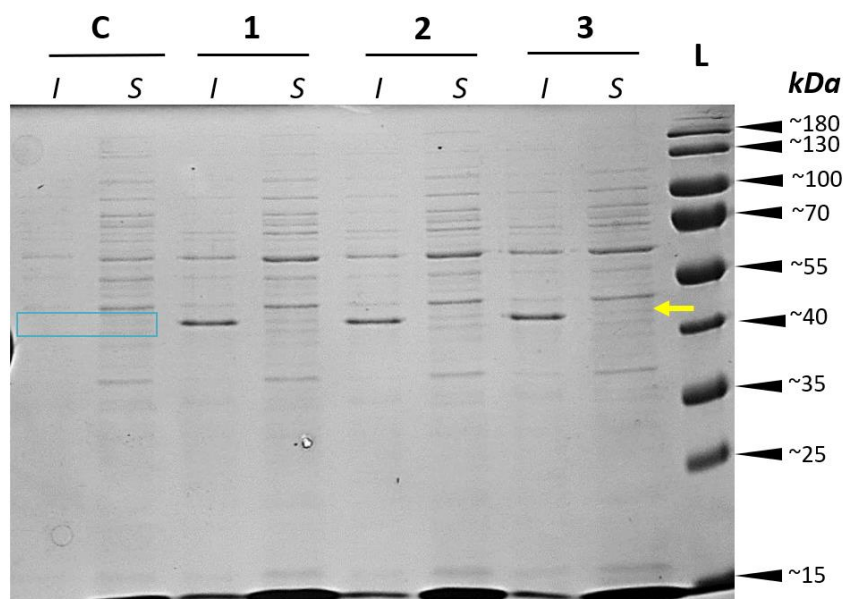


Figure 4.18: SDS-PAGE of induced and non-induced *R. opacus*^{pTip-QC1_ACP-BTE}
I = insoluble fraction; *S* = soluble fraction; *C* = negative control (empty vector);
1, 2 & 3 = replicate induced cultures; *L* = Protein ladder, in kDa;
Expected band size (yellow arrow) = 43.74 kDa (42.92 kDa protein + 0.84 kDa hexahis tag).
 For details see **4.2.8.1**.

To evaluate whether some ACP-BTE activity was occurring an expression assay was carried to investigate whether cells induced to express pTip-QC1_ACP-BTE showed increased lauric acid production. *R. opacus*^{pTip-QC1_ACP-BTE} was grown on OMSW fibre hydrolysate and induced with thiostrepton after 48 hours. As a negative control *R. opacus*^{pTip-QC1} was grown in parallel and induced. The total levels of TAG were measured alongside biomass production over the course of the fermentation (**Figure 4.19**). *R. opacus*^{pTip-QC1_ACP-BTE} and *R. opacus*^{pTip-QC1} exhibited similar growth and TAG production rates for the first 48 hours. However, after induction *R. opacus*^{pTip-QC1_ACP-BTE} accumulated less TAG and grew more slowly overall. The control strain reached a maximum TAG yield of 8.16 ± 1.18 g/L after 96 hours, while *R. opacus*^{pTip-QC1_ACP-BTE} took 120 hours to attain a similar level of TAG (8.42 ± 0.62 g/L). Both strains had a final CDW of ~ 29 g/L but *R. opacus*^{pTip-QC1_ACP-BTE} produced between 5-18% less biomass than the control between 48 and 120 hours. This indicated that expression of the heterologous protein incurred a minor fitness cost.

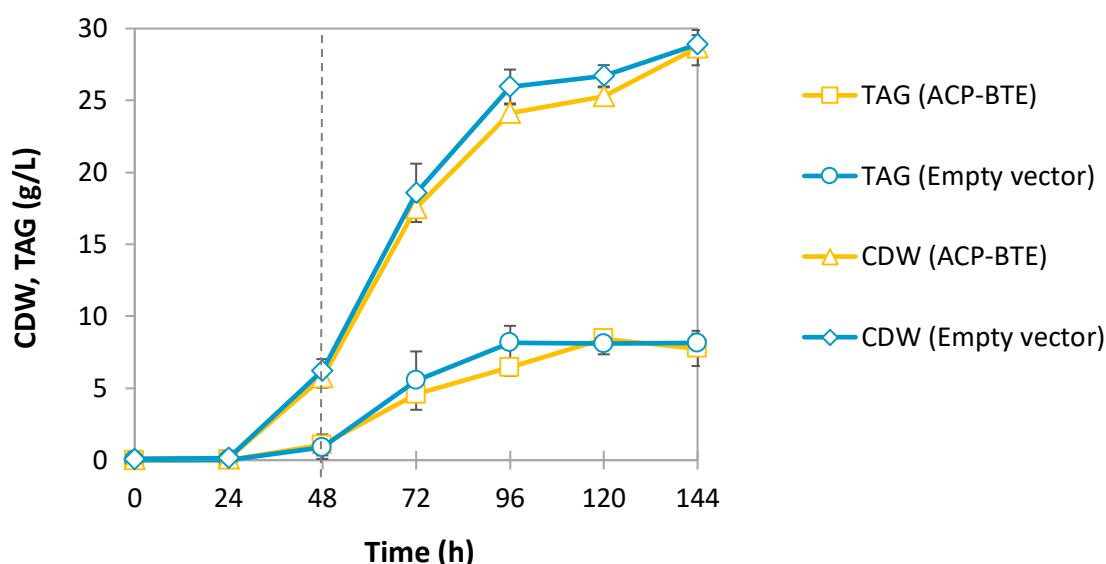


Figure 4.19: Cell dry weight and TAG production over 144 hours by thiostrepton induced *R. opacus*^{pTip-QC1_ACP-BTE} and *R. opacus*^{pTip-QC1}

Total cell dry weight (CDW) and TAG levels measured in *R. opacus*^{pTip-QC1_ACP-BTE} (ACP-BTE) and *R. opacus*^{pTip-QC1} (Empty vector) grown on OMSW fibre hydrolysate supplemented with 1% VYE over six days. Plasmid expression was induced after 48 hours (dashed grey line).

The abundance of lauric acid produced by *R. opacus*^{pTip-QC1_ACP-BTE} over the course of the fermentation was quantified as a percentage of the CDW and in terms of total concentration in the medium (Figure 4.20). The concentration of laurate within the cells remained relatively stable throughout the fermentation at around 0.02-0.04% of CDW, while the total concentration of laurate continued to increase proportionately with biomass production (Figure 4.20, '%CDW (ACP-BTE)' & 'g/L (ACP-BTE)'). Although there was 43% more laurate measured at 48 hours in cells carrying pTip-QC1_ACP-BTE than in the controls, there was a slightly greater abundance of all FAs in this strain at 24 and 48 hours compared to the control (Figure 4.21, '24 h' & '48 h'). Overall the amount of fatty acids produced by *R. opacus*^{pTip-QC1_ACP-BTE} were comparable with the control throughout the fermentation and no noticeable attenuation in LCFAs or increase in lauric acid levels was observed after induction (Figure 4.21). Based on these results it was concluded that ACP-BTE was being expressed non-functionally.

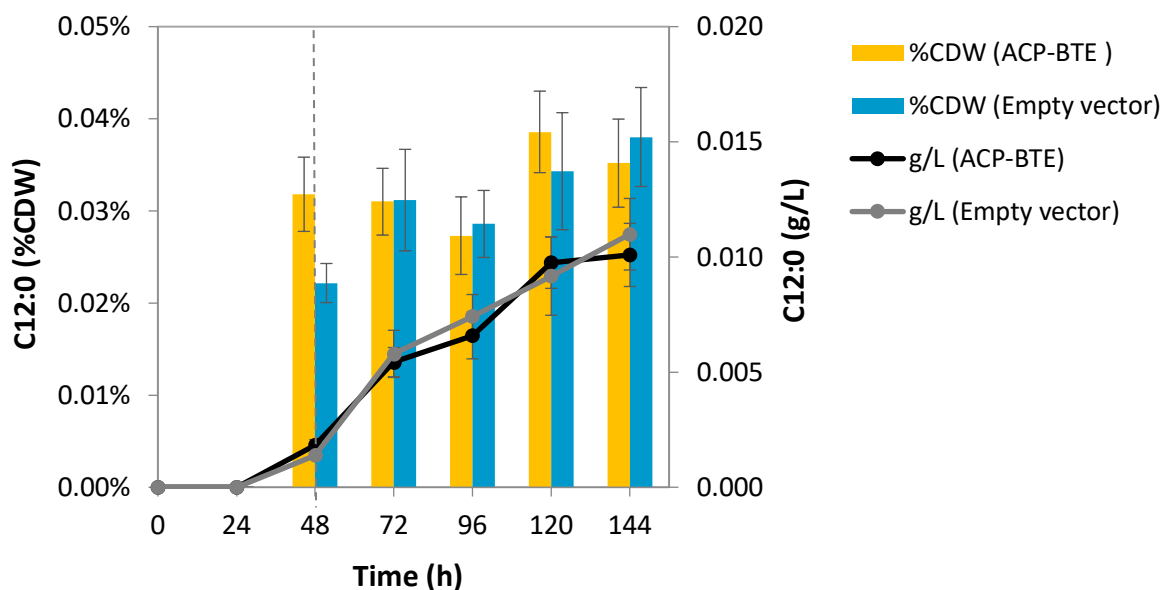


Figure 4.20: Laurate (C12:0) production over time by thiostrepton induced *R. opacus*^{pTip-QC1_ACP-BTE} and *R. opacus*^{pTip-QC1}

Laurate production by *R. opacus*^{pTip-QC1_ACP-BTE} (ACP-BTE) and *R. opacus*^{pTip-QC1} (Empty vector) grown on OMSW fibre hydrolysate supplemented with 1% VYE over six days. Plasmid expression was induced after 48 hours (dashed grey line). Primary Y-axis: laurate as a percentage of cell dry weight (% CDW); Secondary Y-axis: total laurate produced (g/L).

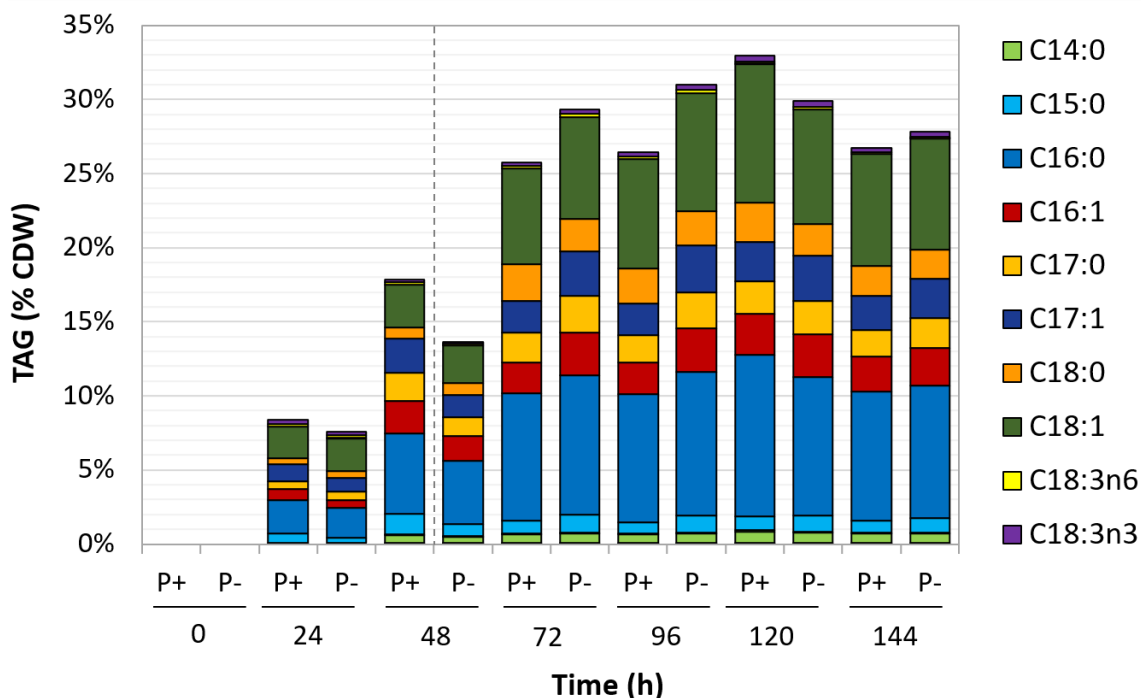


Figure 4.21: Time-course profile of the major long-chain fatty acids produced by *R. opacus*^{pTip-QC1_ACP-BTE} and *R. opacus*^{pTip-QC1}

Percentage abundance of the major long chain fatty acids (LCFAs) in *R. opacus*^{pTip-QC1_ACP-BTE} (P+) and *R. opacus*^{pTip-QC1} (P-) grown on OMSW fibre hydrolysate supplemented with 1% VYE over six days. Plasmid expression was induced after 48 hours (dashed grey line).

4.4 Discussion

Growth assays with the model fermentative species *E. coli* were used to gain a more holistic understanding of OMSW fibre hydrolysate fermentability by disentangling the effects of nutrient limitation from substrate inhibition. Lignocellulose is typically low in nitrogen and phosphorus compared to first generation feedstocks and lignocellulosic hydrolysates often require supplementation with nutrients to enable viable fermentation (Jørgensen, 2009). Identifying specifically which nutrients are limiting in the hydrolysate enables more cost effective and commercially viable nutrient supplements to be identified. The nutrient growth assays demonstrated that growth inhibition of *E. coli* on OMSW fibre hydrolysate was primarily due to a limitation in nitrogen and, to a lesser extent, phosphate (**Figure 4.6**) despite the presence of a range of inhibitory chemicals and metals (**Chapter 3, Table 3.3**). These findings suggested that growth of other fermentative microorganisms might also be supported by OMSW fibre hydrolysate so long as an accessible source of nitrogen and phosphate was supplemented.

As was detailed in the introduction, only a limited number of species have been grown in monoculture on OMSW-derived sugars. Of the eight species screened in this work, only *S. cerevisiae* has previously been grown on hydrolysates of OMSW (Ballesteros et al, 2010; Puri et al, 2013). The other seven species were selected based on their reported biotechnological utility. All eight species grew on OMSW fibre hydrolysate supplemented with 1% VYE to some degree, but there was significant variability between their relative productivities (**Table 4.10**). The poorest performing species, *C. saccharoperbutylacetonicum* (**Figure 4.7**) and *G. thermoglucosidasius* (**Figure 4.9**), exhibited strong substrate inhibition that resulted in premature entry into stationary phase, utilisation of less than 50% of metabolically available sugars and no product synthesis.

Although further studies are needed to identify the precise cause of inhibition, previous work has shown that growth of solventogenic Clostridia on lignocellulosic hydrolysates is primarily inhibited by formic acid, phenol and furfural (Liu et al, 2019). Formic acid could not be measured in the OMSW fibre hydrolysate and furfural was absent, however, 21 mM of vanillin, the marker inhibitor for the presence of phenolic compounds, was detected (**Chapter 3, Table 3.3**). Furthermore, the dark brown colour of the hydrolysis liquid indicated an abundance of tannins, which are polyphenolic compounds that can incapacitate enzymes by forming hydrogen crosslinks with carbonyl groups (Field &

Lettinga, 1992). Previous work with closely related *C. acetobutylicum* has shown that extracting phenolics and tannins from OMSW fibre hydrolysate with ethanol (Farmanbordar et al, 2018b) or organosolv pre-treatment (Farmanbordar et al, 2018a) alleviated growth inhibition. It is possible therefore that *C. saccharoperbutylacetonicum* is more sensitive to phenolic compounds than *C. acetobutylicum*.

It has also been observed that Gram-positive microbes are generally more susceptible to tannin inhibition, possibly because the outer membrane of Gram-negatives affords greater protection against hydrogen bonding by polyphenols (Field & Lettinga, 1992). There are no publications specifically investigating the effects of lignocellulosic inhibitors on *G. thermoglucosidasius*, but as a Gram-positive it could have been affected by phenolics. *R. opacus* on the other hand is also Gram-positive but did not show signs of substrate inhibition. This may be because *R. opacus* has an unusually complex outer envelope composed of mycolic acids which are associated with phenol tolerance and enable it to grow on phenol as a sole carbon source (Henson et al, 2018). *P. putida* exhibited growth inhibition after utilising only ~63% of metabolically available sugars (**Figure 4.10**). However, *P. putida* strains are known for having high tolerance to aromatic compounds and phenol degradation capabilities (El-Naas et al, 2009; Pini et al, 2009; Wong et al, 1978). *P. putida* was therefore more likely inhibited by autoacidification on OMSW fibre hydrolysate, as discussed in **4.1.1.3**.

Due to significant physiological variation between the eight candidate species the fermentation screening conditions were kept consistent for as many variables as possible – the starting inoculum OD₆₀₀, medium volume, nutrient levels and sampling times were identical and only temperature and aeration were changed to suit each microorganism. Growth conditions were primarily based on the optimal conditions reported for each strain and little species-specific optimisation was carried out beforehand. Thus, strains that grew relatively well but did not produce high levels of product, such as *S. pombe*, *E. coli* and *P. putida* still merit further study as their performance could likely be improved by optimising culture conditions.

So far there is only a single published study in which *S. pombe* was grown on lignocellulosic hydrolysates. Tura et al, (2018) compared the growth of *S. pombe* to *S. cerevisiae* on sugarcane bagasse pre-treated with ionic liquids and found that *S. pombe* produced ethanol to 78% of theoretical maximum yield while *S. cerevisiae* produced only 56%. Although the performance of *S. pombe* on OMSW fibre hydrolysate was poorer than

S. cerevisiae (**Figure 4.13**), *S. pombe* clearly has potential as an industrial ethanol producer. Further exploration of *S. pombe* strains could help identify superior phenotypes for fermenting lignocellulosic feedstocks. This has already been done using biochemical screening and selection to identify *S. pombe* strains with beneficial characteristics for winemaking (Benito et al, 2016).

Similarly, *E. coli* LW06 exhibited very robust growth on OMSW fibre hydrolysate. Although the ethanol yield attained via the heterologous ethanol pathway in this strain was relatively poor (34% of maximum theoretical yield), *E. coli* is an established industrial microorganism with an extensive repertoire of genetic engineering tools, opening up the potential for advanced strain manipulation to produce a wide range of natural products from OMSW fibre (Jung et al, 2010; Park et al, 2018; Wang et al, 2017).

The species that emerged as the most promising candidates for fermentation of OMSW fibre were *R. opacus*, *S. cerevisiae* and *Z. mobilis*. *S. cerevisiae* and *Z. mobilis* are the most widely studied and developed species for cellulosic ethanol production (Panesar et al, 2006; Petrovič, 2015). Their intrinsic aptitude for fermenting a wide variety of lignocellulosic feedstocks was further confirmed by their excellent performance on OMSW fibre hydrolysate: *S. cerevisiae* and *Z. mobilis* were closely tied in terms of fermentation efficiency, producing ethanol to about 70% of theoretical maximum with a productivity of $\sim 0.74 \text{ g/L.h}^{-1}$ and final yield of $\sim 18 \text{ g/L}$ (**Table 4.10**). Although promising, to ensure commercial viability microorganisms must be capable of producing ethanol to $>90\%$ of theoretical yield with a productivity of $>1 \text{ g/L.h}^{-1}$ and have tolerance to ethanol concentrations above 40 g/L (Dien et al, 2003). Attaining these yields on OMSW fibre hydrolysate is difficult without utilising a wider repertoire of sugars, particularly D-xylose. Genetic and adaptive engineering approaches have already been used to generate D-xylose utilising strains of *Z. mobilis* (Agrawal et al, 2010; De Graaf et al, 1999; Mohagheghi et al, 2014; Zhang et al, 1995) and to enable D-xylose fermentation in *S. cerevisiae* ATCC 200026, the strain used in this project (Smith et al, 2014). An important next step toward developing a bioprocess for bioethanol production from OMSW fibre would be to trial some of these D-xylose fermenting strains.

R. opacus MITXM-61 was the most productive strain identified through this project, primarily due to its ability to efficiently and simultaneously catabolise D-glucose and D-xylose. Kurosawa et al (2014) generated MITXM-61 through adaptive evolution of an *R. opacus* strain suspected of carrying potential D-xylose utilisation genes based on previous

work (Kurosawa et al, 2013). The same group were able to engineer *R. opacus* to metabolise L-arabinose (Kurosawa et al, 2015b), demonstrating that the sugar utilisation repertoire of MITXM-61 could be expanded even further to improve fermentation productivity. Overall *R. opacus* exhibited robust growth on OMSW fibre hydrolysate, reaching exceptionally high biomass density (final CDW 32.7%) and producing TAG to 72% of theoretical yield, equivalent to nearly half of CDW (Table 4.10). Growth on OMSW fibre hydrolysate produced an FA profile typical of *R. opacus* strains, containing an abundance of straight-chain FAs between 16-18 carbons long (Table 4.11) (Alvarez & Steinbüchel, 2002). Different carbon sources and the presence of inhibitors have been shown to affect FA branching and abundance in *R. opacus* (Tsitko et al, 1999). However, the identity and abundance of major FAs was highly consistent with those reported in previous studies of MITXM-61 (Figure 4.22), demonstrating that although OMSW fibre hydrolysate is a highly heterogeneous feedstock FA biosynthesis was not perturbed.

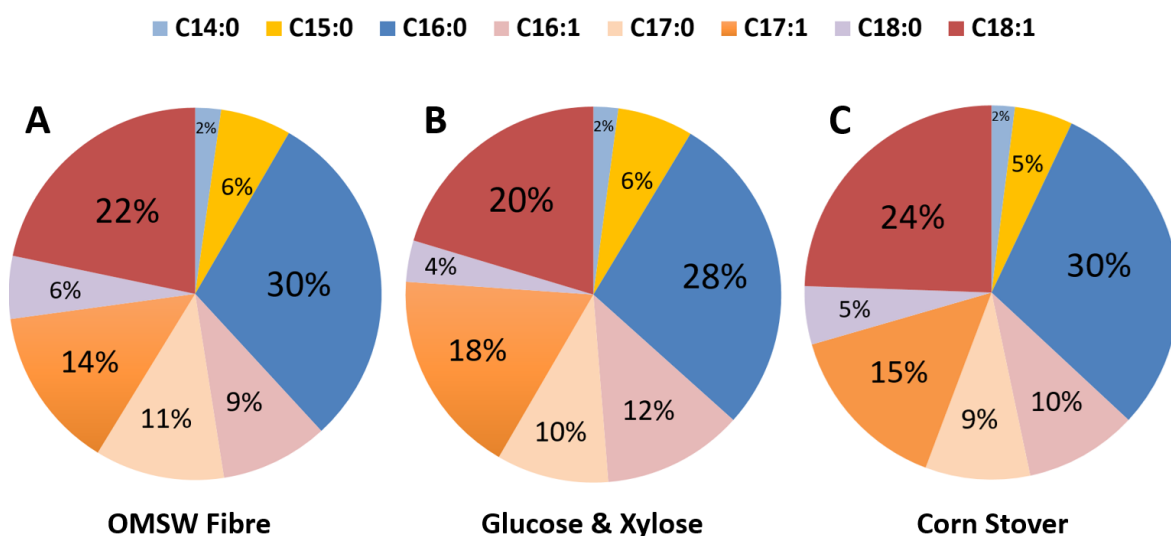


Figure 4.22: Percentage abundance of the major fatty acids produced by *R. opacus* MITXM-61 reported in the literature compared to this project

(Figure by author using data published by Kurosawa et al, (2014) and Fei et al, (2015))

- A. Fatty acid profile of *R. opacus* MITXM-61 grown on OMSW fibre hydrolysate for 72 hours (data presented in Table 4.11).
- B. FA profile reported by Fei et al, (2015) for *R. opacus* MITXM-61 grown on a mixture of D-glucose and D-xylose in 500 ml conical flasks via a two-stage batch culture (nitrogen rich conditions followed by nitrogen limiting conditions).
- C. FA profile reported by Kurosawa et al (2014) for *R. opacus* MITXM-61 grown on alkali-pretreated corn stover hydrolysate by batch fermentation in a 2 L fermentor.

Furthermore, the total TAG yield attained on OMSW fibre (15.2 ± 1.1 g/L) corresponds well with work by Kurosawa et al, (2014) wherein MITXM-61 grown on corn stover hydrolysate produced a 15.9 g/L TAG. However, the overall productivity of MITXM-61 was significantly greater on OMSW fibre (0.21 ± 0.02 g/L.h⁻¹) compared to corn stover (0.13 g/L.h⁻¹) (Kurosawa et al, 2014) due to a shorter lag phase. There was a 48 hour lag phase before growth commenced on corn stover, (Kurosawa et al, 2014) whereas in the two fermentation trials carried out with *R. opacus* on OMSW fibre the lag phase only lasted ~12 to 24 hours (**Figure 4.11** and **4.17**). Similarly, there was a ~96 hour lag phase during growth of *R. opacus* on hardwood pulp (Kurosawa et al, 2013). This demonstrates that OMSW fibre hydrolysate is a significantly more favourable feedstock for *R. opacus* compared to other lignocellulosic hydrolysates.

Unlike ethanol fermentation where a high volumetric productivity is desirable, TAG accumulates intracellularly and attaining efficient productivity therefore requires a delicate balance between biomass and product synthesis. The critical parameter for achieving this in oleaginous species is the C/N ratio (Alvarez & Steinbüchel, 2002). The C/N ratio for OMSW fibre hydrolysate supplemented with 1% VYE was calculated as 44.2, although it may have been slightly higher because about 4% of total YAN was inaccessible to *R. opacus* (**Figure 4.17**). In several studies of *R. opacus* Kurosawa et al (2015c; 2013; 2014) optimised the C/N ratio using response surface methodology (RSM), a statistical technique for optimising experimental methods when there are several dependent variables. The optimal C/N ratio determined for MITXM-61 grown on a mixture of D-glucose and D-xylose with (NH₄)₂SO₄ as the sole nitrogen source was 62.3 (Kurosawa et al, 2014). TAG production from OMSW fibre hydrolysate could therefore be improved further by adding about 29% less VYE to the hydrolysate to give a C/N ratio of ~62.3. On a side note, in all relevant publications by the Sinskey group the C/N ratio is calculated by dividing the carbon source concentration in g/L by the nitrogen source concentration in g/L (Fei et al, 2015; Kurosawa et al, 2010; Kurosawa et al, 2015c; Kurosawa et al, 2013; Kurosawa et al, 2014). (NH₄)₂SO₄ was usually used to supplement nitrogen in these studies, but this method produces inaccurate results when different nitrogen sources are used because the amount of nitrogen present varies between compounds. To compare the results from these publications to this study the results were converted to the true ratio of carbon to nitrogen using **Equation 4.6 (4.2.6.5)**.

FAs produced by *R. opacus* have the optimal length for biodiesel production (Fei et al, 2015) and can also be converted to aviation fuel via a series of chemical processing steps (Jiménez-Díaz et al, 2016). That said, directly producing MCFAs in *R. opacus* would eliminate the need for hydrocracking and reduce the number of steps for aviation fuel production. In general, the possibility of developing an *R. opacus* strain capable of producing custom FAs is an intriguing concept as the ability to produce a diverse range of products within an integrated biorefinery provides commercial flexibility and greater overall economic stability. Unfortunately, our attempt to manipulate the FA profile of *R. opacus* toward lauric acid production by expressing the thioesterase ACP-BTE has so far been unsuccessful. No increase in lauric acid was measured (**Figure 4.21**) and no obvious changes in the abundance of other fatty acids was observed (**Figure 4.20**), indicating that the protein is likely misfolded. Further work is needed to confirm the hypothesis that overexpression of ACP-BTE can promote an increase in MCFA accumulation during transition-phase. The identity and functionality of the enriched bands observed in crude cell lysate of induced *R. opacus*^{pTip-QC1_ACP-BTE} (**Figure 4.18**) need to be established. This could be done either by western blotting against the hexahistidine tag or by histidine tag purification of the protein followed by matrix-assisted laser desorption/ionization-time of flight (MALDI-TOF) mass spectrometry (MS). *In-vitro* acyl-CoA thioesterase activity assays are also available to measure catalytic activity of ACP-BTE and determine if the purified enzyme is functional (Hunt et al, 2002; McMahon & Prather, 2014).

Troubleshooting of ACP-BTE misfolding is also required. Heterologous protein expression in bacterial systems at high expression levels often leads to misfolding and aggregation in inclusion bodies (Kunze et al, 1995). pTip-QC1 was designed for overexpressing proteins for biochemical studies because *Rhodococcus* species can grow over a broad temperature range (4-35°C), which can improve expression of more complex protein targets (Nakashima & Tamura, 2004b). As our aim was to produce cytoplasmically active protein, not material for biochemical studies, it is possible that switching to a less efficient promoter or using a different vector will be necessary to enable functional expression of ACP-BTE. Furthermore, eukaryotic proteins expressed in the bacterial cytoplasm cannot form disulphide bridges, potentially disrupting protein integrity (de Marco, 2009). Analysis of putative disulphide bridges in the ACP-BTE protein sequence was carried out using the DiANNA web server (Ferrè & Clote, 2005) and showed three predicted disulphide bonds between cysteines at positions 11 – 187, 206 – 215 and 320 – 343.

Although this did not influence functionality when ACP-BTE was expressed in *E. coli* (Voelker & Davies, 1994) it could have contributed to misfolding in *R. opacus*. In general, expressing plant proteins in bacteria is challenging and it may be more effective to express a bacterial MCFA thioesterase or an autologous C12-active thioesterase. However, when Huang et al, (Huang et al, 2016) overexpressed four putative thioesterases from *R. opacus* PD630 in *R. opacus* and *E. coli* they found that all four increased C16:1 and C18:1 FA yields in *E. coli* but only two were effective in *R. opacus*, indicating that there may be greater regulatory complexity in its FA biosynthesis pathway.

Over 261 genes have been implicated in TAG metabolism through transcriptomics, bioinformatic analyses and metabolic reconstruction (Amara et al, 2016; Holder et al, 2011) and recent functional genomic analyses have revealed that at least ten putative copies exist for many major TAG biosynthesis and β -oxidation pathway genes (Holder et al, 2011). Therefore even if ACP-BTE is functionally expressed, it is possible that the extensive redundancy and complexity of FA metabolism in this species may obfuscate any heterologous thioesterase activity. Previous work has shown that knocking out the major diacylglycerol acyltransferases (DGATs) *atf1* and *atf2* reduced TAG yields by 30 and 50% respectively, but did not eliminate TAG production entirely (Hernandez et al, 2013). Overall, this indicates that different isozymes are likely to be differentially regulated and contribute to TAG biosynthesis via highly coordinated metabolic circuits (Alvarez et al, 2019). Furthermore, acyl-CoA synthase, the major β -oxidation pathway enzyme that was knocked out in *E. coli* expressing ACP-BTE to enable greater lauric acid production, exists as 15 isozymes in *R. opacus* (Holder et al, 2011; Voelker & Davies, 1994). Disabling the β -oxidation pathway to increase MCFA yields is therefore probably not a viable approach in *R. opacus*. In general, manipulating the FA profile in *R. opacus* could pose a significant genetic engineering challenge, but also presents an exciting opportunity to develop this robust and highly productive species into a unique and valuable industrial platform.

Chapter 5: General Discussion

OMSW has considerable potential as a renewable feedstock for sustainably producing fuels and bio-based chemicals - it is abundant, high in lignocellulose, produced continuously and does not directly compete with agriculture. Furthermore, integrated MSW biorefineries could augment operational costs with gate fees and by recycling inorganic MSW components. Thus far however, research into the amenability of OMSW for biorefining has been limited in comparison to other lignocellulosic feedstocks (Matsakas et al, 2017). The work presented in this thesis aimed to evaluate OMSW as a feedstock for bio-manufacturing and identify candidate species with promising characteristics for OMSW fermentation.

The OMSW used for research purposes is typically acquired by manually sampling and sorting mixed MSW from local establishments (Adhikari et al, 2013; Aiello-Mazzarri et al, 2006; Lay et al, 1999), acquired from nearby waste treatment plants (Farmanbordar et al, 2018b; Ghanavati et al, 2015; Hartmann & Ahring, 2005; Jensen et al, 2011; Lavagnolo et al, 2018) or simply replaced with an OMSW-like material (McCaskey et al, 1994) Ma et al, 2009 (Dang et al, 2017). By contrast, the OMSW fibre used in this project was produced on an industrial autoclave system using a predetermined mixture of MSW, constructed according to national averages for the composition of MSW across the UK. Very recently, Althuri & Venkata (2019) used a custom mixture of organic materials, including food waste, yard trimmings, newspaper, cardboard, textiles and wood chips, to generate a reproducible and heterogeneous source of OMSW, but did not report the basis for the quantities used in their mixture. The approach used in this thesis enabled OMSW fibre to be produced reproducibly with a realistic composition that, by extension, also reflects OMSW from other high-income nations with similar consumption patterns. On the whole, the constructed OMSW fibre used throughout this PhD is more representative and of greater industrial relevance compared to the OMSW sources described in the literature so far for bioprocessing applications.

Autoclaving is an established industrial method for MSW management that is implemented around the world (Wojnowska-Baryła et al, 2019). There is a general consensus in the literature that hydrothermal pre-treatments like autoclaving produce fewer inhibitors than other processes but can effectively increase cellulose accessibility in a variety of feedstocks (Jönsson & Martin, 2016). Work from this PhD showed that autoclave pre-treated OMSW was low in most major inhibitors associated with

lignocellulosic hydrolysates, while the major problem inhibitors furfural and 5-HMF were absent. Additionally, autoclaving made the cellulose in OMSW more accessible, enabling a relatively high hydrolysis efficiency to be achieved (75%) at an industrially relevant solids loading of 20%, despite the poor rheology of the lab scale hydrolysis set-up.

Although the hydrolysis results were promising, the enzyme loading used for this work were highly impracticable. Cellulolytic enzymes are the most prohibitive overhead cost in lignocellulosic bioprocesses (Klein-Marcuschamer et al, 2012) and must be used as economically as possible while still ensuring efficient saccharification. Furthermore, in the context of a fully functioning MSW biorefinery based around the Wilson System[®], autoclaving and hydrolysis are predicted to be the most energy intensive processes, respectively accounting for 42% and 32% of total heat and 41% and 0.4% of total electricity (Meng et al, 2019). Optimising autoclave conditions and hydrolysis methods are therefore vital for developing a viable bioprocess around OMSW. This will also ensure efficient process flow for the MSW biorefinery as whole so that margins are maximised. Any future research endeavours in this area should draw on the large body of work that has already been published on OMSW hydrolysis methodology (Jensen et al, 2011; Jensen et al, 2010; Li et al, 2012a; Mahmoodi et al, 2018a; Puri et al, 2013) and aim to make full use of the Wilson Bio-Chemical pilot rig which offers a unique opportunity for optimising OMSW production and pre-treatment conditions rapidly and in a scalable manner.

Finding applications for waste streams is a critical but often neglected aspect of bioprocess development. My work showed that AD of the residual material from OMSW fibre hydrolysis produced greater methane yields than AD of the un-hydrolysed OMSW fibre. This suggests that rather than sending OMSW fibre directly to AD it is potentially more valuable to produce higher-value bio-products from OMSW fibre hydrolysate and use waste streams such as hydrolysis residuals to power biorefinery processes.

This reasoning is further supported by a life cycle analysis for an MSW biorefinery based around the Wilson System[®] carried out by Meng et al, (2019). Their model showed that the energetic requirements of the entire processing plant (29.03 kWh electricity and 660 MJ of heat) could be fully sustained from biogas produced by AD of process waste water and by heat recovery from incineration of hydrolysis residues, waste water sludge and fermentation residues (266 kWh electricity and 1,108 MJ heat) (Meng et al, 2019). Although the results of this LCA are encouraging, several life cycle analyses comparing AD

and incineration for energy production from OMSW draw varying conclusions about the efficiency and sustainability of one over the other (Di Maria & Micale, 2015; Fernández-González et al, 2017; Tan et al, 2015). Further work is therefore required to determine whether AD or incineration are the best options for dealing with the various waste streams from OMSW bioprocessing in the context of developing a viable and sustainable MSW biorefinery.

Moreover, Meng et al, (2019) did not consider the potential impacts of metal accumulation from various waste streams over time, such as in incineration fly ash which is considered a hazardous waste with limited disposal options (Margallo et al, 2015). Work from this PhD showed that toxic metals become concentrated in the residuals fraction and are relatively abundant in the liquid hydrolysate, indicating that they could also become concentrated in fermentation residues. Although these metals could be immobilised through AD and composting (Dong et al, 2013; Smith, 2009), diminishing metal supplies are of global concern and some metals from these waste streams have significant commercial value (Chojnacka, 2010). Furthermore, as discussed in **Chapter 2**, fluctuations in metal levels on an industrial scale could potentially affect fermentative microorganisms. A possible approach could be to detoxify and recycle metals from OMSW fibre hydrolysate and other bioprocess waste streams using materials designed for selective metal adsorption. For example, up to 70% of Ni, 40% of Zn and 25% of Cd present in residual material from hydrolysis of maize processing waste could be removed by circulation over a macroporous polyacrylamide column for 6 days (Selling et al, 2008). Alternately, a carbonaceous mesoporous material called Starbon[®], produced using waste polysaccharides, can selectively and reversibly bind precious metals from a mixture of abundant earth metals and could be used to remove metals from OMSW hydrolysate before fermentation (García et al, 2015). These and other metal reclamation technologies should be investigated in the interest of developing a truly circular economy around MSW.

Although the initial compositional analysis of the OMSW fibre identified some protein (3%) and oil (2%), the concentration of microbially accessible nitrogen and phosphate measured in the hydrolysate were suboptimal. Other studies of OMSW composition report highly variable protein and lipid levels, averaging 14% and 9% respectively, with the highest levels found in regions with high food waste production (Barampouti et al, 2019). In some countries the lipid fraction of OMSW is even large enough to be extracted for biodiesel

production (Barik et al, 2018). Because OMSW is such a heterogeneous and variable feedstock, an affordable and abundant nutrient source is crucial to allow fermentation conditions to be optimised, particularly for strains like *R. opacus* where the C/N ratio is critical for optimal performance.

My work demonstrated that supplementing OMSW fibre hydrolysate with 1% VYE abolished nitrogen and phosphate limitation and promoted efficient growth of most microorganisms trialled in this study. On an industrial scale VYE could be substituted with autolysed spent yeast, a waste product that is generated in substantial volumes in the brewing industry. An average medium sized brewery in the UK has a batch capacity of 1,000-2,000 L and generates thousands of Kg of spent yeast per week. Alternative applications of waste yeast are limited to animal feed, anaerobic digestion or fertiliser and offsite transport is expensive, therefore 40-70% is usually disposed directly into sewage systems (Kerby & Vriesekoop, 2017). Combining these two waste streams could effectively meet the needs of both industries and presents an appealing opportunity for circular economy.

It was postulated that a highly robust and physiologically well-adapted species would be required to develop a bioprocess around OMSW fibre due to the heterogeneous, variable and complex nature of the feedstock. As such, a substrate-oriented screening approach was chosen to identify candidate species for this project. In general, the use of a product-oriented screening approach, in which a microorganism is selected based on its ability to efficiently produce a product of commercial interest, has been favoured in academic and industrial settings (Rumbold et al, 2010). Only a handful of publications report the use of a substrate-oriented approach for second-generation feedstock fermentation: Rumbold et al (2009; 2010) published two studies in which yeasts (*S. cerevisiae*, *Pichi stipites*), bacteria (*Corynebacterium glutamicum*, *E. coli*) and fungi (*Aspergillus niger*, *Trichoderma reesei*) were screened for the ability to ferment a range of lignocellulosic hydrolysates or glycerol and Lau et al, (2010) compared the fermentation performance of three ethanologens (*Z. mobilis*, *S. cerevisiae* and *E. coli*) on AFEX-pretreated corn stover.

The species used in these three publications are all extensively studied for lignocellulosic feedstock fermentation and industrial biotechnology applications. However, the disparate pre-treatment chemistries and inhibitor profiles of second-generation

feedstocks, along with the variations in published experimental conditions like the concentration of sugars, nutrients, inoculum size and the type of bioreactor used, limit the possibility of confidently comparing the performance of a species across publications. The same is true of OMSW-derived feedstocks, which, as discussed above, are highly heterogeneous and frequently irreproducible in composition, leading to greatly varied fermentation profiles even when the same microorganism is used (Ballesteros et al, 2010; Puri et al, 2013). In general, substrate-oriented screening entails more work in the early stages of process development but ultimately enables each species' intrinsic fermentation abilities and robustness to be more systematically and rigorously evaluated with the feedstock of interest, thereby also increasing the likelihood of successfully developing a microbial production platform (Lau & Dale, 2009; Rumbold et al, 2009; Rumbold et al, 2010).

The robustness of each microorganism trialled in this project was quantitatively evaluated and compared, enabling species of biotechnological significance to be selected based on their intrinsic ability to thrive on OMSW fibre hydrolysate. *R. opacus*, *S. cerevisiae* and *Z. mobilis* demonstrated excellent growth and produced near theoretical yields (>69%) of product. However, the fermentation assay developed in this project was exclusively carried out in conical flasks, which do not enable monitoring of critical variables (i.e. oxygen transfer rate (OTR) and oxygen uptake rate (OUR), CO₂ production, temperature, pH) that are necessary to facilitate bioprocess scale-up (Neubauer et al, 2013). Scale-up is the most challenging step in bioprocess development and many species that do well in shake flasks become inviable under bioreactor conditions due sheer forces, heat transfer and mixing inefficiencies, temperature and pH variability and oxygen transfer limitation (Humphrey, 1998).

Physiology also has a significant influence on a species' scalability and viability for fermenting a feedstock. For example, scaling-up aerobic bioprocesses is more challenging than fermentations with anaerobes or facultative anaerobes like *Z. mobilis* and *S. cerevisiae*. Shake flasks have a well-defined gas/liquid mass transfer area that mostly enables oxygen transfer independently of changes in medium composition, making them excellent for preliminary high-throughput fermentation screens (Büchs, 2001). However, fermentation broth viscosity limits oxygen solubility and under bioreactor conditions any changes in hydrodynamics will reduce oxygen transfer into the system (Garcia-Ochoa et al,

2010). Such changes are influenced by operational conditions, physicochemical properties of the culture (i.e. density, viscosity, surface tension), bioreactor geometry and cell density (Paulová & Brányik, 2013). *R. opacus* has a highly aerobic metabolism and growth in stirred tank bioreactors requires at least 60% dissolved oxygen to ensure efficient growth (Kurosawa et al, 2014). The sensitivity of TAG biosynthesis to aeration was observed when *R. opacus* cultures grown in shake flask assays with 40 ml instead of 10 ml OMSW fibre hydrolysate exhibited slower rates of growth and TAG accumulation. High culture densities are required for viable TAG production in *R. opacus*, therefore it is critical that dissolved oxygen levels can be efficiently sustained throughout fermentation.

Aerobic fermentations are not impossible to engineer (the antibiotic fermentations developed in the 1940's were all highly aerobic processes (Humphrey, 1998)), however aerobic bioreactors such as airlift fermentors and bubble columns require significant power consumption which contributes to operating costs (Garcia-Ochoa & Gomez, 2009). Therefore in general, anaerobic or microaerobic processes can be more reliably scaled-up and economically operated. Although all three candidate species demonstrated considerable promise for biofuel and chemical production from OMSW fibre, bioprocess scalability must be validated at higher volumes with online monitored bioreactors in order to fully assess their industrial viability (Büchs, 2001; Neubauer et al, 2013). Furthermore, techno-economic and life cycle analyses are valuable tools for comparing different microbial platforms and should be used to comprehensively evaluate the practicability of each species in the context of an integrated MSW biorefinery (Julio et al, 2017).

Finally, efficient downstream processing is of particular importance for ensuring bioprocess viability. Ethanol is secreted into the medium and can be isolated relatively rapidly and economically by distillation so long as concentrations of at least 4% w/w are obtained (Huang & Zhang, 2011). Conversely, extracting TAG from intracellular lipid inclusions requires extensive purification for which industrial scale technologies are currently underdeveloped and uneconomical. Industrial methods for TAG purification from microbial biomass have been extensively reviewed by Dong et al, (2016) who highlight the critical importance of efficient cell disruption. Viable disruption technologies should release lipids effectively while avoiding the formation of stable emulsions that impede phase separation and eliminating cellular debris which reduces extraction efficiency at high cell densities. Effective lipid extraction is also a limiting step, requiring nonpolar solvents that

are water-immiscible but also volatile enough to be economically recovered by low-energy phase-separation and evaporation (Dong et al, 2016).

On the whole methods for extracting lipids from wet microbial biomass require further development to be practical for industry. Any potential technologies must also be evaluated in conjunction with other downstream processing necessary for transforming extracted triglycerides into biodiesel and other products (Lestari et al, 2009). Engineering the TAG pathway to produce more valuable fatty acids could offer a way balance out the higher costs of product purification. However, our current understanding of how TAG metabolism is regulated in *R. opacus* is incomplete and the biochemistry of key processes, such as how sugar metabolism is coupled to lipid synthesis, are still unclear (Alvarez et al, 2019). Additionally, the high level of functional redundancy among proteins in this pathway limits the options for systematic studies (Holder et al, 2011).

To our knowledge this is the first time an attempt has been made to manipulate FA chain length in *R. opacus*. However, as discussed in **Chapter 4**, further work is needed to resolve the non-functional expression of ACP-BTE. Alternative engineering targets and approaches should also be explored. Although *R. opacus* is a non-model organism, an expanded repertoire of genetic engineering tools has become available in recent years, including a library of promoters, reporters, selection markers and plasmids, as well as genomic integration cassettes. Neutral target integration sites to enable stable genomic integration of heterologous genes have also been identified (DeLorenzo et al, 2018). Interestingly, CRISPR interference (CRISPRi) (Larson et al, 2013) has recently been developed for targeted gene repression in *Rhodococcus* (DeLorenzo et al, 2018) opening up the possibility of disabling functionally redundant enzymes in the TAG metabolic network.

There is an urgent need for innovative and holistic waste management systems to cope with increasing volumes of MSW, mitigate the environmental impacts of poor waste disposal and enable our finite resources to be recycled. At the same time, a pressing search is underway to find viable renewable alternatives to petroleum that will ensure the long-term sustainability of our industries. Developing an integrated biorefinery around MSW has the potential to significantly alleviate the social, economic and environmental burdens of inadequate waste management. This thesis has demonstrated that autoclave pre-treated OMSW fibre can be used as a feedstock for producing renewable fuels and chemicals.

Several biotechnologically useful microorganisms were identified that are intrinsically well suited for fermenting OMSW. These species are promising candidates for the development of OMSW-based biorefining processes and provide a foundation for further studies that aim to valorise this underexplored feedstock. Future work should focus on evaluating the performance of candidate species in bioreactors under scalable conditions and at greater volumes. Furthermore, bioprocess viability should be investigated through LCAs and TEAs to determine which microbial platform would be most viable in an OMSW biorefinery.

Appendices

Appendix I: Percentage composition of constructed OMSW fibre

Table AI-1: Components of OMSW fibre were measured by a range of established methods. For details see materials and methods in **Chapter 2**. Oil and protein were measured separately but are ethanol and water soluble, respectively, and are thus shown as a fraction of non-structural components extracted by water or ethanol. A breakdown of the monosaccharides measured in the hemicellulose fraction are given as percentages of the total dry weight of fibre. All data are averages of at least triplicate analyses. \pm SD = Standard deviation of minimum triplicate measurements.

Glu = Glucose; *Xyl* = Xylose; *Man* = Mannose; *Fuc* = Fucose; *Ara* = Arabinose; *Rha* = Rhamnose; *Gal* = Galactose; *GalA* = Galacturonic acid. *n/a* = not applicable.

| Component | Percentage of total dry mass (%) | \pm SD |
|------------------------------|----------------------------------|-------------|
| Cellulose | 37.61 | 2.73 |
| Hemicellulose | | |
| <i>Fuc</i> | 0.02 | 0.002 |
| <i>Ara</i> | 0.27 | 0.02 |
| <i>Rha</i> | 0.06 | 0.002 |
| <i>Gal</i> | 0.41 | 0.02 |
| <i>Glu</i> | 1.10 | 0.08 |
| <i>Xyl</i> | 1.34 | 0.03 |
| <i>Man</i> | 0.95 | 0.10 |
| <i>GalA</i> | 0.10 | 0.02 |
| Total: | 4.25 | 0.14 |
| Lignin | 15.78 | 0.37 |
| Ash | 14.74 | 1.47 |
| Metals | 1.33 | 0.26 |
| Extractives (water) | | |
| <i>Protein</i> | 3.23 | 0.40 |
| <i>Extractives (other)</i> | 5.92 | <i>n/a</i> |
| Total: | 9.15 | 2.62 |
| Extractives (ethanol) | | |
| <i>Oil</i> | 1.72 | 0.25 |
| <i>Extractives (other)</i> | 6.23 | <i>n/a</i> |
| Total: | 7.95 | 0.92 |
| SUM: | 90.83 | 4.21 |
| Other (remaining): | 9.17 | <i>n/a</i> |

Appendix II: Concentration of metals measured in constructed OMSW fibre

Table AII-1: Metals were measured by ionisation coupled plasma mass spectrometry (ICPMS) against Agilent certified multi-element environmental calibration standard No. 5183-4688. Note that units change as concentrations range from mol/Kg to $\mu\text{mol/Kg}$.

$\pm\text{SD}$ = Standard deviation of triplicates. n/d = Not detected.

| Metal | Concentration | $\pm\text{SD}$ | Units |
|------------------------|----------------------|----------------------------------|--------------------|
| Ca⁴³ | 1.03 | 0.12 | mol/Kg |
| Ca⁴⁴ | 1.06 | 0.14 | mol/Kg |
| Al | 166.90 | 27.50 | mmol/Kg |
| K | 66.53 | 6.44 | mmol/Kg |
| Fe | 62.44 | 28.48 | mmol/Kg |
| Na | 57.48 | 5.43 | mmol/Kg |
| Mg | 44.44 | 6.00 | mmol/Kg |
| Zn | 2.47 | 1.65 | mmol/Kg |
| Mn | 0.76 | 0.06 | mmol/Kg |
| Ni | 0.33 | 0.25 | mmol/Kg |
| Cu | 0.33 | 0.06 | mmol/Kg |
| Ba | 0.16 | 0.02 | mmol/Kg |
| Cr | 0.11 | 0.01 | mmol/Kg |
| V | 0.04 | 0.01 | mmol/Kg |
| Pb | 0.01 | 0.00 | mmol/Kg |
| Sb | 0.01 | 0.00 | mmol/Kg |
| V | 39.98 | 5.08 | $\mu\text{mol/Kg}$ |
| Pb | 13.77 | 3.10 | $\mu\text{mol/Kg}$ |
| Sb | 10.39 | 0.63 | $\mu\text{mol/Kg}$ |
| Co | 9.29 | 0.87 | $\mu\text{mol/Kg}$ |
| As | 1.20 | 0.66 | $\mu\text{mol/Kg}$ |
| U | 0.46 | 0.09 | $\mu\text{mol/Kg}$ |
| Cd | 0.30 | 0.09 | $\mu\text{mol/Kg}$ |
| Tl | 0.03 | 0.02 | $\mu\text{mol/Kg}$ |
| Th | n/d | n/d | - |
| Mo | n/d | n/d | - |
| Ag | n/d | n/d | - |

Appendix III: Shannon Index

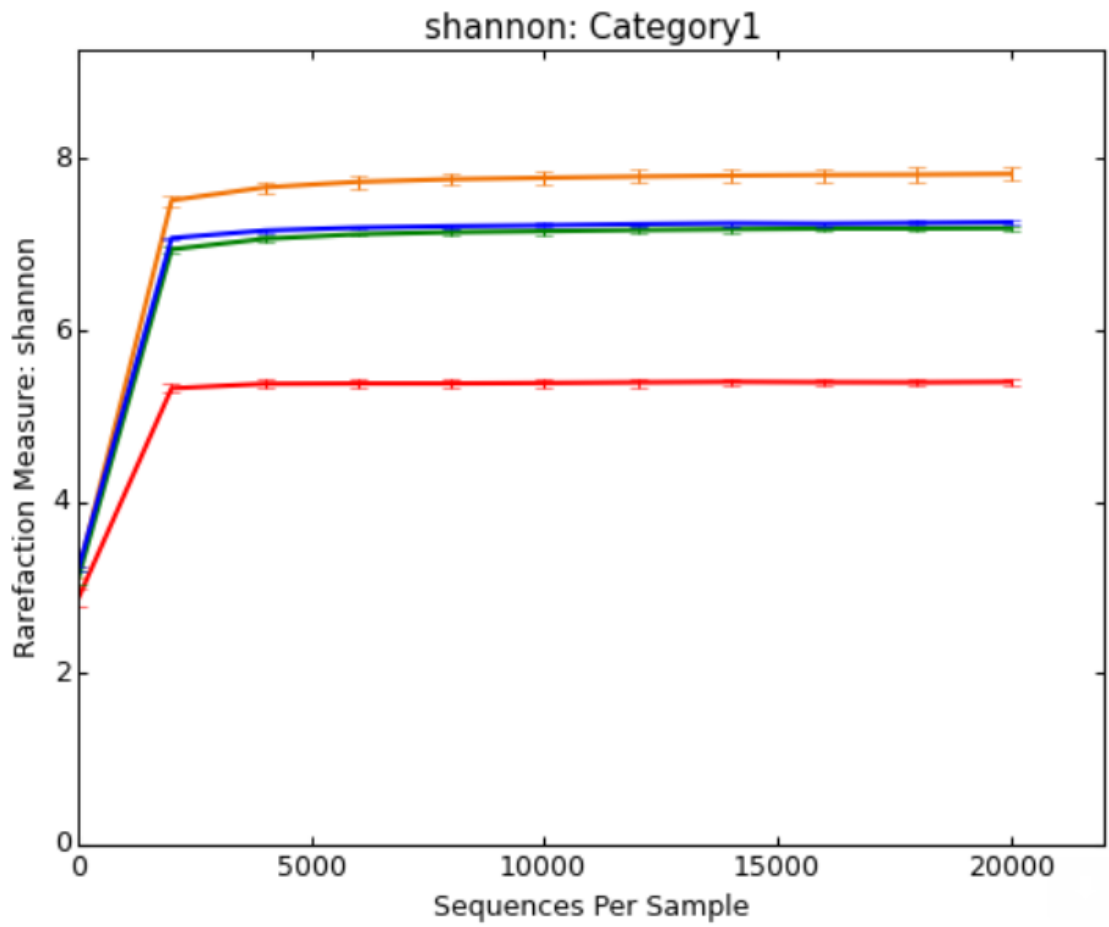


Figure AIII-1: Shannon index plot (measure of sequencing depth) for reads from microbial community sequencing (for details see Chapter 3, 3.2.8.2)

Appendix IV: Taxonomic Tables of AD Community Analysis

Table AIV-1: Taxonomic abundance to the phylum level for microbial communities fed with OMSW fibre (MFW.1, MFW.2) and residuals from OMSW fibre hydrolysis (MFW.3, MFW.4) after 43 days of anaerobic digestion with OMSW fibre or residuals, based on groupings of 16s rRNA sequences. For details see Methods in **Chapter 3 (3.2.8.2)**.

| Legend | Taxonomy | Total % | MFW.1 % | MFW.2 % | MFW.3 % | MFW.4 % |
|--------|--|---------|---------|---------|---------|---------|
| | None:Other | 3.4% | 3.9% | 4.0% | 3.6% | 3.9% |
| | k__Archaea;p__Euryarchaeota | 7.0% | 7.4% | 8.1% | 7.3% | 7.0% |
| | k__Archaea;p__Miscellaneous Crenarchaeotic Group | 0.0% | 0.0% | 0.0% | 0.0% | 0.0% |
| | k__Bacteria;p__Acidobacteria | 1.2% | 0.8% | 0.9% | 1.0% | 1.0% |
| | k__Bacteria;p__Actinobacteria | 4.9% | 1.4% | 1.3% | 1.4% | 1.3% |
| | k__Bacteria;p__Aminicenantes | 0.2% | 0.0% | 0.0% | 0.0% | 0.0% |
| | k__Bacteria;p__Armatimonadetes | 0.3% | 0.1% | 0.2% | 0.2% | 0.2% |
| | k__Bacteria;p__Atribacteria | 0.1% | 0.4% | 0.4% | 0.4% | 0.4% |
| | k__Bacteria;p__Bacteroidetes | 24.5% | 23.9% | 23.7% | 24.1% | 24.7% |
| | k__Bacteria;p__Caldiserica | 0.1% | 0.1% | 0.1% | 0.1% | 0.1% |
| | k__Bacteria;p__Chlamydiae | 0.0% | 0.0% | 0.0% | 0.0% | 0.0% |
| | k__Bacteria;p__Chlorobi | 0.0% | 0.0% | 0.0% | 0.0% | 0.0% |
| | k__Bacteria;p__Chloroflexi | 5.3% | 14.5% | 14.7% | 14.5% | 13.9% |
| | k__Bacteria;p__Cloacimonetes | 8.6% | 1.4% | 1.4% | 1.4% | 1.4% |
| | k__Bacteria;p__Cyanobacteria | 0.1% | 0.0% | 0.0% | 0.0% | 0.0% |
| | k__Bacteria;p__Deinococcus-Thermus | 0.0% | 0.0% | 0.0% | 0.0% | 0.0% |
| | k__Bacteria;p__Elusimicrobia | 0.0% | 0.0% | 0.0% | 0.0% | 0.0% |
| | k__Bacteria;p__Fibrobacteres | 0.3% | 1.2% | 1.1% | 1.2% | 1.2% |
| | k__Bacteria;p__Firmicutes | 17.5% | 15.6% | 15.1% | 15.4% | 16.0% |
| | k__Bacteria;p__Gemmatimonadetes | 0.0% | 0.0% | 0.0% | 0.0% | 0.0% |
| | k__Bacteria;p__Hydrogenedentes | 1.3% | 1.1% | 1.1% | 1.4% | 1.3% |
| | k__Bacteria;p__Lentisphaerae | 0.2% | 0.6% | 0.5% | 0.6% | 0.5% |
| | k__Bacteria;p__Microgenomates | 0.5% | 1.5% | 1.5% | 1.5% | 1.5% |
| | k__Bacteria;p__NA | 3.4% | 3.7% | 3.7% | 3.6% | 3.5% |
| | k__Bacteria;p__Nitrospirae | 0.1% | 0.5% | 0.4% | 0.4% | 0.4% |
| | k__Bacteria;p__Omnitrophica | 0.1% | 0.1% | 0.1% | 0.1% | 0.1% |
| | k__Bacteria;p__Parcubacteria | 0.3% | 0.3% | 0.3% | 0.3% | 0.2% |
| | k__Bacteria;p__Planctomycetes | 0.5% | 0.3% | 0.3% | 0.3% | 0.3% |
| | k__Bacteria;p__Proteobacteria | 9.3% | 7.0% | 6.8% | 7.0% | 6.9% |
| | k__Bacteria;p__Saccharibacteria | 0.2% | 0.0% | 0.0% | 0.0% | 0.0% |
| | k__Bacteria;p__Spirochaetae | 5.0% | 9.1% | 9.2% | 9.1% | 9.0% |
| | k__Bacteria;p__Synergistetes | 3.2% | 3.3% | 3.5% | 3.7% | 3.6% |
| | k__Bacteria;p__Tenericutes | 0.7% | 0.0% | 0.0% | 0.0% | 0.0% |
| | k__Bacteria;p__Thermotogae | 0.2% | 0.0% | 0.0% | 0.0% | 0.0% |
| | k__Bacteria;p__Verrucomicrobia | 1.6% | 1.6% | 1.6% | 1.5% | 1.6% |

Table AIV-2: Taxonomic abundance to the phylum level for microbial communities fed with OMSW fibre (MFW.1, MFW.2) and residuals from OMSW fibre hydrolysis (MFW.3, MFW.4) after 43 days of anaerobic digestion with OMSW fibre or residuals, based on groupings of 16s rRNA sequences. For details see Methods in **Chapter 3 (3.2.8.2).**

| Legend | Taxonomy | MFW.1 | MFW.2 | MFW.3 | MFW.4 |
|--------|---|-------|-------|-------|-------|
| | | % | % | % | % |
| | None;Other:Other:Other | 3.9% | 4.0% | 3.6% | 3.9% |
| | k_Archaea;p_Euryarchaeota;c_Methanobacteria;o_Methanobacteriales | 0.0% | 0.0% | 0.0% | 0.0% |
| | k_Archaea;p_Euryarchaeota;c_Methanomicrobia;o_Methanomicrobiales | 2.4% | 2.7% | 2.5% | 2.5% |
| | k_Archaea;p_Euryarchaeota;c_Methanomicrobia;o_Methanosarcinales | 4.9% | 5.3% | 4.8% | 4.4% |
| | k_Archaea;p_Euryarchaeota;c_Thermoplasmata;o_Thermoplasmatales | 0.1% | 0.1% | 0.1% | 0.1% |
| | k_Archaea;p_Miscellaneous Crenarchaeotic Group;c_NA;o_NA | 0.0% | 0.0% | 0.0% | 0.0% |
| | k_Bacteria;p_Acidobacteria;c_Acidobacteria;o_NA | 0.2% | 0.2% | 0.2% | 0.3% |
| | k_Bacteria;p_Acidobacteria;c_Holophagae;o_Holophagales | 0.0% | 0.0% | 0.0% | 0.0% |
| | k_Bacteria;p_Acidobacteria;c_Holophagae;o_NA | 0.6% | 0.6% | 0.7% | 0.7% |
| | k_Bacteria;p_Actinobacteria;c_Acidimicrobia;o_Acidimicrobiales | 0.2% | 0.1% | 0.1% | 0.2% |
| | k_Bacteria;p_Actinobacteria;c_Actinobacteria;o_Actinomycetales | 0.0% | 0.0% | 0.0% | 0.0% |
| | k_Bacteria;p_Actinobacteria;c_Actinobacteria;o_Bifidobacteriales | 0.0% | 0.0% | 0.0% | 0.0% |
| | k_Bacteria;p_Actinobacteria;c_Actinobacteria;o_Corynebacteriales | 0.1% | 0.1% | 0.1% | 0.1% |
| | k_Bacteria;p_Actinobacteria;c_Actinobacteria;o_Frankiales | 0.0% | 0.0% | 0.0% | 0.0% |
| | k_Bacteria;p_Actinobacteria;c_Actinobacteria;o_Kineosporiales | 0.3% | 0.2% | 0.3% | 0.3% |
| | k_Bacteria;p_Actinobacteria;c_Actinobacteria;o_Micrococcales | 0.2% | 0.2% | 0.2% | 0.2% |
| | k_Bacteria;p_Actinobacteria;c_Actinobacteria;o_Micromonosporales | 0.0% | 0.0% | 0.0% | 0.0% |
| | k_Bacteria;p_Actinobacteria;c_Actinobacteria;o_NA | 0.1% | 0.1% | 0.1% | 0.1% |
| | k_Bacteria;p_Actinobacteria;c_Actinobacteria;o_Propionibacteriales | 0.0% | 0.0% | 0.0% | 0.0% |
| | k_Bacteria;p_Actinobacteria;c_Actinobacteria;o_Streptomyces | 0.0% | 0.0% | 0.0% | 0.0% |
| | k_Bacteria;p_Actinobacteria;c_Coriobacterii;o_Coriobacteriales | 0.0% | 0.0% | 0.0% | 0.0% |
| | k_Bacteria;p_Actinobacteria;c_NA;o_NA | 0.1% | 0.0% | 0.0% | 0.1% |
| | k_Bacteria;p_Actinobacteria;c_Thermoleophila;o_Gaieilales | 0.4% | 0.4% | 0.4% | 0.3% |
| | k_Bacteria;p_Thermoleophila;o_Thermoleophila;o_Solirubrobacteriales | 0.0% | 0.0% | 0.0% | 0.0% |
| | k_Bacteria;p_Aminicenantes;c_NA;o_NA | 0.0% | 0.0% | 0.0% | 0.0% |
| | k_Bacteria;p_Armatimonadetes;c_Chthonomonadetes;o_Chthonomonadales | 0.0% | 0.0% | 0.0% | 0.0% |
| | k_Bacteria;p_Armatimonadetes;c_NA;o_NA | 0.1% | 0.2% | 0.2% | 0.2% |
| | k_Bacteria;p_Atribacteria;c_NA;o_NA | 0.4% | 0.4% | 0.4% | 0.4% |
| | k_Bacteria;p_Bacteroidetes;c_Bacteroidia;o_Bacteroidales | 8.6% | 8.5% | 8.2% | 8.8% |
| | k_Bacteria;p_Bacteroidetes;c_Bacteroidia;o_NA | 6.3% | 6.3% | 6.3% | 6.5% |
| | k_Bacteria;p_Bacteroidetes;c_Cytophagia;o_Cytophagales | 0.0% | 0.0% | 0.0% | 0.0% |
| | k_Bacteria;p_Bacteroidetes;c_Flavobacteria;o_Flavobacteriales | 0.0% | 0.0% | 0.0% | 0.0% |
| | k_Bacteria;p_Bacteroidetes;c_NA;o_NA | 6.0% | 6.0% | 6.8% | 6.5% |
| | k_Bacteria;p_Bacteroidetes;c_Sphingobacteria;o_Sphingobacteriales | 2.9% | 2.8% | 2.7% | 2.9% |
| | k_Bacteria;p_Caldiserica;c_Caldiserica;o_Caldisericales | 0.1% | 0.1% | 0.1% | 0.1% |
| | k_Bacteria;p_Chlamydiae;c_Chlamydiae;o_Chlamydiales | 0.0% | 0.0% | 0.0% | 0.0% |
| | k_Bacteria;p_Chlorobi;c_Chlorobia;o_Chlorobiales | 0.0% | 0.0% | 0.0% | 0.0% |
| | k_Bacteria;p_Chloroflexi;c_Anaerolineae;o_Anaerolineales | 13.6% | 13.8% | 13.6% | 13.0% |
| | k_Bacteria;p_Chloroflexi;c_Caldilineae;o_Caldilineales | 0.0% | 0.0% | 0.0% | 0.0% |

| | | | | | |
|---|-------|-------|-------|-------|-------|
| k_Bacteria;p_Chloroflexi;c_NA;o_wastewater_metagenome | 0.0% | 0.0% | 0.0% | 0.0% | 0.0% |
| k_Bacteria;p_Chloroflexi;c_Thermomicrobia;o_NA | 0.2% | 0.1% | 0.1% | 0.1% | 0.1% |
| k_Bacteria;p_Cloacimonetes;c_NA;o_NA | 1.4% | 1.4% | 1.4% | 1.4% | 1.4% |
| k_Bacteria;p_Cyanobacteria;c_Melainabacteria;o_Obscuribacteriales | 0.0% | 0.0% | 0.0% | 0.0% | 0.0% |
| k_Bacteria;p_Deinococcus-Thermus;c_Deinococci;o_NA | 0.0% | 0.0% | 0.0% | 0.0% | 0.0% |
| k_Bacteria;p_Elusimicrobia;c_Elusimicrobia;o_NA | 0.0% | 0.0% | 0.0% | 0.0% | 0.0% |
| k_Bacteria;p_Fibrobacteres;c_Fibrobacteria;o_Fibrobacteriales | 1.2% | 1.1% | 1.2% | 1.2% | 1.2% |
| k_Bacteria;p_Firmicutes;c_Bacilli;o_Bacillales | 0.0% | 0.0% | 0.0% | 0.0% | 0.0% |
| k_Bacteria;p_Firmicutes;c_Bacilli;o_Lactobacillales | 1.8% | 1.6% | 1.7% | 1.7% | 1.6% |
| k_Bacteria;p_Firmicutes;c_Clostridia;o_Clostridiales | 11.1% | 10.7% | 11.1% | 11.1% | 11.7% |
| k_Bacteria;p_Firmicutes;c_Clostridia;o_NA | 0.9% | 0.9% | 0.8% | 0.8% | 0.9% |
| k_Bacteria;p_Firmicutes;c_Clostridia;o_Thermoanaerobacteriales | 1.5% | 1.4% | 1.4% | 1.4% | 1.5% |
| k_Bacteria;p_Firmicutes;c_Erysipelotrichia;o_Erysipelotrichales | 0.1% | 0.1% | 0.1% | 0.1% | 0.1% |
| k_Bacteria;p_Firmicutes;c_NA;o_NA | 0.0% | 0.0% | 0.0% | 0.0% | 0.0% |
| k_Bacteria;p_Firmicutes;c_Negativicutes;o_Selenomonadales | 0.2% | 0.2% | 0.2% | 0.2% | 0.3% |
| k_Bacteria;p_Gemmatimonadetes;c_Gemmatimonadetes;o_Gemmatimonadales | 0.0% | 0.0% | 0.0% | 0.0% | 0.0% |
| k_Bacteria;p_Hydrogenedentes;c_NA;o_NA | 1.1% | 1.1% | 1.4% | 1.4% | 1.3% |
| k_Bacteria;p_Lentisphaerae;c_NA;o_NA | 0.6% | 0.5% | 0.6% | 0.5% | 0.5% |
| k_Bacteria;p_Lentisphaerae;c_Oligosphaeria;o_Oligosphaerales | 0.0% | 0.0% | 0.0% | 0.0% | 0.0% |
| k_Bacteria;p_Microgenomates;c_NA;o_NA | 1.5% | 1.5% | 1.5% | 1.5% | 1.5% |
| k_Bacteria;p_NA;c_NA;o_NA | 3.7% | 3.7% | 3.6% | 3.6% | 3.5% |
| k_Bacteria;p_Nitrospirae;c_Nitrospira;o_Nitrospirales | 0.5% | 0.4% | 0.4% | 0.4% | 0.4% |
| k_Bacteria;p_Omnitrophica;c_NA;o_NA | 0.1% | 0.1% | 0.1% | 0.1% | 0.1% |
| k_Bacteria;p_Parcubacteria;c_NA;o_NA | 0.3% | 0.3% | 0.3% | 0.3% | 0.2% |
| k_Bacteria;p_Plancntomyces;c_Phycisphaerae;o_NA | 0.2% | 0.2% | 0.2% | 0.2% | 0.2% |
| k_Bacteria;p_Plancntomyces;c_Phycisphaerae;o_Phycisphaerales | 0.0% | 0.0% | 0.0% | 0.0% | 0.0% |
| k_Bacteria;p_Plancntomyces;c_Plancntomycetacia;o_Plancntomycetales | 0.0% | 0.1% | 0.0% | 0.0% | 0.0% |
| k_Bacteria;p_Proteobacteria;c_Alphaproteobacteria;o_Caulobacteriales | 0.0% | 0.1% | 0.0% | 0.0% | 0.0% |
| k_Bacteria;p_Proteobacteria;c_Alphaproteobacteria;o_NA | 0.0% | 0.0% | 0.0% | 0.0% | 0.0% |
| k_Bacteria;p_Proteobacteria;c_Alphaproteobacteria;o_Parvularculales | 0.0% | 0.0% | 0.0% | 0.0% | 0.0% |
| k_Bacteria;p_Proteobacteria;c_Alphaproteobacteria;o_Rhizobiales | 0.2% | 0.2% | 0.2% | 0.2% | 0.2% |
| k_Bacteria;p_Proteobacteria;c_Alphaproteobacteria;o_Rhodobacteriales | 0.0% | 0.0% | 0.0% | 0.0% | 0.0% |
| k_Bacteria;p_Proteobacteria;c_Alphaproteobacteria;o_Rhodospirillales | 0.3% | 0.3% | 0.3% | 0.3% | 0.3% |
| k_Bacteria;p_Proteobacteria;c_Alphaproteobacteria;o_Rickettsiales | 0.0% | 0.0% | 0.0% | 0.0% | 0.0% |
| k_Bacteria;p_Proteobacteria;c_Alphaproteobacteria;o_Sphingomonadales | 0.0% | 0.0% | 0.0% | 0.0% | 0.0% |
| k_Bacteria;p_Proteobacteria;c_Betaproteobacteria;o_Burkholderiales | 0.3% | 0.2% | 0.3% | 0.3% | 0.3% |
| k_Bacteria;p_Proteobacteria;c_Betaproteobacteria;o_Methylophilales | 0.0% | 0.0% | 0.0% | 0.0% | 0.0% |
| k_Bacteria;p_Proteobacteria;c_Betaproteobacteria;o_NA | 0.0% | 0.0% | 0.0% | 0.0% | 0.0% |
| k_Bacteria;p_Proteobacteria;c_Betaproteobacteria;o_Neisseriales | 0.0% | 0.0% | 0.0% | 0.0% | 0.0% |
| k_Bacteria;p_Proteobacteria;c_Betaproteobacteria;o_Nitrosomonadales | 0.0% | 0.0% | 0.0% | 0.0% | 0.0% |
| k_Bacteria;p_Proteobacteria;c_Betaproteobacteria;o_Rhodocyclales | 0.0% | 0.0% | 0.0% | 0.0% | 0.0% |
| k_Bacteria;p_Proteobacteria;c_Deltaproteobacteria;o_Bdellovibrionales | 2.0% | 1.9% | 2.0% | 2.0% | 2.0% |

| | | | | |
|--|------|------|------|------|
| k_Bacteria;p_Proteobacteria;c_Betaproteobacteria;o_Burkholderiales | 0.0% | 0.0% | 0.0% | 0.0% |
| k_Bacteria;p_Proteobacteria;c_Betaproteobacteria;o_Methylophilales | 0.0% | 0.0% | 0.0% | 0.0% |
| k_Bacteria;p_Proteobacteria;c_Betaproteobacteria;o_NA | 0.3% | 0.2% | 0.3% | 0.3% |
| k_Bacteria;p_Proteobacteria;c_Betaproteobacteria;o_Neisseriales | 0.0% | 0.0% | 0.0% | 0.0% |
| k_Bacteria;p_Proteobacteria;c_Betaproteobacteria;o_Nitrosomonadales | 0.0% | 0.0% | 0.0% | 0.0% |
| k_Bacteria;p_Proteobacteria;c_Betaproteobacteria;o_Rhodocyclales | 0.0% | 0.0% | 0.0% | 0.0% |
| k_Bacteria;p_Proteobacteria;c_Deltaproteobacteria;o_Bdellovibrionales | 0.0% | 0.0% | 0.0% | 0.0% |
| k_Bacteria;p_Proteobacteria;c_Deltaproteobacteria;o_Desulfuovibrionales | 2.0% | 1.9% | 2.0% | 2.0% |
| k_Bacteria;p_Proteobacteria;c_Deltaproteobacteria;o_Desulfuromonadales | 0.0% | 0.0% | 0.0% | 0.0% |
| k_Bacteria;p_Proteobacteria;c_Deltaproteobacteria;o_Myxococcales | 0.7% | 0.7% | 0.8% | 0.8% |
| k_Bacteria;p_Proteobacteria;c_Deltaproteobacteria;o_NA | 0.3% | 0.3% | 0.3% | 0.3% |
| k_Bacteria;p_Proteobacteria;c_Deltaproteobacteria;o_Oligoflexales | 0.0% | 0.0% | 0.0% | 0.0% |
| k_Bacteria;p_Proteobacteria;c_Deltaproteobacteria;o_Syntrophobacteriales | 2.6% | 2.5% | 2.6% | 2.5% |
| k_Bacteria;p_Proteobacteria;c_Epsilonproteobacteria;o_Campylobacteriales | 0.0% | 0.0% | 0.0% | 0.0% |
| k_Bacteria;p_Proteobacteria;c_Gammaproteobacteria;o_Cellvibrionales | 0.0% | 0.0% | 0.0% | 0.0% |
| k_Bacteria;p_Proteobacteria;c_Gammaproteobacteria;o_Chromatiales | 0.0% | 0.0% | 0.0% | 0.0% |
| k_Bacteria;p_Proteobacteria;c_Gammaproteobacteria;o_Oceanospirillales | 0.0% | 0.0% | 0.0% | 0.0% |
| k_Bacteria;p_Proteobacteria;c_Gammaproteobacteria;o_Pseudomonadales | 0.1% | 0.0% | 0.1% | 0.0% |
| k_Bacteria;p_Saccharibacteria;c_NA;o_NA | 0.1% | 0.1% | 0.1% | 0.1% |
| k_Bacteria;p_Spirochaetae;c_Spirochaetes;o_Spirochaetales | 0.0% | 0.0% | 0.0% | 0.0% |
| k_Bacteria;p_Synergistetes;c_Synergistia;o_Synergistales | 9.1% | 9.2% | 9.1% | 9.0% |
| k_Bacteria;p_Tenericutes;c_Mollicutes;o_Acholeplasmatales | 3.3% | 3.5% | 3.7% | 3.6% |
| k_Bacteria;p_Tenericutes;c_Mollicutes;o_NA | 0.0% | 0.0% | 0.0% | 0.0% |
| k_Bacteria;p_Thermotogae;c_Thermotogae;o_Kosmotogales | 0.0% | 0.0% | 0.0% | 0.0% |
| k_Bacteria;p_Thermotogae;c_Thermotogae;o_Thermotogales | 0.0% | 0.0% | 0.0% | 0.0% |
| k_Bacteria;p_Verrucomicrobia;c_NA;o_NA | 1.3% | 1.4% | 1.3% | 1.3% |
| k_Bacteria;p_Verrucomicrobia;c_Opitutae;o_Opitutales | 0.1% | 0.1% | 0.1% | 0.1% |
| k_Bacteria;p_Verrucomicrobia;c_Opitutae;o_Punicicoccales | 0.0% | 0.0% | 0.0% | 0.0% |
| k_Bacteria;p_Verrucomicrobia;c_Verrucomicrobiae;o_Verrucomicrobiales | 0.1% | 0.1% | 0.1% | 0.1% |

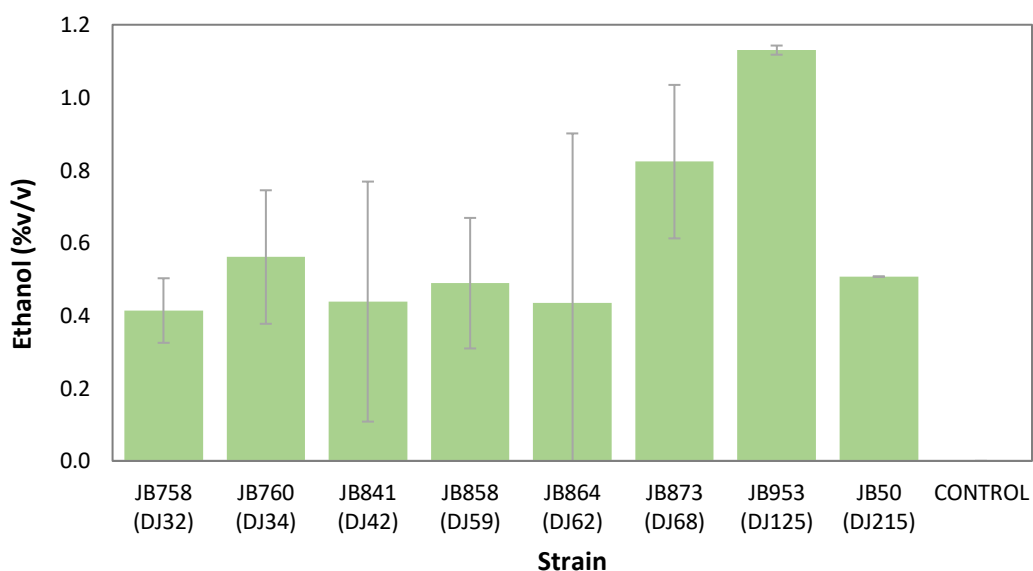
Appendix V: Screening of *Schizosaccharomyces pombe* strains

Schizosaccharomyces pombe strains were grown overnight in YES medium at 32°C with shaking at 200 rpm. Cells were washed and resuspended in water to give a final OD₆₀₀ of 0.4. 5 µl of this suspension was transferred to a well in an optical plate well containing 195 µl of MSW fibre hydrolysate supplemented with 1% vitamin-enriched yeast extract and 40 mM MOPS buffer. Plates were wrapped in Parafilm and then incubated with shaking at 200 rpm for 24 hours.

Negative control (-) : MSW fibre hydrolysate supplemented with 1% vitamin-enriched yeast extract and MOPS buffer. 5µl water instead of cells.

After 24 hours 10 ul of broth was collected and analysed for ethanol content by GC-MS as described in **Chapter 4 (4.2.6.2)**. Strain JB953 produced the highest ethanol titre and was selected as the strain for this project.

Table AV-1: Ethanol production by eight *Shizosaccharomyces pombe* strains grown on MSW fibre hydrolysate over 24 hours



Appendix VI: Sugar fermentation data for each species

Table AVI-1: Sugars fermented by each microorganism grown on OMSW fibre hydrolysate supplemented with 1% vitamin-enriched yeast extract. For methods see Chapter 4, 4.2.6.4. This data was used to calculate the yield parameters reported in Chapter 4, Table 4.10.

| Species | Total sugar consumed (g/L) | Total sugar consumed \pm SD | Total glucose consumed (%) | Total glucose consumed \pm SD | Total xylose consumed (%) | Total xylose consumed \pm SD | Total available sugars consumed (%) | Total available sugars consumed \pm SD |
|--------------------------------------|----------------------------|-------------------------------|----------------------------|---------------------------------|---------------------------|--------------------------------|-------------------------------------|--|
| <i>R. wratislaviensis</i> | 66.76 | 1.61 | 99.46 | 2.95 | 100.00 | 2.48 | 99.57 | 2.41 |
| <i>P. putida</i> | 43.70 | 3.93 | 73.08 | 7.19 | 26.33 | 17.36 | 63.42 | 5.70 |
| <i>S. cerevisiae</i> | 50.24 | 1.20 | 99.30 | 2.37 | -3.71 | 10.60 | 99.30 | 2.37 |
| <i>G. thermoglucosidarius</i> | 18.32 | 2.99 | 20.26 | 5.06 | 47.45 | 6.86 | 25.99 | 4.24 |
| <i>C. saccharoperbutylacetonicum</i> | 3.01 | 3.71 | 5.61 | 6.93 | 0.92 | 7.31 | 4.45 | 5.49 |
| <i>Z. mobilis</i> | 49.48 | 2.89 | 98.36 | 5.74 | 32.02 | 9.95 | 98.36 | 5.74 |
| <i>S. pombe</i> | 56.72 | 3.45 | 99.76 | 6.07 | 73.95 | 9.50 | 99.76 | 6.07 |
| <i>E. coli</i> | 62.63 | 4.33 | 99.12 | 6.22 | 61.64 | 18.43 | 91.02 | 6.30 |

Appendix VII: Fatty acid profile of *Rhodococcus opacus* MITXM-61 grown in 40 ml OMSW fibre hydrolysate supplemented with 1% vitamin-enriched yeast extract

Table AVII-1: Fatty acid percentages are shown by dry weight (%CDW). \pm SD = Standard deviation of triplicate measurements. Samples analysed by GC-MS as described in Chapter 4, 4.2.6.6. Note C:21 was used as an internal standard. For details see Chapter 4, 4.2.4.3.

| | C10:0 | | C11:0 | | C12:0 | | C13:0 | | C14:0 | |
|------|---------|----------|---------|----------|---------|----------|---------|----------|---------|----------|
| Time | mg/mg | \pm SD | mg/mg | \pm SD | mg/mg | \pm SD | mg/mg | \pm SD | mg/mg | \pm SD |
| 0 | 0.0000 | 0.0000 | 0.0000 | 0.0000 | 0.0000 | 0.0000 | 0.0000 | 0.0000 | 0.0000 | 0.0000 |
| 12 | 0.0000 | 0.0000 | 0.0000 | 0.0000 | 0.0000 | 0.0000 | 0.0000 | 0.0000 | 0.0000 | 0.0000 |
| 24 | 0.0000 | 0.0000 | 0.0000 | 0.0000 | 0.0000 | 0.0000 | 0.0000 | 0.0000 | 0.0000 | 0.0000 |
| 48 | 0.0000 | 0.0000 | 0.0000 | 0.0000 | 0.0553 | 0.0537 | 0.1406 | 0.1148 | 1.5268 | 1.1185 |
| 72 | 0.0000 | 0.0000 | 0.0000 | 0.0000 | 0.1239 | 0.1854 | 0.0712 | 0.0267 | 0.6346 | 0.2291 |
| 96 | 0.0000 | 0.0000 | 0.0000 | 0.0000 | 0.0156 | 0.0271 | 0.1095 | 0.0306 | 0.9582 | 0.2228 |
| 120 | 0.0000 | 0.0000 | 0.0000 | 0.0000 | 0.0264 | 0.0236 | 0.0909 | 0.0113 | 0.8172 | 0.0808 |
| 144 | 0.0000 | 0.0000 | 0.0000 | 0.0000 | 0.0421 | 0.0308 | 0.1137 | 0.0129 | 1.0084 | 0.1498 |
| | C14:1 | | C15:0 | | C15:1 | | C16:0 | | C16:1 | |
| Time | mg/mg | \pm SD | mg/mg | \pm SD | mg/mg | \pm SD | mg/mg | \pm SD | mg/mg | \pm SD |
| 0 | 0.0000 | 0.0000 | 0.0000 | 0.0000 | 0.0000 | 0.0000 | -0.5953 | 0.2960 | 0.0000 | 0.0000 |
| 12 | 0.0000 | 0.0000 | 0.0000 | 0.0000 | 0.0000 | 0.0000 | 0.7578 | 0.1741 | 0.0000 | 0.0000 |
| 24 | 0.0000 | 0.0000 | -0.0506 | 0.0876 | 0.0000 | 0.0000 | -0.4624 | 0.2295 | -0.0835 | 0.1446 |
| 48 | 0.0835 | 0.1147 | 2.7138 | 1.7041 | 0.3998 | 0.3050 | 12.5696 | 5.7802 | 5.5867 | 3.6005 |
| 72 | 0.0354 | 0.0363 | 1.4581 | 0.5824 | 0.1948 | 0.0518 | 6.4728 | 2.7202 | 2.4316 | 1.0668 |
| 96 | 0.0857 | 0.0178 | 2.9188 | 0.7256 | 0.3815 | 0.0945 | 10.8334 | 2.4540 | 4.1823 | 0.9744 |
| 120 | 0.0778 | 0.0238 | 2.3915 | 0.2318 | 0.3348 | 0.0488 | 9.3328 | 0.8606 | 3.5431 | 0.3776 |
| 144 | 0.1075 | 0.0144 | 2.8352 | 0.4694 | 0.4121 | 0.0764 | 11.0421 | 1.5939 | 4.2563 | 0.6324 |
| | C17:0 | | C17:1 | | C18:0 | | C18:1 | | C18:2 | |
| Time | mg/mg | \pm SD | mg/mg | \pm SD | mg/mg | \pm SD | mg/mg | \pm SD | mg/mg | \pm SD |
| 0 | 0.0000 | 0.0000 | 0.0000 | 0.0000 | 0.0000 | 0.0000 | 0.0000 | 0.0000 | 0.0000 | 0.0000 |
| 12 | 0.0000 | 0.0000 | 0.0000 | 0.0000 | 0.0000 | 0.0000 | 0.2423 | 0.4196 | 0.0000 | 0.0000 |
| 24 | -0.1290 | 0.1336 | -0.1942 | 0.1795 | -0.1057 | 0.0923 | -0.3936 | 0.2847 | 0.0000 | 0.0000 |
| 48 | 3.3730 | 1.2254 | 3.7856 | 1.8083 | 1.7739 | 0.4948 | 6.7310 | 2.4881 | 0.0080 | 0.0092 |
| 72 | 2.5798 | 1.0960 | 1.8915 | 1.1609 | 1.4522 | 0.5750 | 3.5225 | 1.6631 | 0.0035 | 0.0061 |
| 96 | 4.6734 | 0.9404 | 5.8771 | 1.4805 | 1.7125 | 0.2841 | 6.7788 | 1.2236 | 0.0000 | 0.0000 |
| 120 | 3.8125 | 0.1817 | 5.1326 | 0.5151 | 1.4462 | 0.0469 | 6.1025 | 0.5956 | 0.0000 | 0.0000 |
| 144 | 4.4275 | 0.6672 | 6.1853 | 1.0521 | 1.6430 | 0.2666 | 7.3095 | 0.8141 | 0.0035 | 0.0071 |
| | C18:3n6 | | C18:3n3 | | C20:0 | | C20:1 | | C20:2 | |
| Time | mg/mg | \pm SD | mg/mg | \pm SD | mg/mg | \pm SD | mg/mg | \pm SD | mg/mg | \pm SD |
| 0 | 0.0000 | 0.0000 | 0.0000 | 0.0000 | 0.0000 | 0.0000 | 0.0000 | 0.0000 | 0.0000 | 0.0000 |
| 12 | 0.0000 | 0.0000 | 0.0000 | 0.0000 | 0.0000 | 0.0000 | 0.0000 | 0.0000 | 0.0000 | 0.0000 |
| 24 | 0.0000 | 0.0000 | -0.0340 | 0.0589 | 0.0000 | 0.0000 | -0.0196 | 0.0339 | 0.0000 | 0.0000 |
| 48 | 0.2935 | 0.0486 | 0.3340 | 0.1620 | 0.3913 | 0.1488 | 0.0515 | 0.0506 | 0.0495 | 0.0714 |
| 72 | 0.2940 | 0.0946 | 0.2259 | 0.1058 | 0.3437 | 0.1666 | 0.0753 | 0.0664 | 0.0090 | 0.0155 |
| 96 | 0.2940 | 0.0484 | 0.5985 | 0.1967 | 0.1738 | 0.0613 | 0.1813 | 0.0946 | 0.0392 | 0.0679 |
| 120 | 0.2260 | 0.0470 | 0.5373 | 0.1311 | 0.1300 | 0.0107 | 0.1533 | 0.0589 | 0.0068 | 0.0118 |
| 144 | 0.2579 | 0.0436 | 0.5787 | 0.0963 | 0.1609 | 0.0552 | 0.1848 | 0.0515 | 0.0225 | 0.0261 |

| | C21:0 | | C20:4 | | C20:5 | | C20:3 | | C22:0 | |
|-------------|--------------|------------|--------------|------------|--------------|------------|--------------|------------|--------------|------------|
| Time | mg/mg | ±SD | mg/mg | ±SD | mg/mg | ±SD | mg/mg | ±SD | mg/mg | ±SD |
| 0 | -71.8279 | 21.1205 | 0.0000 | 0.0000 | 0.0000 | 0.0000 | 0.0000 | 0.0000 | 0.0000 | 0.0000 |
| 12 | 163.0790 | 17.5048 | 0.0000 | 0.0000 | 0.0000 | 0.0000 | 0.0000 | 0.0000 | 0.0000 | 0.0000 |
| 24 | -44.0357 | 4.9847 | 0.0000 | 0.0000 | 0.0000 | 0.0000 | -0.5388 | 0.9333 | -0.2535 | 0.4391 |
| 48 | 6.6620 | 0.6528 | 0.0168 | 0.0290 | 0.0112 | 0.0194 | 0.0038 | 0.0065 | 0.2917 | 0.1160 |
| 72 | 3.4187 | 0.3890 | 0.0000 | 0.0000 | 0.0105 | 0.0182 | 0.1182 | 0.2047 | 0.1684 | 0.1545 |
| 96 | 5.3591 | 0.1950 | 0.0790 | 0.1369 | 0.0000 | 0.0000 | 0.0000 | 0.0000 | 0.1458 | 0.0349 |
| 120 | 5.2295 | 0.0951 | 0.0854 | 0.1479 | 0.0000 | 0.0000 | 0.0393 | 0.0681 | 0.1020 | 0.1054 |
| 144 | 5.4938 | 0.5262 | 0.0000 | 0.0000 | 0.0161 | 0.0321 | 0.0000 | 0.0000 | 0.1091 | 0.0851 |
| | C22:1 | | C22:2 | | C22:6 | | C23:0 | | C24:0 | |
| Time | mg/mg | ±SD | mg/mg | ±SD | mg/mg | ±SD | mg/mg | ±SD | mg/mg | ±SD |
| 0 | 0.0000 | 0.0000 | 0.0000 | 0.0000 | 0.0000 | 0.0000 | 0.0000 | 0.0000 | 0.0000 | 0.0000 |
| 12 | 0.0000 | 0.0000 | 0.0000 | 0.0000 | 0.0000 | 0.0000 | 0.0000 | 0.0000 | 0.0000 | 0.0000 |
| 24 | -0.4477 | 0.7755 | -0.9977 | 1.7281 | 0.0000 | 0.0000 | -0.3177 | 0.5503 | -0.1384 | 0.2398 |
| 48 | 0.0133 | 0.0230 | 0.0113 | 0.0196 | 0.1225 | 0.1101 | 0.0615 | 0.1065 | 0.0048 | 0.0083 |
| 72 | 0.0000 | 0.0000 | 0.0356 | 0.0617 | 0.2248 | 0.1357 | 0.0804 | 0.0705 | 0.0000 | 0.0000 |
| 96 | 0.0000 | 0.0000 | 0.0565 | 0.0625 | 0.1285 | 0.0372 | 0.0599 | 0.1038 | 0.0000 | 0.0000 |
| 120 | 0.0000 | 0.0000 | 0.0475 | 0.0823 | 0.1016 | 0.1196 | 0.0524 | 0.0908 | 0.0000 | 0.0000 |
| 144 | 0.0313 | 0.0625 | 0.0361 | 0.0431 | 0.0768 | 0.0611 | 0.0000 | 0.0000 | 0.0000 | 0.0000 |

Appendix VIII: Cloning of ACP-BTE into pTip-QC1

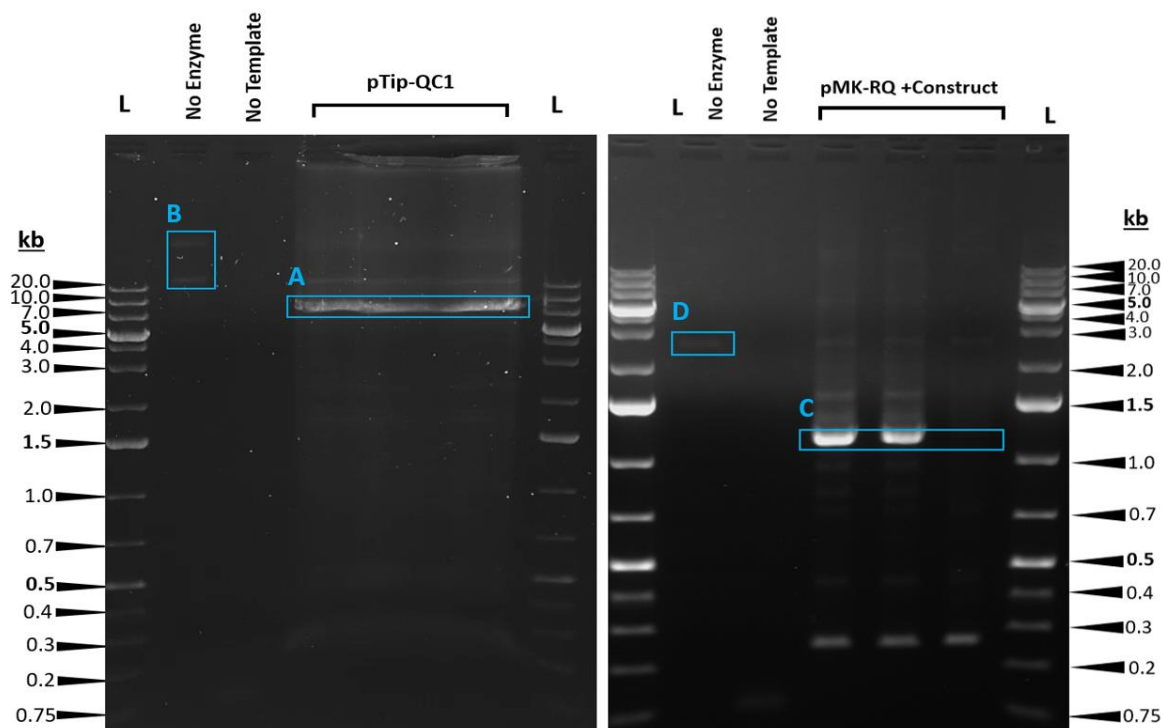


Figure AVIII-1: PCR linearization of *pTip-QC1* and *ACP-BTE*

PCR was carried out as described in **Chapter 4, 4.2.7.2.**

A: Linearised vector *pTip-QC1*. Expected size = 8,384 bp;

B: Negative control – *pTip-QC1* without addition of Phusion polymerase;

C: Linearised construct *ACP-BTE*, isolated by PCR from *pMK-RQ*. Expected size = 1,191 bp;

D: Negative control – *pMK-RQ* without addition of Phusion polymerase;

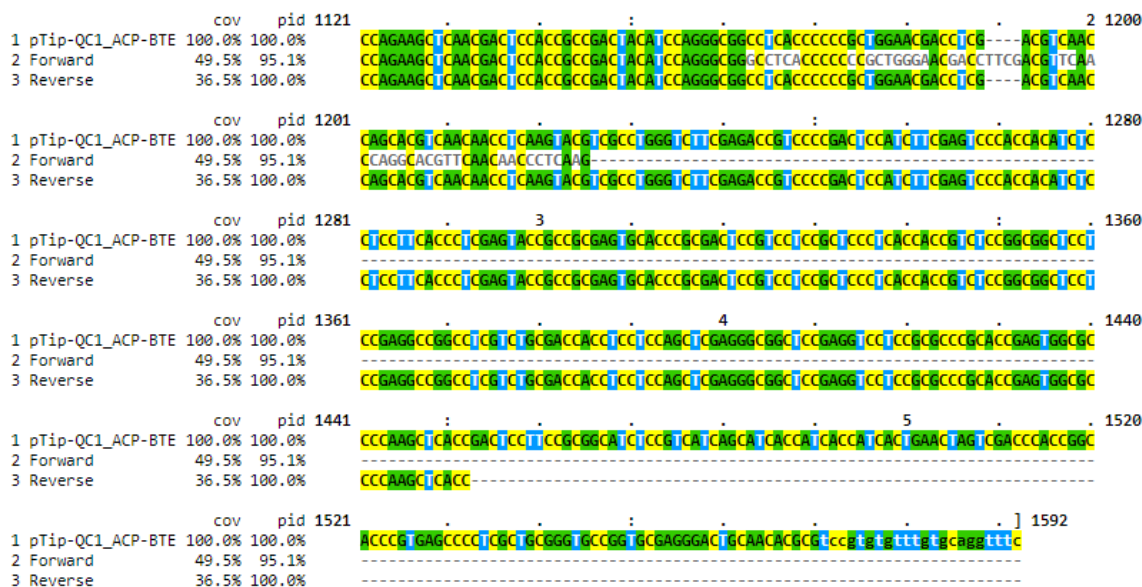
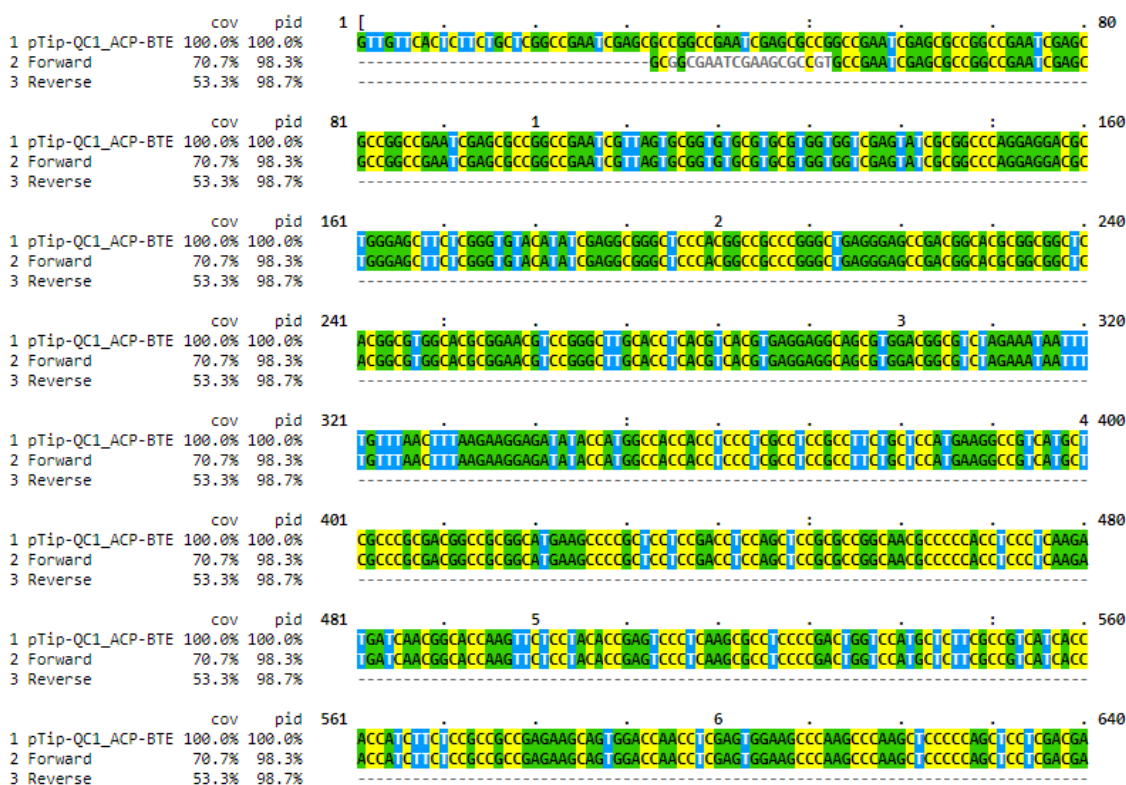


Figure AVIII-3: Sequence alignment of the MCS region of pTip-QC1_ACP-BTE purified from *R. opacus*^{pTip-QC1_ACP-BTE}

Sequencing was carried out as described in Chapter 4, 4.2.7.2. Sequence alignment against the expected vector backbone was carried out using Clustal Omega Multiple Sequence Alignment.

Row 1: Expected sequence (sequence starts 3,753 bp upstream and ends 4,246 bp downstream of insert ACP-BTE).

Row 2: Sequencing results, forward primer.



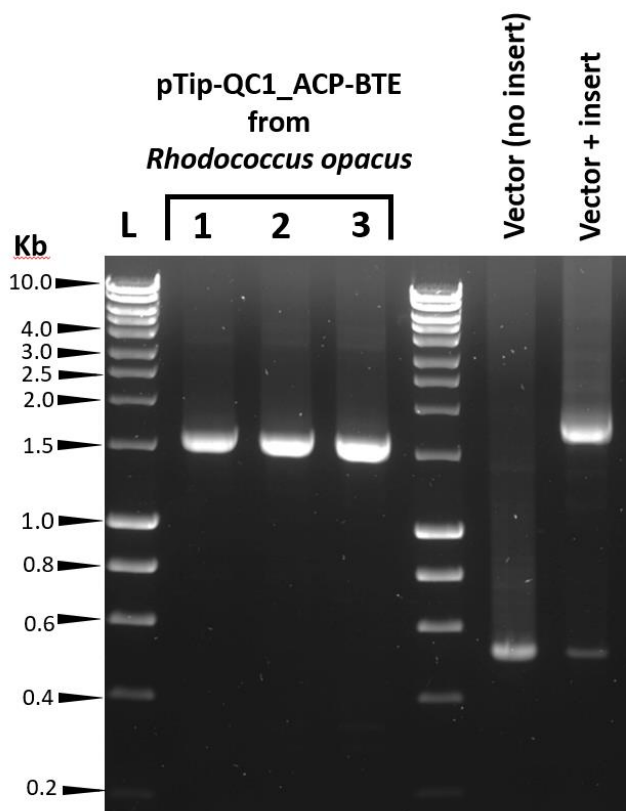
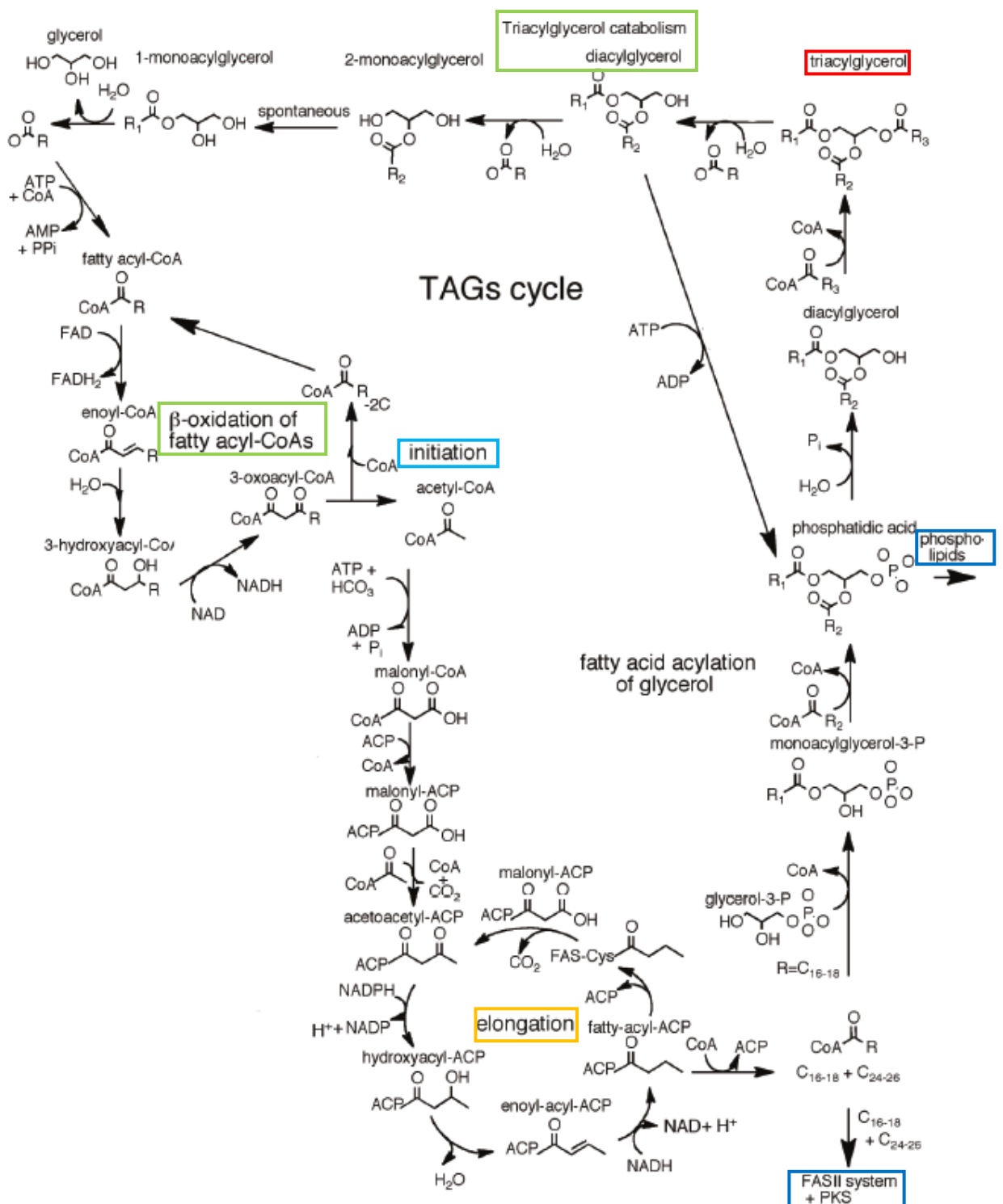


Figure AVIII-4: PCR amplification of the MCS of pTip-QC1_ACP-BTE purified from of *R. opacus*^{pTip-QC1_ACP-BTE}

*Bands in lanes 1, 2 and 3 are PCR products amplified from plasmids purified from *R. opacus*^{pTip-QC1_ACP-BTE}. Expected size for plasmids with insert = 1,587 bp; Expected size for empty vector = 529 bp; As controls plasmids pTip-QC1_ACP-BTE and pTip-QC1 originally purified from *E. coli* were run in parallel.*

Appendix IX: Biochemical steps in the TAG biosynthesis pathway of oleaginous *Rhodococcus* species

The biosynthesis of triacylglycerol (TAG) is shown below (adapted from Holder et al, 2011). Synthesis starts with the precursor acetyl-CoA (**initiation**) which is condensed with malonyl-CoA and propionyl-CoA by dedicated fatty acid (FA) synthases that produce fatty acids of varying carbon chain lengths (**elongation**). To produce a molecule of **triacylglycerol** (TAG), diacylglycerol is condensed with three FA chains. When the cell enters a state of starvation, TAG is broken down via the **β -oxidation pathway**, in which the TAG molecule is split into its constituent FAs and a glycerol. Some FAs are elongated further and transferred to the fatty acid synthase II (FAS II) system and polyketide synthesis (PKS). Alternately, they can be phosphorylated to produce **phospholipids** that make up the cell membrane.



Index of Abbreviations

| | |
|----------------|--|
| ACP | Acyl Carrier Protein |
| ACP-BTE | Acyl-acyl Carrier Protein Thioesterase BTE |
| AD | Anaerobic Digestion |
| BMP | Biomethane Potential |
| C/N | Carbon to Nitrogen ratio |
| C:D | Lipid number (Carbon atoms to Double bonds) |
| CCR | Carbon Catabolite Repression |
| CDW | Cell Dry Weight |
| CN | Cetane Number |
| CoA | Coenzyme A |
| COD | Chemical Oxygen Demand |
| CSL | Corn Steep Liquor |
| DGAT | Diacylglycerol Acyltransferase |
| ED | Entner-Doudoroff pathway |
| EDTA | Ethylenediaminetetraacetic acid |
| FA | Fatty Acid |
| FAMES | Fatty acid methyl esters |
| FPU | Filter Paper Units |
| GC-FID | Gas Chromatography with Flame Ionisation Detection |
| Glu | D-glucose |
| h | Hours |
| HPAEC | High-Performance Anion Exchange Chromatography |
| ICP-MS | Ionisation-coupled Plasma Mass Spectrometry |
| IPTG | Isopropyl- β -D-thiogalactoside |
| JCat | Java Codon Adaptation Tool |

| | |
|-------------------------|---|
| L-Arg | L-Arginine |
| LB | Luria-Bertani Medium |
| LCFAs | Long-Chain Fatty Acids |
| M.I.C. | Minimum Inhibitory Concentration |
| MBTH | 3-methyl-2-benzothiazolinonehydrazone |
| MCFAs | Medium-Chain Fatty Acids |
| MCS | Multiple Cloning Site |
| Min. | Minutes |
| MOPS | 3-(N-morpholino)propanesulfonic acid |
| MSW | Municipal Solid Waste |
| OD₆₀₀ | Optical Density at 600 nm |
| OMSW | Organic fraction of Municipal Solid Waste |
| PAN | Primary Amino Nitrogen |
| PCR | Polymerase Chain Reaction |
| RCM | Reinforced Clostridial Medium |
| RM | Rich Medium |
| RT | Room Temperature |
| SCFAs | Short-Chain Fatty Acids |
| SHF | Separate Hydrolysis and Fermentation |
| SSF | Simultaneous Saccharification and Fermentation |
| TAG | Triacylglycerol |
| TS | Total Solids |
| TSB | Tryptic Soy Broth |
| UPLC-MS | Ultra-Performance Liquid Chromatography (UPLC) with Mass Spectrometry (MS). |
| VYE | Vitamin-enriched Yeast Extract |
| x g | Times gravity, equivalent to Relative Centrifugal Force (RCF) |

| | |
|--------------|--|
| Xyl | D-xylose |
| YAN | Yeast Available Nitrogen |
| YES | Yeast Extract with Supplements |
| YPD | Yeast Peptone Dextrose medium |
| 5-HMF | 5-Hydroxymethylfurfural |
| % v/v | Percentage Volume by Volume |
| % w/v | Percentage Weight by Volume |
| ±SD | Standard Deviation (positive or negative relative to the mean) |

References

- Abas, N., Kalair, A. & Khan, N. (2015) Review of fossil fuels and future energy technologies. *Futures*, 69, 31-49.
- Abdel-Rahman, M. A., Tashiro, Y. & Sonomoto, K. (2013) Recent advances in lactic acid production by microbial fermentation processes. *Biotechnol Adv*, 31.
- Abdhulla, J. J. (2016) *Viability of Autoclaved Municipal Solid Waste as a source for Biofuels and other products*. Doctor of Philosophy University of Nottingham.
- Abdullah, J. & Greetham, D. (2016) Optimizing Cellulase Production from Municipal Solid Waste (MSW) using Solid State Fermentation (SSF). *Journal of Fundamentals of Renewable Energy and Applications*, 06.
- Abrahms, B., DiPietro, D., Graffis, A. & Hollander, A. (2017) Managing biodiversity under climate change: challenges, frameworks, and tools for adaptation. *Biodiversity and Conservation*, 26(10), 2277-2293.
- Adeboye, P. T., Bettiga, M. & Olsson, L. (2014) The chemical nature of phenolic compounds determines their toxicity and induces distinct physiological responses in *Saccharomyces cerevisiae* in lignocellulose hydrolysates. *AMB Express*, 4(46).
- Adhikari, B. K., Trémier, A., Barrington, S., Martinez, J. J. W. & Valorization, B. (2013) Biodegradability of Municipal Organic Waste: A Respirometric Test, 4(2), 331-340.
- Adhikari, S., Nam, H. & Chakraborty, J. P. (2018) Chapter 8 - Conversion of Solid Wastes to Fuels and Chemicals Through Pyrolysis, in Bhaskar, T., Pandey, A., Mohan, S. V., Lee, D.-J. & Khanal, S. K. (eds), *Waste Biorefinery* Elsevier, 239-263.
- Adney, B. & Baker, J. (2008) *Measurement of Cellulase Activities*.
- Agrawal, M., Mao, Z. & Chen, R. R. (2010) Adaptation yields a highly efficient xylose-fermenting *Zymomonas mobilis* strain. *Biotechnology and Bioengineering*, 108(4), 777-785.
- Aidelberg, G., Towbin, B. D., Rothschild, D., Dekel, E., Bren, A. & Alon, U. (2014) Hierarchy of non-glucose sugars in *Escherichia coli*. *Bmc Systems Biology*, 8.
- Aiello-Mazzarri, C., Agbogbo, F. K. & Holtzapple, M. T. (2006) Conversion of municipal solid waste to carboxylic acids using a mixed culture of mesophilic microorganisms. *Bioresource Technology*, 97(1), 47-56.
- Aleklett, K. & Campbell, C. J. (2003) The Peak and Decline of World Oil and Gas Production. *Minerals & Energy - Raw Materials Report*, 18(1), 5-20.
- Almeida, J. R., Röder, A., Modig, T., Laadan, B., Lidén, G. & Gorwa-Grauslund, M. F. (2008) NADH- vs NADPH-coupled reduction of 5-hydroxymethyl furfural (HMF) and its implications on product distribution in *Saccharomyces cerevisiae*. *Appl Microbiol Biotechnol*, 78.

- Almeida, J. R. M., Bertilsson, M., Gorwa-Grauslund, M. F., Gorsich, S. & Liden, G. (2009) Metabolic effects of furaldehydes and impacts on biotechnological processes. *Applied Microbiology and Biotechnology*, 82(4), 625-638.
- Althuri, A. & Venkata, M. S. (2019) Single pot bioprocessing for ethanol production from biogenic municipal solid waste. *Bioresource Technology*, 283, 159-167.
- Alvarez, H., Silva, R., O. Herrero, M., Hernández, M. & S. Villalba, M. (2013) *Metabolism of triacylglycerols in Rhodococcus species: insights from physiology and molecular genetics*, *J Mol. Biochem.*
- Alvarez, H. & Steinbüchel, A. (2002) Triacylglycerols in prokaryotic microorganisms. *Applied Microbiology and Biotechnology*, 60(4), 367-376.
- Alvarez, H. M., Herrero, O. M., Silva, R. A., Hernández, M. A., Lanfranconi, M. P. & Villalba, M. S. (2019) Insights into the Metabolism of Oleaginous *Rhodococcus* spp. *Applied and Environmental Microbiology*, 85(18), e00498-19.
- Alvarez, H. M., Mayer, F., Fabritius, D. & Steinbüchel, A. (1996) Formation of intracytoplasmic lipid inclusions by *Rhodococcus opacus* strain PD630. *Archives of Microbiology*, 165(6), 377-386.
- Alvira, P., Tomas-Pejo, E., Ballesteros, M. & Negro, M. J. (2010) Pretreatment technologies for an efficient bioethanol production process based on enzymatic hydrolysis: A review. *Bioresource Technology*, 101(13), 4851-4861.
- Amara, S., Seghezzi, N., Otani, H., Diaz-Salazar, C., Liu, J. & Eltis, L. D. (2016) Characterization of key triacylglycerol biosynthesis processes in rhodococci. *Scientific Reports*, 6, 24985.
- Amlinger, F., Pollak, M. & Favoino, E. (2004) *Heavy Metals and Organic Compounds from Wastes Used as Organic Fertilizers*.
- Andlar, M., Rezić, T., Marđetko, N., Kracher, D., Ludwig, R. & Šantek, B. (2018) Lignocellulose degradation: An overview of fungi and fungal enzymes involved in lignocellulose degradation, 18(11), 768-778.
- Anyao, C. C. & Baroutian, S. (2018) Decentralized anaerobic digestion systems for increased utilization of biogas from municipal solid waste. *Renewable and Sustainable Energy Reviews*, 90, 982-991.
- Aracil, C., Haro, P., Giuntoli, J. & Ollero, P. (2017) Proving the climate benefit in the production of biofuels from municipal solid waste refuse in Europe. *Journal of Cleaner Production*, 142, Part 4, 2887-2900.
- Arantes, V. & Saddler, J. N. (2011) Cellulose accessibility limits the effectiveness of minimum cellulase loading on the efficient hydrolysis of pretreated lignocellulosic substrates. *Biotechnology for Biofuels*, 4, 16.
- Archimedes & Heath, T. (1897) *The Works of Archimedes* Cambridge University Press.

- Ballesteros, M., Oliva, J., Manzanares, P., Negro, M. J. & Ballesteros, I. (2002) Ethanol production from paper material using a simultaneous saccharification and fermentation system in a fed-batch basis. *World J Microbiol Biotechnol*, 18.
- Ballesteros, M., Sáez, F., Ballesteros, I., Manzanares, P., Negro, M. J., Martínez, J. M., Castañeda, R. & Oliva Dominguez, J. M. (2010) Ethanol Production from the Organic Fraction Obtained After Thermal Pretreatment of Municipal Solid Waste. *Applied Biochemistry and Biotechnology*, 161(1), 423-431.
- Barampouti, E. M., Mai, S., Malamis, D., Moustakas, K. & Loizidou, M. (2019) Liquid biofuels from the organic fraction of municipal solid waste: A review. *Renewable and Sustainable Energy Reviews*, 110, 298-314.
- Barik, S., Paul, K. K. & Priyadarshi, D. (2018) Utilization of kitchen food waste for biodiesel production, *8th International Conference on Environment Science and Engineering (ICESE)*. Barcelona, SPAIN, Mar 11-13.
- Beard, S. J., Hashim, R., Membrillo-Hernandez, J., Hughes, M. N. & Poole, R. K. (1997) Zinc(II) tolerance in *Escherichia coli* K-12: evidence that the *zntA* gene (o732) encodes a cation transport ATPase. *Mol Microbiol*, 25(5), 883-91.
- Belda, E., van Heck, R. G. A., Lopez-Sanchez, M. J., Cruveiller, S., Barbe, V., Fraser, C., Klenk, H. P., Petersen, J., Morgat, A., Nikel, P. I., Vallenet, D., Rouy, Z., Sekowska, A., dos Santos, V., de Lorenzo, V., Danchin, A. & Medigue, C. (2016) The revisited genome of *Pseudomonas putida* KT2440 enlightens its value as a robust metabolic chassis. *Environmental Microbiology*, 18(10), 3403-3424.
- Benito, Á., Jeffares, D., Palomero, F., Calderón, F., Bai, F.-Y., Bähler, J. & Benito, S. (2016) Selected *Schizosaccharomyces pombe* Strains Have Characteristics That Are Beneficial for Winemaking. *PLOS ONE*, 11(3), e0151102.
- Berlin, A., Balakshin, M., Gilkes, N., Kadla, J., Maximenko, V., Kubo, S. & Saddler, J. (2006) Inhibition of cellulase, xylanase and beta-glucosidase activities by softwood lignin preparations. *Journal of Biotechnology*, 125(2), 198-209.
- Berntsson, T., Sanden, B., Olsson, L. & Asbald, A. (2014) Chapter 2: What is a Biorefinery?, *Systems Perspectives on Biorefineries* Chalmers University of Technology.
- Bird, L. J., Coleman, M. L. & Newman, D. K. (2013) Iron and Copper Act Synergistically To Delay Anaerobic Growth of Bacteria. *Applied and Environmental Microbiology*, 79(12), 3619.
- Borjesson, J., Engqvist, M., Sipos, B. & Tjerneld, F. (2007) Effect of poly(ethylene glycol) on enzymatic hydrolysis and adsorption of cellulase enzymes to pretreated lignocellulose. *Enzyme and Microbial Technology*, 41(1-2), 186-195.
- Boudreau, T. F., Peck, G. M., O'Keefe, S. F. & Stewart, A. C. (2018) Free amino nitrogen concentration correlates to total yeast assimilable nitrogen concentration in apple juice. *Food Science & Nutrition*, 6(1), 119-123.

Broeker, J., Mechelke, M., Baudrexl, M., Mennerich, D., Hornburg, D., Mann, M., Schwarz, W. H., Liebl, W. & Zverlov, V. V. (2018) The hemicellulose-degrading enzyme system of the thermophilic bacterium *Clostridium stercorarium*: comparative characterisation and addition of new hemicellulolytic glycoside hydrolases. *Biotechnology for Biofuels*, 11(1), 229.

Bucholz, S. E., Dooley, M. M. & Eveleigh, D. E. (1987) *Zymomonas* - an alcoholic enigma. *Tibtech*, 5, 199-204.

Büchs, J. (2001) Introduction to advantages and problems of shaken cultures. *Biochemical Engineering Journal*, 7(2), 91-98.

Buehler, E. A. & Mesbah, A. (2016) Kinetic Study of Acetone-Butanol-Ethanol Fermentation in Continuous Culture. *Plos One*, 11(8).

Callahan, B., McMurdie, P., Rosen, M., Han, A., Johnson, A. & Holmes, S. (2016) DADA2: High-resolution sample inference from Illumina amplicon data. *Nature Methods*, 13, 581-583.

Calusinska, M., Goux, X., Fossépré, M., Muller, E. E. L., Wilmes, P. & Delfosse, P. (2018) A year of monitoring 20 mesophilic full-scale bioreactors reveals the existence of stable but different core microbiomes in bio-waste and wastewater anaerobic digestion systems. *Biotechnology for Biofuels*, 11(1), 196.

Caporaso, J., Kuczynski, J., Stombaugh, J., Bittinger, K., Bushman, F., Costello, E., Fierer, N., Gonzalez, P., Goodrich, J., Gordon, J., Huttley, G., Kelley, S., Knights, D., Koenig, J., Ley, R., Lozupone, C., McDonald, D., Muegge, B., Pirrung, M., Reeder, J., Sevinsky, J., Turnbaugh, P., Walters, W., Widmann, J., Yatsunenko, T., Zaneveld, J. & Knight, R. (2010) QIIME allows analysis of high-throughput community sequencing data. *Nature Methods* 7(5), 335-336.

Cassia, R., Nocioni, M., Correa-Aragunde, N. & Lamattina, L. (2018) Climate Change and the Impact of Greenhouse Gasses: CO₂ and NO, Friends and Foes of Plant Oxidative Stress, 9(273).

Cavicchioli, R., Ripple, W. J., Timmis, K. N., Azam, F., Bakken, L. R., Baylis, M., Behrenfeld, M. J., Boetius, A., Boyd, P. W., Classen, A. T., Crowther, T. W., Danovaro, R., Foreman, C. M., Huisman, J., Hutchins, D. A., Jansson, J. K., Karl, D. M., Koskella, B., Mark Welch, D. B., Martiny, J. B. H., Moran, M. A., Orphan, V. J., Reay, D. S., Remais, J. V., Rich, V. I., Singh, B. K., Stein, L. Y., Stewart, F. J., Sullivan, M. B., van Oppen, M. J. H., Weaver, S. C., Webb, E. A. & Webster, N. S. (2019) Scientists' warning to humanity: microorganisms and climate change. *Nature Reviews Microbiology*, 17(9), 569-586.

CEN (2009) *EN 590:2009, Automotive fuels -Diesel-Requirements and test methods*.

Available online:

http://www.envirochem.hu/www.envirochem.hu/documents/EN_590_2009_hhV05.pdf
[Accessed

Chandrangsu, P., Rensing, C. & Helmann, J. D. (2017) Metal homeostasis and resistance in bacteria. *Nat Rev Micro*, 15(6), 338-350.

- Chen, H., Venditti, R. A., Jameel, H. & Park, S. (2012) Enzymatic Hydrolysis of Recovered Office Printing Paper with Low Enzyme Dosages to Produce Fermentable Sugars. *Applied Biochemistry and Biotechnology*, 166(5), 1121-1136.
- Chen, H. Z. & Liu, Z. H. (2017) Enzymatic hydrolysis of lignocellulosic biomass from low to high solids loading. *Engineering in Life Sciences*, 17(5), 489-499.
- Chen, R. & Dou, J. (2015) Biofuels and bio-based chemicals from lignocellulose: metabolic engineering strategies in strain development. *Biotechnology Letters*, 38(2), 213-221.
- Cherubini, F. (2010) The biorefinery concept: Using biomass instead of oil for producing energy and chemicals. *Energy Conversion and Management*, 51(7), 1412-1421.
- Cherubini, F., Jungmeier, G., Wellisch, M., Willke, T., Skiadas, I., Van Ree, R. & de Jong, E. (2009) Toward a common classification approach for biorefinery systems, 3(5), 534-546.
- Chojnacka, K. (2010) Biosorption and bioaccumulation - the prospects for practical applications. *Environment International*, 36(3), 299-307.
- Chun, A. Y., Yunxiao, L., Ashok, S., Seol, E. & Park, S. (2014) Elucidation of toxicity of organic acids inhibiting growth of *Escherichia coli* W. *Biotechnology and Bioprocess Engineering*, 19(5), 858-865.
- Clarke, W. P. (2018) The uptake of anaerobic digestion for the organic fraction of municipal solid waste – Push versus pull factors. *Bioresource Technology*, 249, 1040-1043.
- Conway, T. (1992) THE ENTNER-DOUDOROFF PATHWAY - HISTORY, PHYSIOLOGY AND MOLECULAR-BIOLOGY. *Fems Microbiology Letters*, 103(1), 1-28.
- Cripps, R. E., Eley, K., Leak, D. J., Rudd, B., Taylor, M., Todd, M., Boakes, S., Martin, S. & Atkinson, T. (2009) Metabolic engineering of *Geobacillus thermoglucosidasius* for high yield ethanol production. *Metabolic Engineering*, 11(6), 398-408.
- Dang, Y., Sun, D., Woodard, T. L., Wang, L.-Y., Nevin, K. P. & Holmes, D. E. (2017) Stimulation of the anaerobic digestion of the dry organic fraction of municipal solid waste (OFMSW) with carbon-based conductive materials. *Bioresource Technology*, 238(Supplement C), 30-38.
- de Coninck, H., A. Revi, M. Babiker, P. Bertoldi, M. Buckeridge, A. Cartwright, W. Dong, J. Ford, S. Fuss, J.-C. Hourcade, D. Ley & R. Mechler, P. N., A. Revokatova, S. Schultz, L. Steg, and T. Sugiyamde Coninck, H., A. Revi, M. Babiker, P. Bertoldi, M. Buckeridge, A. Cartwright, W. Dong, J. Ford, S. Fuss, J.-C. Hourcade, D. Ley, R. Mechler, P. Newman, A. Revokatova, S. Schultz, L. Steg, and T. Sugiyam (2018) *Global Warming of 1.5°C*.
- De Graaf, A. A., Striegel, K., Wittig, R. M., Laufer, B., Schmitz, G., Wiechert, W., Sprenger, G. A. & Sahm, H. (1999) Metabolic state of *Zymomonas mobilis* in glucose-, fructose-, and xylose-fed continuous cultures as analysed by C-13- and P-31-NMR spectroscopy. *Archives of Microbiology*, 171(6), 371-385.
- de Marco, A. (2009) Strategies for successful recombinant expression of disulfide bond-dependent proteins in *Escherichia coli*. *Microbial cell factories*, 8, 26-26.

- DEFRA (2013) *Mechanical Biological Treatment of Municipal Solid Waste*. Crown.
- DEFRA (2015a) *Anaerobic Digestion Strategy and Action Plan*.
- DEFRA (2015b) *Digest of Waste and Resource Statistics - 2015 Edition* Crown.
- DEFRA (2018) *Digest of waste and resource statistics - 2018 edition* Crown.
- DeLorenzo, D. M., Rottinghaus, A. G., Henson, W. R. & Moon, T. S. (2018) Molecular Toolkit for Gene Expression Control and Genome Modification in *Rhodococcus opacus* PD630. *ACS Synthetic Biology*, 7(2), 727-738.
- DeSantis, T., Hugenholtz, P., Larsen, N., Rojas, M., Brodie, E., Keller, K. & al., e. (2006) Greengenes, a chimera-checked 16S rRNA gene database and workbench compatible with ARB. *Applied and Environmental Microbiology*, 72(7), 5069-5072.
- Di Maria, F. & Micale, C. (2015) Life cycle analysis of incineration compared to anaerobic digestion followed by composting for managing organic waste: the influence of system components for an Italian district. *International Journal of Life Cycle Assessment*, 20(3), 377-388.
- Dien, B. S., Cotta, M. A. & Jeffries, T. W. (2003) Bacteria engineered for fuel ethanol production: current status. *Appl Microbiol Biotechnol*, 63.
- Dong, B., Liu, X. G., Dai, L. L. & Dai, X. H. (2013) Changes of heavy metal speciation during high-solid anaerobic digestion of sewage sludge. *Bioresource Technology*, 131, 152-158.
- Dong, T., Knoshaug, E. P., Pienkos, P. T. & Laurens, L. M. L. (2016) Lipid recovery from wet oleaginous microbial biomass for biofuel production: A critical review. *Applied Energy*, 177, 879-895.
- Dunlop, M. J. (2011) Engineering microbes for tolerance to next-generation biofuels. *Biotechnology for Biofuels*, 4(1), 32.
- Dvořák, P. & de Lorenzo, V. (2018) Refactoring the upper sugar metabolism of *Pseudomonas putida* for co-utilization of cellobiose, xylose, and glucose. *Metabolic Engineering*, 48, 94-108.
- EC (2011) *Roadmap to a resource efficient Europe*. Brussels:
- EC (2019) *Waste Framework Directive: End-of-Waste Criteria*, 2019. Available online: https://ec.europa.eu/environment/waste/framework/end_of_waste.htm [Accessed.
- Edinger, R. & Kaul, S. (2000) Humankind's detour toward sustainability: past, present, and future of renewable energies and electric power generation. *Renewable and Sustainable Energy Reviews*, 4(3), 295-313.
- El-Naas, M. H., Al-Muhtaseb, S. A. & Makhoulouf, S. (2009) Biodegradation of phenol by *Pseudomonas putida* immobilized in polyvinyl alcohol (PVA) gel. *Journal of Hazardous Materials*, 164(2-3), 720-725.

- Farmanbordar, S., Amiri, H. & Karimi, K. (2018a) Simultaneous organosolv pretreatment and detoxification of municipal solid waste for efficient biobutanol production. *Bioresource Technology*, 270, 236-244.
- Farmanbordar, S., Karimi, K. & Amiri, H. (2018b) Municipal solid waste as a suitable substrate for butanol production as an advanced biofuel. *Energy Conversion and Management*, 157, 396-408.
- Fei, Q., Wewetzer, S. J., Kurosawa, K., Rha, C. & Sinskey, A. J. (2015) High-cell-density cultivation of an engineered *Rhodococcus opacus* strain for lipid production via co-fermentation of glucose and xylose. *Process Biochemistry*, 50(4), 500-506.
- Feldman, D., Kowbel, D. J., Glass, N. L., Yarden, O. & Hadar, Y. (2015) Detoxification of 5-hydroxymethylfurfural by the *Pleurotus ostreatus* lignolytic enzymes aryl alcohol oxidase and dehydrogenase. *Biotechnology for Biofuels*, 8.
- Fenske, J. J., Griffin, D. A. & Penner, M. H. (1998) Comparison of aromatic monomers in lignocellulosic biomass prehydrolysates. *J Ind Microbiol Biotechnol*, 20.
- Fernández-González, J. M., Grindlay, A. L., Serrano-Bernardo, F., Rodríguez-Rojas, M. I. & Zamorano, M. (2017) Economic and environmental review of Waste-to-Energy systems for municipal solid waste management in medium and small municipalities. *Waste Management*, 67, 360-374.
- Fernando, S., Adhikari, S., Chandrapal, C. & Murali, N. (2006) Biorefineries: Current Status, Challenges, and Future Direction. *Energy & Fuels*, 20(4), 1727-1737.
- Ferrè, F. & Clote, P. (2005) DiANNA: a web server for disulfide connectivity prediction. *Nucleic acids research*, 33(Web Server issue), W230-W232.
- Field, J. A. & Lettinga, G. (1992) TOXICITY OF TANNIC COMPOUNDS TO MICROORGANISMS. *Plant Polyphenols : Synthesis, Properties, Significance*, 59, 673-692.
- Folland, C. K., Boucher, O., Colman, A. & Parker, D. E. (2018) Causes of irregularities in trends of global mean surface temperature since the late 19th century. *Science Advances*, 4(6), eaao5297.
- Garcia-Ochoa, F. & Gomez, E. (2009) Bioreactor scale-up and oxygen transfer rate in microbial processes: An overview. *Biotechnology Advances*, 27(2), 153-176.
- Garcia-Ochoa, F., Gomez, E., Santos, V. E. & Merchuk, J. C. (2010) Oxygen uptake rate in microbial processes: An overview. *Biochemical Engineering Journal*, 49(3), 289-307.
- García, A. M., Hunt, A. J., Budarin, V. L., Parker, H. L., Shuttleworth, P. S., Ellis, G. J. & Clark, J. H. (2015) Starch-derived carbonaceous mesoporous materials (Starbon®) for the selective adsorption and recovery of critical metals. *Green Chemistry*, 17(4), 2146-2149.
- Garrote, G., Dominguez, H. & Parajo, J. C. (1999) Hydrothermal processing of lignocellulosic materials. *Holz Als Roh-Und Werkstoff*, 57(3), 191-202.
- Gavrilescu, M. & Chisti, Y. (2005) Biotechnology-a sustainable alternative for chemical industry. *Biotechnol Adv*, 23(7-8), 471-99.

- Ghanavati, H., Nahvi, I. & Karimi, K. (2015) Organic fraction of municipal solid waste as a suitable feedstock for the production of lipid by oleaginous yeast *Cryptococcus aerius*. *Waste Management*, 38, 141-148.
- Ghatak, H. R. (2011) Biorefineries from the perspective of sustainability: Feedstocks, products, and processes. *Renewable & Sustainable Energy Reviews*, 15(8), 4042-4052.
- Giakoumis, E. G. (2013) A statistical investigation of biodiesel physical and chemical properties, and their correlation with the degree of unsaturation. *Renewable Energy*, 50, 858-878.
- Gomez, L. D., Whitehead, C., Barakate, A., Halpin, C. & McQueen-Mason, S. J. (2010) Automated saccharification assay for determination of digestibility in plant materials. *Biotechnology for Biofuels*, 3(23).
- Gregson, N., Crang, M., Fuller, S. & Holmes, H. (2015) Interrogating the circular economy: the moral economy of resource recovery in the EU. *Economy and Society*, 44(2), 218-243.
- Grote, A., Hiller, K., Scheer, M., Munch, R., Nortemann, B., Hempel, D. C. & Jahn, D. (2005) JCat: a novel tool to adapt codon usage of a target gene to its potential expression host. *Nucleic Acids Research*, 33, W526-W531.
- Guo, J. H., Peng, Y. Z., Ni, B. J., Han, X. Y., Fan, L. & Yuan, Z. G. (2015) Dissecting microbial community structure and methane-producing pathways of a full-scale anaerobic reactor digesting activated sludge from wastewater treatment by metagenomic sequencing. *Microbial Cell Factories*, 14.
- Haddadi, M. H., Aiyelabegan, H. T. & Negahdari, B. (2018) Advanced biotechnology in biorefinery: a new insight into municipal waste management to the production of high-value products. *International Journal of Environmental Science and Technology*, 15(3), 675-686.
- Hartmann, H. & Ahring, B. K. (2005) Anaerobic digestion of the organic fraction of municipal solid waste: influence of co-digestion with manure. *Water Res*, 39(8), 1543-52.
- Have, R. & Teunissen, P. J. M. (2001) Oxidative Mechanisms Involved in Lignin Degradation by White-Rot Fungi. *Chemical Reviews*, 101(11), 3397-3414.
- Hayles, J. & Nurse, P. (1992) Genetics of the Fission Yeast *Schizosaccharomyces Pombe*, 26(1), 373-402.
- Heer, D. & Sauer, U. (2008) Identification of furfural as a key toxin in lignocellulosic hydrolysates and evolution of a tolerant yeast strain. *Microbial biotechnology*, 1(6), 497-506.
- Henson, W. R., Hsu, F.-F., Dantas, G., Moon, T. S. & Foston, M. (2018) Lipid metabolism of phenol-tolerant *Rhodococcus opacus* strains for lignin bioconversion. *Biotechnology for Biofuels*, 11(1), 339.
- Hernandez, M. A., Arabolaza, A., Rodriguez, E., Gramajo, H. & Alvarez, H. M. (2013) The *atf2* gene is involved in triacylglycerol biosynthesis and accumulation in the oleaginous *Rhodococcus opacus* PD630. *Applied Microbiology and Biotechnology*, 97(5), 2119-2130.

- Holder, J. W., Ulrich, J. C., DeBono, A. C., Godfrey, P. A., Desjardins, C. A., Zucker, J., Zeng, Q., Leach, A. L. B., Ghiviriga, I., Dancel, C., Abeel, T., Gevers, D., Kodira, C. D., Desany, B., Affourtit, J. P., Birren, B. W. & Sinskey, A. J. (2011) Comparative and Functional Genomics of *Rhodococcus opacus* PD630 for Biofuels Development. *PLoS Genetics*, 7(9), e1002219.
- Höök, M. & Tang, X. (2013) Depletion of fossil fuels and anthropogenic climate change—A review. *Energy Policy*, 52, 797-809.
- Hoorweg, D., Bhada-Tata, P., and Kennedy, C. (2013) Waste production must peak this century. *Nature*, 502, 615-617.
- Hoorweg, D. a. B.-T., P. (2012) *What a waste: A global review of solid waste management* Urban Development & Local Government Unit World Bank 1818 H Street, N. W., DC 20433 USA.
- Hossain, S. T., Mallick, I. & Mukherjee, S. K. (2012) Cadmium toxicity in *Escherichia coli*: Cell morphology, Z-ring formation and intracellular oxidative balance. *Ecotoxicol Environ Saf*, 86, 54-9.
- Hou, J., Ding, C., Qiu, Z., Zhang, Q. & Xiang, W.-N. (2017) Inhibition efficiency evaluation of lignocellulose-derived compounds for bioethanol production. *Journal of Cleaner Production*, 165, 1107-1114.
- Huang, L., Zhao, L., Zan, X., Song, Y. & Ratledge, C. (2016) Boosting fatty acid synthesis in *Rhodococcus opacus* PD630 by overexpression of autologous thioesterases. *Biotechnology Letters*, 38(6), 999-1008.
- Huang, W. D. & Zhang, Y. H. P. (2011) Analysis of biofuels production from sugar based on three criteria: Thermodynamics, bioenergetics, and product separation. *Energy & Environmental Science*, 4(3), 784-792.
- Hubbe, M. A. & Gill, R. A. (2016) Fillers for papermaking: A review of their properties, usage practices, and their mechanistic role *Bioresources*, 11(1), 2886-2963.
- Huffer, S., Roche, C. M., Blanch, H. W. & Clark, D. S. (2012) *Escherichia coli* for biofuel production: bridging the gap from promise to practice. *Trends in Biotechnology*, 30(10), 538-545.
- Humphrey, A. (1998) Shake Flask to Fermentor: What Have We Learned? *Biotechnology Progress*, 14(1), 3-7.
- Hungate, R. E. (1969) Chapter IV A Roll Tube Method for Cultivation of Strict Anaerobes, in Norris, J. R. & Ribbons, D. W. (eds), *Methods in Microbiology* Academic Press, 117-132.
- Hunt, M. C., Solaas, K., Kase, B. F. & Alexson, S. E. H. (2002) Characterization of an acyl-CoA thioesterase that functions as a major regulator of peroxisomal lipid metabolism. *Journal of Biological Chemistry*, 277(2), 1128-1138.
- IEA (2008) *Biorefinery Fact Sheets*.
- IEA (2013) *Bio-Based Chemicals: Value Added Products from Biorefineries*.

IEA (2016) *Key World Energy Statistics 2016*.

IEA (2018) *The role of Anaerobic Digestion and Biogas in the Circular Economy*.

Jang, Y. S., Malaviya, A., Cho, C., Lee, J. & Lee, S. Y. (2012) Butanol production from renewable biomass by clostridia. *Bioresour Technol*, 123, 653-63.

Jeffares, D. C. (2018) The natural diversity and ecology of fission yeast. *Yeast*, 35(3), 253-260.

Jeffares, D. C., Rallis, C., Rieux, A., Speed, D., Prevorovsky, M., Mourier, T., Marsellach, F. X., Iqbal, Z., Lau, W., Cheng, T. M. K., Pracana, R., Mulleder, M., Lawson, J. L. D., Chessel, A., Bala, S., Hellenthal, G., O'Fallon, B., Keane, T., Simpson, J. T., Bischof, L., Tomiczek, B., Bitton, D. A., Sideri, T., Codlin, S., Hellberg, J., van Trigt, L., Jeffery, L., Li, J. J., Atkinson, S., Thodberg, M., Febrer, M., McLay, K., Drou, N., Brown, W., Hayles, J., Salas, R. E. C., Ralsler, M., Maniatis, N., Balding, D. J., Balloux, F., Durbin, R. & Bahler, J. (2015) The genomic and phenotypic diversity of *Schizosaccharomyces pombe*. *Nature Genetics*, 47(3), 235-+.

Jeffries, T. W. & Kurtzman, C. P. (1994) Strain selection, taxonomy, and genetics of xylose-fermenting yeasts. *Enzyme and Microbial Technology*, 16, 922-932.

Jensen, J. W., Felby, C. & Jørgensen, H. (2011) Cellulase Hydrolysis of Unsorted MSW. *Applied Biochemistry and Biotechnology*, 165(7), 1799-1811.

Jensen, J. W., Felby, C., Jørgensen, H., Ronsch, G. O. & Norholm, N. D. (2010) Enzymatic processing of municipal solid waste. *Waste Management*, 30(12), 2497-2503.

Jimenez-Diaz, L., Caballero, A., Perez-Hernandez, N. & Segura, A. (2017) Microbial alkane production for jet fuel industry: motivation, state of the art and perspectives. *Microbial Biotechnology*, 10(1), 103-124.

Jiménez-Díaz, L., Caballero, A., Pérez-Hernández, N. & Segura, A. (2016) Microbial alkane production for jet fuel industry: motivation, state of the art and perspectives. *Microbial biotechnology*, 10(1), 103-124.

Jönsson, L. J., Alriksson, B. & Nilvebrant, N. O. (2013) Bioconversion of lignocellulose: inhibitors and detoxification. *Biotechnology for Biofuels*, 6, 10.

Jönsson, L. J. & Martin, C. (2016) Pretreatment of lignocellulose: Formation of inhibitory by-products and strategies for minimizing their effects. *Bioresource technology*, 199, 103-12.

Jönsson, L. J., Palmqvist, E., Nilvebrant, N. O. & Hahn-Hagerdal, B. (1998) Detoxification of wood hydrolysates with laccase and peroxidase from the white-rot fungus *Trametes versicolor*. *Applied Microbiology and Biotechnology*, 49(6), 691-697.

Jørgensen, H. (2009) Effect of Nutrients on Fermentation of Pretreated Wheat Straw at very High Dry Matter Content by *Saccharomyces cerevisiae*. *Applied Biochemistry and Biotechnology*, 153(1), 44-57.

- Jorgensen, H., Kristensen, J. B. & Felby, C. (2007) Enzymatic conversion of lignocellulose into fermentable sugars: challenges and opportunities. *Biofuels Bioproducts & Biorefining-Biofpr*, 1(2), 119-134.
- Jouhara, H., Khordehgah, N., Almahmoud, S., Delpech, B., Chauhan, A. & Tassou, S. A. (2018) Waste heat recovery technologies and applications. *Thermal Science and Engineering Progress*, 6, 268-289.
- Jozala, A. F., Geraldés, D. C., Tundisi, L. L., Feitosa, V. d. A., Breyer, C. A., Cardoso, S. L., Mazzola, P. G., Oliveira-Nascimento, L. d., Rangel-Yagui, C. d. O., Magalhães, P. d. O., Oliveira, M. A. d. & Pessoa, A., Jr. (2016) Biopharmaceuticals from microorganisms: from production to purification. *Brazilian journal of microbiology : [publication of the Brazilian Society for Microbiology]*, 47 Suppl 1(Suppl 1), 51-63.
- Julio, R., Albet, J., Vialle, C., Vaca-Garcia, C. & Sablayrolles, C. (2017) Sustainable design of biorefinery processes: existing practices and new methodology, 11(2), 373-395.
- Jung, Y. K., Kim, T. Y., Park, S. J. & Lee, S. Y. (2010) Metabolic engineering of *Escherichia coli* for the production of polylactic acid and its copolymers, 105(1), 161-171.
- Kalantari, N. (2008) *Evaluation of Toxicity of Heavy Metals for Escherichia coli Growth*, 5.
- Kampen, W. H. (2014) Chapter 4 - Nutritional Requirements in Fermentation Processes, in Vogel, H. C. & Todaro, C. M. (eds), *Fermentation and Biochemical Engineering Handbook (Third Edition)*. Boston: William Andrew Publishing, 37-57.
- Karimi, K. & Taherzadeh, M. J. (2016) A critical review of analytical methods in pretreatment of lignocelluloses: Composition, imaging, and crystallinity. *Bioresource Technology*, 200, 1008-1018.
- Kaza, S., Yao, L., Bhada-Tata, P. & and Van Woerden, F. (2018) *What a Waste 2.0: A Global Snapshot of Solid Waste Management to 2050*Bank, W. D. W.
- Kerby, C. & Vriesekoop, F. (2017) An Overview of the Utilisation of Brewery By-Products as Generated by British Craft Breweries. *Beverages*, 3(2), 24.
- Kim, D. (2018) Physico-Chemical Conversion of Lignocellulose: Inhibitor Effects and Detoxification Strategies: A Mini Review. *Molecules*, 23(2).
- Kim, S. R., Park, Y. C., Jin, Y. S. & Seo, J. H. (2013) Strain engineering of *Saccharomyces cerevisiae* for enhanced xylose metabolism. *Biotechnology Advances*, 31(6), 851-861.
- Kircher, M. (2015) Sustainability of biofuels and renewable chemicals production from biomass. *Curr Opin Chem Biol*, 29, 26-31.
- Klein-Marcuschamer, D., Oleskiewicz-Popiel, P., Simmons, B. A. & Blanch, H. W. (2012) The challenge of enzyme cost in the production of lignocellulosic biofuels. *Biotechnology and Bioengineering*, 109(4), 1083-1087.
- Klindworth, A., Pruesse, E., Schweer, T., Peplies, J., Quast, C., Horn, M. & Glöckner, F. O. (2013) Evaluation of general 16S ribosomal RNA gene PCR primers for classical and next-generation sequencing-based diversity studies. *Nucleic acids research*, 41(1), e1-e1.

- Klinke, H. B., Olsson, L., Thomsen, A. B. & Ahring, B. K. (2003) Potential inhibitors from wet oxidation of wheat straw and their effect on ethanol production of *Saccharomyces cerevisiae*: Wet oxidation and fermentation by yeast. *Biotechnol Bioeng*, 81.
- Klinke, H. B., Thomsen, A. B. & Ahring, B. K. (2001) Potential inhibitors from wet oxidation of wheat straw and their effect on growth and ethanol production by *Thermoanaerobacter mathranii*. *Applied Microbiology and Biotechnology*, 57(5-6), 631-638.
- Klopfenstein, W. E. (1982) ESTIMATION OF CETANE INDEX FOR ESTERS OF FATTY-ACIDS. *Journal of the American Oil Chemists Society*, 59(12), 531-533.
- Koh, B. T., Nakashimada, U., Pfeiffer, M. & Yap, M. G. S. (1992) Comparison of acetate inhibition on growth of host and recombinant *E. coli* K12 strains. *Biotechnol Lett*, 14.
- Kristensen, J. B., Felby, C. & Jørgensen, H. (2009a) Yield-determining factors in high-solids enzymatic hydrolysis of lignocellulose. *Biotechnology for Biofuels*, 2, 10.
- Kristensen, J. B., Felby, C. & Jørgensen, H. (2009b) Determining Yields in High Solids Enzymatic Hydrolysis of Biomass. *Applied Biochemistry and Biotechnology*, 156(1), 127-132.
- Kunze, R., Fußwinkel, H. & Feldmar, S. (1995) Chapter 34 Expression of Plant Proteins in Baculoviral and Bacterial Systems, in Galbraith, D. W., Bourque, D. P. & Bohnert, H. J. (eds), *Methods in Cell Biology* Academic Press, 461-479.
- Kurosawa, K., Boccazzi, P., de Almeida, N. M. & Sinskey, A. J. (2010) High-cell-density batch fermentation of *Rhodococcus opacus* PD630 using a high glucose concentration for triacylglycerol production. *Journal of Biotechnology*, 147(3-4), 212-218.
- Kurosawa, K., Laser, J. & Sinskey, A. J. (2015a) Tolerance and adaptive evolution of triacylglycerol-producing *Rhodococcus opacus* to lignocellulose-derived inhibitors. *Biotechnology for Biofuels*, 8, 14.
- Kurosawa, K., Plassmeier, J., Kalinowski, J., Ruckert, C. & Sinskey, A. J. (2015b) Engineering L-arabinose metabolism in triacylglycerol-producing *Rhodococcus opacus* for lignocellulosic fuel production. *Metabolic Engineering*, 30, 89-95.
- Kurosawa, K., Radek, A., Plassmeier, J. K. & Sinskey, A. J. (2015c) Improved glycerol utilization by a triacylglycerol-producing *Rhodococcus opacus* strain for renewable fuels. *Biotechnology for Biofuels*, 8(1), 31.
- Kurosawa, K., Wewetzer, S. J. & Sinskey, A. J. (2013) Engineering xylose metabolism in triacylglycerol-producing *Rhodococcus opacus* for lignocellulosic fuel production. *Biotechnology for Biofuels*, 6(1), 134.
- Kurosawa, K., Wewetzer, S. J. & Sinskey, A. J. (2014) Triacylglycerol production from corn stover using a xylose-fermenting *Rhodococcus opacus* strain for lignocellulosic biofuels. *Journal of Microbial & Biochemical Technology*, 6(5), 254-259.

- Lamb, D. T., Venkatraman, K., Bolan, N., Ashwath, N., Choppala, G. & Naidu, R. (2014) Phytocapping: An Alternative Technology for the Sustainable Management of Landfill Sites. *Critical Reviews in Environmental Science and Technology*, 44(6), 561-637.
- Larsen, J., Petersen, M. O., Thirup, L., Li, H. W. & Iversen, F. K. (2008) The IBUS process - Lignocellulosic bioethanol close to a commercial reality. *Chemical Engineering & Technology*, 31(5), 765-772.
- Larson, M. H., Gilbert, L. A., Wang, X., Lim, W. A., Weissman, J. S. & Qi, L. S. (2013) CRISPR interference (CRISPRi) for sequence-specific control of gene expression. *Nature Protocols*, 8, 2180.
- Lau, M. W. & Dale, B. E. (2009) Cellulosic ethanol production from AFEX-treated corn stover using *Saccharomyces cerevisiae* 424A(LNH-ST). *Proceedings of the National Academy of Sciences of the United States of America*, 106(5), 1368-1373.
- Lau, M. W., Gunawan, C., Balan, V. & Dale, B. E. (2010) Comparing the fermentation performance of *Escherichia coli* KO11, *Saccharomyces cerevisiae* 424A(LNH-ST) and *Zymomonas mobilis* AX101 for cellulosic ethanol production. *Biotechnology for Biofuels*, 3, 11-11.
- Lavagnolo, M. C., Girotto, F., Rafieenia, R., Danieli, L. & Alibardi, L. (2018) Two-stage anaerobic digestion of the organic fraction of municipal solid waste – Effects of process conditions during batch tests. *Renewable Energy*, 126, 14-20.
- Lay, J.-J., Lee, Y.-J. & Noike, T. (1999) Feasibility of biological hydrogen production from organic fraction of municipal solid waste. *Water Research*, 33(11), 2579-2586.
- LBNNet (2017) *UK Top Bio-Based Chemicals Opportunities*.
- Lee, S.-M., Jellison, T. & Alper, H. S. (2012) Directed evolution of xylose isomerase for improved xylose catabolism and fermentation in the yeast *Saccharomyces cerevisiae*. *Appl Environ Microbiol*, 78.
- Lee, S. Y. & Kim, H. U. (2015) Systems strategies for developing industrial microbial strains. *Nat Biotechnol*, 33(10), 1061-72.
- Lemire, J. A., Harrison, J. J. & Turner, R. J. (2013) Antimicrobial activity of metals: mechanisms, molecular targets and applications. *Nat Rev Micro*, 11(6), 371-384.
- Lestari, S., Mäki-Arvela, P., Beltramini, J., Lu, G. Q. M. & Murzin, D. Y. (2009) Transforming Triglycerides and Fatty Acids into Biofuels. *ChemSusChem*, 2(12), 1109-1119.
- Li, H., Wu, M., Xu, L., Hou, J., Guo, T., Bao, X. & Shen, Y. (2015) Evaluation of industrial *Saccharomyces cerevisiae* strains as the chassis cell for second-generation bioethanol production. *Microbial Biotechnology*, 8(2), 266-274.
- Li, S., Zhang, X. & Andresen, J. M. (2012a) Production of fermentable sugars from enzymatic hydrolysis of pretreated municipal solid waste after autoclave process. *Fuel*, 92(1), 84-88.

- Li, S. J., Zhang, X. N. & Andresen, J. M. (2012b) Production of fermentable sugars from enzymatic hydrolysis of pretreated municipal solid waste after autoclave process. *Fuel*, 92(1), 84-88.
- Li, W. C., Tse, H. F. & Fok, L. (2016) Plastic waste in the marine environment: A review of sources, occurrence and effects. *Science of The Total Environment*, 566–567, 333-349.
- Liggett, R. W. & Koffler, H. (1948) CORN STEEP LIQUOR IN MICROBIOLOGY. *Bacteriological Reviews*, 12(4), 297-311.
- Liu, H. H., Zhang, J., Yuan, J., Jiang, X. L., Jiang, L. Y., Zhao, G., Huang, D. & Liu, B. (2019) Omics-based analyses revealed metabolic responses of *Clostridium acetobutylicum* to lignocellulose-derived inhibitors furfural, formic acid and phenol stress for butanol fermentation. *Biotechnology for Biofuels*, 12.
- Loeschcke, A. & Thies, S. (2015) *Pseudomonas putida*-a versatile host for the production of natural products. *Applied Microbiology and Biotechnology*, 99(15), 6197-6214.
- Lopes, A. M., Ferreira Filho, E. X. & Moreira, L. R. S. (2018) An update on enzymatic cocktails for lignocellulose breakdown, 125(3), 632-645.
- Mahmoodi, P., Karimi, K. & Taherzadeh, M. J. (2018a) Efficient conversion of municipal solid waste to biofuel by simultaneous dilute-acid hydrolysis of starch and pretreatment of lignocelluloses. *Energy Conversion and Management*, 166, 569-578.
- Mahmoodi, P., Karimi, K. & Taherzadeh, M. J. (2018b) Hydrothermal processing as pretreatment for efficient production of ethanol and biogas from municipal solid waste. *Bioresource Technology*, 261, 166-175.
- Majtan, T., Frerman, F. E. & Kraus, J. P. (2011) Effect of cobalt on *Escherichia coli* metabolism and metalloporphyrin formation. *BioMetals*, 24(2), 335-347.
- Margallo, M., Taddei, M. B. M., Hernandez-Pellon, A., Aldaco, R. & Irabien, A. (2015) Environmental sustainability assessment of the management of municipal solid waste incineration residues: a review of the current situation. *Clean Technologies and Environmental Policy*, 17(5), 1333-1353.
- Marriott, P. E., Gomez, L. D. & McQueen-Mason, S. J. (2016) Unlocking the potential of lignocellulosic biomass through plant science. *New Phytol*, 209(4), 1366-81.
- Matsakas, L., Gao, Q., Jansson, S., Rova, U. & Christakopoulos, P. (2017) Green conversion of municipal solid wastes into fuels and chemicals. *Electronic Journal of Biotechnology*, 26, 69-83.
- McCaskey, T. A., Zhou, S. D., Britt, S. N. & Strickland, R. (1994) Bioconversion of municipal solid waste to lactic acid by *Lactobacillus* species. *Applied Biochemistry and Biotechnology*, 45(1), 555-568.
- McMahon, M. D. & Prather, K. L. J. (2014) Functional Screening and In Vitro Analysis Reveal Thioesterases with Enhanced Substrate Specificity Profiles That Improve Short-Chain Fatty Acid Production in *Escherichia coli*. *Applied and Environmental Microbiology*, 80(3), 1042-1050.

- Meng, F., Ibbett, R., de Vrije, T., Metcalf, P., Tucker, G. & McKechnie, J. (2019) Process simulation and life cycle assessment of converting autoclaved municipal solid waste into butanol and ethanol as transport fuels. *Waste Management*, 89, 177-189.
- Meng, X., Yang, J., Xu, X., Zhang, L., Nie, Q. & Xian, M. (2009) Biodiesel production from oleaginous microorganisms. *Renewable Energy*, 34(1), 1-5.
- Mitchell, T. (2009) Carbon democracy. *Economy and Society*, 38(3), 399-432.
- Modenbach, A. A. & Nokes, S. E. (2012) The use of high-solids loadings in biomass pretreatment-a review. *Biotechnology and Bioengineering*, 109(6), 1430-1442.
- Mohagheghi, A., Linger, J., Smith, H., Yang, S. H., Dowe, N. & Pienkos, P. T. (2014) Improving xylose utilization by recombinant *Zymomonas mobilis* strain 8b through adaptation using 2-deoxyglucose. *Biotechnology for Biofuels*, 7.
- Mossberg, J., Söderholm, P., Hellsmark, H. & Nordqvist, S. (2018) Crossing the biorefinery valley of death? Actor roles and networks in overcoming barriers to a sustainability transition. *Environmental Innovation and Societal Transitions*, 27, 83-101.
- Myhre, G., D. Shindell, F.-M. Bréon, W. Collins, J. Fuglestedt, J. Huang, D. Koch, J.-F. Lamarque, D. Lee, B. Mendoza, T. Nakajima, A. Robock, G. Stephens, T. Takemura and H. Zhang, (2013) Anthropogenic and Natural Radiative Forcing, in Stocker, T. F., D. Qin, G.-K. Plattner, M. Tignor, S.K. Allen, J. Boschung, A. Nauels, Y. Xia, V. Bex and P.M. Midgley (eds.) (ed), *Climate Change 2013: The Physical Science Basis, Contribution of Working Group I to the Fifth Assessment Report of the Intergovernmental Panel on Climate Change*. United Kingdom and New York, NY, USA.: Cambridge University Press, Cambridge.
- Nakashima, N. & Tamura, T. (2004a) Isolation and characterization of a rolling-circle-type plasmid from *Rhodococcus erythropolis* and application of the plasmid to multiple-recombinant-protein expression. *Applied and environmental microbiology*, 70(9), 5557-5568.
- Nakashima, N. & Tamura, T. (2004b) A novel system for expressing recombinant proteins over a wide temperature range from 4 to 35°C. *Biotechnology and Bioengineering*, 86(2), 136-148.
- Narihiro, T. & Sekiguchi, Y. (2007) Microbial communities in anaerobic digestion processes for waste and wastewater treatment: a microbiological update. *Current Opinion in Biotechnology*, 18(3), 273-278.
- Neidhardt, F. C., Bloch, P. L. & Smith, D. F. (1974) Culture Medium for Enterobacteria. *Journal of Bacteriology*, 119(3), 736-747.
- Nelson, M. C., Morrison, M. & Yu, Z. (2011) A meta-analysis of the microbial diversity observed in anaerobic digesters. *Bioresource Technology*, 102(4), 3730-3739.
- Neubauer, P., Cruz, N., Glauche, F., Junne, S., Knepper, A. & Raven, M. (2013) Consistent development of bioprocesses from microliter cultures to the industrial scale. *Engineering in Life Sciences*, 13(3), 224-238.

- Nguyen, T. Y., Cai, C. M., Kumar, R. & Wyman, C. E. (2017) Overcoming factors limiting high-solids fermentation of lignocellulosic biomass to ethanol. *Proceedings of the National Academy of Sciences of the United States of America*, 114(44), 11673-11678.
- Nies, D. H. (1999) Microbial heavy-metal resistance. *Applied Microbiology and Biotechnology*, 51(6), 730-750.
- Nikel, P. I. & de Lorenzo, V. (2014) Robustness of *Pseudomonas putida* KT2440 as a host for ethanol biosynthesis. *N Biotechnol*, 31(6), 562-71.
- Nizami, A. S., Rehan, M., Waqas, M., Naqvi, M., Ouda, O. K. M., Shahzad, K., Miandad, R., Khan, M. Z., Syamsiro, M., Ismail, I. M. I. & Pant, D. (2017) Waste biorefineries: Enabling circular economies in developing countries. *Bioresource Technology*, 241, 1101-1117.
- NNFCC (2019) *Anaerobic digestion deployment in the United Kingdom*.
- Noguchi, T., Tashiro, Y., Yoshida, T., Zheng, J., Sakai, K. & Sonomoto, K. (2013) Efficient butanol production without carbon catabolite repression from mixed sugars with *Clostridium saccharoperbutylacetonicum* N1-4. *Journal of Bioscience and Bioengineering*, 116(6), 716-721.
- Novozymes (2016) *Novozymes and DONG Energy enter into agreement on biological waste sorting*, 2016. Available online: <https://www.novozymes.com/en/news/news-archive/2016/06/novozymes-and-dong-energy-enter-into-agreement-on-biological-waste-sorting> [Accessed].
- Novozymes (2019) *SynTec, Synthetic Biology Project - Cellic CTec.*, 2019. Available online: <http://www.synbioproject.org/cpi/applications/cellic-ctec/> [Accessed].
- O'Callaghan, K. (2016) Technologies for the utilisation of biogenic waste in the bioeconomy. *Food Chemistry*, 198, 2-11.
- Pandey, A., Hoefler, R., Taherzadeh, M., Nampoothiri, K. M., C., L. & (2015) *Industrial Biorefineries and White Biotechnology*. U.S.A.: Elsevier B.V.
- Panesar, P. S., Marwaha, S. S. & Kennedy, J. F. (2006) *Zymomonas mobilis*: an alternative ethanol producer. *Journal of Chemical Technology and Biotechnology*, 81(4), 623-635.
- Pappas, K. M., Kouvelis, V. N., Saunders, E., Brettin, T. S., Bruce, D., Detter, C., Balakireva, M., Han, C. S., Savvakis, G., Kyrpides, N. C. & Typas, M. A. (2011) Genome Sequence of the Ethanol-Producing *Zymomonas mobilis* subsp *mobilis* Lectotype Strain ATCC 10988. *Journal of Bacteriology*, 193(18), 5051-5052.
- Park, S. Y., Yang, D., Ha, S. H. & Lee, S. Y. (2018) Metabolic Engineering of Microorganisms for the Production of Natural Compounds, 2(1), 1700190.
- Paulová, L. & Brányik, T. (2013) Chapter 4: Advanced Fermentation Processes, *Engineering Aspects of Food Biotechnology*, 89-105.
- Pethica, J. & Ostriker, J. (2014) *Climate Change: Evidence & Causes, An Overview from The Royal Society and the US National Academy of Sciences*.

- Petrovič, U. (2015) Next-generation biofuels: a new challenge for yeast. *Yeast*, 32(9), 583-593.
- Pini, C. V., Bernal, P., Godoy, P., Ramos, J. L. & Segura, A. (2009) Cyclopropane fatty acids are involved in organic solvent tolerance but not in acid stress resistance in *Pseudomonas putida* DOT-T1E. *Microbial Biotechnology*, 2(2), 253-261.
- Puri, D. J. (2014) *Process improvement for the production of fermentable sugars using paper pulp derived from municipal solid waste*. Doctor of Philosophy University of Southampton, 15.09.2014.
- Puri, D. J., Heaven, S. & Banks, C. J. (2013) Improving the performance of enzymes in hydrolysis of high solids paper pulp derived from MSW. *Biotechnology for Biofuels*, 6(107).
- Quiros, R., Gabarrell, X., Villalba, G., Barrena, R., Garcia, A., Torrente, J. & Font, X. (2015) The application of LCA to alternative methods for treating the organic fiber produced from autoclaving unsorted municipal solid waste: case study of Catalonia. *Journal of Cleaner Production*, 107, 516-528.
- Razavi, A. S., Hosseini Koupaie, E., Azizi, A., Hafez, H. & Elbeshbishy, E. (2019) Bioenergy production data from anaerobic digestion of thermally hydrolyzed organic fraction of municipal solid waste. *Data in Brief*, 22, 1018-1026.
- Rivard, C. J., Nagle, N. J., Adney, W. S. & Himmel, M. E. (1993) Anaerobic bioconversion of municipal solid wastes. *Applied Biochemistry and Biotechnology*, 39(1), 107.
- Rumbold, K., van Buijsen, H. J., Overkamp, K. M., van Groenestijn, J. W., Punt, P. J. & Werf, M. J. v. d. J. M. C. F. (2009) Microbial production host selection for converting second-generation feedstocks into bioproducts, 8(1), 64.
- Rumbold, K., van Buijsen, H. J. J., Gray, V. M., van Groenestijn, J. W., Overkamp, K. M., Slomp, R. S., van der Werf, M. J. & Punt, P. J. (2010) Microbial renewable feedstock utilization: a substrate-oriented approach. *Bioengineered bugs*, 1(5), 359-366.
- Saini, J. K., Saini, R. & Tewari, L. (2015) Lignocellulosic agriculture wastes as biomass feedstocks for second-generation bioethanol production: concepts and recent developments. *3 Biotech*, 5(4), 337-353.
- Salmond, G. P. C. & Whittenbury, R. (1985) BIOLOGY OF MICROORGANISMS, 4TH EDITION - BROCK,TD, SMITH,DW, MADIGAN,MT. *Nature*, 314(6006), 49-49.
- Selling, R., Hakansson, T. & Bjornsson, L. (2008) Two-stage anaerobic digestion enables heavy metal removal. *Water Science and Technology*, 57(4), 553-558.
- Sezonov, G., Joseleau-Petit, D. & D'Ari, R. (2007) *Escherichia coli* physiology in Luria-Bertani broth. *Journal of Bacteriology*, 189(23), 8746-8749.
- Shah, A. T., Favaro, L., Alibardi, L., Cagnin, L., Sandon, A., Cossu, R., Casella, S. & Basaglia, M. (2016) *Bacillus* sp. strains to produce bio-hydrogen from the organic fraction of municipal solid waste. *Applied Energy*, 176, 116-124.

- Shao, Z., Dick, W. A. & Behki, R. M. (1995) An improved Escherichia coli-Rhodococcus shuttle vector and plasmid transformation in Rhodococcus spp. using electroporation. *Letters in Applied Microbiology*, 21(4), 261-266.
- Sharma, P. & Melkania, U. (2018) Effect of sulfate on hydrogen production from the organic fraction of municipal solid waste using co-culture of E. coli and Enterobacter aerogenes. *International Journal of Hydrogen Energy*, 43(2), 676-684.
- Silver, S., Budd, K., Leahy, K. M., Shaw, W. V., Hammond, D., Novick, R. P., Willsky, G. R., Malamy, M. H. & Rosenberg, H. (1981) Inducible plasmid-determined resistance to arsenate, arsenite, and antimony (III) in escherichia coli and Staphylococcus aureus. *Journal of Bacteriology*, 146(3), 983.
- Singh, Y. & Bihari Satapathy, K. (2018) *Conversion of Lignocellulosic Biomass to Bioethanol: An Overview with a Focus on Pretreatment*, 15.
- Sluiter, A., Ruiz, R., Scarlata, C., Sluiter, J. & Templeton, D. (2008) *Determination of extractives in biomass - laboratory analytical procedure*.
- Smith, J., van Rensburg, E. & Gorgens, J. F. (2014) Simultaneously improving xylose fermentation and tolerance to lignocellulosic inhibitors through evolutionary engineering of recombinant Saccharomyces cerevisiae harbouring xylose isomerase. *Bmc Biotechnology*, 14.
- Smith, S. R. (2009) A critical review of the bioavailability and impacts of heavy metals in municipal solid waste composts compared to sewage sludge. *Environment International*, 35(1), 142-156.
- Sorek, N., Yeats, T. H., Szemenyei, H., Youngs, H. & Somerville, C. R. (2014) The Implications of Lignocellulosic Biomass Chemical Composition for the Production of Advanced Biofuels. *BioScience*, 64(3), 192-201.
- Spindler, D. D., Wyman, C. E., Grohmann, K. & Mohagheghi, A. (1989) SIMULTANEOUS SACCHARIFICATION AND FERMENTATION OF PRETREATED WHEAT STRAW TO ETHANOL WITH SELECTED YEAST STRAINS AND BETA-GLUCOSIDASE SUPPLEMENTATION. *Applied Biochemistry and Biotechnology*, 20-1, 529-540.
- Srivastava, N., Rawat, R., Oberoi, H. S. & Ramteke, P. W. (2015) A Review on Fuel Ethanol Production From Lignocellulosic Biomass. *International Journal of Green Energy*, 12(9), 949-960.
- Stewart, V. & Macgregor, C. H. (1982) NITRATE REDUCTASE IN ESCHERICHIA-COLI K-12 - INVOLVEMENT OF CHLC, CHLE, AND CHLG LOCI. *Journal of Bacteriology*, 151(2), 788-799.
- Sundberg, C., Al-Soud, W. A., Larsson, M., Alm, E., Yekta, S. S., Svensson, B. H., Sorensen, S. J. & Karlsson, A. (2013) 454 pyrosequencing analyses of bacterial and archaeal richness in 21 full-scale biogas digesters. *Fems Microbiology Ecology*, 85(3), 612-626.
- Swings, J. & De Lay, J. (1977) The Biology of Zymomonas. *Bacteriological Reviews*, 41(1), 1-46. Available online: [Accessed.

- Takkellapati, S., Li, T. & Gonzalez, M. A. (2018) An overview of biorefinery-derived platform chemicals from a cellulose and hemicellulose biorefinery. *Clean Technologies and Environmental Policy*, 20(7), 1615-1630.
- Tan, S. T., Ho, W. S., Hashim, H., Lee, C. T., Taib, M. R. & Ho, C. S. (2015) Energy, economic and environmental (3E) analysis of waste-to-energy (WTE) strategies for municipal solid waste (MSW) management in Malaysia. *Energy Conversion and Management*, 102, 111-120.
- Tchounwou, P. B., Yedjou, C. G., Patlolla, A. K. & Sutton, D. J. (2012) Heavy metal toxicity and the environment. *Experientia supplementum* (2012), 101, 133-164.
- Thomas, C. D., Cameron, A., Green, R. E., Bakkenes, M., Beaumont, L. J., Collingham, Y. C., Erasmus, B. F. N., de Siqueira, M. F., Grainger, A., Hannah, L., Hughes, L., Huntley, B., van Jaarsveld, A. S., Midgley, G. F., Miles, L., Ortega-Huerta, M. A., Townsend Peterson, A., Phillips, O. L. & Williams, S. E. (2004) Extinction risk from climate change. *Nature*, 427(6970), 145-148.
- Todar, K. (2012) *Diversity of Metabolism in Prokaryotes*, 2012. Available online: http://textbookofbacteriology.net/metabolism_3.html [Accessed].
- Tsitko, I. V., Zaitsev, G. M., Lobanok, A. G. & Salkinoja-Salonen, M. S. (1999) Effect of Aromatic Compounds on Cellular Fatty Acid Composition of *Rhodococcus opacus*. *Applied and Environmental Microbiology*, 65(2), 853.
- Tura, A., Fontana, R. C., Camassola, M. J. A. B. & Biotechnology (2018) *Schizosaccharomyces pombe* as an Efficient Yeast to Convert Sugarcane Bagasse Pretreated with Ionic Liquids in Ethanol, 186(4), 960-971.
- Turner, P., Mamo, G. & Karlsson, E. N. (2007) Potential and utilization of thermophiles and thermostable enzymes in biorefining. *Microbial Cell Factories*, 6.
- Tyagi, V. K., Fdez-Güelfo, L. A., Zhou, Y., Álvarez-Gallego, C. J., Garcia, L. I. R. & Ng, W. J. (2018) Anaerobic co-digestion of organic fraction of municipal solid waste (OFMSW): Progress and challenges. *Renewable and Sustainable Energy Reviews*, 93, 380-399.
- UNEP (2015) *The Emissions Gap Report 2015*. Nairobi: (UNEP), U. N. E. P.
- UNFCCC (2015) *Synthesis report on the aggregate effect of the intended nationally determined contributions.*, 2015. Available online: unfccc.int/resource/docs/2015/cop21/eng/07.pdf [Accessed].
- Uría-Martínez, R., Leiby, P. N. & Brown, M. L. (2018) Energy security role of biofuels in evolving liquid fuel markets, 12(5), 802-814.
- Valle, A., Cabrera, G., Cantero, D. & Bolivar, J. (2015) Identification of enhanced hydrogen and ethanol *Escherichia coli* producer strains in a glycerol-based medium by screening in single-knock out mutant collections. *Microbial Cell Factories*, 14.
- Van Dyk, J. S. & Pletschke, B. I. (2012) A review of lignocellulose bioconversion using enzymatic hydrolysis and synergistic cooperation between enzymes—Factors affecting enzymes, conversion and synergy. *Biotechnology Advances*, 30(6), 1458-1480.

- Venkata, M. S., Nikhil, G. N., Chiranjeevi, P., Nagendranatha Reddy, C., Rohit, M. V., Kumar, A. N. & Sarkar, O. (2016) Waste biorefinery models towards sustainable circular bioeconomy: Critical review and future perspectives. *Bioresour Technol*, 215, 2-12.
- Voelker, T. A. & Davies, H. M. (1994) Alteration of the specificity and regulation of fatty acid synthesis of *Escherichia coli* by expression of a plant medium-chain acyl-acyl carrier protein thioesterase. *Journal of Bacteriology*, 176(23), 7320.
- Voelker, T. A., Worrell, A. C., Anderson, L., Bleibaum, J., Fan, C., Hawkins, D. J., Radke, S. E. & Davies, H. M. (1992) Fatty acid biosynthesis redirected to medium chains in transgenic oilseed plants. *Science*, 257(5066), 72.
- Wältermann, M., Luftmann, H., Baumeister, D., Kalscheuer, R. & Steinbüchel, A. (2000) *Rhodococcus opacus* strain PD630 as a new source of high-value single-cell oil? Isolation and characterization of triacylglycerols and other storage lipids. *Microbiology*, 146(5), 1143-1149.
- Wang, C., Pflieger, B. F. & Kim, S.-W. (2017) Reassessing *Escherichia coli* as a cell factory for biofuel production. *Current Opinion in Biotechnology*, 45(Supplement C), 92-103.
- Wang, J. L., Yan, D. L., Dixon, R. & Wang, Y. P. (2016) Deciphering the Principles of Bacterial Nitrogen Dietary Preferences: a Strategy for Nutrient Containment. *Mbio*, 7(4).
- Wang, W., Kang, L., Wei, H., Arora, R. & Lee, Y. Y. (2011a) Study on the Decreased Sugar Yield in Enzymatic Hydrolysis of Cellulosic Substrate at High Solid Loading. *Applied Biochemistry and Biotechnology*, 164(7), 1139-1149.
- Wang, X., Song, A., Li, L., Li, X., Zhang, R. & Bao, J. (2011b) Effect of calcium carbonate in waste office paper on enzymatic hydrolysis efficiency and enhancement procedures. *Korean Journal of Chemical Engineering*, 28(2), 550-556.
- Warnecke, T. & Gill, R. T. (2005) Organic acid toxicity, tolerance, and production in *Escherichia coli* biorefining applications. *Microb Cell Fact*, 4.
- WilsonBio-Chemical (2018) *The Autoclave: Process Overview*, 2018. Available online: <http://wilsonbio-chemical.co.uk/the-wilson-system/> [Accessed].
- Wojnowska-Baryła, I., Kulikowska, D., Bernat, K., Kasiński, S., Zaborowska, M. & Kielak, T. (2019) Stabilisation of municipal solid waste after autoclaving in a passively aerated bioreactor. *Waste Management & Research*, 37(5), 542-550.
- Wong, C. L., Leong, R. W. M. & Dunn, N. W. (1978) MUTATION TO INCREASED RESISTANCE TO PHENOL IN *PSEUDOMONAS-PUTIDA*. *Biotechnology and Bioengineering*, 20(6), 917-920.
- Wood, J. M. & Wang, H.-K. (1983) Microbial resistance to heavy metals. *Environmental Science & Technology*, 17(12), 582A-590A.
- Woodruff, L. B., May, B. L., Warner, J. R. & Gill, R. T. (2013) Towards a metabolic engineering strain "commons": an *Escherichia coli* platform strain for ethanol production. *Biotechnol Bioeng*, 110(5), 1520-6.

- WRAP (2018) *Comparing the cost of alternative waste treatment options*.
- Wu, X. H., Altman, R., Eiteman, M. A. & Altman, E. (2014) Adaptation of *Escherichia coli* to Elevated Sodium Concentrations Increases Cation Tolerance and Enables Greater Lactic Acid Production. *Applied and Environmental Microbiology*, 80(9), 2880-2888.
- Ximenes, E., Kim, Y., Mosier, N., Dien, B. & Ladisch, M. (2010) Inhibition of cellulases by phenols. *Enzyme and Microbial Technology*, 46(3), 170-176.
- Xu, Y. & Ramanathan, V. (2017) Well below 2 °C: Mitigation strategies for avoiding dangerous to catastrophic climate changes. *Proceedings of the National Academy of Sciences*, 114(39), 10315.
- Yamakawa, C. K., Qin, F. & Mussatto, S. I. (2018) Advances and opportunities in biomass conversion technologies and biorefineries for the development of a bio-based economy. *Biomass and Bioenergy*, 119, 54-60.
- Yang, S. H., Fei, Q., Zhang, Y. P., Contreras, L. M., Utturkar, S. M., Brown, S. D., Himmel, M. E. & Zhang, M. (2016) *Zymomonas mobilis* as a model system for production of biofuels and biochemicals. *Microbial Biotechnology*, 9(6), 699-717.
- Yuan, X. F., Wen, B. T., Ma, X. G., Zhu, W. B., Wang, X. F., Chen, S. J. & Cui, Z. J. (2014) Enhancing the anaerobic digestion of lignocellulose of municipal solid waste using a microbial pretreatment method. *Bioresource Technology*, 154, 1-9.
- Zaldivar, J. & Ingram, L. O. (1999) Effect of organic acids on the growth and fermentation of ethanologenic *Escherichia coli* LY01. *Biotechnol Bioeng*, 66.
- Zaldivar, J., Martinez, A. & Ingram, L. O. (1999) Effect of selected aldehydes on the growth and fermentation of ethanologenic *Escherichia coli*. *Biotechnol Bioeng*, 65.
- Zeigler, D. R. (2014) The *Geobacillus paradox*: why is a thermophilic bacterial genus so prevalent on a mesophilic planet? *Microbiology*, 160(1), 1-11.
- Zhang, G.-C., Liu, J.-J., Kong, I. I., Kwak, S. & Jin, Y.-S. (2015) Combining C6 and C5 sugar metabolism for enhancing microbial bioconversion. *Current Opinion in Chemical Biology*, 29, 49-57.
- Zhang, M., Eddy, C., Deanda, K., Finkestein, M. & Picataggio, S. (1995) METABOLIC ENGINEERING OF A PENTOSE METABOLISM PATHWAY IN ETHANOLOGENIC *ZYMOMONAS-MOBILIS*. *Science*, 267(5195), 240-243.
- Zhang, Y., Banks, C. J. & Heaven, S. (2012) Anaerobic digestion of two biodegradable municipal waste streams. *Journal of Environmental Management*, 104, 166-174.
- Zhao, X. B., Zhang, L. H. & Liu, D. H. (2012) Biomass recalcitrance. Part I: the chemical compositions and physical structures affecting the enzymatic hydrolysis of lignocellulose. *Biofuels Bioproducts & Biorefining-Biofpr*, 6(4), 465-482.
- Zhen, G., Kobayashi, T., Lu, X., Kumar, G., Hu, Y., Bakonyi, P., Rózsenszki, T., Koók, L., Nemestóthy, N., Bélafi-Bakó, K. & Xu, K. (2016) Recovery of biohydrogen in a single-chamber microbial electrohydrogenesis cell using liquid fraction of pressed municipal

solid waste (LPW) as substrate. *International Journal of Hydrogen Energy*, 41(40), 17896-17906.

Zhou, J. W., Wu, K. & Rao, C. V. (2016) Evolutionary Engineering of *Geobacillus thermoglucosidasius* for Improved Ethanol Production. *Biotechnology and Bioengineering*, 113(10), 2156-2167.